Development of Novel Pantothenate Synthetase and Lysine Aminotransferase Inhibitors against Active and Dormant Tuberculosis

THESIS

Submitted in partial fulfilment

of the requirements for the degree of

DOCTOR OF PHILOSOPHY

by

BRINDHA DEVI P

ID No. 2012PHXF518H

Under the supervision of

Prof. P. YOGEESWARI

BITS Pilani

Pilani | Dubai | Goa | Hyderabad

BIRLA INSTITUTE OF TECHNOLOGY AND SCIENCE, PILANI

2015

BIRLA INSTITUTE OF TECHNOLOGY AND SCIENCE, PILANI

CERTIFICATE

This is to certify that the thesis entitled "**Development of Novel Pantothenate Synthetase and Lysine Aminotransferase Inhibitors against Active and Dormant Tuberculosis**" and submitted by **BRINDHA DEVI P** ID No. **2012PHXF518H** for award of Ph.D. of the Institute embodies original work done by her under my supervision.

Signature of the Supervisor **:**

Name in capital letters **: P. YOGEESWARI**

Designation **: Professor**

Date:

Acknowledgement

*First and foremost I would like to thank **God Almighty** who has given me this opportunity.*

Any attempt to list the people and opportunities with which my life has been richly blessed would be like trying to count the stars in the heaven.

*It's a great pleasure and immense satisfaction in expressing my deep gratitude towards my research supervisor, **Prof. P. Yogeeswari**, Professor, Department of Pharmacy, BITS, Pilani-Hyderabad campus, for her guidance, suggestions and support which she bestowed to me. Mere acknowledging with words is inadequate to express my gratitude to her. She was always an inspiration to me in research. The work environment given to me under her, the experiences gained from her and her creative working culture are treasured and will be remembered throughout my life.*

*I deeply acknowledge and heartfelt thanks to **Prof. D. Sriram**, Professor, Department of Pharmacy, BITS, Pilani-Hyderabad campus, for his valuable suggestions, guidance and precious time which he offered me throughout my research.*

*I am thankful to acknowledge my DAC members **Dr. V.V.Vamsi Krishna** and **Dr.Arti Dhar** for their support and encouragement during this period.*

*I am grateful to **Prof. Bijendra Nath Jain**, Vice-Chancellor (BITS) and Director **Prof. V.S.Rao** (Hyderabad campus), for allowing me to carry out my doctoral research work in the institute.*

*I am thankful to **Prof. M. M. S.Anand,** Registrar and **Prof. S.K.Verma,** Dean, Academic Research (Ph.D. Programme), BITS Pilani for their support to do my research work.*

*I would like to express my sincere thanks to **Prof. M.B.Srinivas,** Dean, Administration and **Dr. Vidya Rajesh,** Associate Dean, Academic Research (Ph.D. Programme), BITS-Pilani, Hyderabad campus for their continuous support and encouragement during my research work.*

*I would like to express my gratitude to **Dr. Shrikanth Y. Charde**, Head of the Department, Pharmacy, for providing me with all the necessary laboratory facilities and for having helped me at various stages of my research work.*

*I sincerely acknowledge the help rendered by **Dr.Punna Rao Ravi**,,**Dr.Sajeli Begum**, **Dr.Balram Ghosh**,, **Dr. Swati Biswas** and **Dr.Onkar Kulkherni**, faculty at the BITS-Pilani, Hyderabad campus.*

I acknowledge ***Dr. David Eisenberg*** *and* ***Dr. Shuishu Wang****, Department of Biochemistry and Molecular Biology, USUHS, Maryland (USA), for providing the Mtb PS clone.*

I sincerely acknowledge to ***Dr. E.G. Salina*** *and her group, Institute of the Russian Academy of Sciences, Moscow (Russia) for carrying out my dormant studies for Mycobacterium tuberculosis PS inhibitors.*

I owe a great deal of appreciation and gratitude to ***Dr. Vinay Kumar Nandicoori****, Scientist, and his group at National Institute of Immunology, New Delhi, India for providing Mycobacterium tuberculosis LAT clone.*

I take this opportunity to sincerely acknowledge the Open source Drug Discovery and Development (OSDD)-CSIR, Government of India, New Delhi, for providing me financial assistance. I'm also thankful to the Department of Science and Technology, New Delhi, India (SR/S1/OC-70/2010) and the Program of the Presidium of the Russian Academy of Sciences "Molecular and Cellular Biology" for financial assistance.

I am very much grateful to all my friends ***Ganesh S, Manoj, Ganesh P, Jean, Sridhar, Parameshwar, Sridevi, Mallika, Shalini, Reshma A, Reshma S, Vijay, Renuka, Koushik, Madhu, Saketh Sriram, Priyanka P, Priyanka S, Hasitha, Patrisha, Ram, Brahmam, Bobesh, Radhika, Gangadhar, Srikanth, Shubam, Praveen, Suman, Mahibalan, Rukaiyya, Shailendar, Poorna, Santosh, Preethi, Omkar, Anup, Shubmita, Vishnu*** *for the time they had spent for me and making my stay at campus a memorable one. I take this opportunity to thank one and all for their help directly or indirectly.*

I take this opportunity to thank the project students, especially, ***Monika, Renu*** *and* ***Sridevi K,***

I express my thanks to our laboratory assistants, ***Mrs. Saritha****,* ***Mr. Rajesh****,* ***Mr. Ramu****,* ***Mr.Seenu*** *and* ***Mrs. Rekha****.*

I would like to begin by dedicating this piece of work to my parents ***Mr. T. Parthiban and Mrs. P. Muthu Lakshmi****, whose dreams had come to life with me getting the highest degree in education. I owe my doctorate degree to my parents who kept with their continuous care, support and encouragement my morale high. Thanks are due if I don't dedicate this thesis to my brother* ***Dhambi Raj and my family*** *whose constant and continuous support, love and affection made me reaching this height.*

To those I may have Wronged,

I ask Forgiveness.

To those I may have Helped,

I wish I did More.

To those I Neglected to help,

I ask for Understanding.

To those who helped me,

I sincerely Thank you

So much…

Date: *BRINDHA DEVI P*

Abstract

Tuberculosis (TB) is the leading disease in the world today causing world-wide death among the infectious diseases and is responsible for the greatest morbidity and mortality. In this study we have focused on developing novel leads for the enzyme targets of infectious disease tuberculosis in both active and dormant forms.

We employed computer-aided drug design tool, to identify new leads for *Mycobacterium tuberculosis* (Mtb) enzyme targets pantothenate synthetase (PS) and lysine aminotransferase (LAT). For Mtb PS we utilized the reaction intermediate and the inhibitor bound with active site of the protein. Energy-based pharmacophore hypotheses based on the crystal structures of Mtb PS bound to reaction intermediate and inhibitor were generated and validated using enrichment calculations. Further virtual high-throuput screening and docking were performed to identify new inhibitors for the targets. The leads identified were further modified using medicinal chemistry approach. From the first set of optimized leads, compounds **Pa-9** and **Pa-12** emerged as most potent Mtb PS leads with IC_{50}s of 0.35±0.81 μM and 0.37±0.92 respectively; Mtb MIC of 0.38 μM and 0.85 μM respectively in the presence of efflux inhibitors. The stabilization of protein-ligand complexes was re-ascertained by differential scanning fluorimetry, wherein the melting temperature was monitored. All the top active hits showed a shift in T_m in the range of 2-4.3°C compared to the native protein which implied binding of inhibitors towards the protein. Compound **Pa-12** was found to be effective against dormant Mtb.

For the second enzyme target Mtb LAT, we employed similar approach as mentioned above. As there were no inhibitors available for this enzyme target, we employed two crystal structures from protein data bank that were bound with substrates like lysine and α-ketoglutarte to design leads. Compounds **La-1** and **La-17** exhibited good inhibition of Mtb LAT at IC_{50}s of 4.09±0.09 μM and 4.34±0.01 μM respectively; whereas, compounds **La-28** and **La-30** showed IC_{50}s of 1.02±0.08 μM and 0.81±0.08 μM respectively. From the second set of optimized leads, compounds **Lb-29** and **Lb-12** with IC_{50}s of 1.72±0.64 μM and 4.01±0.31 μM respectively showed ~2.8 logarithmic reduction of bacterial growth in nutrient starved condition when compared with standard first line drugs isoniazid (~1.2) and rifampicin (~2.0) and moxifloxacin (~2.3).

Thus, with an urgent need of anti-mycobacterial drugs for tackling dormant forms, we believe that the present class of drugs could be useful as potential leads for further optimization through in-vivo studies, mutagenesis, and pharmacokinetic approaches.

Table of Contents

List of Tables

List of Figures

List of Abbreviations

μM	:	Micromolar
δ	:	Chemical shift
^{13}C NMR	:	Carbon Nuclear Magnetic Resonance
^{1}H NMR	:	Proton Nuclear Magnetic Resonance
ActD	:	Actinomycin D
AMP	:	Adenosine Monophosphate
AMPCPP	:	α,β-Methyleneadenosine 5'-triphosphate
ATP	:	Adenosine Triphosphate
BCG	:	Bacillus Calmette-Guerin
CFU	:	Colony Forming Unit
CG	:	Conjugate Gradient
CHN	:	Carbon Hydrogen Nitrogen
CNS	:	Central Nervous System
CoA	:	Coenzyme A
D	:	Hydrogen bond Donor
d	:	Doublet
dd	:	Doublet of Doublet
DMSO	:	Dimethyl Sulphoxide
DMSO d_6	:	Dimethyl Sulphoxide deuterated
DOTS	:	Directly Observed Treatment, Short course
DSF	:	Differential Scanning Flourimetry
EF	:	Enrichment Factor
FBS	:	Fetal Bovine Serum
FDA	:	Food and Drug Administration
GABA	:	γ-Aminobutyrate Aminotransferase
GH	:	Goodness of Hit
GLIDE	:	Grid based Ligand Docking and Energetics
HEPES	:	4-(2-Hydroxyethyl)piperazine-1-ethanesulfonic acid
HIV	:	Human Immunodeficiency Virus
HPLC	:	High Pressure Liquid Chromatography

HTVS	:	High-throughput Virtual Screening
IC_{50}	:	Half maximal Inhibitory Concentration
IPTG	:	Isopropyl β-D-1-thiogalactopyranoside
J	:	Coupling constant
kDa	:	Kilo Daltons
KH_2PO_4	:	Potassium dihydrogen phosphate
K_i	:	Inhibitor constant
K_m	:	Kinetic constant
$KMnO_4$	:	Potassium permanganate
LAT	:	Lysine aminotransferase
LCMS	:	Liquid Chromatography-Mass Spectrometer
LAM	:	Lipoarabinomannan
LM	:	Lipomannan
LTBI	:	Latent Tuberculosis Infection
m	:	Multiplet
M.P	:	Melting point
MABA	:	Microplate Alamar Blue Assay
MCS	:	Multiple Cloning Site
MDR TB	:	Multidrug Resistant Tuberculosis
mg	:	Milligram
$MgCl_2$	:	Magnesium chloride
$MgSO_4$	:	Magnesium sulphate
MIC	:	Minimum Inhibitory Concentration
ml	:	Milliliter
mmol	:	Millimole
MPLC	:	Medium Pressure Liquid Chromatography
MPN	:	Most Probable Number
Mtb	:	*Mycobacterium tuberculosis*
MTT	:	(4,5-dimethylthiazol-2-yl)-2,5-diphenyltetrazolium bromide
N	:	Negative ionisable
NaCl	:	Sodium chloride
NAD	:	Nicotinamide Adenine Dinucleatide
NADH	:	Nicotinamide adenine dinucleotide hydrated

NADPH	:	Nicotinamide adenine dinucleotide phosphate
NaOH	:	Sodium hydroxide
Ni-NTA	:	Nickel-nitroloacetic acid
nM	:	Nanomolar
nm	:	Nanometre
NRP	:	Non-Replicating Persistant
OADC	:	Oleic acid, Albumin, Dextrose, Catalase
OAT	:	Ornithine aminotransferase
OPLS	:	Optimized Potentials for Liquid Simulations
ORF	:	Open Reading Frame
PAGE	:	Polyacrylamide Gel Electrophoresis
PCR	:	Polymerase Chain Reaction
PDB	:	Protein Data Bank
pfu	:	*Pyrococcus furiosus*
PHASE	:	Pharmacophoric Search Engine
PIM	:	Phosphatidyl-myo-inositol mannoside
PLP	:	Pyridoxal 5-phosphate
pM	:	Picomolar
PMP	:	Pyridoxal monophosphate
PMSF	:	Phenylmethyl sulfonyl fluoride
PS	:	Pantothenate Synthetase
QPlogBB	:	QuickProp predicted Blood Brain partition coefficient
QPlogCaco	:	QuickProp predicted Caco-2 cell permeability
QPlogHERG	:	QuickProp predicted the human Ether-a-go-go-Related gene
QPlogP	:	QuickProp predicted Partition coefficient
R	:	Aromatic ring
RFU	:	Relative Fluorescence Units
RMSD	:	Root Mean Square Deviation
RNI	:	Reactive Nitrogen Intermediate
ROI	:	Reactive Oxygen Intermediate
rpm	:	Rotation per minute
rt	:	Room Temperature
RT-PCR	:	Real time Polymerase Chain Reaction

s	:	Singlet
SAR	:	Structure-Activity Relationship
SD	:	Steepest Descent
SDS	:	Sodium Dodecyl Sulphate
SP	:	Standard Precision
t	:	Triplet
TB	:	Tuberculosis
TCA	:	Tricarboxylic acid
TLC	:	Thin Layer Chromatography
T_m	:	Melting temperature
TMS	:	Trimethyl silane
V_{max}	:	Maximum velocity
WHO	:	World Health Organisation
XDR TB	:	Extensively Drug Resistant Tuberculosis
XP	:	Extra Precision
YT	:	Yeast extract Tryptone
$ZnSO_4$	:	Zinc sulphate

Chapter 1
Introduction

Tuberculosis rose slowly, silently, seeping into homes of millions, like an ageless miasma. And once arrived, it never went away again. Year after year, century after century, it tightened its relentless hold, worsening whenever war or famine reduced the peoples' resistance, infecting virtually everybody, inexplicably sparing some while destroying others, bringing the young down onto their sickbeds, where the flesh slowly fell from their bones and they were consumed in the years long fever, their minds brilliantly alert until, in apocalyptic numbers, they died, like the fallen leaves of a dreadful and premature autumn.

The Forgotten Plague:

How the War against Tuberculosis was Won - and Lost

Frank Ryan, 1992

1.1. Tuberculosis

Tuberculosis (TB) is one of the deadliest infectious diseases for humans. In 1882, Robert Koch had identified *Mycobacterium tuberculosis* (Mtb) as the causative agent for TB. It was anticipated earlier that there were about 9.8 million new cases, in any year in the history [Koul A., *et al*., 2011]. This implies that the relative shortcomings of the current treatment for TB and the limited effectiveness of public health, mainly in poor countries where TB is prominent. TB is an air born infection, an obligate aerobic bacillus which divides at a slow rate and highly transmitted as an infectious aerosol. Normally, by inhalation of few droplets of Mtb nuclei which is 2-5 μm in diameter contains 1-3 bacilli. The fate of initial exposure to Mtb varies from immediate elimination of the bacteria from the host's immune system to the infected individuals developing active pulmonary TB. In recent years, TB epidemic has been fully emerged due to multi drug resistant TB (MDR-TB) and extensively drug resistant TB (XDR-TB) strains and that leads to dwindling the treatment options old. To achieve this global control of this infectious disease there seem to be an urgent need for new TB drugs that can,

- Shorten the treatment duration
- Targeting MDR and XDR strains

- Simplifying the treatment by reducing daily medication
- Be co-administered with human immunodeficiency virus (HIV) medications.

The World Health Organization (WHO) reports estimated that almost 8.6 million people developed TB and 1.3 million people died from disease also including 3 lacs deaths from HIV infected people. Globally, majority of TB cases in worldwide in the year were reported in South-East Asia (29%), Africa (27%) and Western Pacific (19%) regions. India and China had accounted 26% and 12% of total cases respectively [Elzinga G., *et al*., 2004]. This implied that there were shortcomings of current treatment strategies for TB and limited effectiveness of public health systems [WHO Report, 2013]. A new emerging issue is co-infection of HIV and Mtb. Currently, almost 15% of new TB patients are also infected with HIV and in some areas the proportions exceed 50% [Cox H.S., *et al*., 2009]. Globally, around one fourth of TB deaths were due to HIV and this was about to one-third of new HIV-positive TB cases.

1.2. Physiology of Mtb

Mtb is a non-motile rod shaped bacterium distantly related to actinomycetes. The rods are of 2-5 μm in length and 0.2-0.5 μm in width. Since it is an obligate aerobe, Mtb complexes are found in upper lobes of lungs in human. Mtb is a facultative intracellular parasite that has slow doubling time, i.e 15-20 hrs, and a characteristic feature that contributes to its virulence. Mtb is classified as neither as Gram-positive nor as Gram-negative because it do not have corresponding characteristics. Hence Mtb is classified specifically as acid-fast bacteria due to their impermeability of specific dyes and stains [Todar K., 2006]. Anti-tuberculosis agents in current development trigger a large panel of biological pathways such as cell wall synthesis, DNA replication, protein synthesis or membrane energy production [Zhang Y., *et al*., 2005].

1.2.1. Cell wall of Mycobacteria

The cell wall of Mtb plays an important role among prokaryotes that determines its virulence (Figure 1.1). The cell wall complex contains peptidoglycan which is composed of complex lipids and almost 60% of mycobacterial cell wall is made of lipids. The lipid fraction of Mtb's cell wall consists of three main components: mycolic acid, cord factor and wax-D.

Mycolic acids are unique α-branched lipids found in cell walls of mycobacterium [Asselineau J., *et al*., 1950]. Mycolic acids are strong hydrophobic molecules that form lipid shell around the organism that affects permeability property in cell surface [Takayama K., *et*

al., 2005]. Mycolic acids prevent mycobacteria from the attack of cationic proteins, lysozyme and oxygen radicals in phagocytic granule. Cord factor are the glycolipids in cell wall, which causes the bacteria to grow in serpentine cords. It helps in induction of granulomatous reactions. Wax-D in cell wall is the major component of Freund's complete adjuvant [Todar K., 2006].

The high concentrations of lipids in mycobacterium cell wall are associated with these properties,

- Impermeability to stains and dyes
- Resistance to many antibiotics
- Resistance to killing by acidic and alkaline compounds
- Resistance to osmotic lysis *via* complement depositon
- Resistance to lethal oxidation and survival inside macrophages

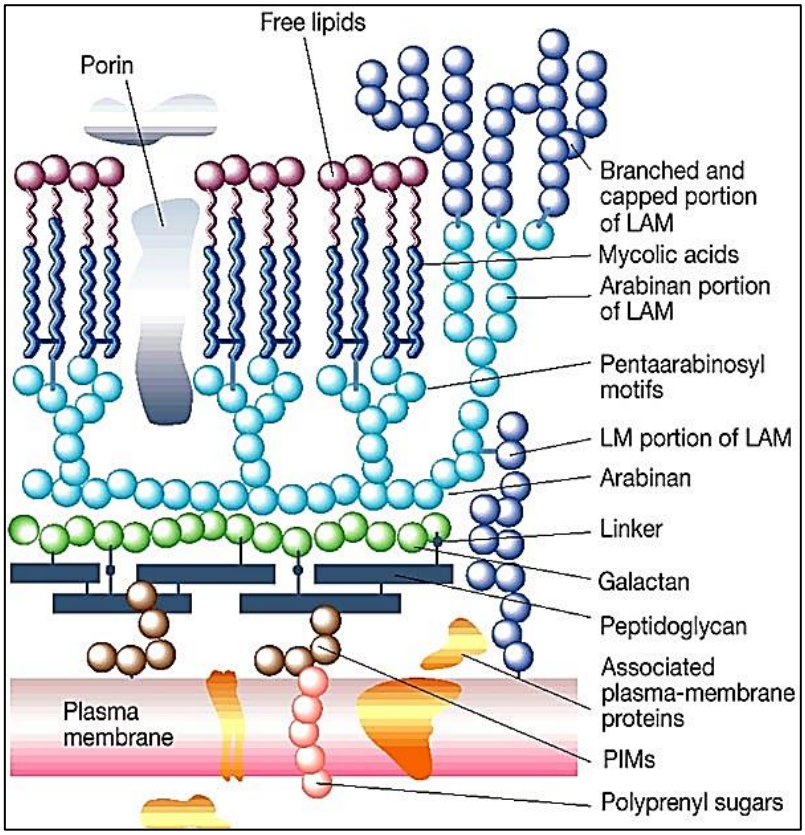

Figure 1.1: Cell wall of Mtb [Park S.H., *et al*., 2000]

1.3. Pathogenesis of TB

Nearly 2 billion people are estimated to be latently infected with Mtb, in a non-replicating or dormant stage. TB can affect any organ but mostly affects lungs. Mtb is transmitted *via* air and reaches pulmonary alveoli where the bacteria are phagocytized by non-activated macrophages. Within the macrophage the bacteria inhibit many cellular mechanisms preventing the fusion between phagosomes and lysosomes [Houben E.N., *et al*., 2006]. The ability of the bacteria to circumvent phagolysosomal degradation allows it to replicate freely and eventually when macrophage lyses the bacteria could invade new macrophage. When large number of macrophage gets infected, they fuse and form multinucleated giant cells called Langhans cells. Other immune cells surround the infected macrophage forming a barrier to the surrounding tissue, thereby creating a compartment called granuloma [Pieters J., *et al*., 2008]. In most cases, the immune system suppresses the infection and the bacteria stop to replicate and enter a dormant state within the granulomas. In these granulomas there is a balance between pathogen virulence factors and the host immune response. Suppression of immune system at later state could result in reactivation of bacterial multiplication and continuation of Mtb infectious cycle (Figure 1.2).

Bacteria inside the granulomas could survive for long time and hence requires longer antibiotic treatment. Most of the commonly available antibiotics are directed towards different parts of replication machinery which are not targeted as effectively in dormant bacteria. Within granulomas the microenvironment could be characterized by hypoxia, nutrient starvation and exposure to reactive oxygen intermediates (ROI) and reactive nitrogen intermediates (RNI) [Vergne I., *et al*., 2004]. These compounds are used by phagocytic cells to eliminate internalized bacteria, yet some pathogenic bacteria like *S. typhimurium* and Mtb were found to avoid elimination, leading to long term survival and the establishment of persistent infection [Zahrt T.C., *et al*., 2002]. The peptidoglycan layer was found to play an important role in the maintenance of bacterial dormancy and variation in specific cross-link during stationary phase adaptation of Mtb.

There is strong evidence that Mtb uses lipids as their major energy source for persistence in the host. Mtb uses the host triacylglycerol to accumulate lipid droplets intracellularly and acquire dormancy phenotype inside macrophage [Fattorini L., *et al*., 2014]. Recently it was reported that, dormant bacteria may be eradicated with antibiotics generated with hydroxyl radicals, suggesting that stimulation of reactive oxygen species provide potential strategy to manage persistent infections [Grant S.S., *et al*., 2012]

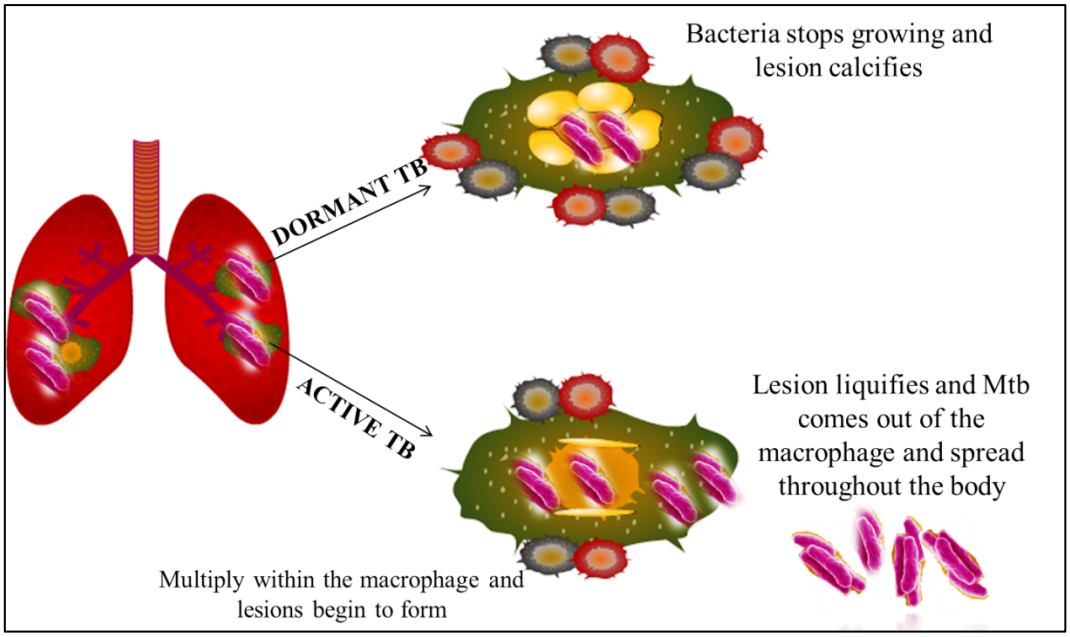

Figure 1.2: Dormant Mtb and active TB differentiation inside the macrophage

1.4. TB chemotherapy

Most of the TB drugs in first-line were discovered in 1950's and 1960's. Streptomycin was first discovered as an effective anti-TB agent [Vilemagne D., *et al*., 2012]. This aminoglycoside interfere with protein biosynthesis through interaction with 30S ribosome subunit [Schatz A., *et al*., 1944; Jones D., *et al*., 1944]. Discovery of mycolic acid synthesis inhibitor INH was one of the most active TB drugs till date [Bernstein J., *et al*., 1944]. The discovery of pyrazinamide, a major breakthrough in TB treatment made significant reduction in treatment period from 9 months to 6 months. In 1961, investigation of polyamines and diamines led to production of a series of diamine analogues that gave rise to discover of ethambutol [Thomas J.P., *et al*., 1961]. Finally rifampicin (RIF) [Binda G., *et al*., 1971] the last member of present first-line drugs was found effective against replicating and non-replicating Mtb. This class of drugs inhibited RNA synthesis by binding to the B-subunit of DNA-dependent polymerase.

In-spite of significant efficiency by these drugs, it was observed that the bacteria rapidly developed resistance to these drugs and stable cure was unattainable with single dose therapy. Inorder to prevent the development of resistance and produce stable cure, combination therapy was introduced. WHO recommended DOTS (Directly observed treatment, short course) anti-TB therapy using combination of four drugs: isoniazid, ethambutol and pyrazinamide for two months followed by rifampicin and isoniazid for four months [Kimerling M.E., *et al*., 1999]. The combination therapy cure rates were found to be 90% in

HIV-negative patients which was a globally accepted standard treatment of active TB. Treatment with these first-line drugs when carried for two months led to destruction of bacteria in all stages of growth and when the treatment continued with rifampicin and isoniazid for four months, residual dormant bacilli was eliminated using rifampicin and any rifampicin resistant mutant was killed by isoniazid.

1.5. Limitations of TB drug therapy

Due to emergence of drug resistant TB and association between HIV and Mtb, DOTS became rapidly ineffective in controlling TB [Kimerling M.E., *et al*., 1999]. The combination of drugs was very expensive and has to be administered for a longer duration which led to significant side effects. The length of therapy makes the patient compliance difficult and these patients would become susceptible to drug-resistant strains. The second major problem was that the current therapies available today were ineffective against persistent bacilli except rifampicin and pyrazinamide. Rifampicin was active against both actively growing and slow metabolizing non-growing bacilli whereas pyrazinamide was active against semi-dormant non-growing bacilli. However there are still dormant bacilli populations not killed by any of the available drugs [Chopra P., *et al*., 2003]. Therefore, there is a need for new drugs that are more active against slowly growing and persistent bacilli to treat populations of bacteria at risk of developing active disease through reactivation. Also, it is important to achieve shortened therapy to slow down the development of drug resistance in mycobacteria.

1.6. Drug resistant TB

MDR-TB is resistant to the first-line anti-TB drugs isoniazid and rifampicin. The term MDR-TB was associated with high mortality rates occurred among HIV-infected patients [WHO report, 2013]. The treatment is quite complicated and it requires second-line drugs some of which are less effective, more toxic and expensive than first-line drugs. XDR-TB is resistant to at least isoniazid and rifampicin and also to fluoroquinolones, capreomycin, kanamycin and amikacin. XDR-TB requires longer treatments with drugs are very costly with limited efficacy and increased side effects. XDR-TB is reported in 77 countries and its prevalence is not clear. Only two of 27 burden MDR-TB countries are routinely testing for the resistance of second-line drugs; since XDR-TB is resistant to first and second-line drugs. The genetic diversity of drug-resistant Mtb indicates that the drug resistance has been evolving due to inappropriate drug treatment [Trauner A., *et al*., 2014]. The ongoing evolution of Mtb, provide excellent opportunity to explore genetic determinants of drugs resistance to Mtb.

Unlike other bacterial pathogens, resistance plasmids and horizontal gene transfer plays no role in drug resistance to Mtb. Efflux mechanism seem to play vital role in developing resistance to this pathogenic bacterium. Due to genetic mutations could be helpful for reliable molecular markers for drug susceptibility testing. The application of this technology to clinical research led to the development of diagnostic tool based on nucleic acid amplification [Trauner A., *et al*., 2014].

1.7. TB drug pipeline

A major advance in the screening efficacy for novel targets was achieved by shifting from enzyme targets to phenotypic screening of whole bacterial cell. Whole bacterial cell screening identified diarylquinolones (bedaquiline), benzothiazines (BTZ-043 and PBTZ-169), and imidazopyridine amide (Q-203) [Zumla A.I., *et al*., 2014] (Figure 1.3).

Bedaquiline (TMC-207), an adenosine triphosphate synthase inhibitor was recently approved by U.S. FDA for the treatment of MDR-TB as a part of new combination therapy. Also, IOC-67683 (delamanid) and TBA-354, a second generation nitroimidazole has also entered phase 3 trials for the treatment of MDR-TB.

Q-203, a compound made from imidazopyridines inhibits the mycobacterial growth by blocking respiratory cytochrome essential for maintaining the proton gradient and ATP synthesis. This drug also has similar property as bedaquiline and inhibits both replicating and non-replicating Mtb. It is active against MDR-TB, XDR-TB and in-vivo data shows there is 100-1000 fold reduction of CFU and blocking of granuloma formation.

Benzothiazinones derivatives, PBTZ-169 and BTZ-043 are in late stage of clinical development. Both drugs inhibits the enzyme, decaprenylphosphory-β-D-ribose 2’ epimerase (DprE1) in Mtb. Inhibition of this enzyme prevents the formation of decaprenylphosphoryl arabinose- a key precursor for biosynthesis of cell wall arabinans, resulting in cell lysis and bacterial death. Both the compounds show 100-1000 fold reduction in CFU in-vivo.

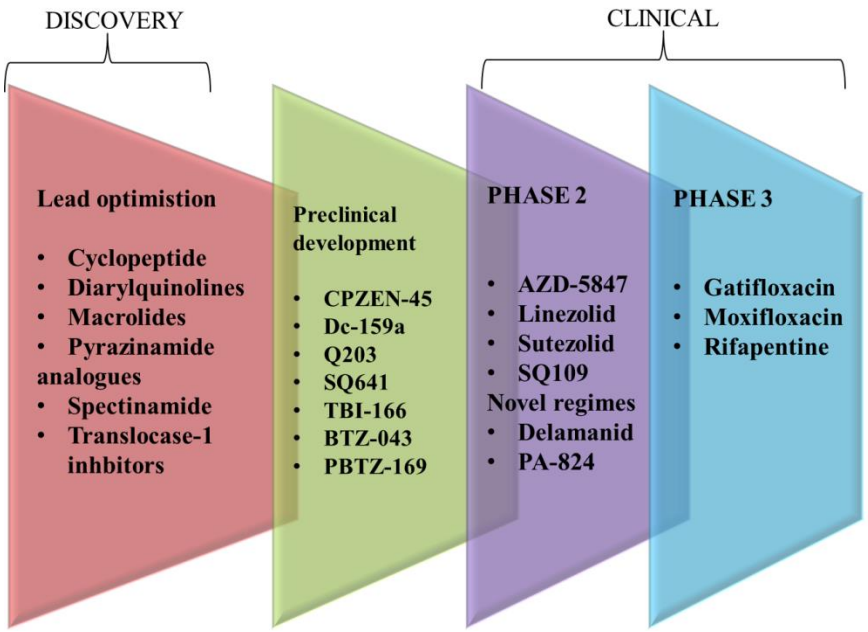

Figure 1.3: Global pipeline of new TB drugs

Chapter 2
Literature Review

Mtb cell wall is comprised of three covalently linked long chain macromolecules such as peptidoglycan, arabinogalactan and mycolic acids. The cell wall biosynthesis represent for good source of molecular targets since the biosynthetic enzymes do not have any homology with the mammalian system. One such attractive target for inhibition of coenzyme A and acyl carrier protein for coordinating acyl group during fatty acid biosynthesis is pantothenate synthetase, the focus of present study. Pantothenate synthetase (PS) (EC: 6.3.2.1), encoded by *panC* gene; also known as D-pantoate:β-alanine ligase. PS catalyses the last step of pantothenate biosynthesis where ATP dependent condensation of pantoate and β-alanine yields pantothenate [Zheng R., *et al*., 2001].

Another target in this study was lysine aminotransferase (LAT) involving in latent TB. It appears to be one such stage and current evidence suggests that Mtb adopts a unique physiological phenotype during latency characterized by bacteriostasis (non-replicating persistence), a switch from aerobic to anaerobic respiration, and increased resistance to several mycobacterial antibiotics. An important target LAT (encoded by the Rv3290c, EC: 2.6.1.36), it is involved in the catalytic reaction of L-lysine where α-amino group is transferred to L-glutamic acid and α-aminoadipic acid. Mtb infection in nutrient deficient mode, LAT gene up-regulation in multiples of 40 times (Betts J.C., *et al*, 2002). Another study showed that mycobacterium adapt to the external environment into the stable and latent infection when, LAT gene is still up-regulated [Voskuil M.I., *et al*., 2004b]. This shows that LAT expression is associated with the dynamics of bacterial infection, which is potentially ideal as drug targets.

A thorough literature study was undertaken on these two less explored targets

2.1. Target I: PANTOTHENATE SYNTHETASE (PS)

PS is a homodimer with a molecular mass of 33 kDa and belongs to cytidylyltransferase superfamily of enzymes (von Delft F., *et al*., 2001). It has two distinct domains:

- Large N-terminal domain from 1-186 residues which forms Rossmann fold

- Smaller C-terminal domain of two layers with the helical layer on top of three stranded antiparallel β-sheet. The β-strands and α-helices are numbered continuously from N-terminus to C-terminus, except the helix α3' which is in one subunit. Three helices are numbered according to the preceding β1 to β4, β6 and β7 that are flanked by α-helices [Wang S., *et al*., 2002].

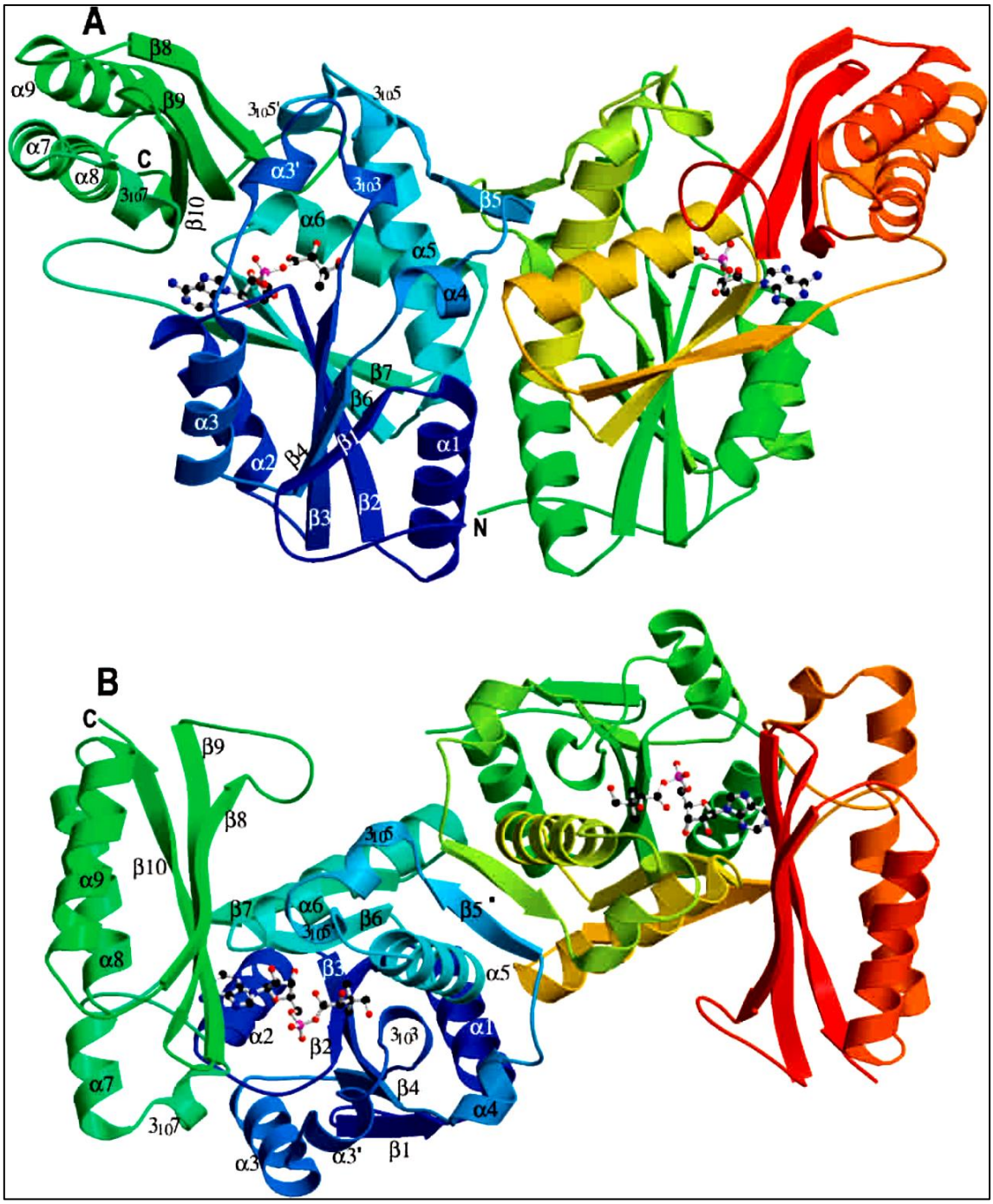

Figure 2.1: (A) Side view of dimer Mtb PS structure; (B) Orthogonal view of (A) from top with two fold.

Residues on β-strands in C-terminal domain have extensive interactions with N-terminal domain. There is a hydrophobic pocket surrounded by Leu123, Leu127, Tyr162, Val166 of N-terminal domain and residues Tyr249, Leu257 and Leu269 of C-terminal domain. Surrounding the hydrophobic pocket, there are three salt bridges, Glu159 to Arg267, Glu128 to Arg278, and Glu126-Arg253. Also there are addional six hydrogen bonding linking the two domains [Wang S., *et al*., 2002]. In additions to these interactions, there are several water-mediated hydrogen bonding interactions.

PS is an ATP-dependent ligase. The formation of the peptide bond between β-alanine and pantoate is catalysed by the formation of pantoyl adenylate from pantoate and ATP (Figure 2.2) with the loss of pyrophosphate [Miyatake K., *et al*., 1979]. This activated ester intermediate is then broken down by the attack of β-alanine, with concomitant formation of pantothenate and AMP. The existence of the intermediate was first proposed in 1960 [Maas W.K., 1960].

The mechanism of PS is based on the binding of ATP followed by D-pantoate and release of PPi and then binding of β-alanine and release of pathothenate and AMP. Based on this reaction, the mechanism has two sequential steps, pantoyl adenylate, a reaction intermediate formation and nucleophilic attack on the mixed anhydride by β-alanine to adenylate. This order of binding suggested that formation of pantoyl adenylate intermediate was forming with the help of enzymatic reaction.

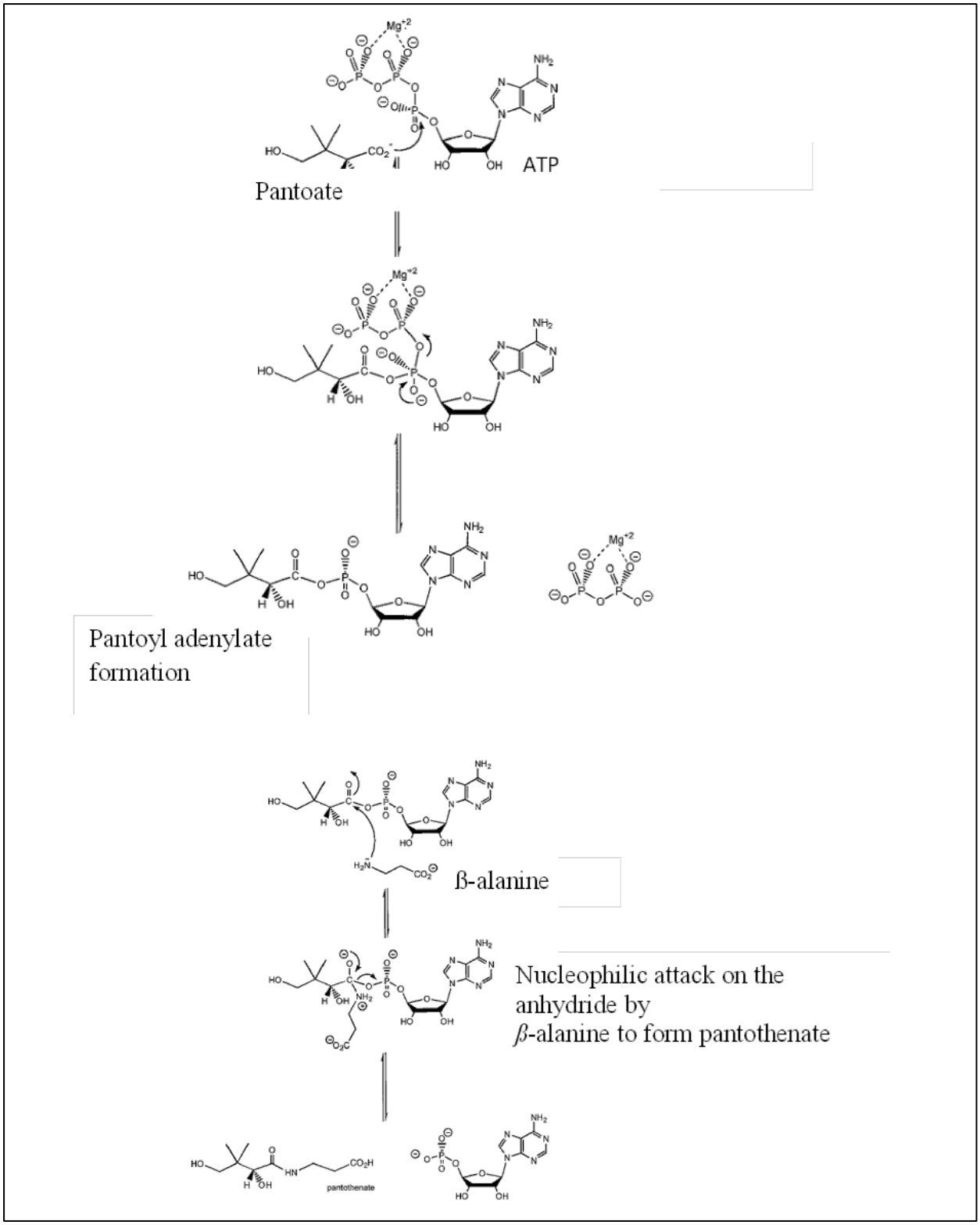

Figure 2.2: Kinetic mechanism of PS reaction: the mechanism shows the structure of pantoyl adenylate intermediate. [Ciulli A., *et al*., 2008]

2.1.1. Binding site analysis of the enzyme PS

The active site of PS is typical of nucleotide binding (Rossmann fold) proteins. The active site of the protein is locked at the C-terminus of the central parallel β-sheet. The cavity is large and there is a cleft between β-strands, β2 and β6. One wall is formed by β2-loop-α-2 and the C-terminus of β7 and the following loop. The flexible residues in the loop-3_{10}3-loop-α3'-loop region fill the gap. Helix 3_{10}7 and the β-strands from the C-terminal domain partially cover the top of the active site region. The bottom of the active site region is mainly hydrophobic, while the top half of the cavity has several charged residues. These positively charged amino acid residues are important for binding of ATP and in the catalytic reaction. The other positively charged arginine side chains, Arg132, Arg273 and Arg278 form a patch by covering the active site region in the enzyme. These positively charged amino acids may steer the negatively charged substrates to the active site cavity [Wang S., *et al*., 2002].

The active site region mainly accompanies ATP and there is little movement of amino acid residues with AMPCPP (adenosine 5′-[α, β-methylene] triphosphate. The adenine group is flanked by Gly46 on helix α2 and Lys160 on the loop after β6. The N1 atom of adenine forms hydrogen bonding interaction to amide nitrogen with the residue Val187. The N6 atom forms the hydrogen bond interaction to carbonyl oxygen at with the residues Met195 and Val187. The N3 atom faces the bottom of the active site cavity, which has two hydrophobic side chains, Val184 and Leu50. The ribose O2* atom show a hydrogen bond to the Oδ2 atoms of Asp161, and the O3* atom forms a hydrogen bond to the amide nitrogen of Gly158, and water-mediated hydrogen bonds to the carbonyl oxygen atoms of Phe156 and Pro38. The phosphate groups turn back towards the top of the active site cavity to the C-terminal domain, and are located near the N-terminal ends of helices α2 and 3_{10}7. Binding of the phosphate groups involves mainly charged side chains [Wang S., *et al*., 2002]. The side chains of Lys160 and Arg198 are partially disordered in the apo enzyme structure but become ordered and move to enable salt bridges to the β- and δ-phosphate groups of AMPCPP, respectively. The α-phosphate group do not have any direct hydrogen bonds with the protein atoms but water-mediated hydrogen bonds to amide nitrogen of Met40 and carbonyl oxygen of Gly41 in Nε2 of His47 side chain are observed.

Researchers have developed Mtb strain that is defective in pantothenate biosynthesis inorder to develop an attenuated Mtb vaccine strain. Many literatures show that a functional pantothenate biosynthetic pathway is required for mycobacterial lipids which are responsible

for virulence of Mtb. Mtb strain lacking gene PanCD, which is responsible for the production of pantothenate failed to revert and were highly atteneutated and less virulent than Bacillus Calmette-Guerin (BCG) vaccine. It was also reported that an auxotrophic mutant of Mtb defective in the de novo biosynthesis of pantothenate was highly attenuated both in immunocompromised mice and immunocompetent mice [Sambdamurthy V.K., *et al*., 2002].

Pantothenate also called as vitamin B5, a water soluble vitamin, is the precursor of 4-phosphopantetheine moiety of coenzyme A [Jackowski S., *et al*., 1996] and acyl carrier protein (ACP), which are required cofactors for many metabolic processes. For the energy-yielding biosynthetic pathways such as TCA and β-oxidation, these cofactors help in the production of fatty acids and isoprenoids. The importance of coenzyme A, ACP and pantothenate in cellular metabolism demonstrated that almost 100 enzymes in *E.coli* required them as a cofactor. This implied that, microorganisms and plants make the vitamin *de novo*, whereas mammals obtain this from their diet [Mass W.K., *et al*., 1960]. Thus this pathway is attractive for the development of non-toxic antibiotics.

2.1.2. Pantothenate biosynthetic pathway

Pantothenate biosynthetic pathway proceeds with α-ketoisovaleric acid [Mass W., *et al*., 1953] followed by enzyme catalysed (ketopantoate hydroxymethyl transferase and ketopantoate reductase) reaction; encoded by *panB* and *panE* to form pantoate. A single step reaction that converts aspartate and β-alanine is catalysed by an enzyme aspartate-1-decarboxylate, encoded by *panD*. Pantothente synthetase catalyses the ATP-dependant condensation of β-alanine and pantoate to form pantothenate (Figure 2.3). The condensation of α-ketoisovalerate with formaldehyde to form α-ketopantoate was already reported in 1942. *PanB* was overexpressed and purified from *E.coli* and was found to be a hexameric protein consists of 28 kDa subunits. The first step involves intramolecular attack of carboxylate ion to form ketopantolactone followed by hydrolysis by nucleophilic attack by one of the water molecule which was coordinated to magnesium ions. *PanE* was cloned, overexpressed and characterized as a monomer with 34 kDa subunits in *E.coli*. Two different mechanisms were proposed for this enzyme mechanism. The only differences between them were the residues donate proton to the ketoacid and the residues that stabilize the hydroxy group of hydrogen bonding. In both the cases, hydrogen of NADPH attacks the carbonyl group of α-ketopantoate. The role of L-aspartate in pantothenate biosynthesis was discovered in 1946. When stimulated with asparagine, pantothenate and aspartate was added to the growth media,

it was found that inhibition of cell growth was occurred. The growth rate was restored when the supplements β-alanine and pantothenate was added. From this analysis, they concluded that β-alanine must be formed from L-aspartate. In the catalytic reaction, the pyruvoyl group bind to L-aspartate to form protonate imine. These binding interactions activate the L-aspartate for decarboxylation and hydrolysis of the Schiff-base that lead to the release of β-alanine and the enzyme.

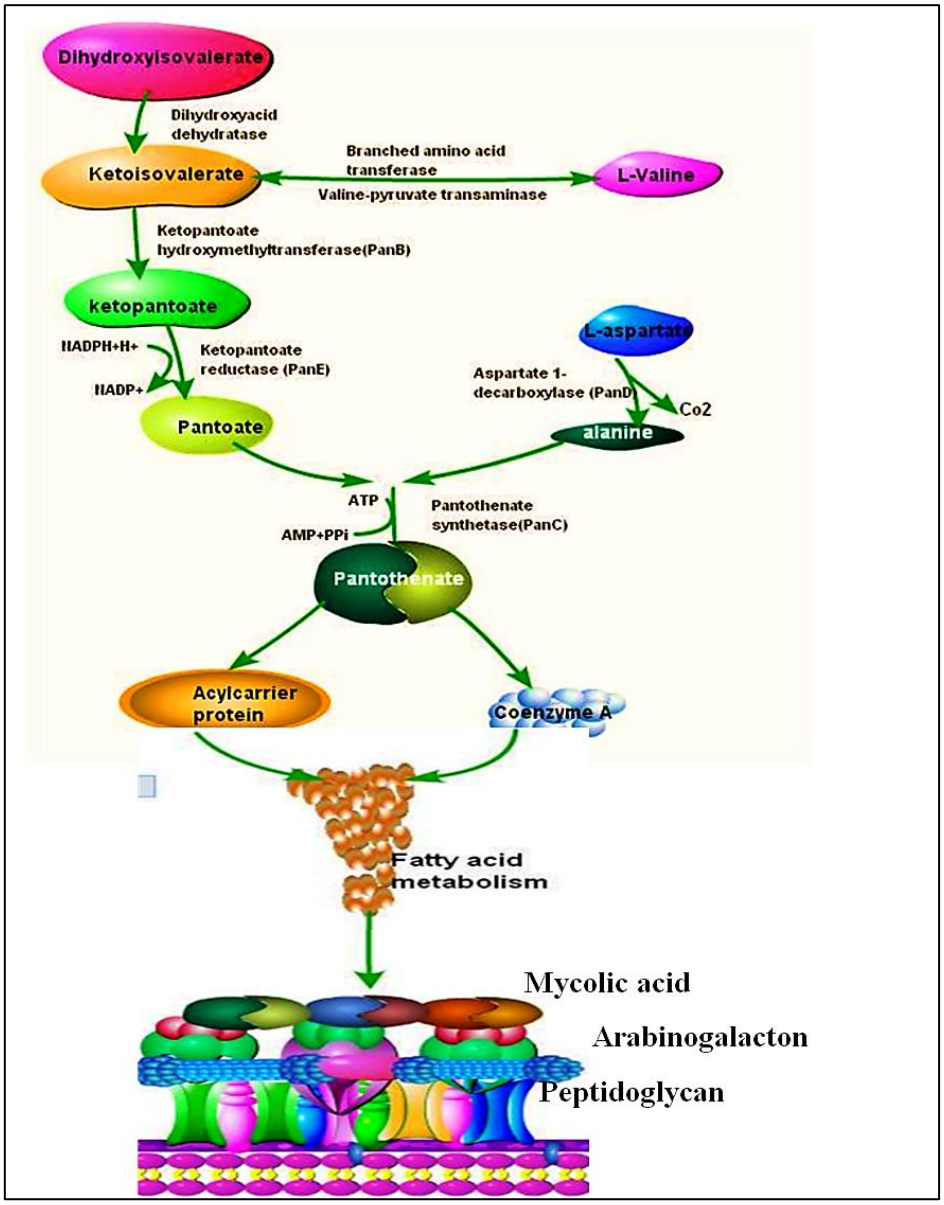

Figure 2.3: Panothenate biosynthetic pathway and the enzymes involved in the pathway

2.1.3. Importance of Mtb PS in dormant TB

Acetyl coA is the central intermediate in primary metabolism with roles in TCA cycle as well as in fatty acid and amino acid biosynthesis [Crick D.C., *et al.*, 2001]. The carbon flux

through acetyl coA is particularly critical to dormant TB. Fatty acids, *via* breakdown to acetyl coA and the use of glyoxylate shunt helps the carbon for carbohydrate synthesis and acetyl coA acts as the gate through which the utilized carbon pool pass. The Mtb cell wall is usually rich in unusual carbohydrates, likely dependent upon this carbon flux through acetyl coA for the maintenance of its cell integrity [Brennan P.J., 2003] (Figure 2.4). As already shown in the Figure 2.3, PS is important in production of pantothenate which leads to the production of acetyl coA and coenzyme A biosynthesis. Thus targeting coenzyme A biosynthesis could disrupt the flux generated through several pathways [Murphy D.J., *et al*., 2007].

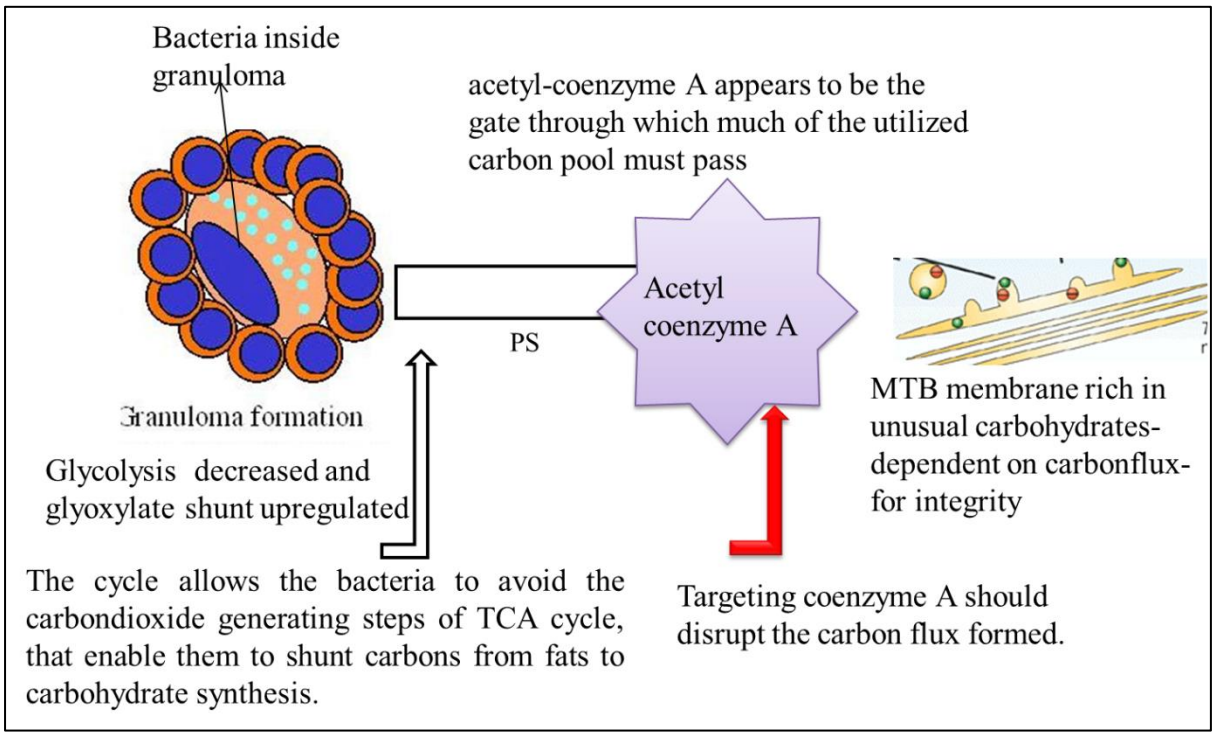

Figure 2.4: Dormant Mtb and its importance with PS

2.1.4. Pantoyl adenylate

The crystal structure of the PS protein in complex with the reaction intermediate shows that the reaction intermediate, pantoyl adenylate, has strong interactions with the active site atoms. This tight binding is necessary to stabilize this highly reactive compound. Pantoyl adenylate has extensive binding interactions with the active site residues with both the pantoate, and the adenylate moiety of the ATP interacting with the protein active site atoms. The pantoate moiety sits in the same position as the pantoate molecule and has identical interactions with the protein atoms, as does the adenosine moiety. However, the α-phosphate group moves closer to pantoate to form a covalent bond with the carboxyl group of pantoate. This allows the α-phosphate to form a direct hydrogen bond to the amide nitrogen of Met40.

The pantoyl adenylate molecule is almost linear and fits snugly in the bottom of the active site cavity. The tight binding of pantoyl adenylate stabilizes this highly reactive intermediate [Zheng R., *et al*., 2001]. This molecule is highly unstable in solution due to the rapid lactonization [Wieland T., *et al*., 1963]. However, inside the active site of the enzyme the molecule is tightly bound with hydrogen bonds to the active site residues, therefore preventing lactonization. With the reaction intermediate in the active site, the flexible wall becomes ordered. This closes the active site cavity, and thus prevents the reaction intermediate from being hydrolysed.

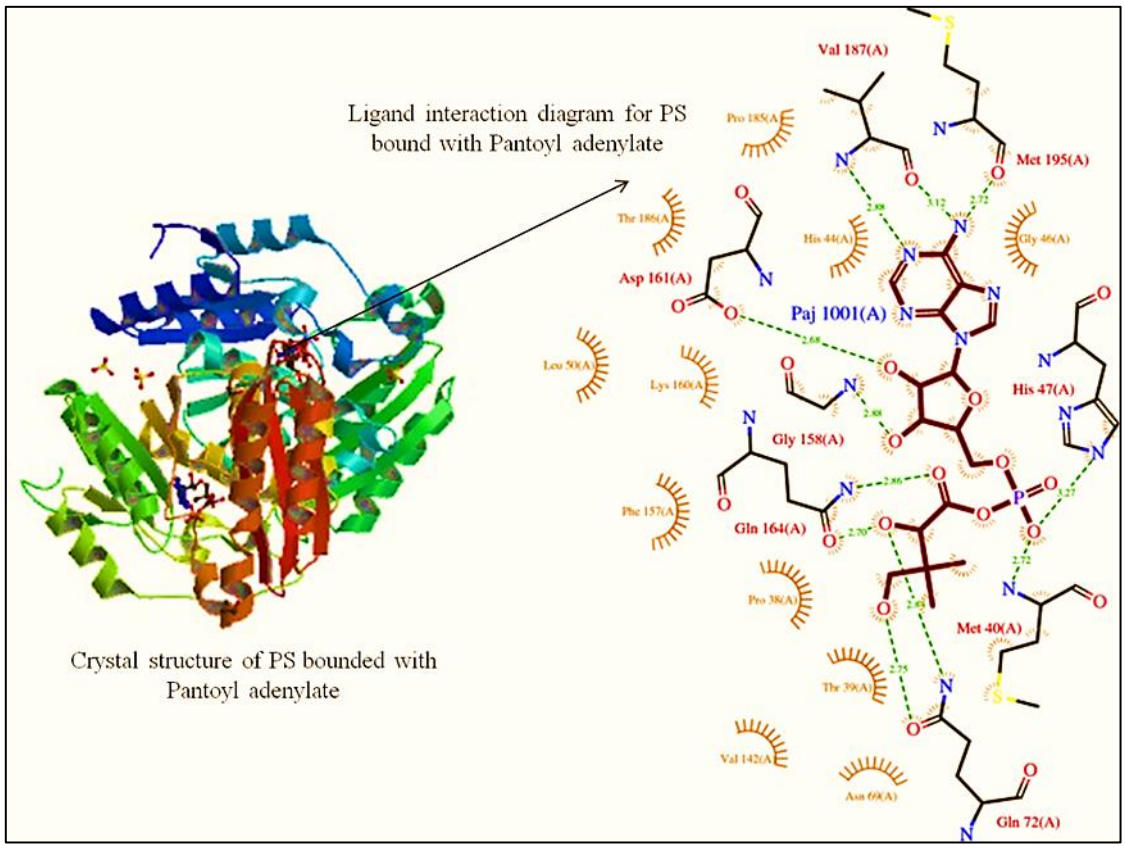

Figure 2.5: Structure of Mtb PS protein and its ligand interaction diagram

2.1.5. Known inhibitors for Mtb PS

Several inhibitors for Mtb PS have been identified with different potency against the enzyme. A high-throughput screening was reported to have identified nafronyl oxalate as an inhibitor of PS with an inhibition constant of 75 μM but there is not satisfactory activity against active Mtb (Figure 2.6D) [White E.L., *et al*., 2007]. Using structure based drug design from fragment screening and substrate and reaction intermediate more potent compounds have been reported [Hung A.W., *et al*., 2009 and Velaparthi S., *et al*., 2008]. The most potent of these displayed nano-molar inhibition towards PS but at the most inhibited bacterial growth

by <50% at 128 μM (Figure 2.6B) [Velaparthi S., *et al*., 2008]. Most recently a combination of high-throughput screening and structure based design yielded an interesting inhibitor of PS whose chemical structure was unrelated to the enzyme substrates. Using enzyme-based assay, actinomycin D (ActD) was identified as inhibitor of Mtb PS [Yang Y., *et al*., 2011]. Molecular docking of ActD cyclopeptide in the active site of Mtb PS was used to identify smaller pharmacophores that might bind in a similar fashion. One compound was identified with activity against active Mtb with an MIC_{99} of 54 μM but did not show satisfactory potency in the biochemical assay (IC_{50}=21.8 μM; Figure 2.6A). Fragment based drug discovery was explored to develop compound (2-(2-(benzofuran-2-ylsulphonylcarbamoyl)-5-methoxy-1H-indol-1-yl) acetic acid) which was bound very efficiently towards the active site cavity and also increased the potency. This compound was found to a competitive inhibitor towards the substrate (K_d =1.8 μM) [Alvin W., *et al*., 2009].

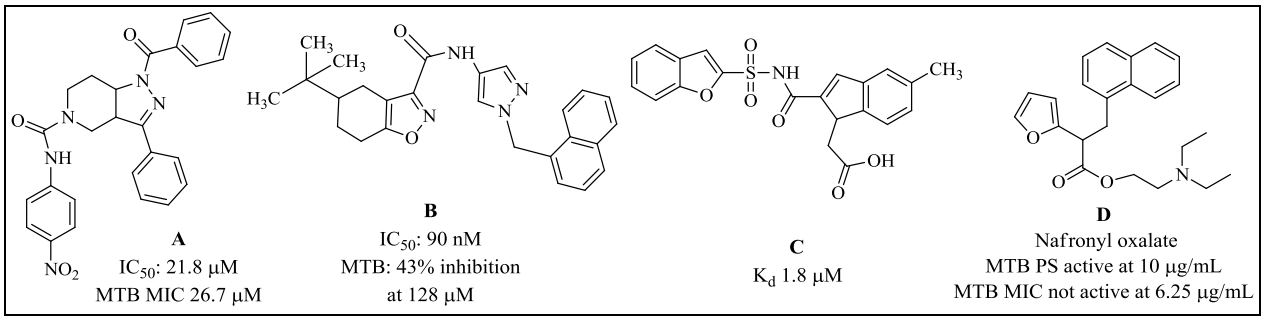

Figure 2.6: Known inhibitors for Mtb PS and their activity data

Compounds with novel chemical structures that could serve as scaffolds for the drug development targeting Mtb PS were identified using screening a large and diverse compound library. Two compounds showed competitive inhibition with respect to pantoate with K_i of 174.1±20.0 nM and 297.1±37.1 nM respectively [Anuradha K., *et al*., 2013]. In order to confirm the growth inhibition against active Mtb, they utilized genetically modified strain of Mtb in which the expression of *PanC* gene is controlled by tetracycline inducible promoter (Abrahams G.L., *et al*., 2012). This promoter replacement strategy was developed to regulate the expression of target genes in Mtb [Ehrt S., *et al*., 2005]. Under these conditions, a panel of known anti-mycobacterial drugs exhibit no shift of MIC implying that the strain was more susceptible to inhibition of unrelated pathway and the inhibitors were specific towards PS. The active two compounds have 4-cyano-1-methyl-3-(4-phenylphenyl)pyrrole-2-carboxylic acid core structure (Figure 2.7).

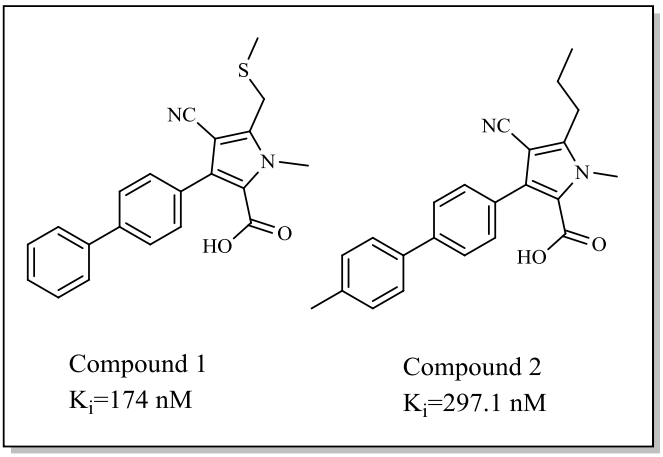

Figure 2.7: The two active molecules proposed by Anuradha K., *et al*., 2013

Novel 3-phenyl-4,5,6,7-tetrahydro-1H-pyrazolo[4,3-c] pyridine derivatives was developed as a novel scaffold for Mtb PS inhibition. Compound 1-nicotinoyl-N,3-diphenyl-6,7-dihydro-1H-pyrazolo[4,3-c]pyridine-5(4H)-carboxamide (Figure 2.8) possess good IC_{50} of 21.8 μM towards Mtb PS and also inhibited the growth of active Mtb with MIC of 26.7 μM. This molecule exhibited no toxicity to mouse macrophage cells (RAW 264.7) till 50 μM [Samala G., *et al*, 2013].

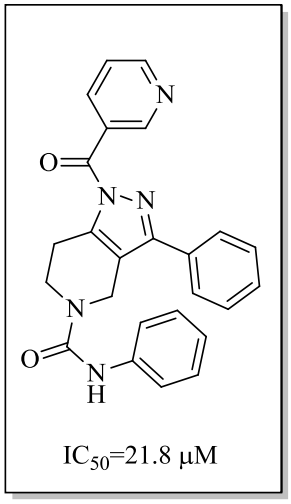

Figure 2.8: Pyridine derivative

Further, the team discovered novel tetrahydrothienol [2,3-c]pyridine-3-carboxamide using molecular hybridization technique [Samala G., *et al*, 2014]. Upon hybridization of reported Mtb PS inhibitor compound (Figure 2.6A) (1-benzoyl-N-(4-nitrophenyl)-3-phenyl-6,7-dihydro-1H-pyrazolo[4,3-c]pyridine-5(4H)-carboxamide) and TAACF inhibitor SID 92097880 (Figure 2.9). Compound 2-((4-nitrophenyl)sulfonyl)-6-(4-nitrothiophene-2-

carboxamido)-2,3,4,5-tetrahydro-1H-cyclopenta[c]pyridine-5-carboxamide showed good MIC in the in-vitro Mtb screening was found to be most potent Mtb PS inhibitor with IC_{50} of 5.77±0.12 µM.

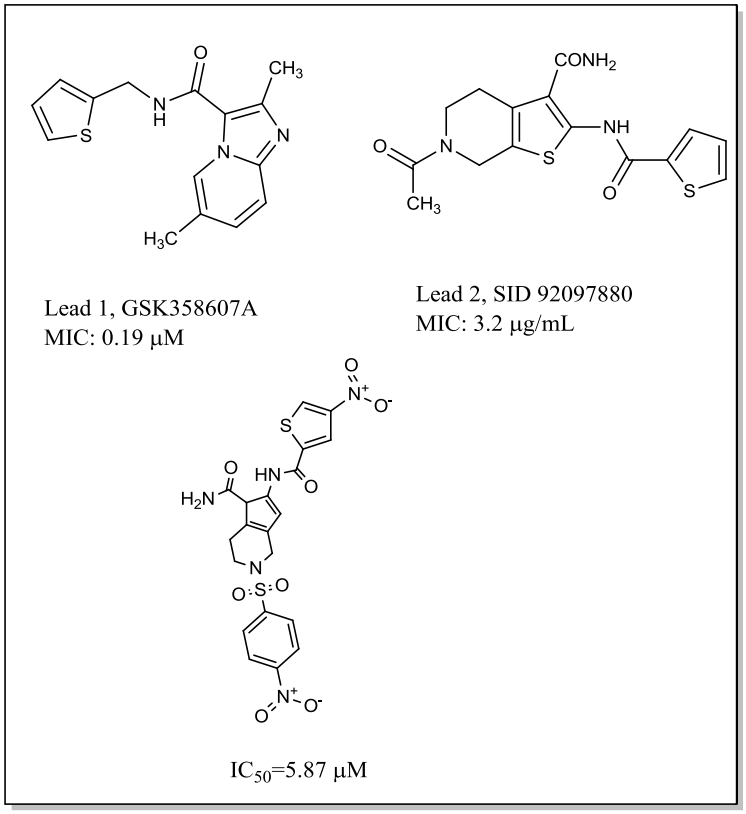

Figure 2.9: Known inhibitors showing potent activity towards Mtb PS

Another series with substituted urea in that substitution with 4-fluorophenyl, chlorophenyl, nitrophenyl and benzyl showed good activity with IC_{50}'s in the range of 6.01 to 13 µM. Due to potency and low cytotoxicity of these active compounds could be valid leads for synthesizing new leads [Ganesh S., *et al*., 2014]. Another series of 2-methylimidazo [1,2-a]pyridine-3-carboxamides derivatives with good activity towards Mtb PS was reported. Compound N'-(1-naphthoyl)-2-methylimidazo [1,2-a]pyridine-3-carbohydrazide emerged as the most active compound with an IC_{50} of 1.90 µM (Figure 2.10). Further to support the activity docking was performed and compound was found with highest docking score of -8.60 kcal mol^{-1} which correlated well with its potency in the enzyme assay [Samala G., *et al*, 2014].

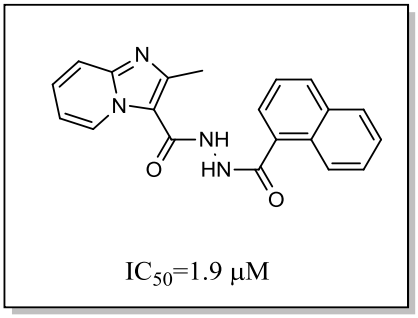

Figure 2.10: Most active imidazo pyridine derivative

2.2. Target II: Mtb LYSINE AMINOTRANSFERASE (LAT)

In Mtb H37Rv, the Rv3290c gene was annotated as putative LAT in gene databases and found to be up-regulated over 40-fold in nutrient starved tuberculosis models. Another study revealed the adaption of the pathogenic bacteria to stationary phase and non-replicating persistence (NRP) showed that LAT was up-regulated. Its regulation level on the other hand decreased long-term latency. These studies, suggested the role of LAT in adaptation of long-term persistence in Mtb [Betts J.C., *et al*., 2002].

Microarray expressions studies were performed to check the expression of genes induction at dormant conditions [Voskuil M.I., *et al*., 2004]. Mtb was found to be induced to enter a state of non-proliferation with two distinct conditions; either entry into stationary phase and oxygen derived non-replicating persistant dormant state [Betts J.C., *et al*., 2002]. In-order to monitor the expression changes in mRNA level, RNA was extracted from typical well aerated Mtb culture grown in 7H9 medium as it progressed from log phase to stationary phase. Still it was unknown at which conditions the stationary phase culture results in cessation of growth. It could be due to, Exhaustion of micronutrients, reduced oxygen availability to the respiring biomass, production of toxic bi-products, growth-limiting quorum-sensing molecules.

There was a dramatic difference between the stationary phase and a NRP expression profile. 102 genes were induced 4-fold or greater in NRP-model compared to only 29 genes during adaptation in stationary phase [Voskuil M.I., *et al*., 2004]. The dormancy genes have specified functions as given in Table 2.1. Induction of these genes may be due to decline in oxygen concentrations in the bacterial culture. During this phase, dormancy regulon was highly induced in NRP model. This dormancy regulon was due to co-regulate cluster of genes under all conditions and was found that LAT gene encoding lysine aminotransferase induced at least 3-fold in both conditions. It was concluded that LAT gene was the most highly-induced gene during nutrition starvation conditions [Voskuil M.I., *et al*., 2003].

Table 2.1: Summary of Sig genes and its regulatory role [Sachdeva P., 2009]

Gene name	Open Reading Frame (ORF)	Proposed regulatory role
SigA	Rv2703	Housekeeping function, Host-pathogen interaction
SigB	Rv2710	Adaptation to cell envelope stress, Hypoxia, Oxidative stress
SigC	Rv2069	Virulence, Immunopathology phenotype
SigD	Rv3414c	Stationary-phase survival, immunopathology phenotype, stringent response, starvation
SigE	Rv1221	Surface stress and heat shock response, immunopathology phenotype, host immune-response modulation, virulence
SigF	Rv3286c	Biosynthesis of mycobacterial cell envelope, immunopathology phenotype
SigG	Rv0182c	SOS response, survival during macrophage infection
SigH	Rv3223c	Oxidative and heat stress, immunopathology phenotype
SigI	Rv1189	Unknown
SigJ	Rv3328c	Oxidative stress
SigK	RV0445c	Unknown
SigL	Rv0735	Virulence
SigM	Rv3911	Long-term in-vivo adaptation

2.2.1. Role of LAT gene in dormant TB

Reports have justified that, LAT gene is a part of *sigG* regulon [Betts J.C., *et al*., 2002]. Based on this interaction from STRING server it implies that there is a functional association that defines as the specific and meaningful interaction between two proteins that can jointly contribute to the same functional process (Figure: 2.11)

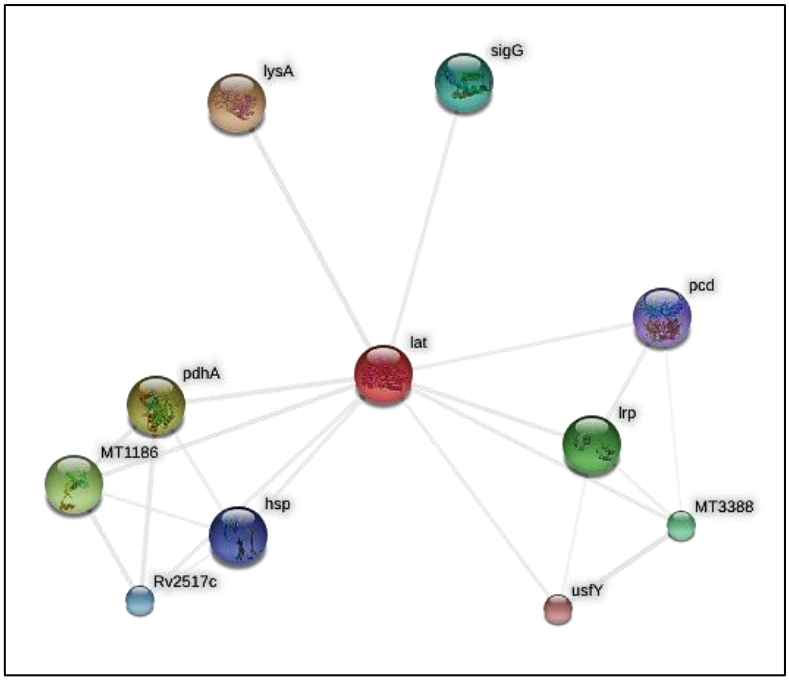

Figure 2.11: LAT protein association network in STRING server (http://string-db.org/)

Mtb has highest alternative sigma factor/ genome size ratio amongst the obligate pathogens suggesting a highly complex regulatory mechanism for its transcription [Manganelli R., *et al*., 2004]. In the course of infection, the bacterial copes with numerous stresses and modulates host responses through coordinated regulation of its gene expression in response to signals encountered in the host body. The sigma factors determine promoter specificity by recognizing and binding to the sequence of the promoter. Mtb has 13 sigma factor genes [Sachdeva P., *et al*., 2009]. *SigA*, the primary or principal σ factor, is indispensable for growth both in Mtb and in *M. smegmatis* [Gomez M., *et al*., 1998]. The Mtb H37Rv sigA transcript is maintained at a constant level under various stress conditions; however, there have been a few reports of its up-regulation during infection in human macrophages and down-regulation during low aeration and stationary-phase growth [Volpe E., *et al*., 2006 and Manganelli R., *et al*., 1999]. During conditions of low aeration and in the stationary phase, the energy available to the bacteria may be quite low and the decreased levels of the *sigA* transcript might reflect a decrease in the mRNA pool relative to the total RNA of the cell. The *sigA* transcript continues to be widely used as an internal standard for normalization in quantitative RT-PCR experiments using Mtb RNA isolated under all conditions. *SigB* the principal factor-like sigma factor of Mtb is very similar to the C-terminal portion of *SigA* [Rodrigue S., *et al*., 2006]. But, unlike *sigA*, it has been found to be dispensable for growth in both *M. smegmatis* [Gomez M., *et al*., 1998] and Mtb. unlike *sigA*, expression of the Mtb

sigB gene increases upon exposure to various environmental stresses such as low aeration, treatment with hydrogen peroxide and heat shock, with a more pronounced effect seen in stationary phase than in logarithmic phase [Hu Y., *et al*., 1999]. *SigC* is conserved across all pathogenic mycobacterial species, including *M. leprae*, and is absent in all non-pathogenic species sequenced to date, such as *M. smegmatis, M. gilvum, M. vanbaalenii, Mycobacterium sp*. MCS [Waagmeester A., *et al*., 2005 and Cole S.T., *et al*., 2001]. It was speculated that Mtb sigC is either translated at a very low efficiency or has a low affinity for RNAP [Manganelli R., *et al*., 1999]. Mtb *sigC* is down-regulated during stationary phase and in response to heat shock and SDS-induced surface stress. *SigD* is expressed at a moderately high and constitutive level during exponential and stationary growth phases and declines significantly, following hypoxia, in a pattern very similar to that of *sigA* in an in vitro culture [Raman S., *et al*., 2004]. Some of the important *sigD*-regulated genes include those encoding proteins involved in lipid metabolism, cell wall-related processes, stress response and DNA binding and repair (Hu Y., *et al*., 2001). *SigE* is one of the two ECF sigma factors encoded by the *M. leprae* genome [Cole S.T., *et al*., 2001]. *SigE* is upregulated in mycobacteria grown within human macrophages compared with those grown in an in-virtually [Graham J.E., *et al*., 1999 and Volpe E., *et al*., 2006]. Its expression also increases following exposure to heat shock, SDS-mediated surface stress, isoniazid and vancomycin [Manganelli R., *et al*., 1999, Pendzich J., *et al*., 2004 and Provvedi R., *et al*., 2009]. Although *sigE* is not essential for growth of *M. smegmatis*, its deletion results in increased susceptibility to oxidative stress and acidic pH [Wu Q.L., *et al*., 1997 and Fernandes N.D., *et al*., 1999]. The expression of Mtb *sigF* is induced under a variety of stress conditions, most notably antibiotic stress (rifampin, ethambutol, streptomycin and cycloserine), nutrient depletion, oxidative stress, cold shock and anaerobic metabolism, particularly in the presence of metronidazole and during stationary-phase growth [Michele T.M., *et al*., 1999]. However, no such marked change in the transcript level of *sigF* was seen in Mtb H37Rv following exposure to cold shock, hypoxia, oxidative stress and entry into stationary phase, suggesting a differential regulation pattern of *sigF* expression in Mtb and *M. bovis* BCG [Manganelli R., *et al*., 1999]. *SigG* is one of the most highly induced genes in Mtb during macrophage infection; [Volpe E., *et al*., 2006 and Cappelli G., *et al*., 2006] and has been shown, in a macrophage infection model, to be required for survival of the bacterium [Lee J.H., *et al*., 2008]. However, its expression is down-regulated upon exposure to various stress conditions, such as mild cold shock, heat shock, low aeration and SDS-mediated surface stress. *SigG* is one of the least represented

mRNAs among all σ factors under normal in vitro growth conditions [Manganelli R., *et al*., 1999].

Similarly, *SigH*, *SigI*, *SigJ*, *SigK*, *SigL*, *SigM* also functions the same alike, the above described sigma factors. But till date *SigI* and *SigK* functions are unknown. Rest all other sigma factors SigH [Fernandes N.D., *et al*., 1999], *SigK*, *SigL* [Hahn M.Y., *et al*., 2005] and *SigM* [Raman S., *et al*., 2006] are involved in oxidation stress and heat shock mechanism in persistent bacteria.

2.2.2. Importance of LAT and its mechanism

Lysine aminotransferase (LAT) is an important enzyme responsible for the conversion of L-lysine to Δ-piperidine-6-carboxylic acid [Miyahara I., *et al*., 1994]. LAT is the member of pyridoxal 5-phosphate (PLP) vitamin B6 dependent aminotransferase family of enzymes [Hayashi H., 1995], which have been divided into several fold types on the basis of structural and evolutionary relatedness. Fold type 1 enzymes are mostly studied and are aspartate aminotransferase (AAT). They are further subdivided into two groups as aspartate aminotransferase belonging to subgroup I [Hayashi H., *et al*., 1995], LAT a member of subgroup II of fold type I aminotransferases that include ornithine aminotransferase (OAT) and γ-aminobutyrate aminotransferase (GABA) [Shen B.W., *et al*., 1998 and Storici P., *et al*., 2004]. It was proposed that the overall reaction of this enzyme family follows Ping-Pong Bi-Bi mechanism [Velick S.F., *et al*., 1962]. This is a special multi-substrate reaction in which two substrates and two products with an enzyme react with one substrate to form a product and modify the enzyme. Later, reacting with the second substrate leads to a final product and regeneration the original enzyme. Mostly complex ping-pong mechanisms exist for the enzymes that have more than two substrates (Figure 2.12).

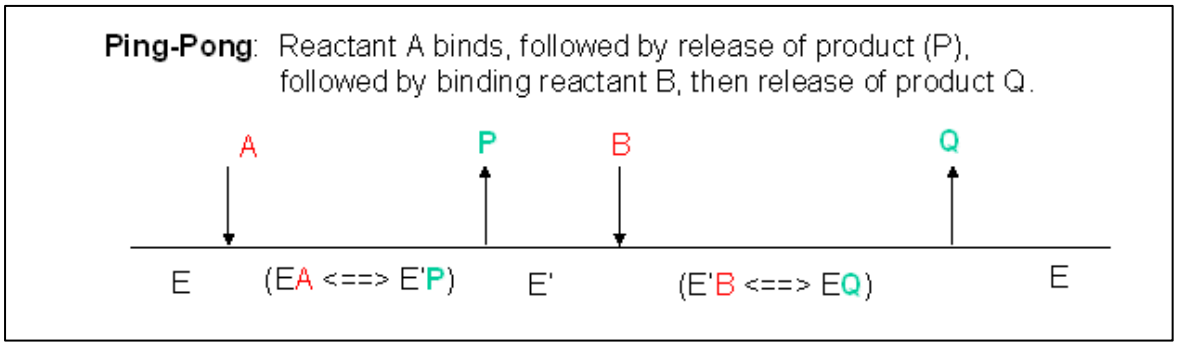

Figure 2.12: General mechanism of Ping-Pong reaction [Velick S.F., *et al*., 1962]

It was demonstrated that LAT enzyme is PLP-dependent and is the member of subgroup II of fold type-I aminotransferases [Mehta P.K., *et al.*, 1993]. The degradation of most of the amino acids will start with the transfer of amino group to α-keto acids. Lysine aminotransferases that belongs to group II aminotransferase family catalyse a reversible transamination reaction between L-lysine and α-keto acid. It was found that the identification and characterization of the product derived from L-lysine was important to obtain information concerning which amino group of L-lysine is transaminated [Tripathi S.M., *et al*., 2006]. Based on these investigations, it has been found that, the terminal amino group of L-lysine was enzymatically transferred to α-ketoglutarate to yield α-aminoadipate-6-semialdehyde which was immediately converted into intramolecularly dehydrated form Δpiperidine-6-carboxylic acid. LAT required PLP as the cofactor for its catalysis of enzyme reaction (Figure: 2.13).

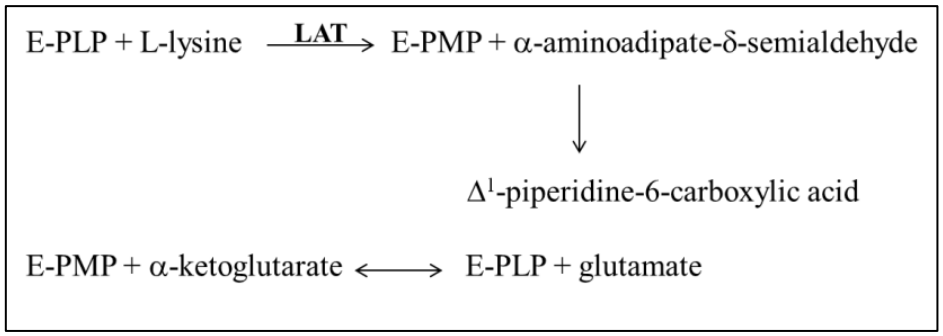

Figure 2.13: LAT enzyme catalysed reaction [Tripathi S.M., *et al.*, 2006]

2.2.3. Binding site analysis of the enzyme LAT

LAT from Mtb subunit consists of 449 amino acid residues with the molecular weight of 50 kDa. It was found that the enzyme was oligomeric and found to be dimer as observed with all members of this family [Tripathi S.M., *et al*., 2006]. In the X-ray structure of LAT enzyme it was found in two forms. Internal aldimine and external aldimine form with L-lysine bound with PLP as a substrate and α-ketoglutarate in its bound form towards LAT. The internal aldimine form of the enzyme exhibited the characteristic Schiff's base linkage with Lys300 in the active site of this enzyme. Residues bound with PLP were Gly128, Ala129, Phe167, His168, Glu238, Asp271, Val273 and Gln274. The two residues Ser329 and Thr330 formed a symmetry-related dimer. N1 of PLP was stabilized by the interaction with the invariant residue Asp 271. The phosphate moiety of PLP anchored the co-factor with hydrogen bond interaction with Thr330, Gly128 and Ala129 and was also involved in water mediated interactions. In the PMP-bound form, there was a change when compared with internal

aldimine structure. Additional interaction of this internal aldimine was compared with the external aldimine which involved interaction with N4 atom of PMP hydrogen bonded with Lys300, Gln243 and a water molecule (Figure 2.14).

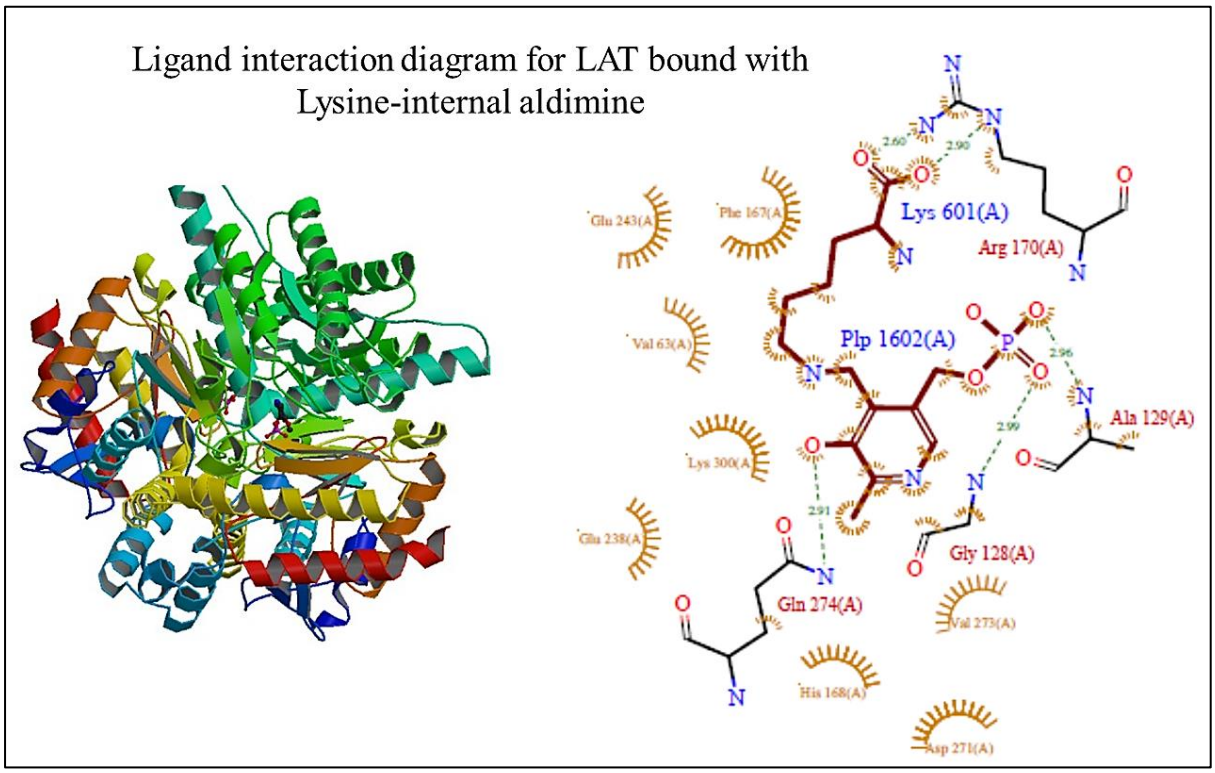

Figure 2.14: Ligand interaction diagram for LAT enzyme bound with lysine and PLP [Tripathi S.M., *et al*., 2006]

The external aldimine form of this enzyme was formed due to presence of excess of substrate. It was expected that the enzyme bound with PMP released the product as an imine form between α-aminoadipate-δ-semialdehyde and PMP [Tripathi S.M., *et al*., 2006]. The carboxylate group of L-lysine was stabilized by bidentate hydrogen bonds with invariant Arg170. The PLP-lysine is naturally stabilized by an internal bond while the non-polar lysine atoms from Cα-Cε extended into the pocket involving Val63, Lys300, Ser329 and Thr 330. Glu243 in this enzyme will shielded the positively charged invariant Arg422 by creating a salt-bridge with the residues. Conceivably Arg422 also prevented the carboxylic group of the substrate L-lysine from interaction inorder to avoid unwanted transamination at the α-amino group which was important for reaction specificity. Also, Cγ-Cδ atoms of this residue showed van der Waals interaction with Cδ and Cε atoms of the substrate. With the breakage of Schiff base, the active site of this enzyme was stabilized by the interaction with Thr330 [Tripathi S.M., *et al*., 2006]. Arg170 was conserved across the large family of PLP-dependent enzymes

whereas; Glu243 was conserved among selected subgroup II enzymes. α-ketoglutarate was bound with the enzyme making interaction of O-1 and O-2 with the invariant Arg422 at one end and O-3 and O-4 to the conserved Arg170 residue at the other end [Tripathi S.M., *et al*., 2006]. Asn328 from the dimeric counterpart was also involved in interaction with O-3 of the substrate α-ketoglutarate and water mediated interactions (Figure 2.15).

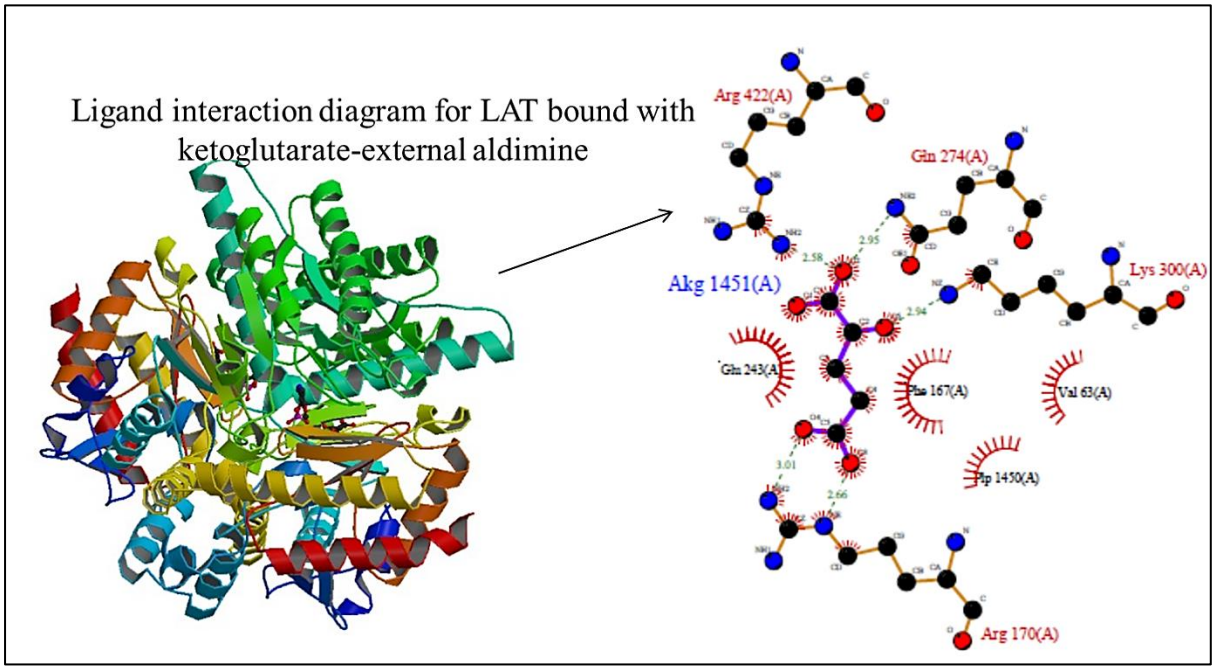

Figure 2.15: Ligand interaction diagram for LAT enzyme bound with α-ketoglutarate [Tripathi S.M., *et al*., 2006]

2.2.4. Inhibitors for LAT

A long-term program for structural elucidation of proteins upregulated during persistent/latent stage of Mtb was initiated earlier inhibitors designed through in-silico approach using Autodock-a three dimensional database search utility to screen in-house database of about 20,000 molecules from the crystal structure available from PDB ID: 2CJH [Voskuil M.I., *et al*., 2004 and Dube D., *et al*., 2008]. Two predicted compounds (Figure 2.16 and 2.17) were identified by in-vitro screening.

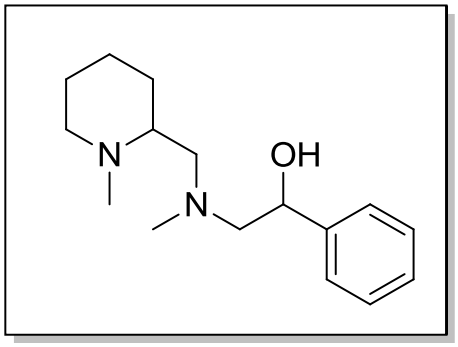

Figure 2.16: Methyl piperidine derivative completely inhibits the enzyme at 400 μM concentration

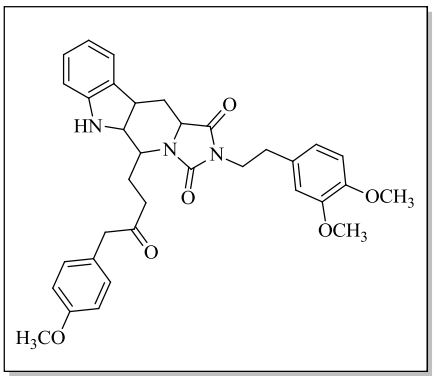

Figure 2.17: 1H-imidazo[1',5':1,6]pyrido[3,4-b]indole derivative inhibits the Mtb LAT enzyme about 60% at 500 μM concentration

There are not much work reported for this target and hence it is considered as an attractive protein to be exploited in this study.

Chapter 3
Objectives and Plan of work

3.1. Objectives

Based on the literature evidences it was clear that TB is a major health problem affecting the global population both in developed and developing countries. In order to accelerate the development of new anti-TB drugs, several strategies have been developed, which could help in shortening the therapy and be effective against both active and latent form of Mtb. The important roles of PS and LAT in Mtb were thoroughly reviewed from various sources. Design of inhibitors for both PS and LAT were considered as prime importance and hence the below mentioned strategy was followed. Clinical studies indicated that a significant number of the strains are resistant to isoniazid, rifampin and pyrazinamide. However, there are still persistent bacterial populations that are not killed by any of the available TB drugs. Therefore, there is a need to design new drugs for actively growing non-persistent bacilli to treat the population at risk of developing active disease through reactivation. As there are only few successful inhibitors available in the market to MDR-TB and XDR-TB, there is an urgency to develop additional therapeutically useful inhibitors. There are limited number of inhibitors against PS and LAT being explored till date and those inhibitors were found to be effective towards TB. Hence for development of novel inhibitors against Mtb targeting PS and LAT, with effectiveness against dormant and active forms of TB was considered important.

The main objectives of the proposed work were:

I. To design Mtb PS and LAT inhibitors by:

- Energy optimised e-pharmacophore modelling
- High throughput virtual screening of commercial database towards the active site of PS and LAT complexes with inhibitor and substrate bound form.

II. In-vitro enzymatic screening of designed molecules for PS and LAT.

III. Development of various analogues of PS and LAT inhibitors based on in-vitro enzymatic screening data.

IV. In-vitro anti-mycobacterial screening for both active and latent forms of Mtb.

V. In-vitro cytotoxicity screening to check the safety profile of the compounds.

VI. Bio-physical characterisation using differential scanning flourimetry to determine the thermal stability of protein and protein-ligand complexes.

3.2. Plan of work

The plan of work has been classified into following categories,

3.2.1. Design of novel inhibitors for Mtb PS and LAT using structure based drug design

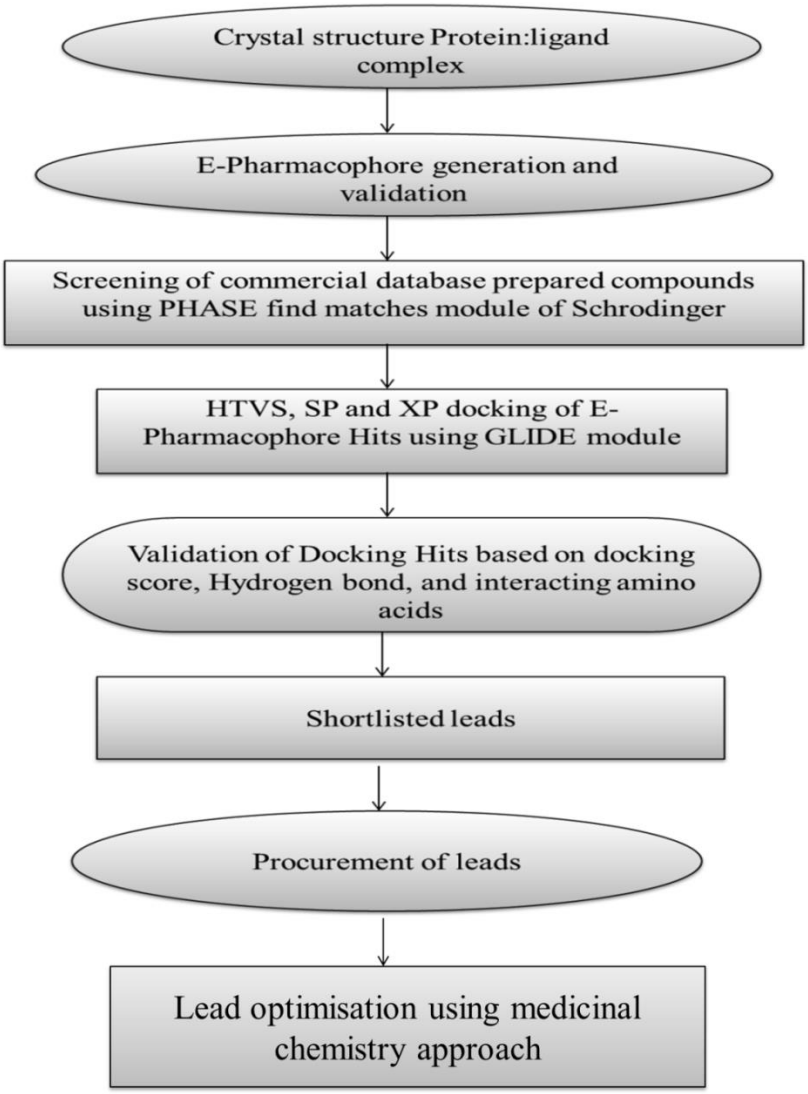

Figure 3.1: Work for drug design and development

3.2.2. In-vitro enzyme inhibition assay

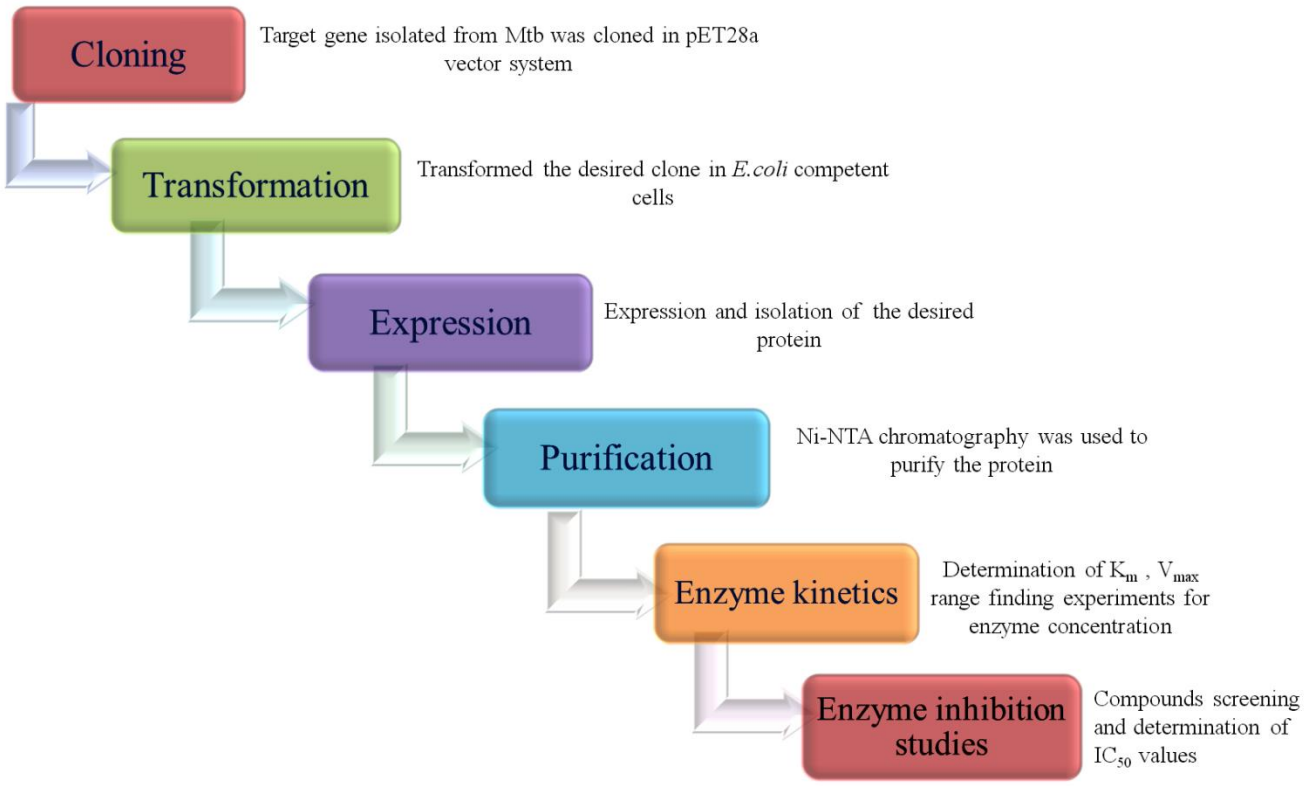

Figure 3.2: Work flow for biological evaluation

3.2.3. Lead modification using synthetic chemistry

The top active molecules were further derivatized using synthetic chemistry utilizing novel/previously reported methodologies as a lead expansion strategy. The synthesis was outsourced to the medicinal chemistry research group at the department of pharmacy.

3.2.4. In-vitro anti-mycobacterial screening

Lead compounds synthesized for Mtb PS and LAT were evaluated for anti-mycobacterial screening using different methods as follows.

I. For Mtb PS

- Using MABA to determine the MIC's.
- Determination of MIC's using reported efflux drugs verapamil and piperine.
- Determination of MIC's in the presence of pantothenic acid in active growing Mtb on the activity of inhibitors.

- Determination of inhibitory effect in dormant bacilli under potassium deficient conditions.

II. For Mtb LAT

- Using MABA to determine the MIC's.
- Determination of inhibitory effect in nutrient starvation model of dormant bacilli

3.2.5. In-vitro toxicity studies

To evaluate the toxicity of the designed and synthesized compounds against RAW 264.7 and HEK 293 cells were utilized and tested at 50 μM concentration using MTT assay to evaluate their toxicity profile.

3.2.6. Biophysical characterization

To evaluate the stabilization of protein-ligand complexes of promising leads, thermal shift assay was performed using differential scanning flourimetry for both Mtb PS and LAT inhibitors.

Chapter 4
Materials and Methods

In search of novel inhibitors for Mtb PS and Mtb LAT for the treatment of TB, we employed computational strategy for screening of large data sets of molecules and evaluated in-vitro for the identification of promising molecules. Virtual screening, a computational method where large libraries of compounds could be assessed for their potential to bind specific sites on target molecules such as proteins, was employed in the study.

We utilized reported crystal structure of the Mtb PS bound to the reaction intermediate complex (PDB ID: 1N2I) and inhibitor complex (PDB ID: 3IVX) as templates for virtual screening of commercial database (Asinex) consisting of 500,000 molecules. Similarly, for Mtb LAT we utilized two approaches with crystal structure of LAT bound with substrate lysine with PLP bound (PDB ID: 2CJD) and α-ketoglutarate with PLP bound (PDB ID: 2CJH) templates for further screening of molecules.

4.1. DESIGN OF NOVEL OF INHIBITORS USING STRUCTURE BASED DRUG DESIGN

4.1.1. Computational Details

All computations were carried out in an Intel Core 2 Duo E7400 2.80 GHz capacity processor with memory of 2GB RAM running with the RHEL 5.2 operating system. PHASE 3.3 implemented with Maestro 9.3 software package (Schrodinger, LLC) was used to generate pharmacophore models. The virtual screening options for HTVS (High Throughput Virtual Screening), SP (Standard Precision) and Glide XP (Extra Precision) docking were all checked to be executed. Glide XP (extra precision) module of Schrodinger 9.3 (Glide, version 5.7, Schrodinger, LLC, New York, NY, 81 2011) was utilised for docking. Bond orders and formal charges were added to the hetero groups and hydrogen atoms were added to all atoms in the system.

4.1.2. Protein preparation

Using protein preparation wizard and impact energy minimization, the protein file was prepared. About 500 cycles of steepest descent (SD) and 5000 cycles of conjugate gradient (CG) methods with optimized potential for liquid simulations (OPLS) 2005 force field using Schrodinger suite version 9.3 were employed. The active site of the protein was located and grid files were generated using receptor grid generation panel. The "Write XP descriptor information" option was selected and "Compute RMSD" option was enabled and rest of the parameters were kept as default. The XP Glide scoring function was used to order the best ranked compounds and the important interactions like π-cation and π-π stacking were analysed using XP visualizer in Glide module. The input RMSD of the crystal ligand was also ascertained.

4.1.3. Development of energy-based pharmacophore models

The hybrid approach of ligand and structure-based technique using docking energy score for finding the bioactive component of ligands against the receptor was employed. Pharmacophore sites were automatically generated with the module PHASE module [Phase, v3.0, Schrodinger, LLC, New York, NY] for the refined crystal ligand [Dixon S.L., *et al*., 2006]. For the generation of energy-based pharmacophore (e-pharmacophore) docking post-processing module of script option was selected and input file was given in .xpdes format [Salam N.K., *et al*., 2009]. A default set of ten chemical features: hydrogen bond acceptor (A), hydrogen bond donor (D), hydrophobic (H), negative ionisable (N), positive ionisable (P) and aromatic ring (R) features were used. Hydrogen bond acceptor sites were represented as vectors along the hydrogen bond axis in accordance with the hybridization of the acceptor atom. Hydrogen bond donors were represented as projected points, located at the corresponding hydrogen bond acceptor positions in the binding site. Projected points allowed the possibility for structurally dissimilar active compounds to form hydrogen bonds to the same location, regardless of their point of origin and directionality. Each pharmacophore feature site was first assigned an energetic value equal to the sum of the Glide XP contributions of the atoms comprising the site, allowing sites. This allowed sites to be quantified and ranked on the basis of these energetic terms [Nagamani S., *et al*., 2012].

4.1.4. Energy based pharmacophore validation

For validating the best of pharmacophore hypotheses, enrichment calculation was performed using a decoy set consisting of 1000 molecules with molecular weight ranging from 400-500

kDa along with known PS inhibitors. As there is no reported inhibitor available till date we didn't perform for LAT. E-Pharmacophore validation was important to check the hypothesis to discriminate the active compounds from the inactive molecules. Enrichment factor (EF), goodness of fit (GH), % actives (%A), and % yield were calculated using the following equations [Sakkiah S., *et al*., 2012].

$$EF=\frac{(H_a \times D)}{(H_t \times A)} \quad (1)$$

$$GH=\left(\left(\frac{H_a}{4H_tA}\right)\times(3A+H_t)\right)\times\left(1-\left(\frac{H_t-H_a}{D-A}\right)\right) \quad (2)$$

$$\%\ Yield=\left[\left(\frac{H_a}{H_t}\right)\times 100\right] \quad (3)$$

$$\%A=\left[\left(\frac{H_a}{A}\right)\times 100\right] \quad (4)$$

Where

'H_t' represented total number of compounds in the hit list

'H_a'represented total number of active molecules in the hit list

'A' represented total number of actives in the decoy set

'D' represented total number of molecules in the decoy set

4.1.5. Preparation of ligands

The commercial database Asinex [ASINEX, ASINEX Platinum Collection, ASINECorp, Winston-Salem, NC, USA. http://www.asinex.com] with 500,000 molecules were processed through redundancy checking and Lipinski filters to select compounds that had better drug property [Knox A.J., *et al*., 2005]. All the structures were prepared using LigPrep (LigPrep v2.2, Schrodinger LLC, New York, NY) along with Epik (Epik v1.6, Schrodinger, LLC, New York, NY) to expand protonation and tautomeric states at 7.0 ± 2.0 pH units. Conformational sampling was also performed for all database molecules using the ConfGen search algorithm. Confgen with OPLS 2005 force field was applied for the generation of conformers with duplicate poses eliminate if the RMSD was less than 2.0 Å. A distance-dependent dielectric

constant of 4 and maximum relative energy difference of 10 kcal mol^{-1} were applied. Using Phase, the database was indexed with automatic creation of pharmacophore sites for each conformer to allow rapid database alignments and screening.

4.1.6. Molecular docking

The best predicted and validated pharmacophore models were utilized to screen against large public compound libraries from Asinex. Virtual screening of the compound library was carried out by using Glide module of Schrodinger, LLC, 2012. Primarily, by using Glide module (Grid based ligand docking with energetics), we examined for favourable interactions between screened ligand hits (from pharmacophore screening) and the protein of interest in the flexible mode docking. The Glide module with three modes of docking, high-throughput virtual screening (HTVS), standard precision (SP), and extra precision (XP) mode were employed sequentially. The XP mode was used for exhaustive sampling and advanced scoring, resulting in even higher enrichment [Friesner R.A., *et al*., 2004 and Kawatkar S., 2009]. Final shortlisting of hit molecules were performed based on visual inspection of important amino acid interactions in the active site cavity, docking scores and the hydrogen bonds involved in binding [Alvarez J., *et al*., 2005]. The selected hits retrieved from the commercial database (Asinex) were purchased for biological evaluations.

4.1.7. ADME prediction

All the selected hit compounds were subjected to in-silico ADME analysis using QikProp module of Schrödinger. Various properties like LogP (octanol water coefficient), % human oral absorption, Lipinski's rule of five, QPlogBB (Predicted brain/blood partition coefficient), QPlogHERG (Predicted IC_{50} values for blockage of HERG K^+ channels), QPPCaco (Predicted apparent Caco-2 cell permeability in nm/s) were predicted for the compounds and were checked for any violations.

4.2. Synthesis and characterization

Synthesis of promising leads (PS and LAT) and their analogues were performed by our medicinal chemistry research group at the Department of Pharmacy. Hit expansion of the lead identified was achieved using the following synthetic protocols (Figure 4.1-Figure 4.4).

4.2.1. Synthesis of Mtb PS leads using reaction intermediate based approach-rhodanine-3-propane hydrazide derivatives

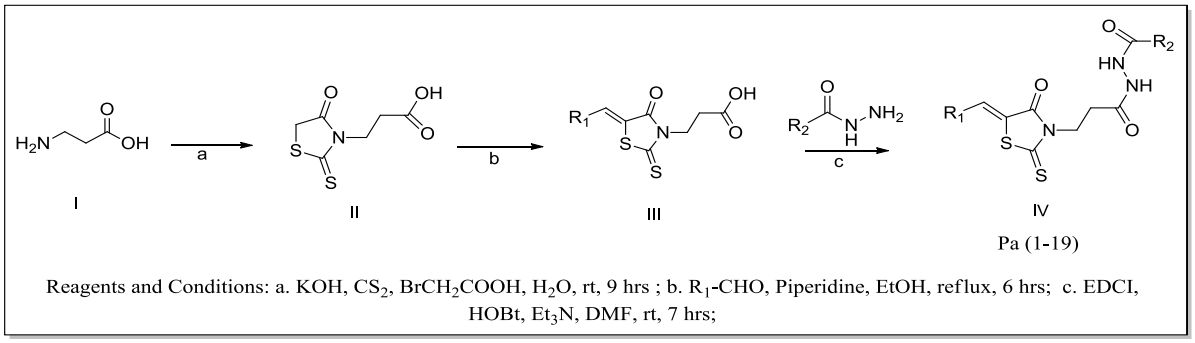

Figure 4.1: Synthetic scheme utilized for Mtb PS leads-reaction intermediate based approach

4.2.2. Synthesis of Mtb PS leads using inhibitor based approach-tryptophan derivatives

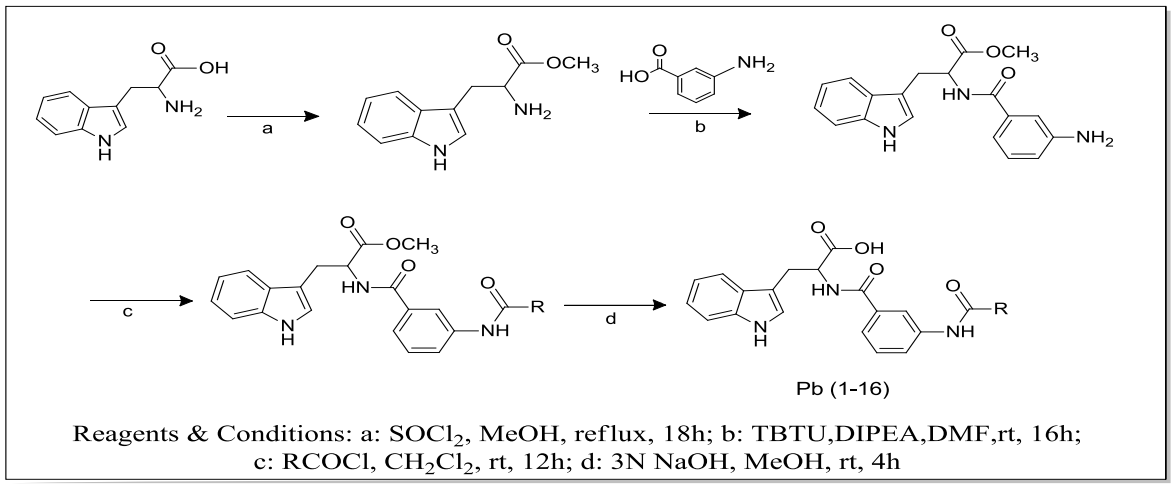

Figure 4.2: Scheme utilized for developing Mtb PS leads-inhibitor based approach

4.2.3. Synthesis of Mtb LAT leads using substrate lysine based approach-glutarohydrazide derivatives

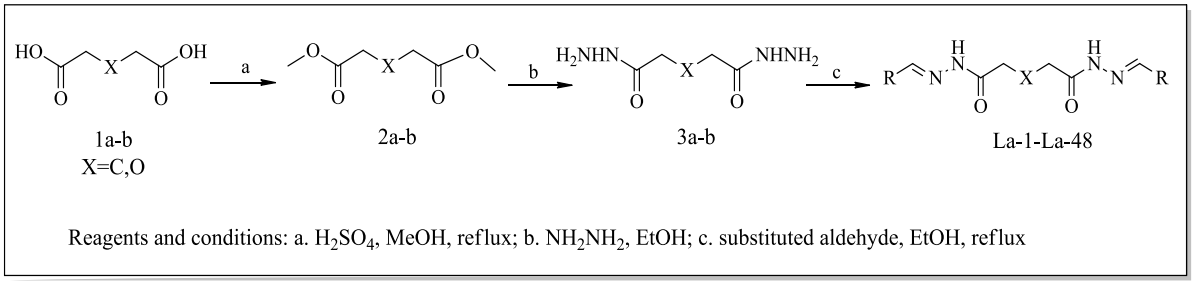

Figure 4.3: Scheme utilized for developing Mtb LAT leads-lysine based approach

4.2.4. Synthesis of Mtb LAT leads using substrate α-ketoglutarate based approach-thiazole derivatives

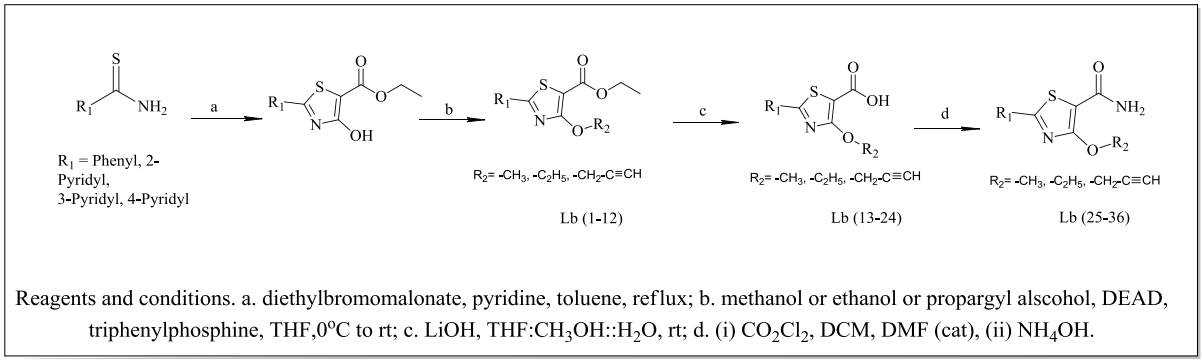

Reagents and conditions. a. diethylbromomalonate, pyridine, toluene, reflux; b. methanol or ethanol or propargyl alscohol, DEAD, triphenylphosphine, THF,0^{o}C to rt; c. LiOH, THF:CH_3OH::H_2O, rt; d. (i) CO_2Cl_2, DCM, DMF (cat), (ii) NH_4OH.

Figure 4.4: Scheme utilized for developing Mtb LAT leads-α-ketoglutarate based approach

All commercially available chemicals and solvents were used without further purification. TLC experiments were performed on aluminimum-backed silica gel 40 F254 plates (Merck, Darmstadt, Germany). The homogeneity of the compounds was monitored by thin layer chromatography (TLC) on silica gel 40 F254 coated on aluminum plates, visualized by UV light and KMnO4 treatment. Purifications were done on Biotage Isolera purification system on silica gel (MPLC grade) by using either hexane:ethylactetae or dichloromethane:methanol as eluent. All ^{1}H and ^{13}C NMR spectra were recorded on a Bruker AM-300 (300.12 MHz, 75.12 MHz) NMR spectrometer, (BrukerBioSpin Corp, Germany). Chemical shifts are reported in ppm (δ) with reference to the internal standard TMS. The signals are designated as follows: s, singlet; d, doublet; dd, doublet of doublets; t, triplet; m, multiplet. Molecular weights of the synthesized compounds were checked by SHIMADZU LCMS-2020 series in ESI mode. Elemental analyses were carried out on elementar vario MICRO CUBE, CHN Analyser. All commercially available chemicals and solvents were used without further purification.

4.3. Biological assessments

All the designed leads and synthesized analogues were evaluated for in-vitro biological assessments Mtb PS enzymatic assay and LAT enzymatic assays, MIC against both active and dormant Mtb, and cytotoxicity studies in eukaryotic cell lines.

4.3.1. Mtb PS inhibitory assay

4.3.1.1. Expression and purification of Mtb PS

The expression and purification of Mtb PS was performed based on the earlier reported literature [Wang S., *et al*., 2003]. The Mtb *panC* gene (Rv3602c) encoding the PS was cloned

and transformed into BL21 (DE3) cells. Transformants were grown in LB broth at 37ºC with constant aeration, in the presence of 50 µg/ml kanamycin. Exponentially growing cultures (A600 of ~0.6) were induced with 0.8 mM IPTG (Isopropyl β-D-1-thiogalactopyranoside) and further grown for 12-16 h at 24ºC. Cells were harvested and lysed by sonication in lysis buffer containing 20 mM HEPES (pH 7.8), 500 mM NaCl, and 0.5 mM PMSF (Phenyl methane sulfonyl fluoride). The cell lysate containing His 6-fusion proteins were equilibrated with Ni-NTA affinity resins and the tagged proteins were eluted with buffer containing 250 mM imidazole. The fractions containing PS protein were pooled and the presence of PS protein was confirmed using sodium dodecyl sulphate polyacrylamide gel electrophoresis (SDS-PAGE). Further the pooled protein samples were used for enzymatic assay.

4.3.1.2. In-vitro PS screening

The Mtb PS enzymatic studies were performed as per the earlier reported literature [Eisenberg L., *et al*., 2006]. To each well of a 96-well plate, 60 µl of PS reaction mixture consisting of 0.4 mM NADH, 5 mM pantoic acid, 10 mM $MgCl_2$, 5mM β-alanine, 10 mM ATP, 1 mM potassium phosphoenol pyruvate, and 20 µl of enzyme mixture consists of 18 units/ml each of chicken muscle myokinase, rabbit muscle pyruvate kinase, and rabbit muscle lactate dehydrogenase diluted in 100 mM HEPES buffer were added. The reaction mixture and enzyme mixture were added to the plate to a final volume of 100 µl with 100 mM HEPES buffer (pH 7.8). Concentration of enzyme was determined based on the range finding experiments by varying the concentration of enzymes. Compounds were then added to the plates and the reaction was initiated with the addition of 10 µL of 4.32 pM of Mtb PS, diluted in buffer. The test plate was immediately transferred to a microplate reader and the depletion of NADH was measured at 340 nm. The reaction components except Mtb PS were mixed in the well and the background reaction was measured; Mtb PS was then added and the reaction kinetics was monitored [White E. L., *et al*., 2006]. Reactions were carried out at 37°C in a heat-controlled PerkinElmer Victor X3 spectrophotometer. % Inhibitions were calculated using following formula

$$\% \text{ Remnant activity} = 100 \times \left[\frac{\text{Control absorbance - Inhibitor absorbance}}{\text{Control absorbance}}\right] \quad (5)$$

$$\% \text{ Inhibition} = 100 - \% \text{ Remnant activity} \quad (6)$$

Inorder to confirm the specific inhibition of Mtb PS, coupled enzyme assay has been performed as described above except the final concentration of lactate dehydrogenase was

kept to 0.2 units/ml and no substrate (pantoate) was added. The assay has initiated with 6.5 mM of AMP instead of Mtb PS.

4.3.2. Mtb LAT inhibitory activity

4.3.2.1. Cloning and purification of Mtb LAT

Cloning to obtain the target protein Mtb LAT was performed as per the earlier reported procedure [Tripathi S.M., *et al*., 2006]. Lysine-epsilon aminotransferase was PCR amplified using specific forward primer (5'CCCAAGCTTATGGCCGCCGTCGTGAAGTCCGTC3') and reverse primer (5'ATGCAAGCTTACGTCACCACCGGTAACGCGCT3') from Mtb genomic DNA. Pfu polymerase was used with 65°C of primer annealing temperature. PCR products were digested with HindIII and cloned into HindIII site of pET28b vector. Sequence confirmed clones were further transformed into C41 (DE3) cells (Lucigen) for expression studies. Further the transformed colonies were expressed and induced with 0.2 mM IPTG grown in YT media (Yeast extract and Tryptone broth) for 12-16 hrs at 20°C. Induced cells were then harvested and lysed by sonication in lysis buffer (50 mM Tris pH-7.2, 300 mM NaCl and 10 mM imidazole) and subsequently centrifugation was done at 10,000 rpm at 4°C for 45 min for clear extract. Later, the cell extracts were loaded into column (Bio-Rad) and equilibrated with Ni-NTA beads at 4°C for 3 hrs. The cell extracts were washed with wash buffer and subsequently the desired protein of interest was eluted with elution buffer containing different concentrations of imidazole from 100 mM to 500 mM. Eluted samples containing the desired protein was identified by SDS PAGE.

4.3.2.2. Mtb LAT enzymatic assay and its kinetics studies

Mtb LAT enzymatic assay was performed in 100 µl volume containing 200 mM phosphate buffer (pH 7.2), 1.5 mM L-Lysine, 1.5 mM α-ketoglutarate, 15 µM pyridoxal 5-phosphate with various concentration of Mtb LAT for 1 hrs at 37°C. Reactions were terminated by adding 10% trichloroacetic acid in ethanol. The Mtb LAT activity was monitored and the end product was detected at an absorbance of 465 nm and 280 nm. To determine the kinetic parameter K_m and V_{max}, either L-lysine or α-ketoglutarate was varied keeping the other substrate constant at 1 mM. Concentration of LAT enzyme was determined based on the range finding experiments. The reactions were performed same as enzymatic assay described and the K_m and V_{max} were obtained using non-linear regression analysis using GraphPad prism software [Jaqtap P.K., *et al*., 2012].

4.3.2.3. In-vitro Mtb LAT enzyme inhibition study

The enzymatic studies were performed similar to the reported literature [Tripathi S.M., *et al*., 2006]. To each well of a 96-well plate, a desired substrate and enzyme concentration as described above was taken. The designed and synthesized compounds were added to the plates in different concentrations from 50 μM to 1 μM. The reaction components except Mtb LAT were mixed in the well and the background reaction was measured. Mtb LAT was then added and the reaction kinetics was monitored. Reactions were carried out at 37°C in a heat-controlled PerkinElmer Victor X3 spectrophotometer. Further the IC_{50} values were calculated using GraphPad Prism analysis software.

4.3.3. In-vitro anti-mycobacterial screening

4.3.3.1. Anti-mycobacterial screening of active Mtb using MABA method

The in-vitro anti-mycobacterial screening against Mtb H37Rv was carried out using MABA method as reported earlier [Leonard B., *et al*., 2008]. The inoculum was prepared and re-suspended in 7H9 medium (7H9 broth, 0.1% casitone, 0.5% glycerol), supplemented 10% with oleic acid, albumin, dextrose, and catalase (OADC), and diluted to 1:20 and 100 µl was used as inoculum. The drug concentration was diluted in 7H9 media and it serially diluted. Growth control without antibiotic and sterile control were also kept in 96 well microtiter plates. Isoniazid and ethambutol were used as positive controls and sterile water was added to all surface wells in order to avoid evaporation during incubation. The plate was incubated for 7 days at 37^{o}C in normal atmosphere. After incubation, 1:1 of alamar blue and 10% tween solution were added to each well, and the plate was re-incubated for 3-4 h. A change in colour from blue (oxidised state) to pink (reduced) indicated the growth of bacteria, and the MIC was defined as the lowest concentration of drug that prevented this change in colour.

4.3.3.2. Efflux studies for Mtb PS leads

As a hypothesis, we tested all the compounds for their MIC's as mentioned in the above method in the presence of reported efflux pump inhibitors verapamil (50 µg/ml) and piperine (8 µg/ml).

4.3.3.3. Effect of Pantothenic acid for Mtb PS leads

For the few promising top lead compounds, we tested Mtb MIC's in the presence of 1% and 5% pantothenic acid. The procedure followed as similar to that mentioned in 4.3.3.1.

4.3.3.4. Dormant model for Mtb screening of Mtb PS leads-potassium deficient condition

This assay was performed at the Institution of the Russian Academy of Sciences, Moscow (Russia). The most promising compounds were examined for their activity against dormant 'non-culturable' Mtb bacilli at 20 and 100 µM. Mtb strain H37Rv was grown from frozen stocks for 10 to 12 days in Sauton medium contained 0.5 g KH_2PO_4, 1.4 g MgSO4·$7H_2O$, 4 g L-asparagine, 60 ml glycerol, 0.05 g ferric ammonium citrate, 2 g sodium citrate, 0.1 ml 1% ZnSO4·$7H_2O$, water to l liter, pH 7.0 (adjusted with 1M NaOH) and supplemented with ADC (Albumin, Glucose, and NaCl) and 0.05% tween 80 (37°C; 200 rpm). To obtain non-culturable (dormant) cells, a culture grown in Sauton medium to an optical density at 600 nm (OD_{600}) of 5 served as an inoculum that was added to potassium-deficient Sauton medium supplemented with ADC and 0.05% tween 80 (37°C; 200 rpm) at a concentration of $5*10^5$ cells per ml. Potassium-deficient Sauton medium contained 8.9 g $Na_2HPO_4·12H_2O$, 1.4 g $MgSO_4·7H_2O$, 4 g L-asparagine; 60 ml glycerol, 0.05 g ferric ammonium citrate, 2 g sodium citrate, 0.1 ml 1% $ZnSO_4·7H_2O$, and water to l liter, pH 7.0 (adjusted with 1M NaOH). The resuscitation procedure was performed in diluted liquid Sauton medium (1:1 [vol/vol]; final concentration of glycerol, 0.6%) supplemented with ADC. Non-culturable cells obtained in potassium-deficient Sauton medium were harvested, washed twice with fresh medium, resuspended in ADC-supplemented diluted Sauton medium, and left standing at 37°C. The 'non-culturable' cells obtained with low metabolic activity were characterized by marked phenotypic resistance to both isoniazid and rifampicin and were unable to form colonies onto agar solidified Sauton's medium but could be reactivated in liquid medium after special procedures of resuscitation described above. Thus these cells met the key criteria of dormancy and were applied as a relevant tool for finding drugs for latent TB. For estimation of inhibitory effect of test compounds, the concentration of both treated and untreated 'non-culturable' cells recovered from dormancy were estimated by MPN assay with the use of statistical approaches [Salina E., *et al*., 2014].

4.3.3.5. Dormant model Mtb screening for LAT compounds-nutrient starved condition

Owing to its simplicity, reproducibility and ease of handling, we employed this model for testing our novel potent LAT inhibitors aimed at persistent bacteria. In this model, cultures of in-vitro grown Mtb bacteria were subjected to nutrient depletion by growing the culture in PBS (Phosphate buffer saline) for 6 weeks. Nutrient starvation using this method triggered dormancy response in the bacilli that was termed as non-replicating persistence (NRP), a

physiological state thought to mimic the one exhibited by Mtb during various stages of persistent infection. After 6 weeks, the culture was treated with the test compounds and standard drugs at a concentration of 10 µg/ml in a tube and incubated at 37°C for 7 days. The treated cell suspensions were diluted 10-fold up to 10^{-6} using Middlebrook 7H9 medium supplemented with OADC and were plated in 48 well plates in triplicates. The plates were incubated at 37°C for 4 weeks and the wells with visible bacterial growth were counted as positive and MPN values were calculated using standard statistical methods.

4.3.4. In-vitro cytotoxicity studies

The synthesized compounds were evaluated for cytotoxicity studies as per the earlier reported literatures [Gerlier D., *et al*., 1986 and Scudiero D.A., *et al*., 1988]. The RAW 264.7/HEK 293 cells were grown in RPMI medium supplemented with 10% fetal bovine serum (FBS), 10,000 units penicillin and 10 mg streptomycin per ml in T25 flasks to attain 80-90% confluency. Cells were scraped and seeded into wells *i.e*. 5,000 cells per well in poly-L-lysine coated plates. The microtiter plates were incubated at 37^{o} C, 5% CO_2, 95% air and 100% relative humidity for 24 hrs prior to addition of experimental drugs. The test compounds at 100 µM concentration were then added to cells and incubated at 37°C for 72 hrs. After 72 hrs of exposure, viability was assessed on the basis of cellular conversion of MTT into a formazan product using the Promega Cell Titer 96 non-radioactive cell proliferation assay. 10 µL of 10 mg/ml concentration of MTT was added and incubated for 3 hrs at 37^{o}C. At the end of incubation formazon crystals were formed and the media from microtiter plates were removed. Later, the bound crystals were subsequently dissolved by adding 100 µL DMSO. Absorbance was then read on plate reader at a wavelength of 595 nm. Relative to the control wells the percent growth was calculated for each well. The percentage of cells killed was calculated from the formula,

$$\% \text{ of cells killed} = 100 \left[\frac{\text{Mean OD sample}}{\text{Mean OD day 0}}\right] \quad (7)$$

4.4 Bio-physical characterization

The transition from native form to denatured form was measured as a function of increase in temperature using the fluorescence of an environmentally-sensitive dye called sypro orange. The DSF study was performed as per the standard protocols [Niesen F.H., *et al*., 2007 and Brvar M., *et al*., 2012]. The real time PCR instrument (Bio-Rad iCycler5) was programmed to equilibrate the samples at 25°C for 3 min and increased temperature upto 95°C, taking fluorescence reading at every 0.1°C rise using a LED/Photodiode set matched to the dye

excitation and emission wavelengths. The melting points of the protein and protein with ligand were obtained as the lowest point of first derivative plot and calculated by the software included with the instrument. Optimum concentration of Mtb PS/LAT and dye was determined by varying different concentrations of protein and dye in analysis buffer. Also the top active compounds were selected and diluted in <10% DMSO. In a 96-well PCR plate, 20 µl of reaction was carried by combining 10 µl of protein solution (75-90 µg/ml) in analysis buffer, 2 µl of 5X dye (diluted from 5000X stock with the sub stock of 50X) and 1.6 µl of ligand solution diluted from its subsequent stock solutions.

Chapter 5

Results and Discussion for Development of Mycobacterial Pantothenate Synthetase Inhibitors

Pantothenate synthetase (PS), the protein responsible for mycolic acid synthesis is important in the production of acetyl coA and coenzyme A synthesis; a peculiar step in fatty acid synthesis for the cell wall in Mtb. Developing novel inhibitors by targeting pantothenate synthetase of Mtb offers an excellent opportunity to address resistance towards the drugs developed so far. The major aim of this study was to explore, novel drug molecules with Mtb PS as a template for targeting Mtb infection. A very useful model for achieving this aim could be structure-based design. It was prerequisite to have accurate starting structures and also to enhance the chances of retrieving similarly active and diverse hits from database screening.

In the present study, we employed two attempts to develop novel diverse inhibitors of Mtb PS as exemplified below.

Design I: Structure-based lead identification of PS inhibitors based on reaction intermediate bound to PS protein

Design II: Structure-based lead identification of PS inhibitors based on inhibitor bound to PS protein.

5.1. DESIGN I: Mtb PS INHIBITORS BASED ON REACTION INTERMEDIATE

There were many crystal structures published in the protein data bank (www.rcsb.org/pdb) on PS in complexes with AMPCPP, pantoate, AMP, ATP, various ligands and fragments developed by fragment-based design with resolutions ranging from 1.6 to 2.33 Å [Wang S., *et al*., 2002 and Hung A.W., *et al*., 2009]. As we attempted to employ a new drug design strategy for PS based on structure-based e-pharmacophore modelling which was not explored for this target, we started with the reaction intermediate pantoyl adenylate bound with protein being crucial in the identification of novel lead molecules. In the present study, we utilized the crystal structure of Mtb PS in complex with a reaction intermediate, pantoyl adenylate (PDB ID: 1N2I) with 1.7 Å resolution [Zheng R., *et al*., 2001] (Figure 5.1).

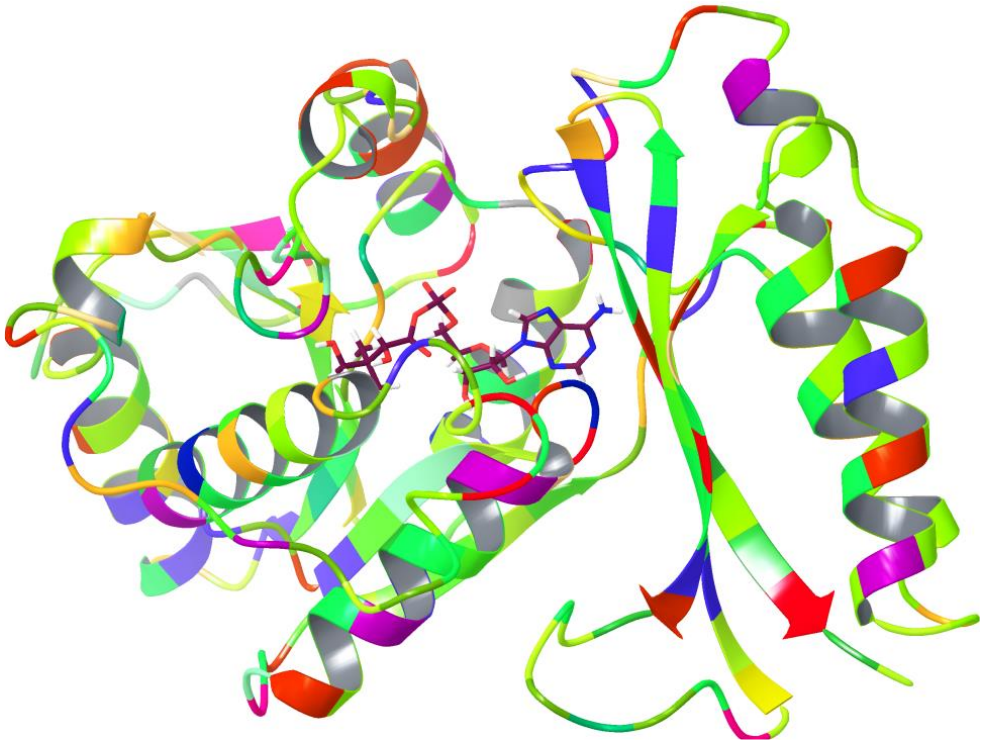

Figure 5.1: Crystal structure of Mtb PS bound with reaction intermediate (1N2I)

5.1.1. Protein preparation and active site cavity validation of the protein PS

The retrieved protein was prepared and hydrogen atoms, water molecules were removed and prepared as described in materials and methods section 4.1.2. The crystal ligand pantoyl adenylate was found to show hydrogen bonding interactions with Val187, Met195, Gln164, Met40, His47, Gly158, Gln72 and Asp161 amino acid residues. In order to validate the docking program utilized for e-pharmacophore generation, the crystal ligand was prepared and redocked on to the grid of the active site. The docking score was found to be -9.649 kcal mol^{-1}. The diagrammatic representation of reference ligand is shown in Figure 5.2. The active site of the protein was located and grid files were generated using receptor grid generation panel. Grid size was found to be 10 Å and is used for all docking analysis.

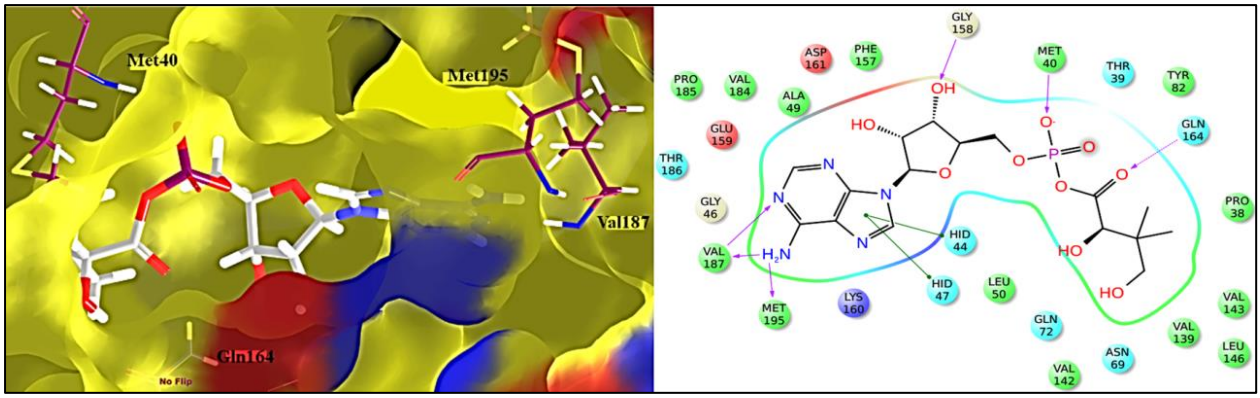

Figure 5.2: Binding analysis and ligand interaction for the reference ligand

Redocking results showed that the compound exhibited similar interactions as that of the original crystal structure which was further confirmed with RMSD of 0.312 Å. The superimposition of docked pose and original crystal ligand pose of pantoyl adenylate is presented in Figure 5.3.

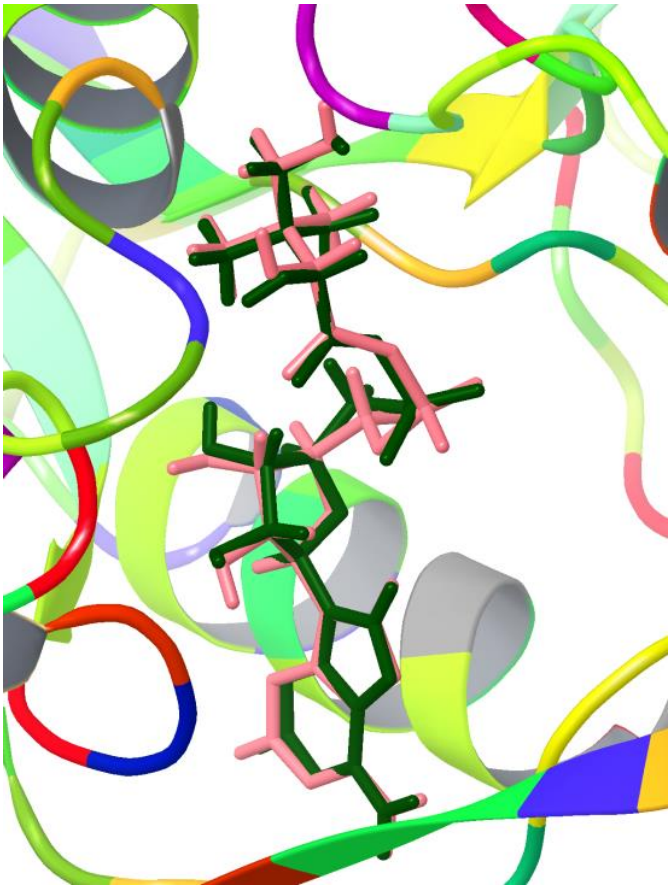

Figure 5.3: Superimposition of docked pose of pantoyl adenylate and original pose of pantoyl adenylate; where pink color indicates the original ligand and the green color represents docked ligand

5.1.2. E-pharmacophore generation

E-pharmacophore hypotheses were developed by mapping the XP energetic terms into pharmacophoric sites which formed the basis of structural and energy information between protein and ligand. Initially, the number of pharmacophore sites was set to ten as default in the program. The generated e-pharmacophore with 10 features was found with 5 acceptors (A), 4 donors (D) and 1 negative ionisable (N) group. Surprisingly the hydrophobic interactions were not mapped as pharmacophore may be due to comparatively high energy. However, hydrophobic interactions were also considered important in further processing of database hits. As this ligand yielded maximum pharmacophore sites which would be difficult to identify best fitting ligand matching all these pharmacophore. Hence based on the energy score and distance we created different hypothesis with the combination of 6 features, 5 features and 4 feature models.

5.1.3. E-pharmacophore validation

The best five hypotheses were taken and validation was performed using decoy set containing 1000 inactives along with 28 Mtb PS active inhibitors (http://www.brenda-enzymes.info). The five best hypotheses were subjected for validation using decoy set containing 1000 inactive along with 28 Mtb PS active inhibitors (http://www.brenda-enzymes.info/). Ligand decoy sets were available for download as provided by Schrodinger (http://www.schrodinger.com/glide_decoy_set). Enrichment factor (EF) was employed for the fraction of known actives recovered when a fraction of database was screened. EF is defined as the ratio of number of actives retrieved relative to the number of database molecules tested. EF is mainly gives the percentage of the database screened. The five hypotheses thus generated validated using decoy set containing 1000 inactive along with 28 reported Mtb PS inhibitors [Samala G., *et al*., 2013, Alvin W., *et al*., 2009, Yang Y., *et al*., 2011, White E L., *et al*., 2007 and Velaparthi S., *et al*., 2008].

Ligand decoy sets were available for download as provided by Schrodinger (http://www.schrodinger.com/glide_decoy_set). The enrichment results for all the 6 pharmacophoric hypotheses were compared based on the enrichment factor, % Yield, GH and % of active based on recovery rate of actives against the ranked decoy database. This helped not only to eliminate the pharmacophore sites which lacked significant interactions but also prioritized the sites for further screening of molecules. By this methodology, we obtained both good enrichment as well as diversity in our hits. The energy contribution between the

ligand and every amino acid in the binding site always were key things in ligand-receptor complex. The enrichment factor reflected the capability of a screening application to detect active ligands (true positives) compared to the random selection of molecules. Thus, its value was expected to be greater than 1 and higher that it, the better the enrichment performance of the virtual screening [Dror O., *et al*., 2009]. Hypothesis **1**, a six point model with 3 acceptors and 3 donors (A2A6A11D16D17) has displayed good enrichment factor, % yield, and goodness of hit and % actives. Whereas, Hypothesis **2** and Hypothesis **5** also exhibited higher % actives in an acceptable range, but considering other parameters like, enrichment factor, goodness of hit and yield, the other hypothesis didn't satisfy the scores corresponding to a true pharmacophore model and hence were not considered.

Table 5.1: E-pharmacophore hypotheses and its validation

Hypothesis	E-pharmacophore features	Number of actives retrieved	EF	GH	% Yield	%A
1	6 Features(A2A6A9A11D16D17)	17	4.05	0.2	11.33	60
2	5 Features(A2A6D15D18N21)	16	1.43	0.09	4	57
3	5 Features(A2A9D15D16N21)	10	0.55	0.03	1.54	35.71
4	4 Features(A2D14A11D17)	11	0.72	0.05	2.01	39.29
5	4 Features(A2A6D16D17)	18	1.05	0.05	2.94	64.29

EF: enrichment factor; GH: goodness of hit; %A: actives

Finally, the six point e-pharmacophore hypothesis as shown in Figure 5.4 was utilized for the virtual screening of commercial database (Asinex).

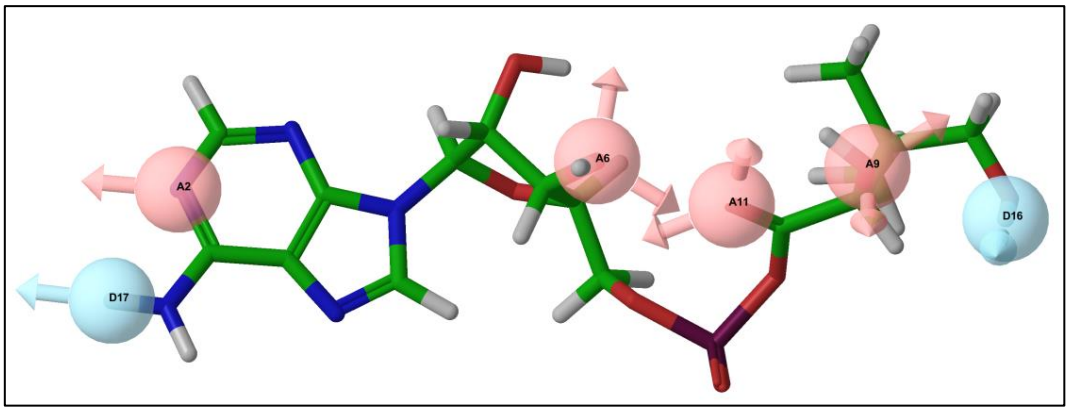

Figure 5.4: Energy based pharmacophore generation for virtual screening of compounds

5.1.4. Virtual screening and docking

Virtual screening of commercial database was performed as high-throughput screening of large database for lead identification. In this study, the six point pharmacophoric model was used as a query to screen commercial database of 500,000 molecules (Asinex). Using PHASE module 40,258 molecules with fitness value above 1.5 were carried forward to HTVS. These ligands were docked into the PS active site using the default grid and finally selected 12,938 molecules as hits from HTVS with the criteria of docking score of ≤ -6.0 kcal mol^{-1} and number of hydrogen bonds ≥ 2. These hits were further docked using Glide SP (Standard precision) docking module and about 6,429 molecules were selected based on the docking score of ≤ -6.0 kcal mol^{-1}, 1.5 with hydrogen bonding and visual inspection of interaction into the pocket. Filtered ligands were subjected to Glide XP which combined accurately physics-based scoring terms and thorough sampling and resulted in compounds with docking scores between -9.649 to -6.222 kcal mol^{-1}. Though the docking score did not indicate the compound's binding affinity but it was helpful in prioritizing/ranking the ligands. Final shortlisting of hit compounds was based on visual inspection of the important amino acid residues involved in binding that included hydrogen bonding with Val187, Met195, Met40, Gln164, Gln72, Gly158, Asp161 and π-π stacking interactions with Hie44 and Hie47 (where Hie was the protonated state of histidine with hydrogen at epsilon position). The fitness, docking score, hydrogen bonding and ligand interaction for the top 41 shortlisted compounds are tabulated in the Table 5.2. The diagrammatic representations of the final selected compounds are depicted in Figures 5.5, 5.6 and 5.7. Further, the ADME properties were predicted using Quikprop module in Schrodinger (Table 5.3).

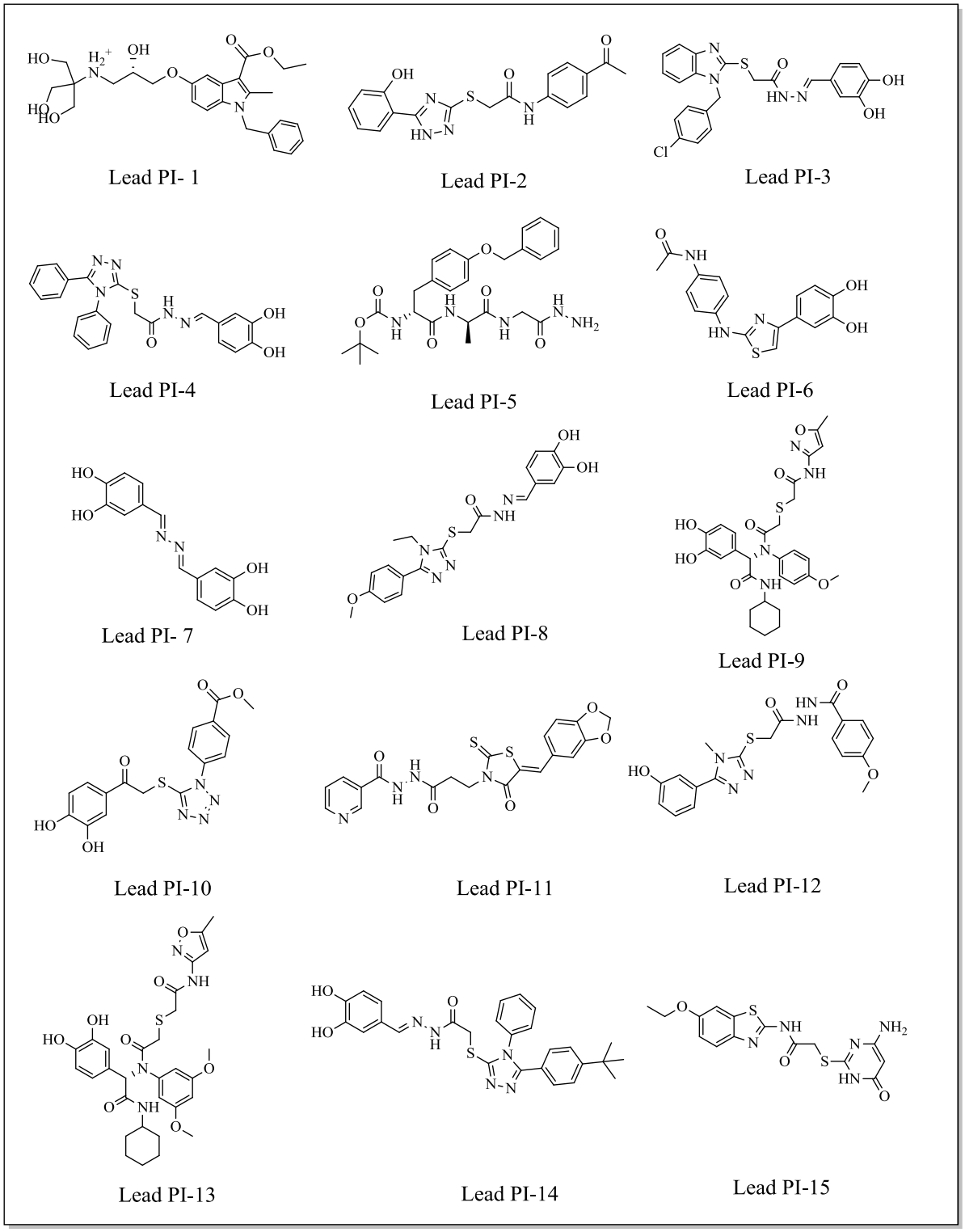

Figure 5.5: Chemical structures of the selected compounds (**Lead PI-1-PI-15**)

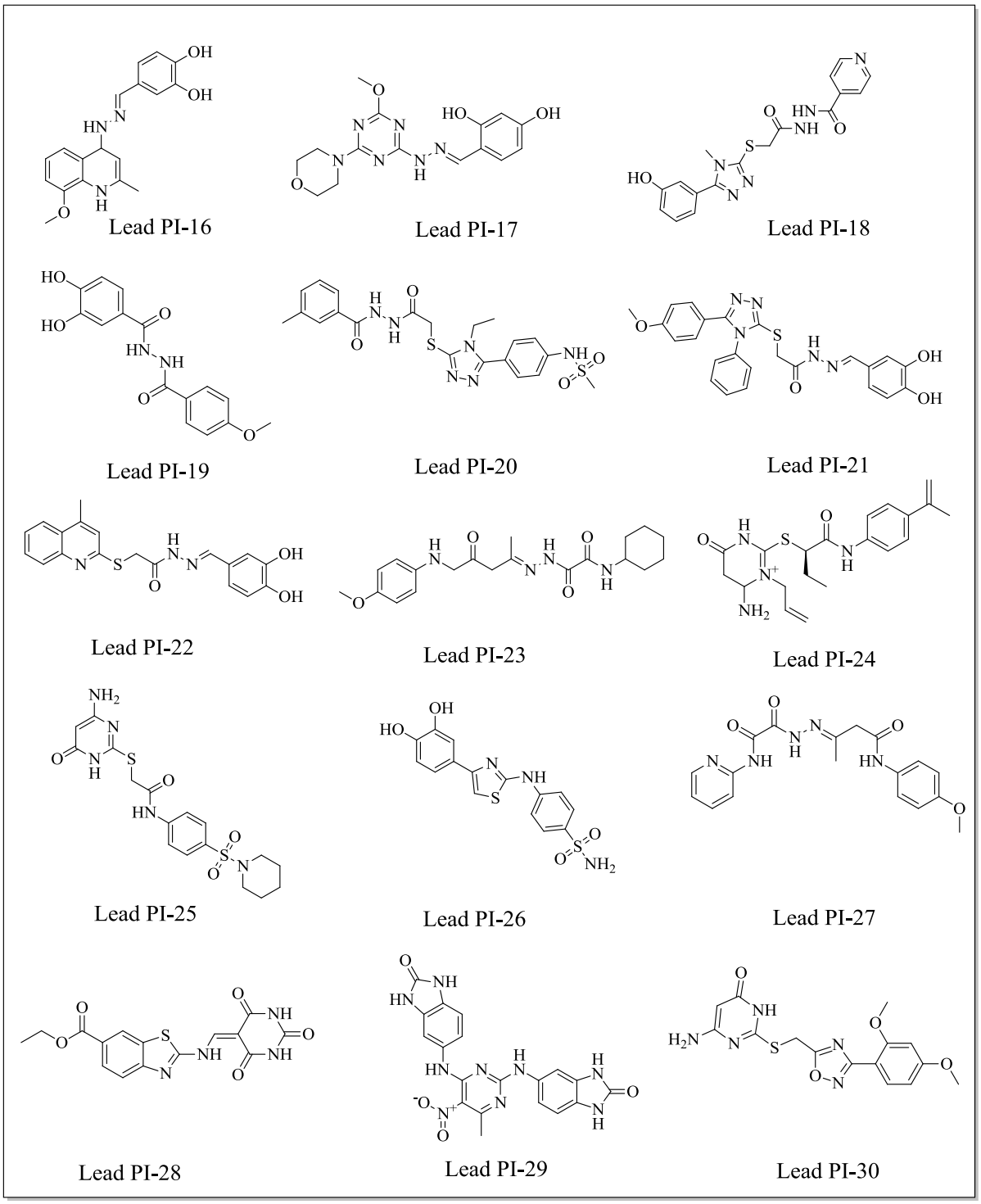

Figure 5.6: Chemical structures of the selected compounds (**Lead PI-16-PI-30**)

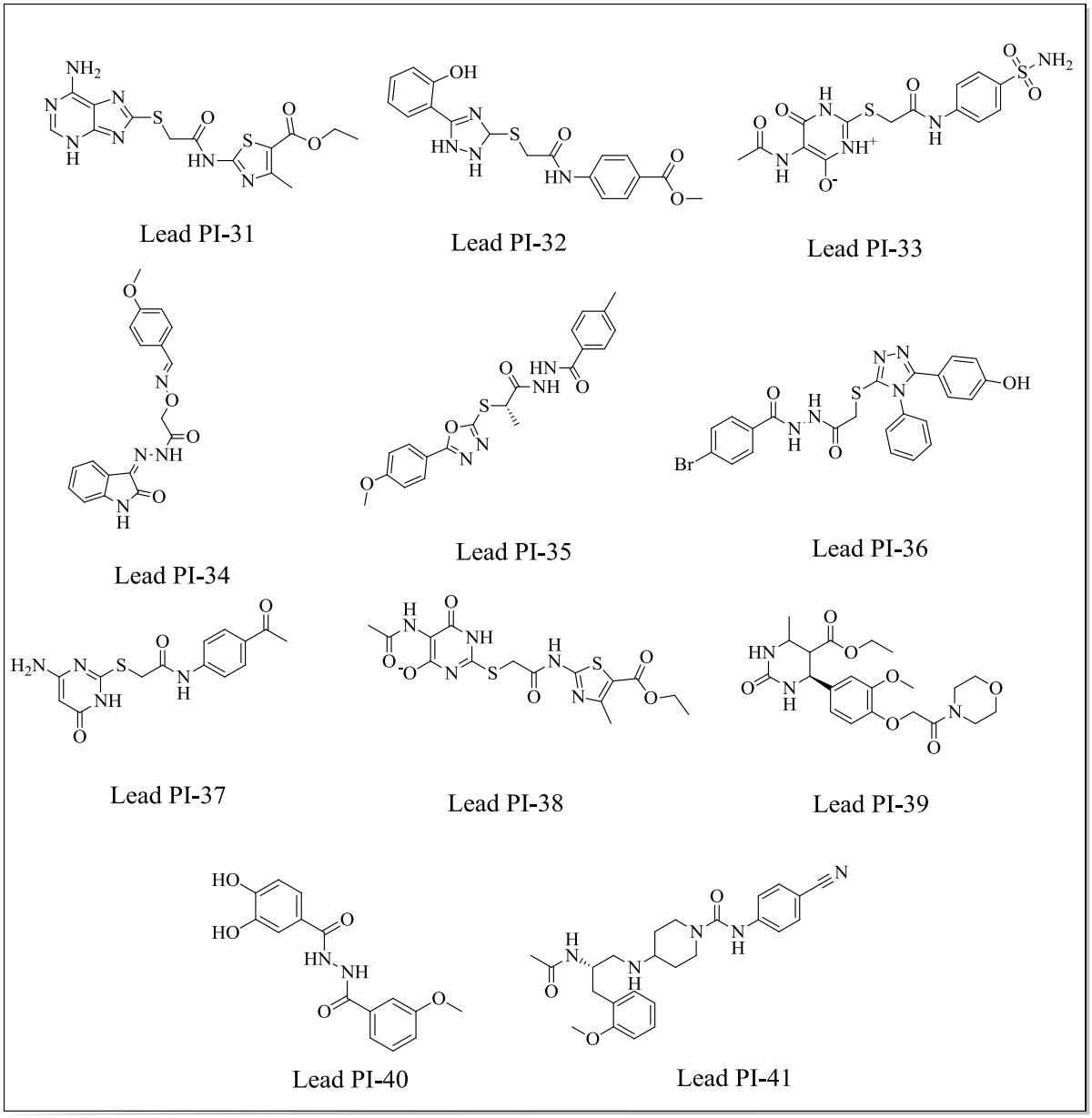

Figure 5.7: Chemical structures of the selected compounds (**Lead PI-31-PI-41**)

Table 5.2: Computational analysis for the designed compounds

Compound ID	Docking score	Hydrogen bond	Fitness	Ligand interaction
Crystal ligand	-9.64	6	1.542	Val187, Met195, Gly158, Met40, Gln164, Hid44/47
Lead PI-1	-9.64	5	1.449	Hie47, Gln72, 3Asp161, Gln164, Glu128
Lead PI-2	-9.21	5	1.383	Gln164, Gln72, Ser187, 2Hie44, Val187
Lead PI-3	-8.96	4	1.491	Hie47, Val187
Lead PI-4	-8.97	4	1.117	Ser197, Ser196, 2val187
Lead PI-5	-8.7	5	1.287	Asp161, Val187, Pro185
Lead PI-6	-8.53	3	1.876	Asp161, Val187
Lead PI-7	-8.56	3	1.34	Gln164, Gln72, Val187
Lead PI-8	-8.47	4	1.94	Gln72, 2Ser196
Lead PI-9	-8.28	6	1.121	Gln72, Gly158, Asp161, Hie44
Lead PI-10	-8.22	4	1.298	Thr39,Gln164
Lead PI-11	-8.17	4	1.057	Asp161, Ser197, Ser196, Gly158
Lead PI-12	-8.06	2	1.862	Met40, Hie47, Tyr82, Lys160, Val187
Lead PI-13	-8.05	5	1.611	Gln72, Pro38, Gly158
Lead PI-14	-7.94	5	1.946	Asp161, Ser196, Ser197, Hie44
Lead PI-15	-7.86	3	1.248	Asp161, Gln164, Hie47, Met195, Val187
Lead PI-16	-7.84	2	1.623	Gln72, 2Val187
Lead PI-17	-7.94	2	1.736	Met195, Val187, Lys160
Lead PI-18	-7.77	1	1.885	Val187, Ser196
Lead PI-19	-7.69	3	1.267	Gly158, Val187, Met195
Lead PI-20	-7.68	3	1.842	Gly158, 2Ser196, Gln72
Lead PI-21	-7.59	5	1.923	Ser196, Val187
Lead PI-22	-7.59	4	1.356	Hie47
Lead PI-23	-7.57	5	1.25	Gly158, Glu128, Hie47
Lead PI-24	-7.55	2	1.247	Asp161, Hie44, Val187
Lead PI-25	-7.43	1	1.887	Hie47, Asp161
Lead PI-26	-7.4	2	1.11	Gln72, Val187
Lead PI-27	-7.23	3	1.69	2Hie47, Met40
Lead PI-28	-7.3	2	1.228	Val187, Met195
Lead PI-29	-7.06	4	1.786	Thr39, Ser197, Val187
Lead PI-30	-7.07	2	1.34	Gly158, Met40, Hie47
Lead PI-31	-7.03	5	1.141	Gln164, Pro185, Val187, Met195, Hie47
Lead PI-32	-6.87	3	1.558	Ser197, 2Hie44, Val187
Lead PI-33	-6.86	4	1.499	Gln72, Hie47
Lead PI-34	-6.82	2	1.34	Met40, Hie47, Gln72
Lead PI-35	-6.81	3	1.196	Asp161, Ser196, Hie44
Lead PI-36	-6.75	2	1.062	Val187, Gln164

Contd.

Compound ID	Docking score	Hydrogen bond	Fitness	Ligand interaction
Lead PI-37	-6.727	5	1.268	Gln164, Gly158, Val187, Hie47, Met40
Lead PI-38	-6.39	5	1.431	Gln164, Met40, 2asp161, Gln164, Glu128
Lead PI-39	-6.25	3	1.218	Gln72, Tyr82
Lead PI-40	-6.22	4	1.997	Hie44, 2Met195
Lead PI-41	-6	3	1.346	Gly74, Hie47

5.1.5. ADME prediction for the designed compounds

All the selected compounds were subjected to *in silico* ADME properties using QikProp module in Schrodinger. The compounds shortlisted were found to be in accordance with Lipinski's rule of five which is the preliminary criteria of drug like molecules. Various other important properties like predicted octanol/water partition coefficient logP, predicted IC_{50} value for blockage of HERG K+ channels, predicted apparent Caco-2 cell permeability in nm/sec, predicted brain/blood partition coefficient, percent human oral absorption were predicted for the selected compounds and checked for any deviations. The lead compounds **PI-7**, **PI-25**, **PI-26**, **PI-29**, **PI-31**, **PI-33**, **PI-37 and PI-38** did not show good partition coefficient (QPlogP) values which were critical for understanding of absorption and distribution of drugs. Factor QPlogCaco-2 property were not in the acceptable range for the lead compounds **PI-25**, **PI-29**, **PI-33** and **PI-38**. This factor determines cell permeability in biological membranes and its metabolism. The critical factor governing drug access to cell membrane could be predicted through cell permeability. Some lead compounds (**PI-5**, **PI-9**, **PI-13**, **PI-39** and **PI-41**) were predicted to be associated with HERG cardiotoxicity which restrict their further development as promising drug molecule. Also, many compounds showed violation of Lipinski's rule of five mainly due to molecular weight (>500), hydrogen donor and acceptor. Lead compounds **PI5**, **PI-9**, **PI-13**, **PI-14**, **PII-29** and **PI-33** violated from Lipinski rule of five. Predicted blood brain barrier and % human oral absorption were in the acceptable range for all the designed leads. This implies that the bioavailability of the lead compounds is good.

Table 5.3: ADME prediction for the designed compounds

Compound ID	QPlogPo/w[a]	QPlogHERG[b]	QPPCaco[c]	QPlogBB[d]	%Human oral absorption[e]	Rule of five[f]
Lead PI-1	2.234	-7.083	27.039	-2.349	65.653	0
Lead PI-2	2.158	-6.62	126.177	-1.888	77.187	0
Lead PI-3	4.318	-6.087	191.207	-1.618	93.061	0
Lead PI-4	3.807	-6.531	85.51	-2.01	83.814	0
Lead PI-5	2.917	-3.535	112.715	-2.127	41.875	3
Lead PI-6	2.139	-6.309	157.52	-1.641	78.797	0
Lead PI-7	0.775	-5.772	75.908	-2.114	65.14	0
Lead PI-8	3.408	-6.774	83.092	-2.519	81.257	0
Lead PI-9	2.594	-3.923	156.903	-2.001	55.515	2
Lead PI-10	1.454	-5.293	36.96	-2.227	63.52	0
Lead PI-11	2.949	-6.529	153.169	-1.711	83.321	0
Lead PI-12	3.238	-6.793	81.275	-2.304	80.087	0
Lead PI-13	2.809	-3.573	218.97	-1.871	59.362	2
Lead PI-14	5.436	-7.681	83.422	-2.593	67.247	2
Lead PI-15	1.43	-5.601	148.011	-1.653	74.161	0
Lead PI-16	2.442	-5.794	410.96	-1.312	88.024	0
Lead PI-17	1.158	-5.4	387.764	-1.356	80.054	0
Lead PI-18	2.202	-6.773	39.866	-2.562	68.487	0
Lead PI-19	1.536	-5.718	94.525	-1.91	71.297	0
Lead PI-20	2.915	-7.031	30.773	-3.106	70.646	0
Lead PI-21	4.31	-7.706	83.43	-2.529	86.572	0
Lead PI-22	3.368	-6.713	161.98	-1.908	86.213	0
Lead PI-23	3.564	-6.332	245.936	-1.972	90.605	0
Lead PI-24	2.687	-5.654	149.367	-0.731	81.592	0
Lead PI-25	0.671	-5.834	23.95	-2.757	55.562	0
Lead PI-26	0.67	-5.89	33.442	-2.274	58.153	0
Lead PI-27	2.586	-6.909	148.845	-2.03	80.974	0
Lead PI-28	1.133	-5.106	26.541	-2.324	59.064	0
Lead PI-29	0.643	-6.567	3.579	-3.803	34.703	2
Lead PI-30	1.225	-5.632	90.117	-1.964	69.108	0
Lead PI-31	0.667	-5.773	28.756	-2.711	56.959	0
Lead PI-32	1.236	-7.566	31.37	-1.57	60.967	0
Lead PI-33	-1.001	-5.936	3.475	-3.865	4.848	2
Lead PI-34	2.552	-6.957	221.711	-1.877	83.872	0
Lead PI-35	3.962	-6.821	222.358	-1.713	92.149	0
Lead PI-36	4.849	-7.503	75.699	-2.098	76.008	1
Lead PI-37	0.36	-5.647	39.12	-2.325	57.551	0

Contd.

Compound ID	QPlogPo/w[a]	QPlogHERG[b]	QPPCaco[c]	QPlogBB[d]	%Human oral absorption[e]	Rule of five[f]
Lead PI-38	0.545	-5.757	11.743	-3.38	36.322	1
Lead PI-39	2.686	-4.441	153.449	-1.636	81.8	0
Lead PI-40	1.545	-5.69	96.855	-1.889	71.542	0
Lead PI-41	2.253	-4.655	34.609	-1.321	67.687	0

[a]Predicted octanol/water partition coefficient logP (acceptable range: −2.0 to 6.5); [b]Predicted IC_{50} value for blockage of HERG K+ channels.(below -5); [c]Predicted apparent Caco-2 cell permeability in nm/sec (<25 poor; >500 great); [d]Predicted brain/blood partition coefficient (-3.0 to 1.2); [e]Percent human oral absorption (<25% is poor and >80% is high); [f]Rule of 5 violation (mol_MW < 500, QPlogPo/w < 5, donorHB ≤5, accptHB ≤10)

5.1.6. Biological assessments

Preliminary enzyme inhibition assay was performed for the designed compounds at a single concentration of 50 μM. The assay was based on coupling of AMP produced in the condensation of β-alanine and pantoate with the oxidation of NADH to NAD+ by myokinase, pyruvate kinase and lactate dehydrogenase. The decrease in the absorbance of NADH was spectrophotometrically monitored at 340 nm. Inorder to confirm specific inhibition of PS apart from the other "coupled enzymes" in the assay, the hits were tested in an assay that was performed with a final concentration of lactate dehydrogenase as 0.2 units ml^{-1} and pantoic acid was not added to the reaction mixture. The "coupling enzyme" assay was initiated with AMP (6.5 mM final concentration) instead of PS. The % inhibition of the 41 lead compounds is tabulated in the Table 5.4.

Table 5.4: In-vitro enzyme inhibition data for 41 lead compounds

Compound ID	% Inhibition at 50 μM concentration	Compound ID	% Inhibition at 50 μM concentration
Lead PI-1	12.7	**Lead PI-22**	7.216
Lead PI-2	25.77	**Lead PI-23**	73.46
Lead PI-3	79.88	**Lead PI-24**	23.47
Lead PI-4	47.22	**Lead PI-25**	13.36
Lead PI-5	40.91	**Lead PI-26**	28.29
Lead PI-6	40.69	**Lead PI-27**	17.67
Lead PI-7	20.67	**Lead PI-28**	88.87
Lead PI-8	12.92	**Lead PI-29**	51.74
Lead PI-9	65.37	**Lead PI-30**	11.65
Lead PI-10	20.6	**Lead PI-31**	41.05
Lead PI-11	93.14	**Lead PI-32**	7.26
Lead PI-12	13.98	**Lead PI-33**	24.44
Lead PI-13	56.22	**Lead PI-34**	73.06

Contd.

Compound ID	% Inhibition at 50 μM concentration	Compound ID	% Inhibition at 50 μM concentration
Lead PI-14	17.75	**Lead PI-35**	11.36
Lead PI-15	0.996	**Lead PI-36**	13.92
Lead PI-16	10.94	**Lead PI-37**	64.45
Lead PI-17	23.59	**Lead PI-38**	11.94
Lead PI-18	69.28	**Lead PI-39**	14.84
Lead PI-19	48.02	**Lead PI-40**	47.88
Lead PI-20	8.134	**Lead PI-41**	18.29
Lead PI-21	14.17		

Ten compounds (**Lead PI-3**, **Lead PI-9**, **Lead PI-11**, **Lead PI-13**, **Lead PI-18**, **Lead PI-23**, **Lead PI-28**, **Lead PI-29**, **Lead PI-34**, and **Lead PI-37**) which showed more than 50% inhibition were further tested in lower concentrations to estimate the IC_{50} values. **Lead PI-11** showed the highest inhibition of 93.14% and **Lead PI-28** showed 88.87% inhibition. The IC_{50} values were calculated using non-linear regression analysis using GraphPad prism software. Among 10 leads, four leads showed IC_{50}s <10 μM. The interaction pictures (Figure 5.9 and Figure 5.10) of these 10 lead compounds were shown that they had H-bond interaction with the amino acid moieties which are crucial for enzyme activity. Compound (Z)-N'-(3-(5-(benzo[d][1,3]dioxol-5-ylmethylene)-4-oxo-2-thioxothiazolidin-3-yl)propanoyl) nicotinohydrazide (**Lead PI-11**) was found to be the most potent inhibitor with an IC_{50} of 1.12±0.12 μM and MIC of 54.81 μM. Comparatively, the reported inhibitor nafronyl oxalate showed IC_{50} of 90 nM and inhibited the bacterial growth by <50% at 128 μM. This result implies that, the reported inhibitor have promising IC_{50} value but failed to kill the bacteria at lower concentration; but the designed **Lead PI-11** showed IC_{50} greater than the reported compound also it killed the bacteria at 54.81 μM makes this compound a promising candidate for initial step of derivatization using medicinal chemistry approach. Table 5.5 represents the IC_{50} values for the designed compounds selected as leads.

Table 5.5: Top active lead compounds inhibitory concentration

Compound ID	IC_{50} values (μM)
Lead PI-3	26.33±1.06
Lead PI-9	38.78±1.16
Lead PI-11	1.128±0.22
Lead PI-13	40.48±0.79
Lead PI-18	26.33±0.68
Lead PI-23	8.92±0.34
Lead PI-28	7.67±0.41
Lead PI-29	47.12±1.24
Lead PI-34	5.97±0.19
Lead PI-37	24.72±1.03

Based on the Quickprop prediction **Lead PI-11** did not show any violation of Lipinski's rule of five. With the aim of getting insights into the structural basis for its activity, this compound was analysed in more detail. The compound was found to display highest docking score among the other identified Asinex hits, with docking score of -7.089 kcal mol^{-1}. The lead compound was found to be associated with four hydrogen bonding interactions with relevant amino acid residues of the protein. Oxygen atom of the benzodioxo group was found to interact with Val187. Oxygen and NH of carbohydrazide group attached to the pyridyl end were found to be interacting with Gln164 and the carbonyl oxygen atom on thiazole ring participated in hydrogen bonding with Hie47 analogous to the one observed in the crystal ligand which showed interaction with His44. In addition to hydrogen bonding interactions; the 3-pyridyl ring was found to be well placed in the hydrophobic pocket consisting of Phe67, Val142, Leu146 and Pro38. Apart from hydrophobic interactions 3-pyridyl ring showed polar contacts with Asn69, Gln72 Ser65 and Thr39, whereas the 5-benzo[d][1,3]dioxo showed polar contacts with Hie47, Ser196 and Thr186 and was also involved in hydrophobic interaction with Met195, Ala49, Leu50 and Val184. The orientation of lead compound was also found to be similar to that of crystal ligand. The binding analysis for the lead molecule is shown in Figure 5.8.

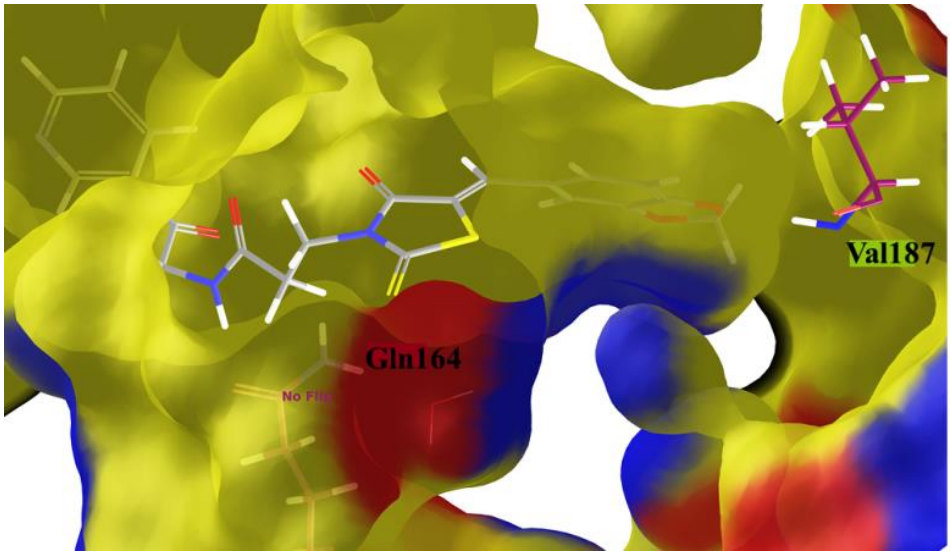

Figure 5.8: Binding analysis for the lead molecule **Lead PI-11**

The binding analysis of leads **PI-3**, **PI-9**, **PI-13** and **PI-18** showed wide range of activity differences. The binding analysis of lead **PI-3** and **PI-18** shared equal IC_{50} values, revealed that Val 187 amino acid is interacting in common; but compounds **PI-3** and **PI-18** failed to produce hydrogen bonding interaction with the side chain of Hie47 and Ser196. The leads **PI-9** and **PI-13** binding pattern revealed that, the cyclo hexyl formamide group in both compounds shared the common interaction with Gln72 as shown in Figure 5.9.

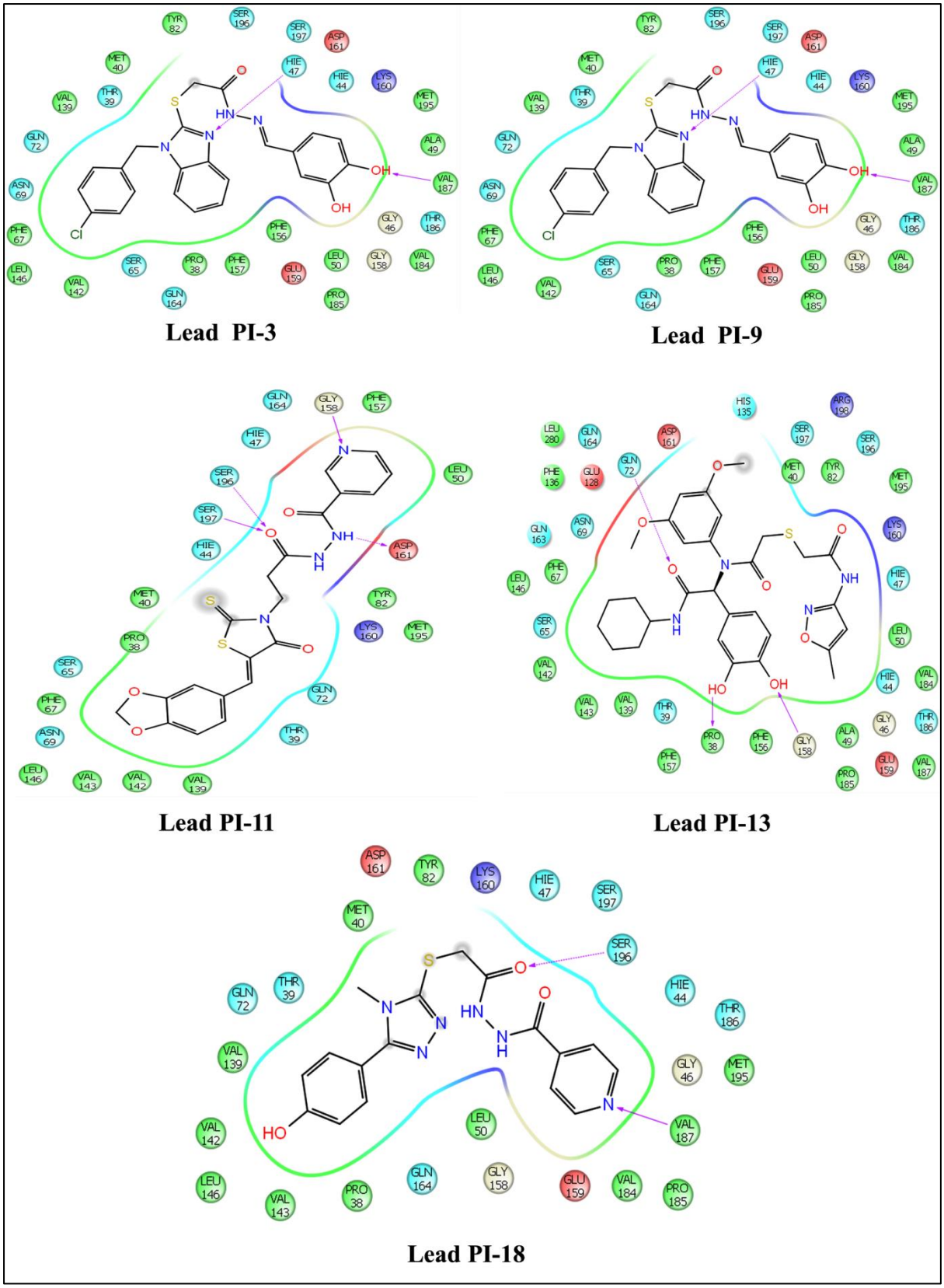

Figure 5.9: Ligand Interaction for the top active compounds (**Lead PI-3**, **PI-9**, **PI-11**, **PI- 13**, and **PI-18**)

The lead compounds **PI-23** and **PI-28**, were found to show two hydrogen bond interactions, one with Met195 and other with Val187 which are the important amino acid interactions shown by selected crystal ligand. This was also well correlated with the enzyme inhibitory activity with the IC_{50}s of 8.92±0.34 μM and 7.67±0.41 μM respectively. Also, in closer analysis of lead compound **PI-34** showed that, it was associated with three hydrogen bonds with Met50, Hie47 and Gln72 which makes this molecule crucial for the enzyme inhibition with an IC_{50} of 5.97±0.19 μM. The lead compounds **PI-29** and **PI-37** was showing three hydrogen bonding interaction with three different amino acids as shown in Figure 5.10. In **PI-29**, the important amino acid Val187 making a hydrogen bonding; whereas in **PI-37**, Met40 and Gln164 was making the hydrogen bond interaction which made **PI-37** (24.72±1.03 μM) comparatively active than **PI-29**.

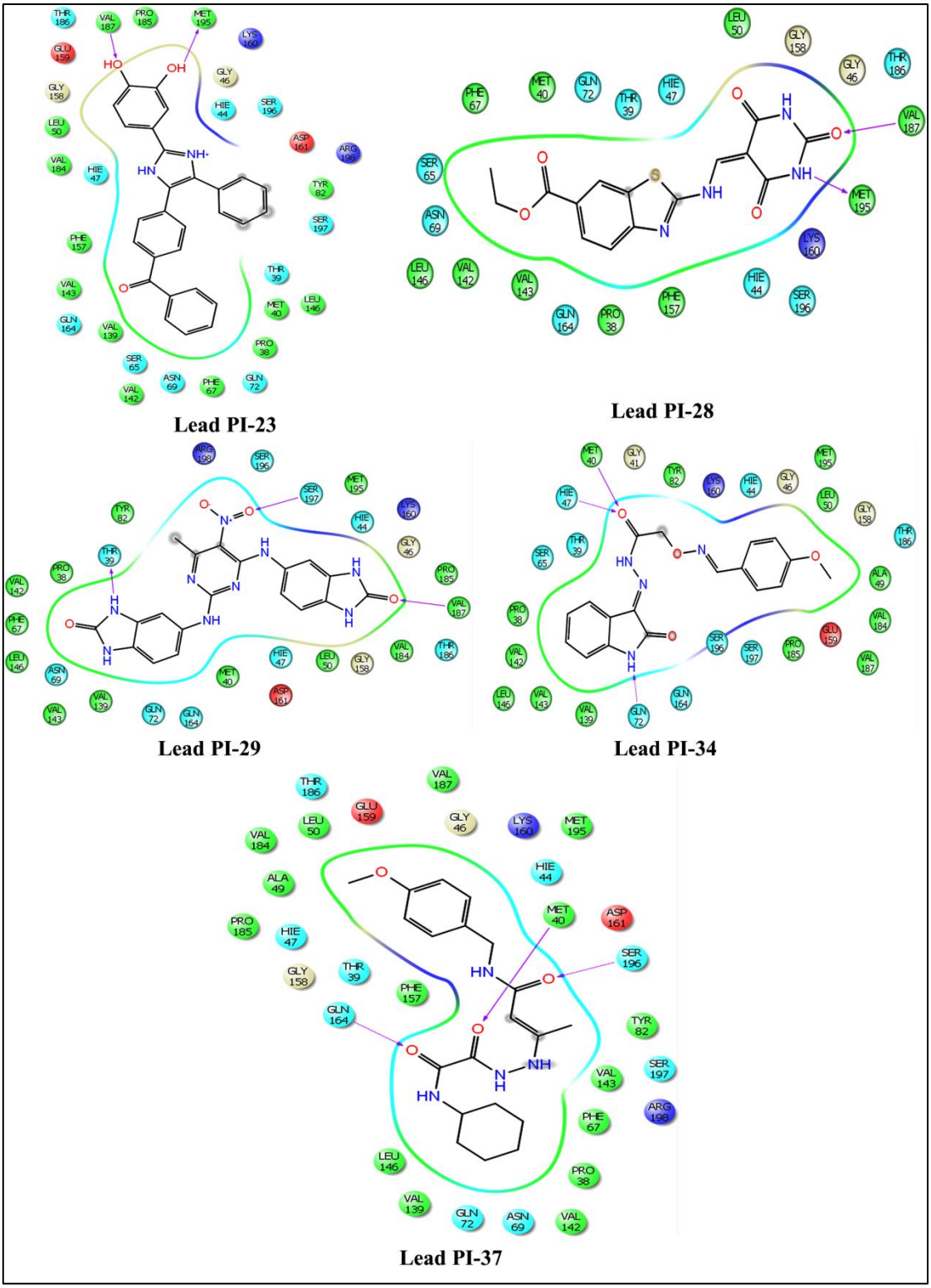

Figure 5.10: Ligand Interaction for the top active compounds (**Lead PI-23**, **PI- 28**, **PI-29**, **Pa-34** and **PI-37**)

5.1.7. Lead optimization using medicinal chemistry

To study the structure-activity relationship of lead compound **Lead PI-11**, we further derivatized it to nineteen compounds and assayed for Mtb PS inhibition. The synthetic pathway employed to achieve the target compounds has been delineated in Figure 5.11.

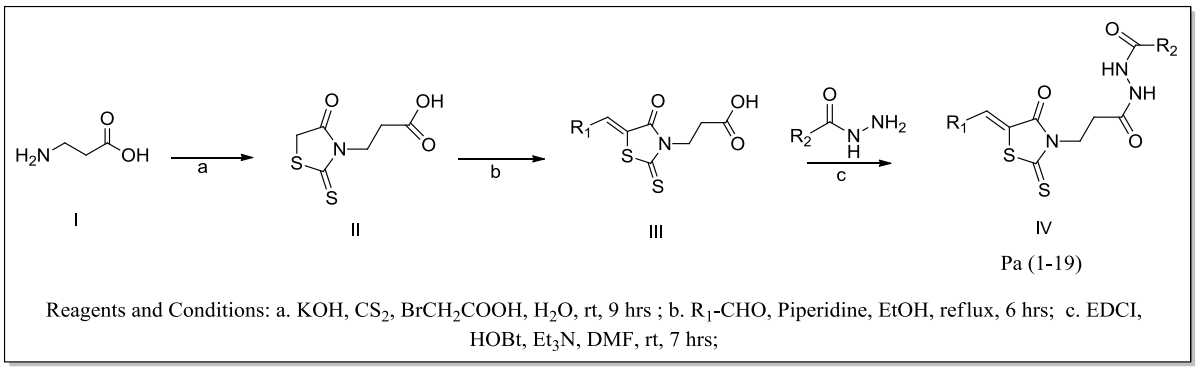

Figure 5.11: Synthetic scheme utilized for Mtb PS leads-reaction intermediate based approach

The final compounds were synthesized in 3 steps; in the first step, β-alanine (**I**) was reacted with carbon disulphide and bromoacetic acid under basic conditions using water as solvent to form compound **II** in good yield (81%). Compound **II** was then subjected to Knoevenagel type of condensation with different aldehydes by refluxing in ethanol using catalytic amount of piperidine to achieve compound **III** in excellent yield (90%) [Suto R.K., *et al*., 2005]. Finally compound **III** was treated with acid hydrazides using EDCI, HOBt and Et_3N, at room temperature, to yield compounds **Pa (1-19)**. The synthesis was carried out by medicinal chemistry research group at the Department of Pharmacy.

5.1.8. In-vitro PS inhibition assay for the synthesized compounds

The enzyme inhibition assay was performed for the synthesized compounds as discussed in section 4.3.1.2. In the initial screening at 25 µM, all the compounds showed more than 50% inhibition against Mtb PS and their IC_{50}s were calculated. Their IC_{50}s were found to be in the range of 0.35±0.81 µM to 5.86±0.11 µM; Five compounds (**Pa-9**, **Pa-12**, **Pa-13**, **Pa-16**, **and Pa-19**) were found to more effective with IC_{50}'s less than 1 µM. The compounds **Pa-2**, **Pa-3**, **Pa-6** and **Pa-9** were equipotent to the parent **Lead PI-11** which possessed enzyme inhibition of 1.12±0.12 µM. Compound **Pa-9** emerged as the most active compound with an IC_{50} of 0.35±0.81µM which was 2 times more potent than parent compound. The in-vitro biological activity data is tabulated in Table 5.5.

Table 5.6: Biological evaluation for the synthesized compounds

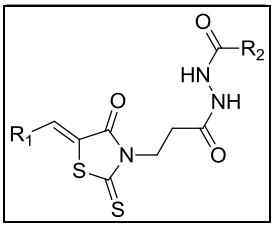

Compoud ID	R_1	R_2	IC_{50} µM[a]	Mtb MIC in µM[b]	Mtb MIC in µM[v]	Mtb MIC in µM[p]	Cytotoxicity at 100 µM[c]
Lead PI-11	5-Benzo[d][1,3]dioxole	3-Pyridyl	1.12±0.12	54.81	13.70	27.40	38.92±0.12
Pa-1	5-Benzo[d][1,3]dioxole	Phenyl	5.86±0.11	54.95	13.73	13.73	63.22±0.26
Pa-2	5-Benzo[d][1,3]dioxole	4-Pyridyl	1.21±0.37	54.82	27.41	27.41	36.55±0.38
Pa-3	5-Benzo[d][1,3]dioxole	1-Naphthyl	1.05±0.53	24.75	3.09	12.37	61.80±0.22
Pa-4	4-Chlorophenyl	Phenyl	4.89±0.22	56.18	7.02	3.51	62.58±1.02
Pa-5	4-Chlorophenyl	4-Pyridyl	3.50±0.43	56.05	14.01	7.00	42.11±0.65
Pa-6	4-Chlorophenyl	1-Naphthyl	1.17±0.72	25.25	12.62	25.25	63.71±2.92
Pa-7	4-Chlorophenyl	3-Pyridyl	1.35±0.43	7.01	7.01	3.50	50.62±3.32
Pa-8	3,4,5-Trimethoxyphenyl	Phenyl	1.39±0.22	6.24	1.56	3.12	45.37±0.33
Pa-9	3,4,5-Trimethoxyphenyl	4-Pyridyl	0.35±0.81	1.55	0.38	0.77	22.21±0.65
Pa-10	3,4,5-Trimethoxyphenyl	1-Naphthyl	1.14±0.34	5.67	5.67	5.67	56.17±0.62
Pa-11	3,4,5-Trimethoxyphenyl	3-Pyridyl	2.12±0.13	49.80	6.22	24.9	35.37±0.26
Pa-12	4-Nitrophenyl	Phenyl	0.37±0.92	1.71	0.85	0.85	50.05±0.53
Pa-13	4-Nitrophenyl	4-Pyridyl	0.59±0.43	13.68	13.68	13.68	21.78±0.47
Pa-14	4-Nitrophenyl	1-Naphthyl	1.40±0.13	12.35	1.54	1.54	41.23±0.66
Pa-15	4-Nitrophenyl	3-Pyridyl	2.51±0.42	3.41	0.85	0.85	32.92±0.29
Pa-16	4-Benzyloxyphenyl	Phenyl	0.79±0.23	24.18	24.18	12.09	43.96±1.05
Pa-17	4-Benzyloxyphenyl	4-Pyridyl	1.54±0.13	24.13	6.03	6.03	53.05±2.23
Pa-18	4-Benzyloxyphenyl	1-Naphthyl	1.70±0.21	88.18	22.04	44.09	27.22±0.64
Pa-19	4-Benzyloxyphenyl	3-Pyridyl	0.51±0.72	12.07	12.07	12.07	28.20±0.93
	Isoniazid		ND	0.72	0.72	0.72	ND
	Ethambutol		ND	7.64	7.64	3.82	ND

[a]Mtb PS enzyme,[b]Minimum inhibitory concentration against *M. tuberculosis* H37 Rv; [v]MIC in presence of verapamil, [p]MIC in presence of piperine, [c]**%** inhibition of RAW 264.7 cells, ND indicates not determined

The dose response curves plotted for the two top active compounds **Pa-9** and **Pa-12** are presented in Figure 5.12.

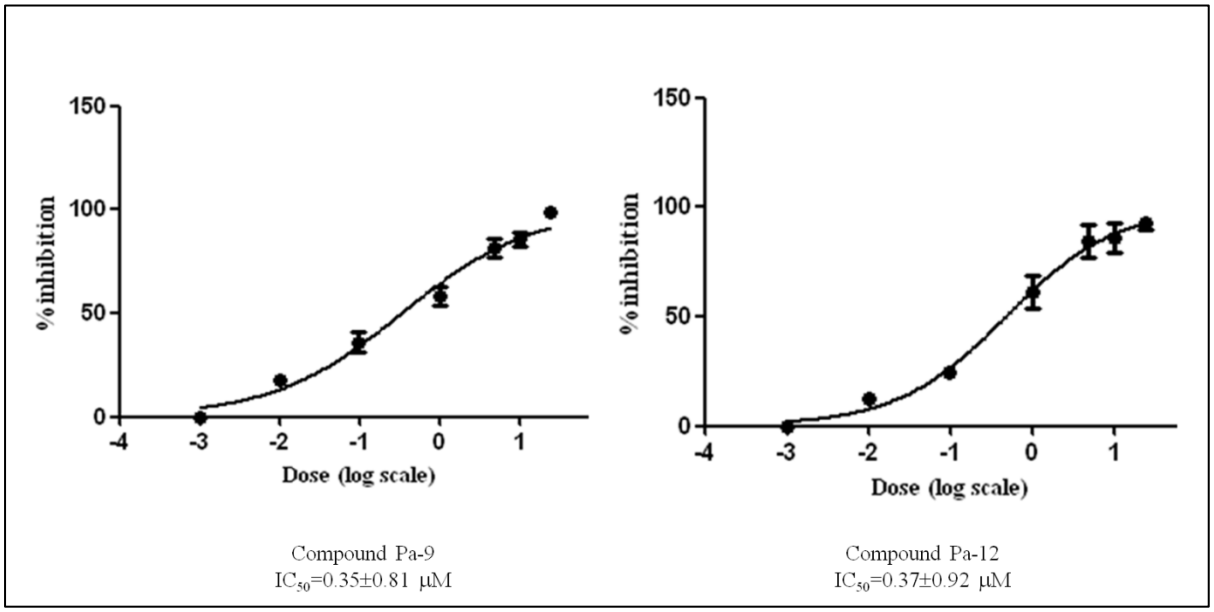

Figure 5.12: Dose response curve for the top active compounds (**Pa-9** and **Pa-12**)

The synthesized compounds were docked to the Mtb PS in order to support the structure-activity relationship. Firstly, R_1 position of the parent compound was substituted with 4-chlorophenyl, 3,4,5-trimethoxy phenyl, 4-nitrophenyl and benzyloxyphenyl groups. Of these derivatives, compounds with 3,4,5-trimethoxy phenyl (**Pa-9**-**Pa-11**), benzyloxyphenyl (**Pa-16-Pa-19**) and 4-nitrophenyl (**Pa-12-Pa-15**) groups showed good activity range (0.35 μM - 2.51 μM) when compared to that with 4-chlorophenyl group (1.17 μM - 4.89 μM). Replacement of benzo[d, 1,3]dioxole with 3,4,5-trimethoxy phenyl and benzyloxyphenyl group at R_1 played important role in enzyme activity. The assay results confirmed that the molecule with 3,4,5-trimethoxy phenyl at R_1 (**Pa-9**) was more active when compared to benzyloxyphenyl group compound (**Pa-19**). This could be attributed to the presence of an extra cation-π interaction between His 47 and phenyl group of the molecule.

Overall compound **Pa-9** emerged as the most potent inhibitor of Mtb PS with a low IC_{50} of 0.35 μM. Closer analysis of compound **Pa-9** in the binding site revealed four hydrogen bonds; carbonyl oxygen atom on thiazolidine ring with Hie44 and NH group on acid hydrazide participated with Tyr82 and Met40. The trimethoxy phenyl group at R_1 position occupied the hydrophobic pocket surrounded by Pro185, Ala49, Val184, Val187, Leu50 and Phe157. Also the trimethoxyl phenyl group was further stabilized by π-π stacking interaction

with Hie47 which made the compound more potent. The binding analysis and the ligand interaction diagram are shown in the Figure 5.13.

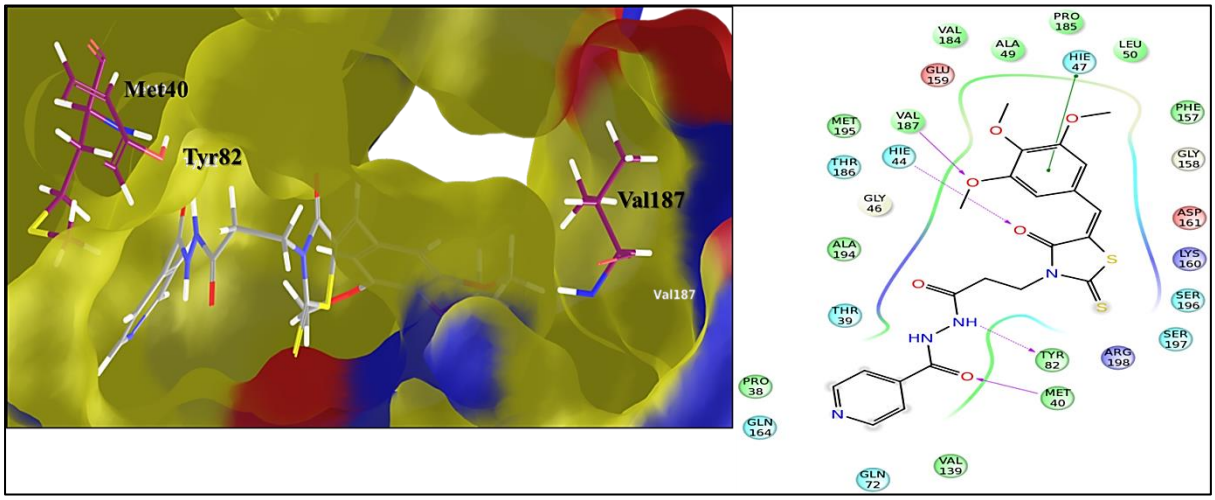

Figure 5.13: Binding analysis and ligand interaction diagram for the top active compound Pa-**9**

The next series of compounds in combinations with 4-nitrophenyl group at R^1 position (**Pa-12- Pa-15**) showed good activity data towards Mtb PS (0.37 µM to 2.51 µM). Compound **Pa-12** showed high activity in Mtb PS assay (0.37±0.92 µM). This could be supported by the strong non-polar interactions at the hydrophobic pocket and cationic interaction between oxygen of nitro group and Lys160 (Figure 5.14). Further substitution of nitrophenyl containing compounds at R_2 position with phenyl, 4-pyridyl, 1-naphthyl and 3-pyridyl moieties showed a decrease in the activity range suggesting the phenyl substitution to be appropriate. Analysis of these compounds revealed that the 4-nitrophenyl substituted derivatives with R_2 phenyl (**Pa-12**) and 4-pyridyl (**Pa-13**) substituted compounds were more potent than R_2 3-pyridyl (**Pa-15**) and Naphthyl (**Pa-14**) substituted compounds. The 4-nitrophenyl substituted compounds were equipotent to trimethoxy phenyl substitution (**Pa-8-Pa-11**). Comparison of the two potent compounds with phenyl and 4-pyridyl substituted group revealed that compound **Pa-12** exhibited significant activity due to hydrophobic interaction and additional cationic interaction with Lys160 amino acid while compound **Pa-13** did not show this cationic interaction.

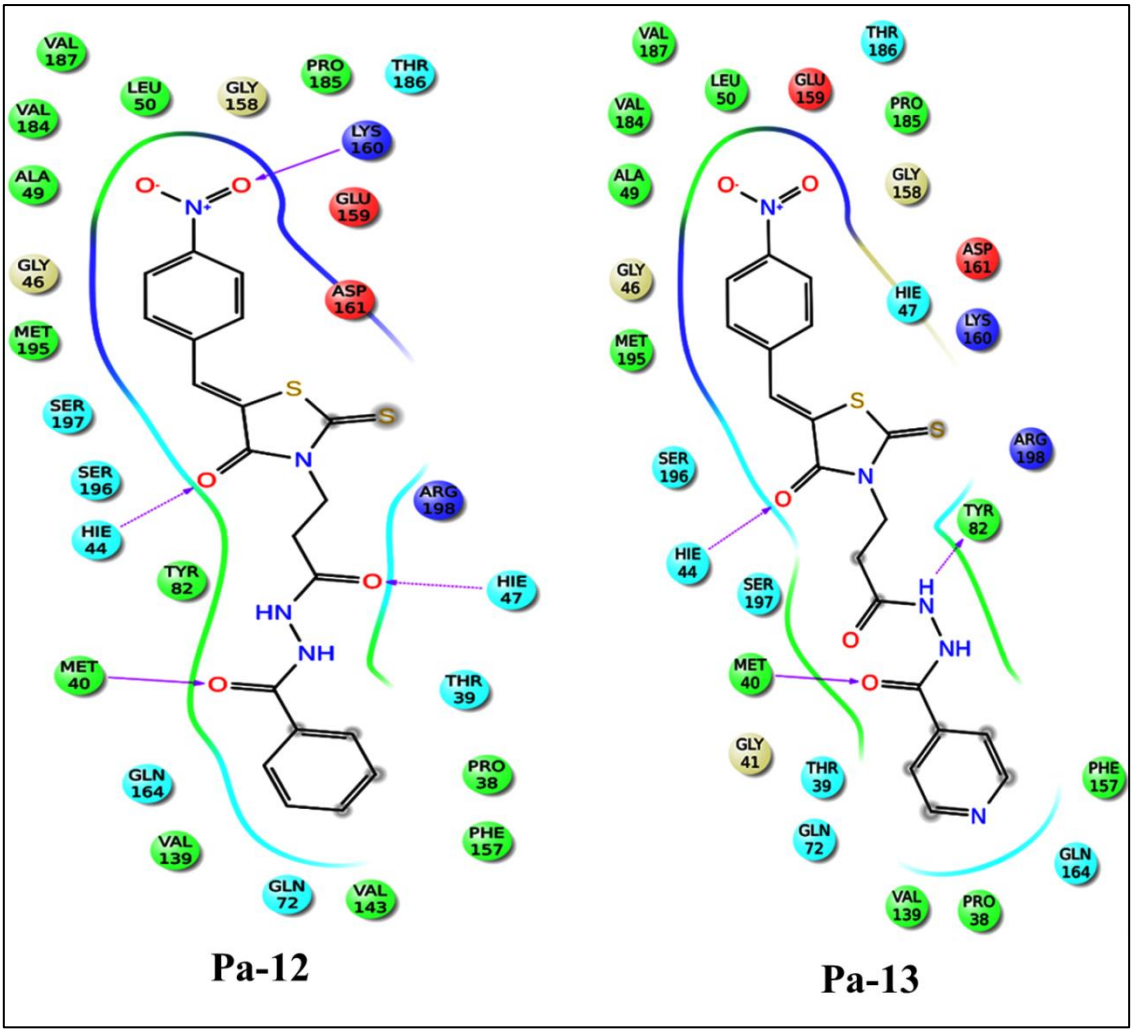

Figure 5.14: Ligand interaction diagram for the compound **Pa-12** and **Pa-13**

Compounds with chloro substitution (**Pa-4**-**Pa-7**) at R_1 position were found to be less active compared to trifluoromethyl and nitro substitutions. Orientation of **Pa-7** compound was found to be different from that of the remaining compounds, probably accounting to its high electronegative nature as shown in Figure 5.15. Compound **Pa-6** was associated with two hydrogen bonding interactions with relevant amino acids Hie44 and Hie47. The 4-chlorophenyl group (**Pa-6**) at R_1 position was inserted into the hydrophobic cavity lined by Pro185, Val187, Val184, Leu50 and Met195.

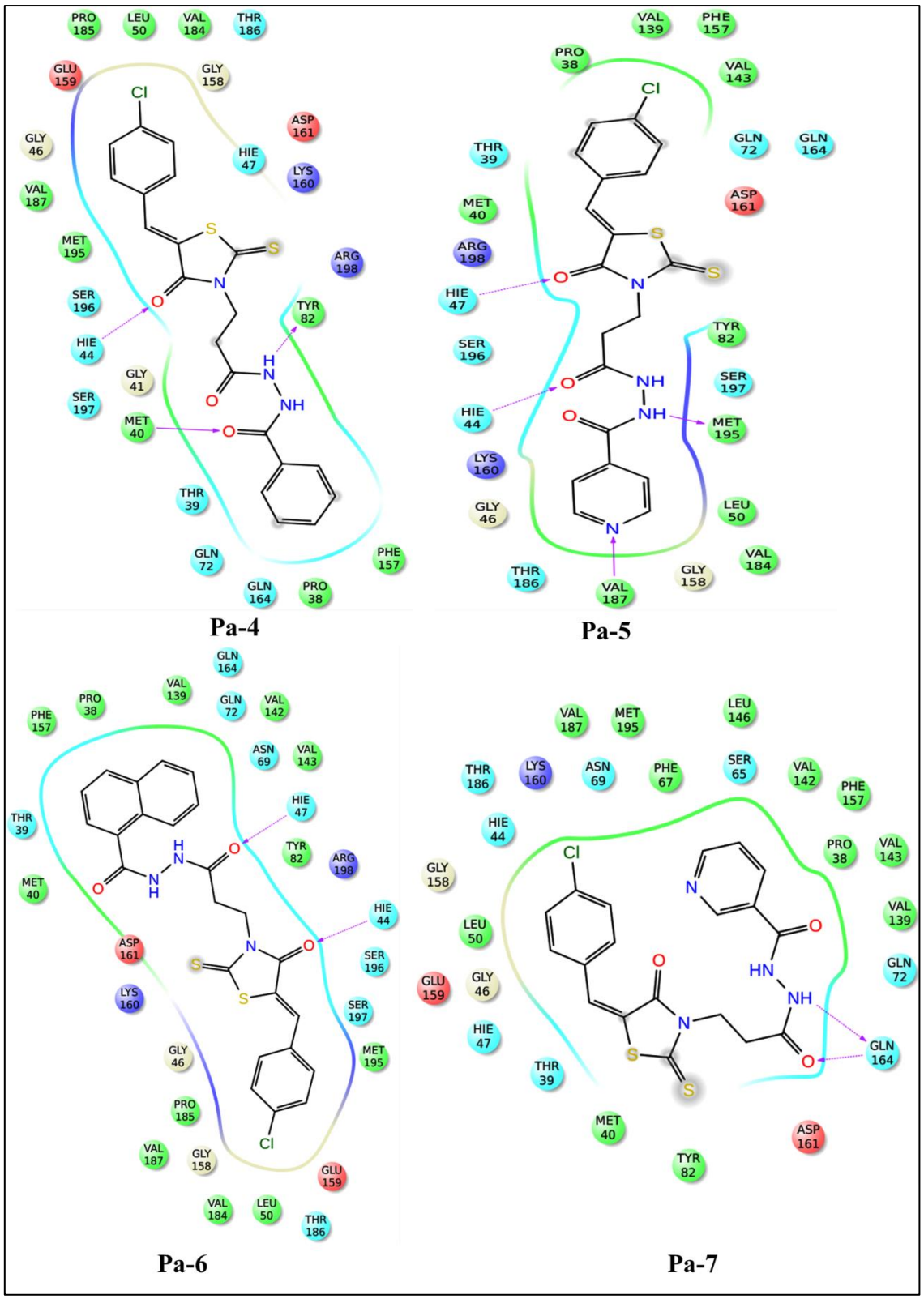

Figure 5.15: Ligand interaction diagram for the compound **Pa-4**, **Pa- 5**, **Pa- 6** and **Pa-7**

The compounds **(Pa-1-Pa-3)** substituted at R_2 position with phenyl, 4-pyridyl, and 1-naphthyl differed in their activity ranges. Comparing the orientation of these molecules at the active site, it was found that the 4-pyridyl (**Pa-2**) and 1-naphthyl (**Pa-3**) moieties were in the hydrophobic pocket in contrast to that of compound with phenyl substitution (**Pa-1**) facing towards the solvent accession. Compounds (**Pa-3**, **Pa-6**, **Pa-10**, **Pa-14**, and **Pa-18**) with 1-naphthyl substitution at R_2 position showed slightly better or equipotent activity (IC_{50} 1.05 µM to 1.70 µM) when compared to parent lead compound (IC_{50} of 1.12 µM). This was well supported by the interaction profile in the docking studies orienting in a similar manner to the crystal ligand and retaining 3-4 hydrogen bonds as observed with reference molecule (Hie44, Asp161, Val187 Ser126 and Ser127). However replacement with phenyl group (compound **Pa-1**) at R_2 position led to a reduction in the activity five times (IC_{50} of 5.86 µM) which was evident from their interaction profile as the molecule took a slightly different orientation/pose, excluding the hydrophobic interactions. The binding pose and the interaction pattern of compound **Pa-1** is depicted in Figure 5.16.

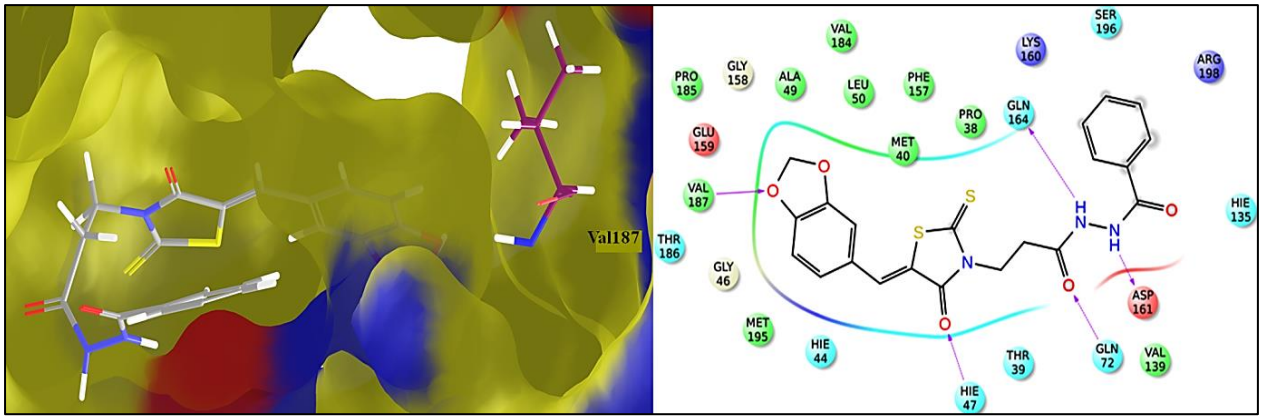

Figure 5.16: Binding pose and its ligand interaction diagram of compound **Pa-1**

When R_2 position was substituted with 4-benzyloxyphenyl group two nanomolar inhibitors **Pa-16** and **Pa-19** emerged with IC_{50}s of 0.79 µM and 0.51 µM respectively. These compounds revealed hydrogen bonding with Hie47, Val187, Hie44, Ser196 and Met195, the 4-benzyloxy phenol group was buried in the hydrophobic pocket with Val143, Val142, Phe157, Val139, Val68 and Phe67. Thus bulkier group at R_2 was favourable for PS inhibition. The ligand interaction diagram for the compound **Pa-16** and **Pa-19** are depicted in Figure 5.17.

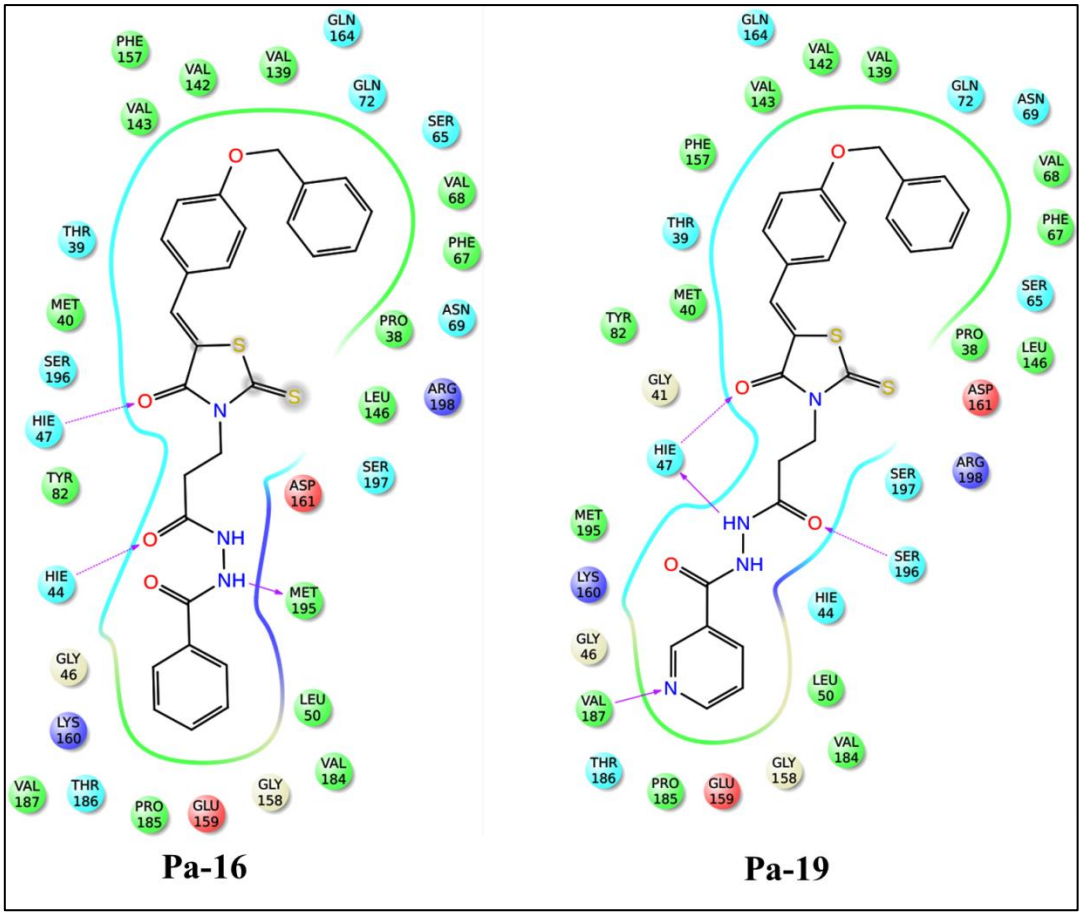

Figure 5.17: Ligand interaction diagram for the compound **Pa-16** and **Pa-19**

5.1.9. In-vitro anti-mycobacterial screening

Further, all the compounds were screened for their in-vitro anti-mycobacterial activity against log phase culture of Mtb H37Rv by MABA assay method for the determination of MIC in duplicates. MICs of the synthesized compounds along with the standard drugs for comparison are presented in Table 5.5. The compounds showed MICs ranging from 1.55-88.18 µM; and six compounds (**Pa-7**, **Pa-8**, **Pa-9**, **Pa-10**, **Pa-12** and **Pa-15)** showed promising activity with MIC less than 10 µM. When compared to standard first line antitubercular drug ethambutol (MIC of 7.64 µM), six compounds (**Pa-7**, **Pa-8**, **Pa-9**, **Pa-10**, **Pa-12** and **Pa-15**) were found to be more active but less active than isoniazid (MIC of 0.72 µM). Among the compounds tested, **Pa-9** the compound with the high activity against PS enzyme was found to be the most active in-vitro with MIC of 1.55 µM. The parent **Lead PI-11** possessed Mtb MIC of 54.81 µM. Thus the most active compound **Pa-9** was more potent than the parent compound. Thus this compound could be considered as the initial lead for further drug development process.

5.1.10. Effect of efflux pump inhibitors

Most of the molecules that showed good Mtb PS enzyme inhibition did not exhibit potent inhibition against Mtb including the parent lead compound. It could be due to involvement of wide array of efflux mechanisms mediated by several ABC (ATP-binding cassette) transporters and major facilitator superfamily (MFS) proteins, or antibiotic-modifying and degrading enzymes, to name a few possibilities. Multiple drugs like verapamil, reserpine, phenothiazines such as thioridazine, and piperine have been shown to inhibit bacterial efflux pumps in-vitro [Pages J.M., *et al*., 2009]. All the synthesized compounds were evaluated for their Mtb MIC at 10 μg/ml in the presence of reported efflux pump inhibitors verapamil and piperine. A 2 to 6 fold decrease in MIC value compared to that of in absence of efflux inhibitors was observed. In most of the cases except **Pa 10**, **Pa-13** and **Pa-19** (Table 5.6) potency improved 2 to 6 fold when compared to that in the absence of efflux pump inhibitors including isoniazid. With compounds **Pa-6, Pa-7** and **Pa-16** including ethambutol MICs were were found to be improved with one of the efflux inhibitor. The parent **Lead PI-11** possessed MIC of 13.70 μM and 27.40 μM in the presence of efflux inhibitor verapamil and piperine respectively.

The series of compounds **(Pa-1-Pa-3)** substituted benzodioxole and various R_2 substitutions showed good MIC values in the presence of both verapamil and piperaine. This might be due to the action of efflux pumps in the bacterial cell wall which could have effluxed the compounds from the outer membrane of the bacteria.

The series of compounds **Pa-4-Pa-7** and **Pa-16-Pa-19**, showed enhanced MIC values in the presence of efflux pump inhibitors. MIC values did not change much in the absence of efflux inhibitors for the compounds (**Pa-6, Pa-16**, and **Pa-19**). This showed that these compounds competed towards the efflux pump present in the bacterial cell wall and entered the cell wall to encounter the bacteria. This could also be attributed to localization of positively charged residues present in these compounds to have achieved optimal activity towards the bacteria.

Finally, the set of compounds **Pa-8-Pa-11** and **Pa-12-Pa-15** showed a decrease in MIC values in the presence of efflux inhibitors; while these compounds were found with good enzyme activity data in nanomolar range. In the absence of efflux inhibitors the MIC values were slightly higher. This experiment was an indication that efflux mechanism could be an important hurdle in the development of anti-tubercular drugs.

5.1.11. Effect of panothenate on activity

Further, the compounds were tested for Mtb MIC in the presence of 1 and 5 % pantothenic acid and there were no difference observed in MICs. In order for a pantothenate biosynthesis inhibitor to be effective, the supply of exogenous pantothenate must be exhausted. Further extensive studies should be carried out on daily intake in animal models or based on overexpression of PS to get a clear understanding.

5.1.12. Dormant anti-mycobacterial screening- Potassium deficient conditions

As discussed earlier, pantothenate is an essential precursor for the biosynthesis of acetyl-coenzyme A, which is a central intermediate in primary metabolism with roles in the TCA cycle as well as fatty acid and amino acid biosynthesis. The flux of carbon through acetyl-coenzyme A was particularly critical to non-replicating Mtb. Fatty acids, *via* breakdown to acetyl-coenzyme A and use of the glyoxylate shunt provided carbon for carbohydrate synthesis and thus acetyl-coenzyme A appear to be a gate through which much of the utilized carbon pool pass. Based on these reports, we examined for the most promising compounds for their activity against dormant bacilli under potassium deficient conditions. This assay was carried out at Institute of Russian academy of sciences, Moscow, Russia. Compounds **Pa-9** and **Pa-12** were tested for their activity against dormant 'non-culturable' Mtb bacilli at 20 and 100 μM concentrations. 'Non-culturable' cells obtained with low metabolic activity were characterized by marked phenotypic resistance to both isoniazid and rifampicin and were unable to form colonies onto agar solidified Sauton's medium but could be reactivated in liquid medium after special procedures of resuscitation. Thus these cells met the key criteria of dormancy and could be applied as a relevant tool for finding drugs for latent TB. For estimation of inhibitory effect of the compounds, the concentration of both treated and untreated 'non-culturable' cells recovered from dormancy were estimated by MPN assay with the use of statistical approaches. It was found that after treatment with compounds **Pa-9** and **Pa-12**, dormant 'non-culturable' cells were less able to recover from dormancy (Figure 5.18). Compound **Pa-12** caused a ~1-log decrease in the viability of dormant cells after incubation with 20 μM for 7 days. Although this effect was quite a modest one, the activity of this compound was comparable to rifampicin in relation to dormant Mtb. These compounds may be regarded as the prominent one for the development of derivatives which were more effective for dormant Mtb cells and latent TB.

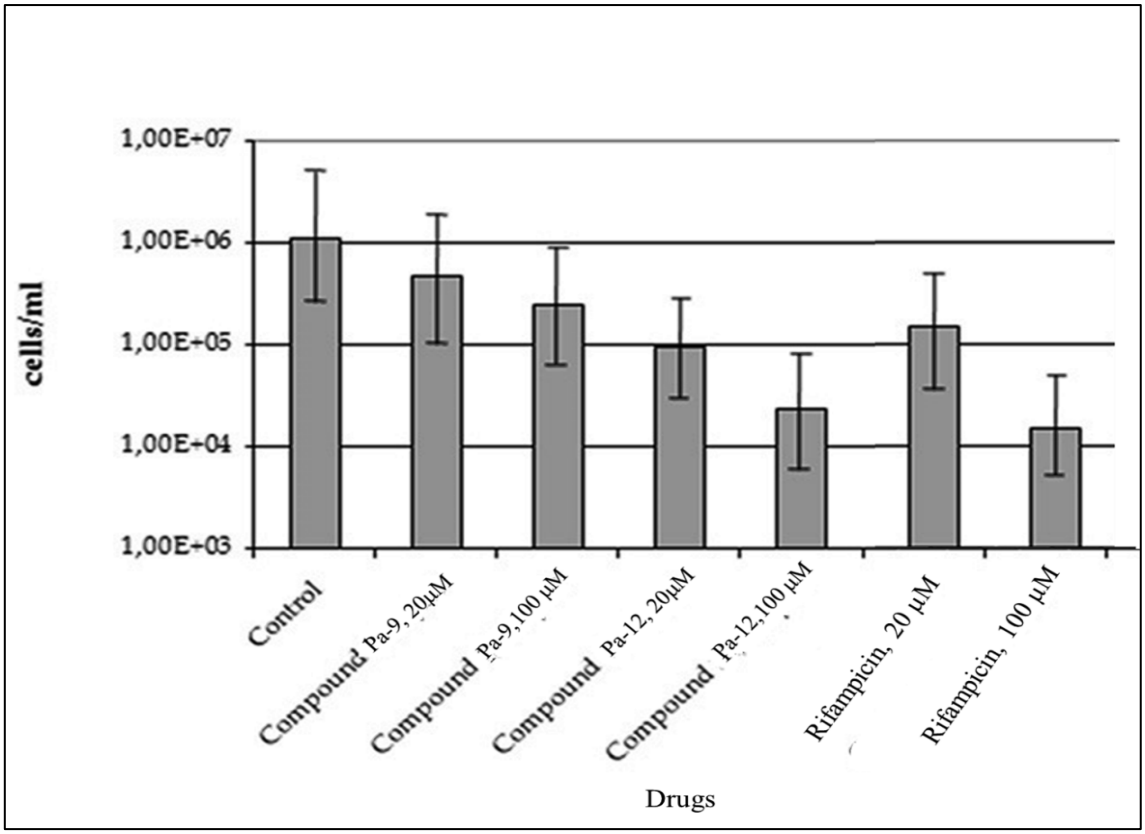

Figure 5.18: The effectiveness of the compounds **Pa-9** and **Pa-12** for killing Mtb dormant 'non-culturable' cells (The error bars represent 95% confidence limits)

5.1.13. In-vitro cytotoxicity evaluation for the synthesized compounds

The synthesized compounds were also tested for their in-vitro cytotoxicity against RAW 264.7 cells (Mouse macrophage) at a high concentration of 100 μM using MTT assay. Since Mtb bacterium resides inside macrophages we have used RAW 264.7 cells. The monocyte macrophage cell lines (RAW 264.7) are mostly used for TB research and compound toxicity studies. Percentage inhibition as reported in Table 5.6 indicated that the compounds inhibits in the range of 21.78-63.71%. The most promising compound **Pa-9** showed only 22.21% cytotoxicity at 100 μM and the selectivity index was >64. **Pa-1**, **Pa-3, Pa-4** and **Pa-5** were found to be toxic at 100 μM concentrations and compound **Pa-7**, **Pa-10**, **Pa-12** and **Pa-17** were found to be in the border line with almost 50% inhibition. Encouragingly, other synthesized molecules were relatively safe to be worked out from a pharmaceutical point of view as potential drug candidate for TB infection.

5.1.14. ADME predictions for the synthesized compounds

Finally, 19 synthesized leads were analysed for ADME prediction using QikProp module in Schrodinger. Predicted Caco-2 value for **Pa-11** was only found low**.** Also, the predicted % human oral absorption and blood brain barrier for all the compounds were found to be good.

With regard to logP predictions all compounds except **Pa-7** were found to be in the acceptable range. HERG toxicity being crucial was predicted for all compounds and was expected to be below -5. All the compounds were found to be safe with no potential cardiotoxicity as predicted by the software.

In the first subset (**Pa-1-Pa-3**) compounds substituted with 5-benzo[d][1,3]dioxole and with R_2 substituent of 1-naphthyl violated from rule of five drug like property. The molecular weight of these compounds were high and also due to high lipophilic nature (PlogP=5.7). Similarly, the compounds (**Pa-5-Pa-7**) substituted with 4-chlorophenyl violated the rule of five. This was due to high molecular weight and logP of the compounds. The most active compound (**Pa-9**) showed good predicted ADME properties. Further studies could be carried out for this compound to make this molecule a potent drug candidate. The ADME properties for the synthesized compounds are shown in Table 5.7.

Table 5.7: ADME predictions for the synthesized compounds

Compound ID	QPlogPo/w[a]	QPlogHERG[b]	QPPCaco[c]	QPlogBB[d]	% Human oral absorption[e]	Rule of 5[f]
Lead PI-11	2.949	-6.529	153.169	-1.711	83.321	0
Pa-1	4.707	-6.85	280.809	-1.763	85.369	1
Pa-2	3.71	-6.665	153.814	-2.061	74.854	1
Pa-3	5.705	-7.412	348.766	-1.709	79.937	2
Pa-4	3.716	-6.678	154.218	-2.063	74.907	1
Pa-5	6.182	-7.433	923.156	-1.023	90.299	2
Pa-6	5.386	-8.464	141.735	-2.277	71.069	2
Pa-7	-0.228	-9.205	321.864	-1.875	89.207	2
Pa-8	5.396	-8.47	144.151	-2.269	71.261	2
Pa-9	3.713	-7.103	296.72	-2.701	76.004	0
Pa-10	2.726	-6.911	656.471	-3.015	65.421	0
Pa-11	4.711	-7.685	18.128	-2.704	70.449	1
Pa-12	2.727	-6.913	237.572	-3.015	65.432	0
Pa-13	4.939	-7.096	285.734	-1.314	100	0
Pa-14	3.947	-6.893	154.07	-1.626	89.21	0
Pa-15	5.931	-7.677	343.379	-1.283	94.097	1
Pa-16	3.947	-6.895	154.143	-1.626	89.218	0
Pa-17	3.919	-6.723	280.894	-1.418	93.719	0
Pa-18	2.928	-6.548	141.714	-1.759	82.597	0
Pa-19	4.907	-7.351	321.769	-1.427	87.6	1

[a]Predicted octanol/water partition coefficient logP (acceptable range: −2.0 to 6.5); [b]Predicted IC_{50} value for blockage of HERG K+ channels.(below -5); [c]Predicted apparent Caco-2 cell permeability in nm/sec (<25 poor; >500 great); [d]Predicted brain/blood partition coefficient (-3.0 to 1.2); [e]Percent human oral absorption (<25% is poor and >80% is high); [f]Rule of 5 violation (mol_MW < 500, QPlogPo/w < 5, donorHB ≤5, accptHB ≤10)

5.1.14. Biophysical characterization for potential compounds

The interaction of the top active leads (**Pa-9** and **Pa-12**) with the protein and their ability to stabilize the protein was evaluated by measuring the fluorescence of the dye in presence of the native protein and protein-ligand complexes using DSF. It measured the thermal stability of a target protein and a subsequent increase in protein melting temperature would indicate binding of a ligand to the protein. Positive shift of T_m corresponding to native protein indicated increased stability due to inhibitor binding. Figure 5.19 and Figure 5.20 shows the melting curve of compounds **Pa-9** and **Pa-12**. The protein Mtb PS showed melting temperature T_m of 52.50 °C, whereas with compound **Pa-9** and **Pa-12** the corresponding T_ms were found to be 56.80 °C and 56.70°C respectively. Thus this study revealed that these compounds could bind to the protein which was indicated by the increased in protein

stability. Further this study indicated that these compounds could be further developed as valuable drug candidates against Mtb PS.

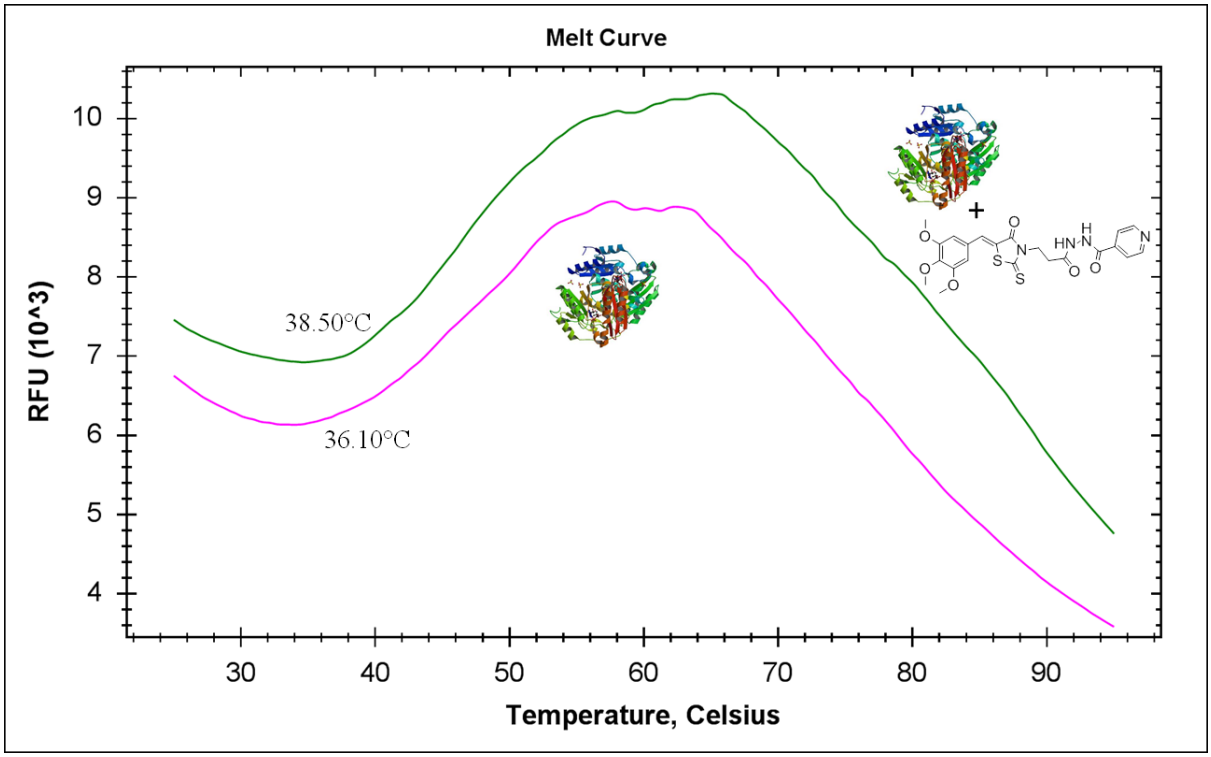

Figure 5.19: Melting curve of the top active compounds **Pa-9**

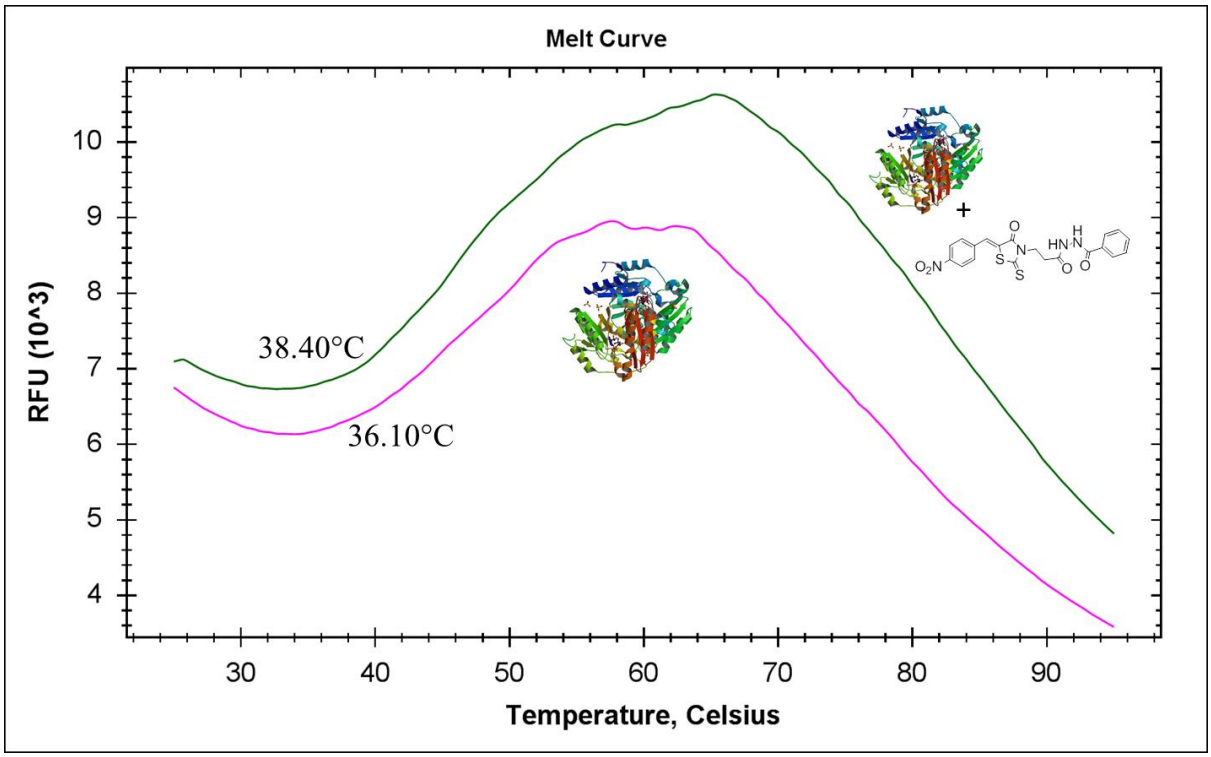

Figure 5.20: Melting curve of the top active compound **Pa-12**

5.2 DESIGN II: Mtb PS INHIBITORS BASED ON BOUND STRUCTURE WITH INHIBITOR

Mycobacterial PS inhibitors from previously reported literatures encouraged us to re-engineer the previously reported inhibitor 2-(2-(benzofuran-2-ylsulfonylcarbamoyl)-5-methoxy-1H-indol-1-yl) acetic acid [Hung A.W., *et al*., 2009] as a template to be utilized as starting point to design and develop inhibitors of Mtb PS. In the present study, the crystal structure of Mtb PS protein co-crystallized with this inhibitor [PDB ID: 3IVX] retrieved from the PDB was utilised as a structural frame work for virtual screening of the Asinex database to discover newer class of PS inhibitors (Figure 5.21). The goal of virtual screening (VS) was to search large chemical databases to find compounds that best matched a given query and also to reduce enormous virtual chemical space of small organic molecules, to a suitable number of compounds that could inhibit the protein with a highest chance to become drug candidates. HTVS, SP, and Glide XP docking options for virtual screening were used. Glide XP module of Schrödinger 9.2 (Glide, version 5.7, Schrödinger, LLC, New York, NY, 2011) was finally utilized for docking as it combined accurate, well defined physics-based scoring terms and thorough sampling of the terms.

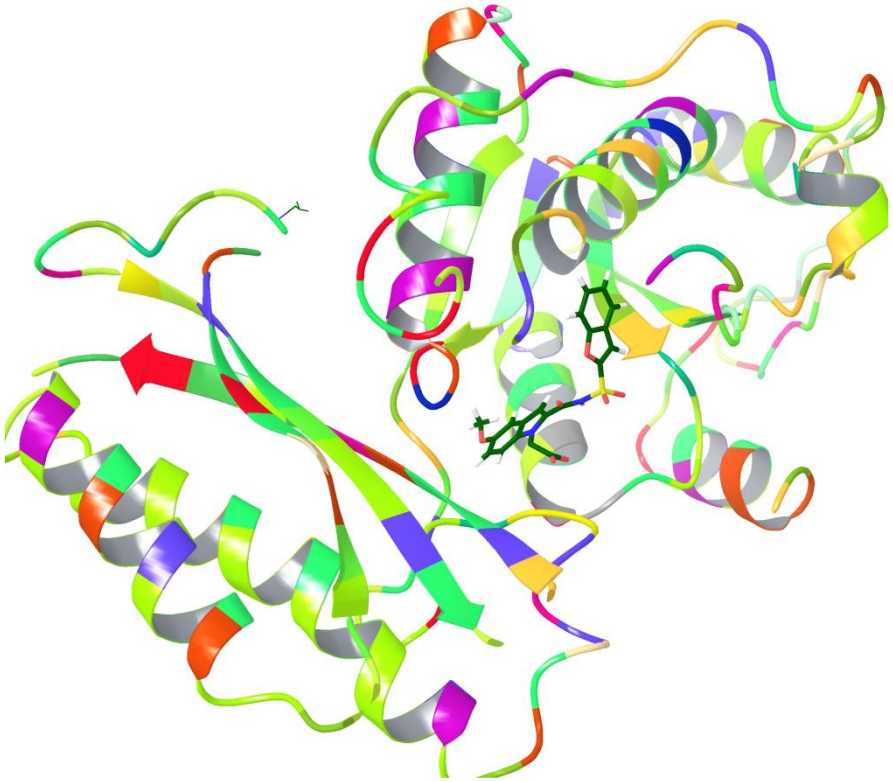

Figure 5.21: Crystal structure of Mtb PS bound with inhibitor (3IVX)

5.2.1. Protein preparation and active site validation of the Mtb PS protein

The retrieved protein was prepared using protein preparation wizard by adding hydrogen atoms, removing water molecules and minimizing energy by converging the heavy atoms using OPLS_2005 as force field. The orientations of the ligand in the active site pocket with the interactions between the ligand and protein atoms were visualized. The reference ligand showed a docking score of -9.75 kcal $mole^{-1}$. Closer analysis of the crystal structure bound with ligand showed key hydrogen bonding with His44, His47, Met40, Ser196, Ser197 and Val187, while the hydrophobic pocket included Pro38, Met40, Thr39, Phe157 and Leu50 residues. This additional hydrophobic wall could be utilized to design compounds against Mtb PS protein. The diagrammatic representation of docking crystal ligand towards the active site of protein and its ligand interaction diagram are shown in Figure 5.22.

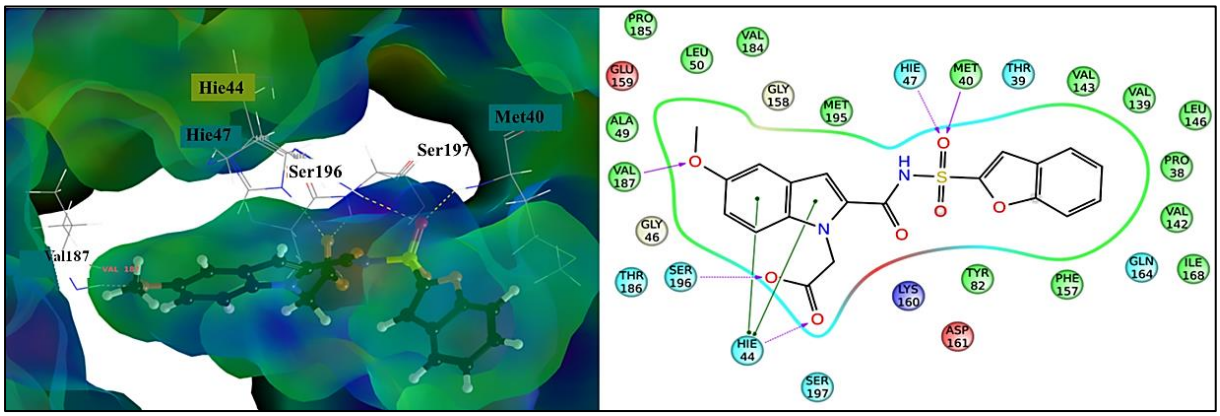

Figure 5.22: Binding analysis and ligand interaction diagram of reference ligand

The active site of the protein was located and grid files were generated using receptor grid generation panel. Grid size was calculated and is used for all docking analysis. The Grid box locating the active site pocket was found to be 18Å. Later, the "Write XP descriptor information" option was selected and "Compute RMSD" option was enabled and rest of the parameters were kept as default. The XP Glide score scoring function was used to order the best ranked compounds and the important interactions like π-cation and π-π stacking were analyzed using XP visualizer in Glide module. The input RMSD of the crystal ligand was also ascertained. To validate the methods in prediction of binding energy and possible interaction between ligands and receptor, at first existing ligand in crystal structure was re-docked in 3IVX. After superimposition, RMSD <2Å was gained and showed that this technique could be applied for next predictions. The RMSD of re-docked ligand and original crystal ligand was found to be 1.13Å. The superimposition of docked pose and crystal ligand towards the active site of the protein is depicted in Figure 5.23**.**

Figure 5.23: Superimposition of docked pose and crystal ligand towards the active site of the protein (Where, Pink represents the original pose of crystal ligand Orange represents the docked pose of crystal ligand)

5.2.2. E-pharmacophore generation

The e-pharmacophore method which combined the aspects of structure-based and ligand was explored for the Mtb PS protein in this study. The result of XP docking was used to determine the pharmacophoric features of the protein. Pharmacophore hypotheses were developed by mapping Glide XP energetic terms onto pharmacophore sites, with the basis of structural and energy information between protein and ligand. The initial number of pharmacophore sites was set up to 10 for the crystal structure. The generated e-pharmacophore showed three aromatic rings (R) required for the hydrophobic interaction within the pocket namely R9 (score -0.56), R11 (score -1.14) and other R12 (score -0.93) together with acceptor site namely A having energy scores -0.35 and one negative ionizable (N) group with the score of -0.76. On an average, there were 7 sites per hypothesis, many of which did not even appear to be directly involved in protein-ligand interactions. For a specified ligand there would be many different pharmacophore sites, in most cases within this pharmacophore it will be difficult to find out which site contribute to the activity. Hence based on energy score and distance between each pharmacophore points of the hypothesis we

made the combination of pharmacophore having 5, 4 and 3 point features totalling to 6 combinations as represented in Table 5.8.

5.2.3. E-pharmacophore validation

The best six hypotheses were taken and validation was performed using decoy set containing 1000 inactives along with 28 Mtb PS reported inhibitors [Samala G., *et al*., 2013; Alvin W., *et al*., 2009; Yang Y., *et al*., 2011; White E L., *et al*., 2007 and Velaparthi S., *et al*., 2008]. Hypothesis 2, a four point model (RRRN) containing three aromatic rings (R) and one negative ionizable group (N) displayed good enrichment factor (EF), goodness of hit (GH) and satisfied all other validation parameters of a true pharmacophore model. Similarly, hypothesis 5, a three point model (RRA) containing two aromatic rings (R) and one hydrogen acceptor (A) also yielded all validation parameters of a true pharmacophore model. Though the hypothesis 6 exhibited higher EF, other parameters like GH and %A were not acceptable. From the overall validations, we could conclude that hypothesis 2 (RRRN) and hypothesis 5 (RRA) could predict most of the experimentally active molecules than the remaining four hypotheses that were compared. The results are as shown in Table 5.6, where hypothesis 2 and hypothesis 5 showed good enrichment at 1% (EF1%) and Goodness of hit values compared with other hypotheses.

Table 5.8: E-pharmacophore hypothesis and its validation

Hypothesis	E-pharm features	No.of actives	EF	GH	%Yield	%A
1	5features(R12,R9,R11,A4,N7)	23	0.91	0.04	2.50	82.14
2	4features (R12,R9,R11,N7)	22	1.88	0.13	5.14	78.57
3	4features (R12,R9,R11,A4)	22	0.95	0.037	2.61	78.50
4	3features (R12,R11,N7)	1	0.63	0.02	1.72	3.44
5	3features (R12,R11,A4)	16	1.69	0.10	4.62	57.72
6	3features (R12,R11,R9)	15	1.86	0.04	5.06	53.57

EF: Enrichment factor; GH: Goodness of hit; %A: Actives

Thus the four point and three point e-pharmacophore models were selected for the virtual screening of commercial database (Asinex). The selected e-pharmacophores are shown in Figure 5.24.

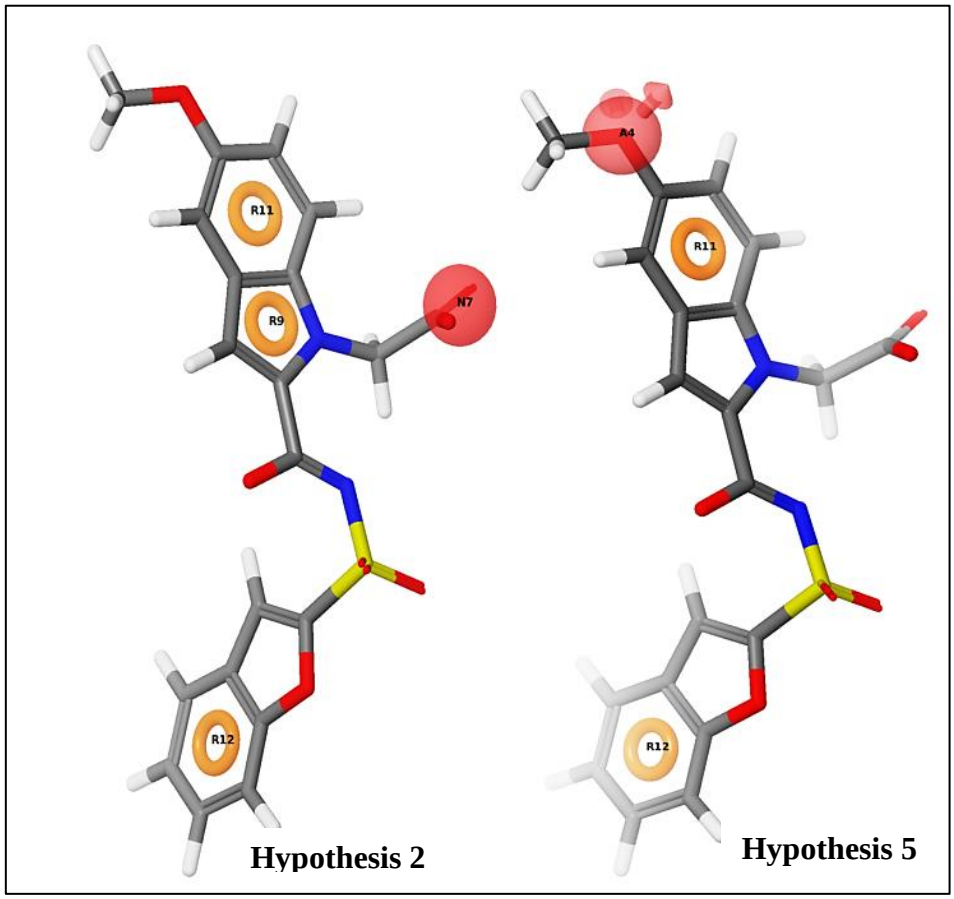

Figure 5.24: Selected e-pharmacophoric hypotheses

5.2.4. Virtual screening of molecules and docking

Virtual screening is of cardinal importance in in-silico drug discovery process to speed up drug development, where it helps in the selection of the best candidate drug. The virtual screening protocol reported in this study was based on the application of sequential filters to select a restricted number of compounds. The validated e-pharmacophore models (hypothesis 2 and hypothesis 5) were used in turn to screen the 500000 compounds of the Asinex database. First using the option implying "phase find matches" hypothesis in Maestro to filter the compounds based on the fit value was used. Fit value was used to check how effectively the ligand fitted to the e-pharmacophore model. In this study, the hits retrieved by the two e-pharmacophore models with a fit value above 1.0 were carried for HTVS. About 11978 hits from HTVS with the docking score of ≤ -6.0 kcal mol^{-1} were subjected to another docking using Glide SP. The selected 270 hits of from preliminary screening were taken to Glide XP

docking. A total of 70 ligands were selected for Glide XP docking. The results of the virtually screened ligands using Glide XP helped us to find accurately the hydrogen-bond interactions, electrostatic interaction, hydrophobic interactions and π-π stacking interactions. The results showed that the docking score ranged from -7.471 to -10.523 kcal mol^{-1}. The docking score of the crystal ligand was -9.75 kcal $mole^{-1}$. In addition to docking scores, final short listing of possible lead molecules were based on visual inspection of important interacting amino acids like Val187, Ser196, Hie44, Hie47 and Met40 residues as reported for the crystal inhibitor bound to PS protein. The active site of the protein with the ligand was figured using ligand interaction diagram in Schrodinger suite. Finally top 14 hits were shortlisted and the selected hits were well fit to the active site of the protein. The shortlisted scaffolds as hits belonged to diverse scaffolds like piperazine, imidazole, thiazole, pyridine, dimethyl benzyl furoyl, pyrrolidine, furan, formamide, pentamide derivatives. The structures of all the selected hits are depicted in Figure 5.25.

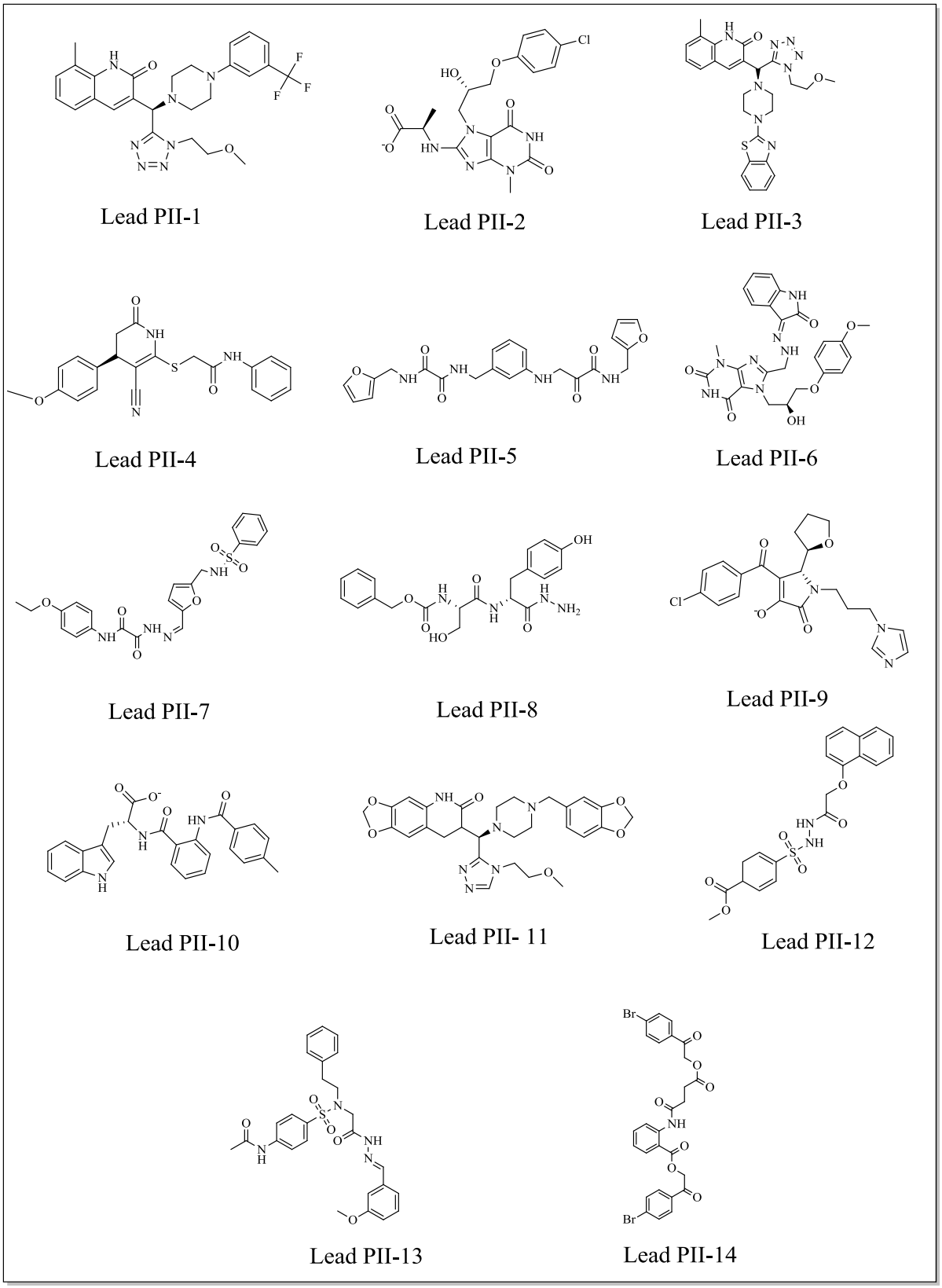

Figure 5.25: Structure of the selected hits molecules by virtual screening

The 14 selected compounds with their fitness values, docking score, hydrogen bonding and ligand interactions are tabulated in Table 5.9. Compared to the crystal ligand, hits **PII-1** and **PII-2** were found to be better and with regard to hydrogen bonding interactions. Hit compounds **PII-2** and **PII-5** were found to show one extra interaction.

Table 5.9: Computational profile of the selected compounds

Compound ID	Fitness	Docking score	Hydrogen bond	Ligand interactions
Crystal ligand	1.568	-9.75	5	Val187, Ser196, Hie44, Hie47, Met 40
Lead PII-1	1.702	-10.117	6	Lys160, Ser197, Hie44, Met195
Lead PII-2	1.942	-10.071	8	Asp161, Gly158, Hie44, Ser197, Ser196, Val187, Gly46
Lead PII-3	1.676	-9.664	7	Ser197, Ser196, Hie44, Lys160, Met195
Lead PII-4	2.421	-10.816	7	Gln164, Ser197, Ser196, Pro38, Gly158, Val187
Lead PII-5	1.668	-10.691	8	Gln164, Pro38, Hie44, Lys160, Ser197, Asp161, Ser196
Lead PII-6	2.105	-10.274	6	Pro38, Val187, Gln164, Lys160, Arg198, Ser197
Lead PII-7	2.226	-10.198	7	Met40, Pro38, Asp161, Lys160, Hie44, Ser197, Gln72
Lead PII-8	2.081	-9.803	7	Gly158, Gln164, Gln72, Hie47, Ser196, Ser197, Asp161, Lys160
Lead PII-9	1.126	-8.713	5	Gln72, Ser197, Ser196, Hie44
Lead PII-10	1.594	-8.401	5	Hie44, Hie47, Ser197, Ser196, Lys160
Lead PII-11	1.825	-9.281	7	Lys160, Hie44, Ser197, Ser196, Val187
Lead PII-12	2.08	-9.135	5	Gln164, Asn161, Lys160, Hie44, Val187
Lead PII-13	2.158	-9	6	Ser196, Val187, Hie44, Hie47, Ser197, Met40
Lead PII-14	1.622	-12.845	7	Arg198, Gln164, Gly158, Ser197, Ser196, Asp161, Hie44

The selected lead compounds were visually inspected for its interaction pattern of amino acids. The ligand interaction diagram for the top 14 hits compounds were depicted in Figures 5.26, 5.27 and 5.28. The common interacting amino acids retained in all the ligand were Ser197/Ser196, Val187 and Hie44.

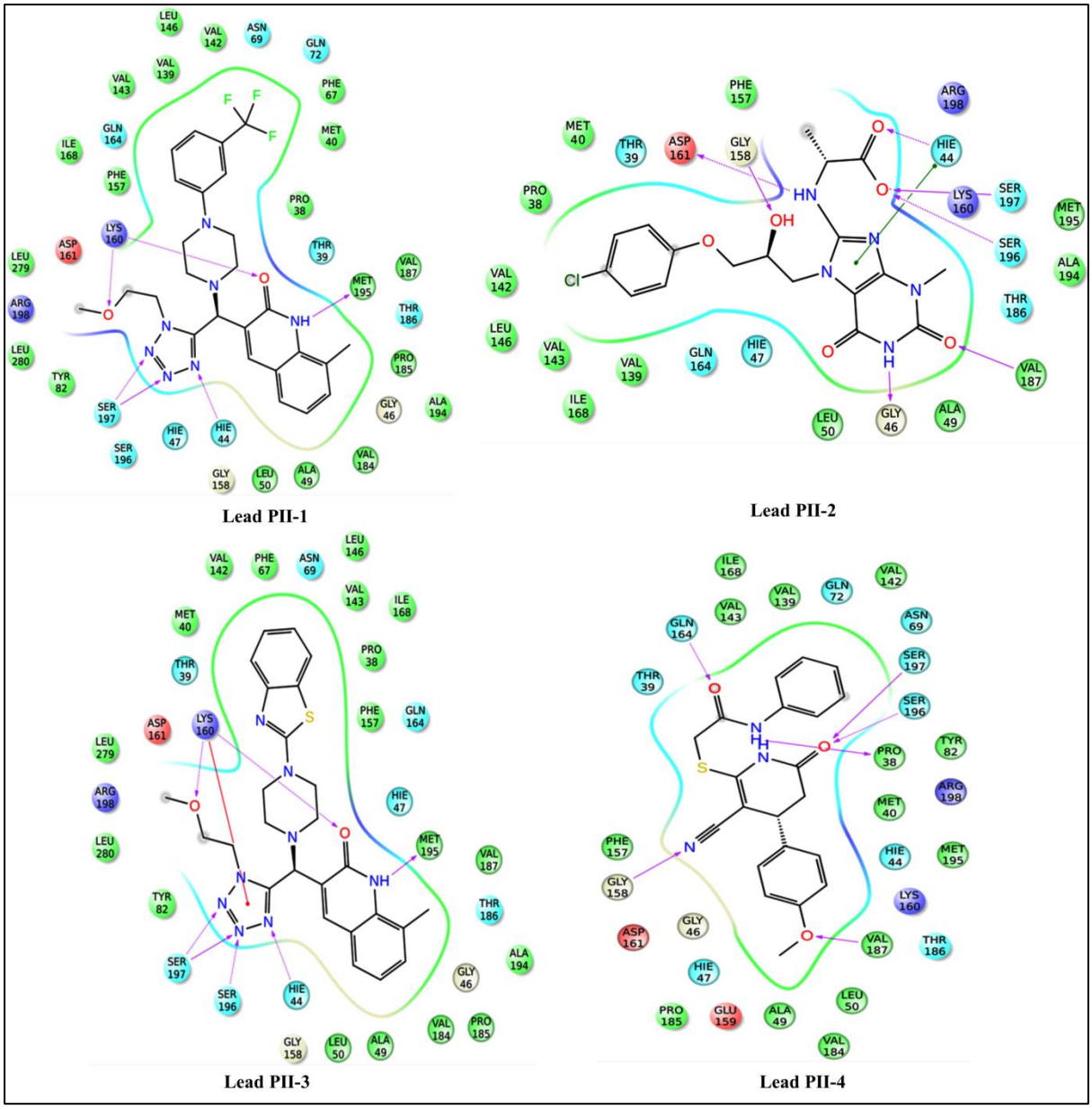

Figure 5.26: Ligand interaction diagram for the selected hits by virtual screening (**Lead PII-1- PII-4**)

As seen in Figure 5.26, among the leads **PII-1-PII-4**, only lead **PII-2** had multiple interactions with Hie44 with hydrogen bonding and π-π stacking. Except **PII-1** all the leads exhibited hydrogen bonding with Ser197 while **PII-1** showed similar interaction with Ser197. Similarly Val187 interaction was exhibited by **PII-2** and **PII-4**, while the hydrogen bonding interactions with Hie47 and Met40 were missing in these compounds.

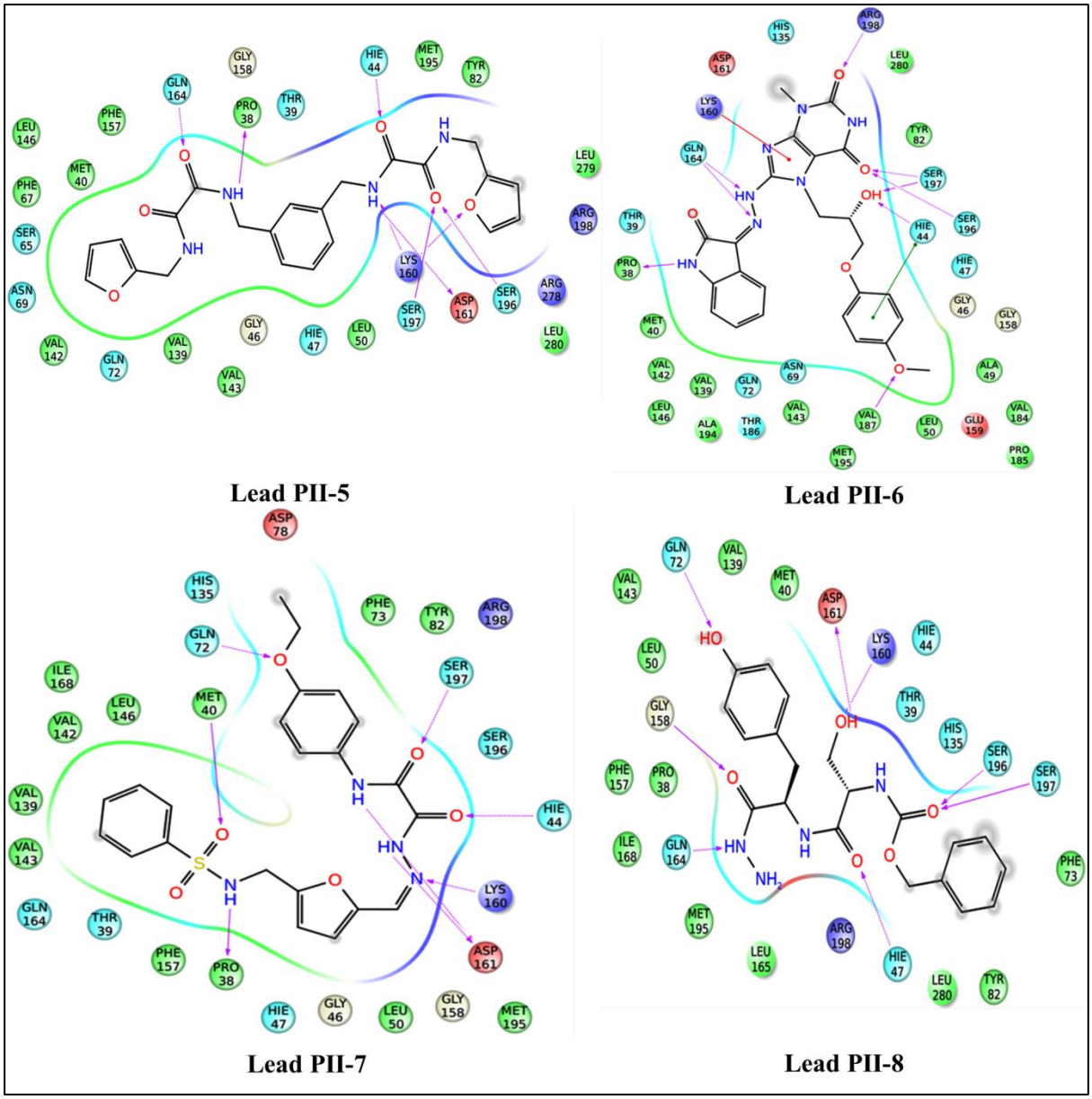

Figure 5.27: Ligand interaction diagram for the selected hits by virtual screening (**Lead PII-5- PII-8**)

In Figure 5.27, the interaction diagram for **Leads PII-5- PII-8** revealed that Hie44 interaction was missing with **PII-8**; while **PII-5** and **PII-7** exhibited only hydrogen bonding with Hie44. The **PII-6** was found to exhibit π-π stacking with Hie44. All the compounds except **PII-7** exhibited interaction with Ser196 /Ser197.

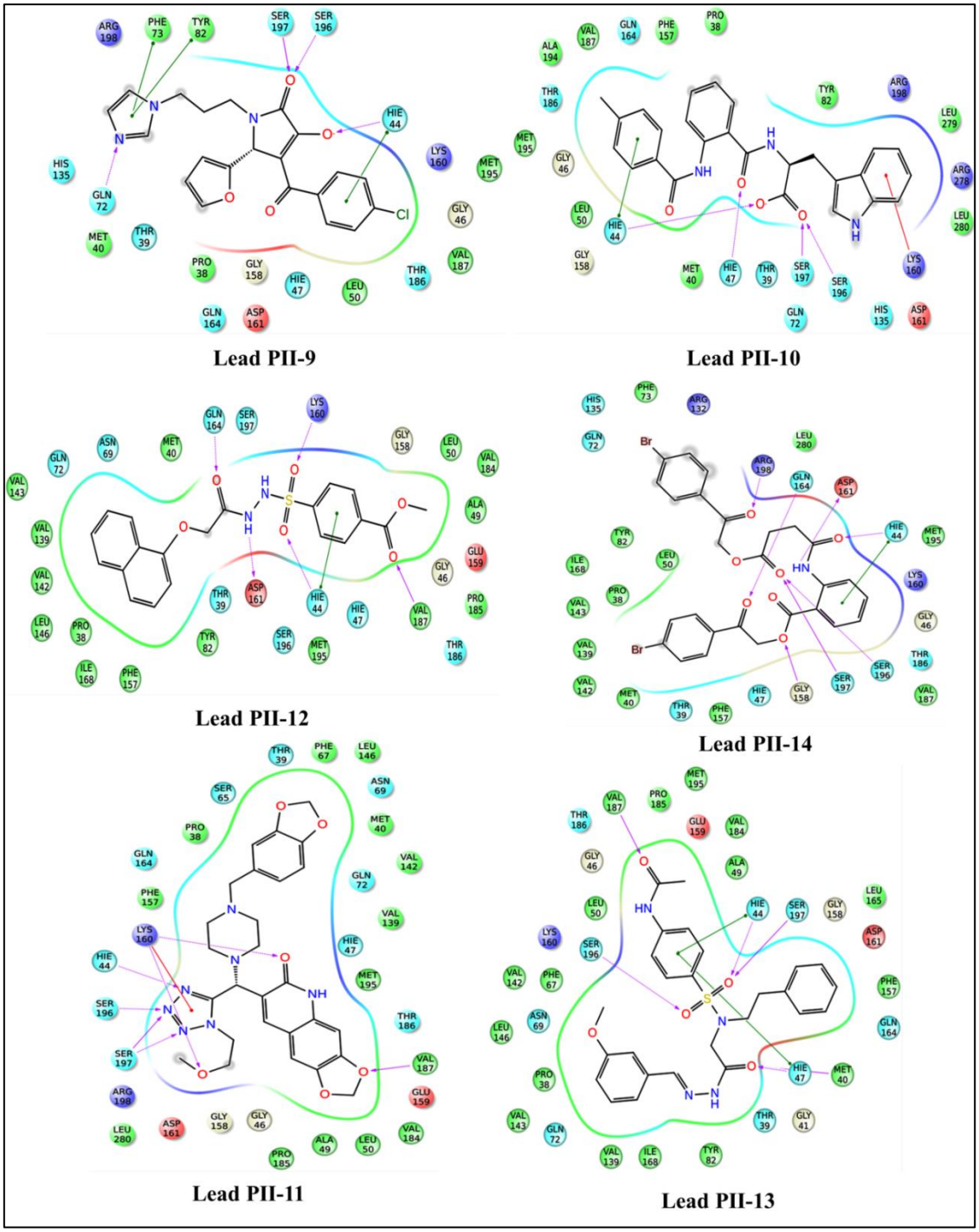

Figure 5.28: Ligand interaction diagram for the selected hits by virtual screening (**Lead PII-9- PII-14**)

As seen in the Figure 5.28, among the compounds **PII-9**-**PII-14**, almost all the hit compounds showed multiple hydrogen bonding interactions. **PII-13** exhibited interaction with Met40 as like crystal ligand, whereas other in other hits this interaction was not found. Similarly, there was an additional positively charged amino acid Lys300 interacting with **PII-**

10, **PII-11** and **PII-12**. Similarly, there were extra two π-π stacking interactions (Phe73 and Tyr82) present only in **PII-9**.

5.2.5. ADME predictions for the designed compounds

ADME predictions could help in identifing selected compounds with pharmaceutical importance which can be further developed into a drug molecule. All the selected compouds were subjected to in-silico ADME properties using QikProp module in Schrodinger. The predicted logP values for the designed compounds were found to be acceptable and the predicted HERG property was also found acceptable except **Lead PII-2** and **Lead PII-10**. Similarly, the blood brain barrier predicted values are in the range *i.e.* -3 to 1.2. The compounds **Lead PII-2** and **Lead PII-8** were found to have less Caco-2 property indicating problems with permeation and absorption through intestine. The predicted % human oral absorption values for the compounds **Lead PII-3**, **PII-4**, **PII-9**, **PII-10**, **PII-11**, **PII-13** and **PII-14** were high (>80%) which implied that the bioavailability of these compounds could be high. The leads (**PII-5** and **PII-6**) were found to have more than one violation which need to be considered seriously during further development. The ADME predictions for the selected compounds were tabulated in the Table 5.10.

Table 5.10: ADME predictions for the designed compounds

Compound ID	QPlogPo/w[a]	QPlogHERG[b]	QPPCaco[c]	QPlogBB[d]	% Human oral absorption[e]	Rule of 5[f]
Lead PII-1	3.737	-6.905	133.187	-0.583	73.892	1
Lead PII-2	2.135	-3.659	10.033	-2.383	44.411	1
Lead PII-3	2	-5.379	217.277	-1.538	82.489	0
Lead PII-4	3.05	-5.107	327.502	-1.121	89.82	0
Lead PII-5	1.76	-7.061	86.03	0	45.962	2
Lead PII-6	2.058	-5.681	74.913	-2.317	46.631	2
Lead PII-7	3.606	-7.232	226.742	-2.025	80.216	0
Lead PII-8	1.485	-5.408	11.906	-3.382	41.933	1
Lead PII-9	3.023	-5.75	523.914	-1.031	93.314	0
Lead PII-10	4.792	-4.165	90.669	-1.512	85.516	0
Lead PII-11	3.66	-7.768	96.3	-2.659	83.879	0
Lead PII-12	2.165	-5.556	178.078	-1.591	79.903	0
Lead PII-13	4.067	-7.57	263.341	-2.092	81.125	1
Lead PII-14	4.827	-7.613	183.258	-1.863	82.756	1

[a]Predicted octanol/water partition coefficient logP (acceptable range: −2.0 to 6.5); [b]Predicted IC_{50} value for blockage of HERG K+ channels.(below -5); [c]Predicted apparent Caco-2 cell permeability in nm/sec (<25 poor; >500 great); [d]Predicted brain/blood partition coefficient (-3.0 to 1.2); [e]Percent human oral absorption (<25% is poor and >80% is high); [f]Rule of 5 violation (mol_MW < 500, QPlogPo/w < 5, donorHB ≤5, accptHB ≤10)

5.2.6 Biological assessments

Further to prove the design concept, the final hits were procured from Asinex database, and subjected to Mtb PS enzyme inhibition study, anti-mycobacterial screening and toxicity studies. The lead compounds were assayed for Mtb PS inhibition utilizing the assay that catalysed the ATP-dependent condensation of pantoate and β-alanine to form pantothenate, AMP and pyrophosphate. The formation of AMP from Mtb PS catalysed reaction was coupled with reactions through myokinase, pyruvate kinase and lactate dehydrogenase. The decrease in the absorbance of NADH was spectrophotometrically monitored at 340 nm. In the initial screening at 50 µM, all the compounds showed more than 50% inhibition against Mtb PS and were further studied for IC_{50} measurements with varying concentrations. The results are tabulated in Table 5.11.

Table 5.11: Biological evaluation for the designed compounds

Compound ID	IC_{50} µM	Compound ID	IC_{50} µM
Lead PII-1	>50	**Lead PII-8**	14.98±0.04
Lead PII-2	11.36±0.05	**Lead PII-9**	16.5±0.02
Lead PII-3	10.77±0.06	**Lead PII-10**	6.63±0.08
Lead PII-4	2.81±0.04	**Lead PII-11**	4.27±0.08
Lead PII-5	2.18±0.02	**Lead PII-12**	>50
Lead PII-6	>50	**Lead PII-13**	23.33±0.01
Lead PII-7	4.04±0.02	**Lead PII-14**	8.75±0.02
Crystal ligand	1.8 (K_d)		

K_d=Dissociation constant

All of the lead compounds inhibited Mtb PS activity with IC_{50}s values ranging from 2.18-23.33 µM except **Leads PII-1, PII-6** and **PII-12** which exhibited >50 µM. The most active molecule was found to be Lead **PII-5** with IC_{50} of 2.18 ± 0.02 µM. Other promising hits included **Lead PII- 4**, **Lead PII- 7**, **Lead PII- 10**, **Lead PII- 11** and **Lead PII- 14** that exhibited IC_{50}'s less than 10 µM. But all the leads designed were less potent than crystal ligand, which has K_d value of 1.8 µM Diagrammatic representation of potent molecule **Lead PII- 5** is shown in Figure 5.29.

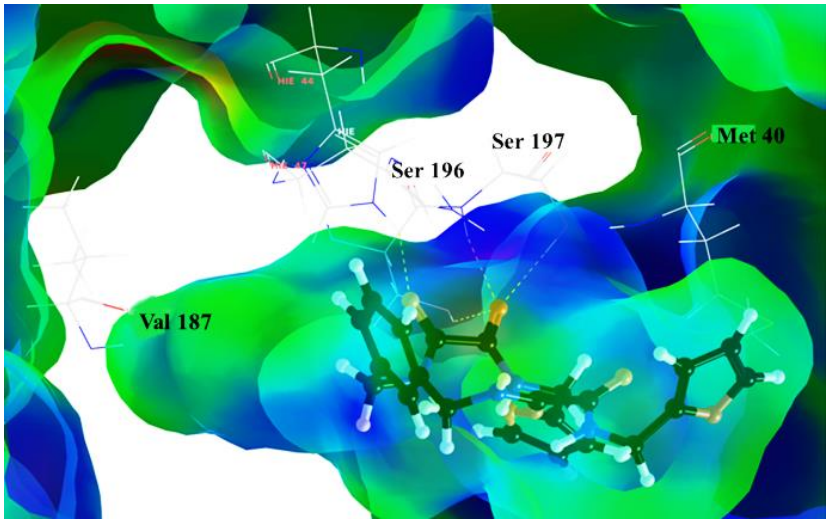

Figure 5.29: Binding analysis and ligand interaction diagram for the top active compound (**Lead PII-5**)

The **Lead PII-10** with the closer analysis revealed that the compound was associated with four hydrogen bonding towards the active site of the protein. The toluene ring in the compound was stabilized with π-π stacking interaction with Hie44. Also, the phenyl ring in the right side of the compound was stabilized with positively charged amino acid Lys160. The compound is well fitted into non-polar amino acid pockets which make the molecule more lipophilic and further modification with this site would easily penetrate into the cell wall of mycobacteria as shown in Figure 5.30.

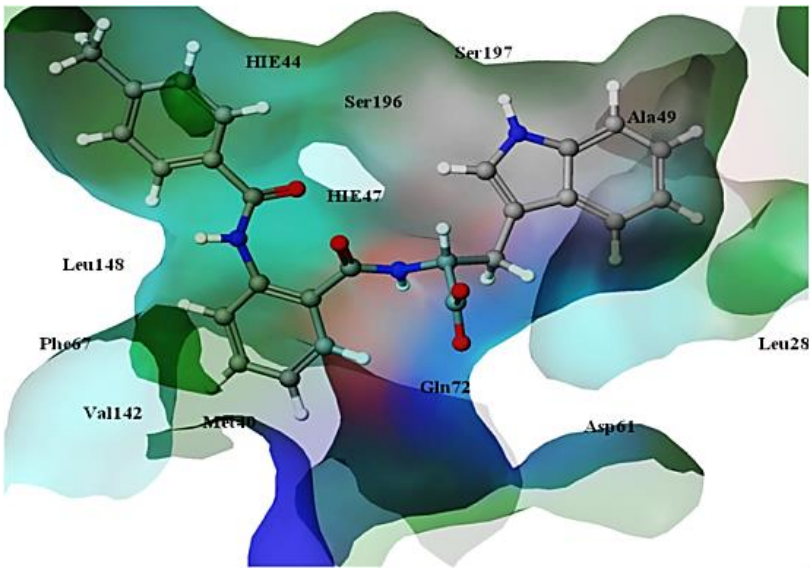

Figure 5.30: Binding analysis for the compound **Lead PII-10**

5.2.7. Lead optimization using medicinal chemistry

Based on the preliminary screening of hits identified by the in-silico modelling, it was evident that e-pharmacophore hypothesis employed in the study was successful in lead identification. To further our medicinal chemistry quest to improve the activity of lead compounds, we attempted to structurally modify **Lead PII-10** to improve the potency and also better understand a structure-activity relationship. The major reason for selecting **PII-10** was due to scaffold similarity with the crystal ligand and good drug- like properties. Considering these properties, we selected **PII-10** as the starting parent molecule to derivatize series of analogues. About 16 compounds with modification of several groups like 2-pyrazine, cyclohexyl, cyclopentyl, 2-thiophene, 4-fluorophenyl, 4-methoxylbenzyl, 2-trifluoromethyl phenyl, 2, 3 and 4-chlorophenyl, 2-furoyl, 3 and 4-nitrophenyl, phenyl, 2-fluoro and 4-*tert*-butyl phenyl were modified at R position. The scheme utilized for synthesizing the compounds was shown in Figure 5.31 and detailed procedures along with structural characteristics are provided in annexure II at the end of the thesis.

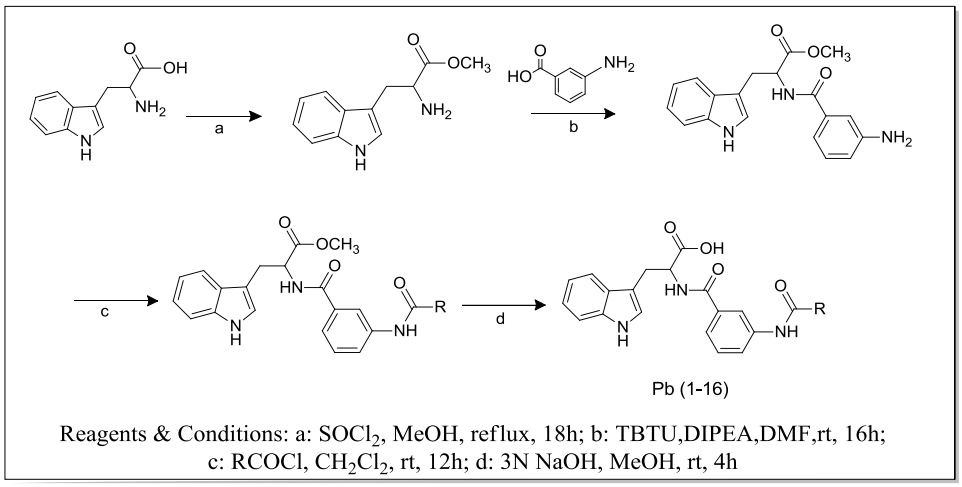

Figure 5.31: Scheme utilized for developing Mtb PS leads-inhibitor based approach

The target molecules were synthesized by following a four step synthetic scheme starting with a commercially available, less expensive 2-amino-3-(1H-indol-3-yl)propanoic acid (**1**). In the first step, the acid group was protected as methyl ester. Then the obtained methyl 2-amino-3-(1H-indol-3-yl)propanoate (**2**) was treated with 3-aminobenzoic acid, TBTU and DIPEA in DMF to afford methyl 2-(3-aminobenzamido)-3-(1H-indol-3-yl)propanoate derivative (**3**). Corresponding acid chlorides were utilized to synthesise final compounds **(Pb-1-Pb-16)**

5.2.8. In-vitro PS inhibition assay for the synthesized leads

The synthesized compounds (**Pb-1-Pb-16**) were evaluated for their in-vitro enzymatic inhibition assay. The coupled assay was found to prove that compounds synthesised were specific towards Mtb PS and were not active against enzymes used in the reaction. The R-position was substituted with different aromatic groups inorder to maintain bulky, hydrophobic group at the protein. Among the synthesized compounds, about six compounds (**Pb-5**, **Pb-8**, **Pb-12**, **Pb-14**, **Pb-15** and **Pb-16**) were found to be more efficient than the parent **Lead PII-10** with IC_{50}s less than 6 µM. Compound **Pb-5** with 4-fluorophenyl substitution was found to exhibit highest activity data with an IC_{50} of 2.28±0.03 µM. Hence post lead optimization, compound **Pb-5** emerged to be three times more potent than the parent molecule (**Lead PII-10**) having IC_{50} of 6.63±0.08 µM. The IC_{50}s, MICs and cytotoxicity results of all 16 compounds are represented in Table 5.12.

Table 5.12: Biological activity data for the synthesized compounds

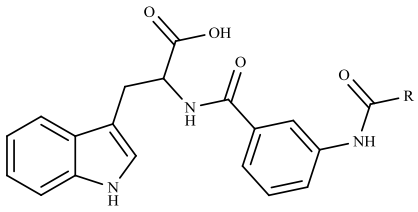

Compound ID	R	IC_{50} (μM)[a]	MIC(μM)[b]	% Cytotoxicity 50μM[c]
Lead PII-10	4-Methyl phenyl	6.63±0.08	56.80	38.16±0.89
Pb-1	2-Pyrazine	10.68±0.02	56.37	48.15±0.01
Pb-2	Cyclohexyl	7.74±0.04	55.86	25.19±0.27
Pb-3	Cyclopentyl	7.14±0.08	28.83	38.20±1.24
Pb-4	2-Thiophene	9.30±0.01	55.86	40.22±2.01
Pb-5	4-Fluoro phenyl	2.28±0.03	27.20	24.84±1.09
Pb-6	4-Methoxybenzyl	15.63±0.06	13.25	63.35±2.01
Pb-7	2-Trifluoromethyl phenyl	8.52±0.01	24.53	32.12±2.85
Pb-8	4-Chlorophenyl	5.23±0.05	52.53	22.69±1.19
Pb-9	3-Chlorophenyl	10.87±0.08	52.53	43.34±2.13
Pb-10	2-Furoyl	6.82±0.04	28.97	37.03±1.22
Pb-11	2-Chlorophenyl	10.06±0.06	52.53	53.59±2.41
Pb-12	3-Nitrophenyl	2.86±0.07	51.39	43.52±1.13
Pb-13	4-Nitrophenyl	9.59±0.04	102.79	32.21±0.95
Pb-14	Phenyl	3.59±0.06	28.34	39.86±0.76
Pb-15	2-Fluoro	5.68±0.02	54.41	56.29±0.94
Pb-16	4-*tert*-Butyl phenyl	4.47±0.01	12.56	50.34±0.51
	Isoniazid	ND	0.72	NIL
	Ethambutol	ND	7.64	NIL

[a]Mtb PS enzyme inhibitory assay; [b]Minimum Inhibitory concentration against Mtb H37 Rv; [c]% inhibition of HEK293 cells. ND indicates not determined

The dose response curve for the compound **Pb-5** was plotted against log of concentration of inhibitor and % inhibition using Graph pad prism software (Figure 5.32).

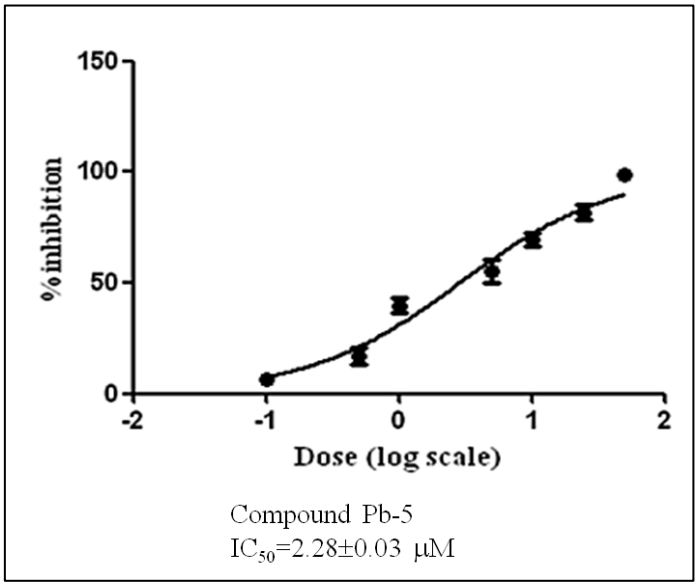

Figure 5.32: Dose response curve for the top active compound **Pb-5**

Compounds substituted with 2-pyrazinyl, 2-thiophene, methoxy benzoyl and 2-furoyl at R-position exhibited IC_{50}s in the range of 6.82 μM-15.63 μM. These molecules exhibit common π-π interaction with Hie44 except **Pb-6** as shown in Figure 5.33. The prominent hydrogen bonding interactions with Ser197 and Asp161 were found to be associated in all these molecules. Due to lack of hydrogen bonding with Gln72 and Ser196 make the molecule **Pb-6** less potent than other compounds (**Pb-1**, **Pb-4** and **Pb-10**).

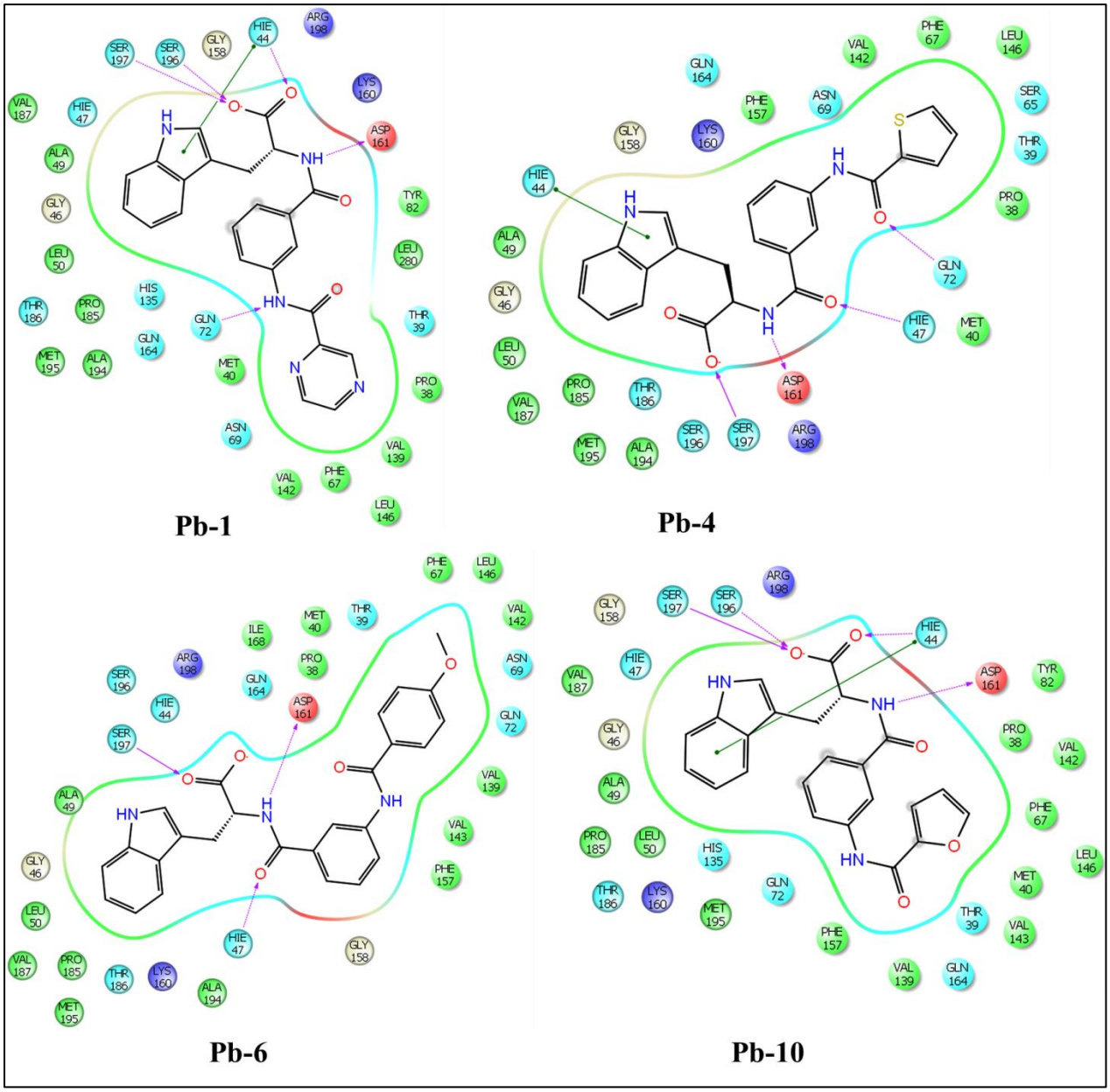

Figure 5.33: Ligand interaction diagram for the compound **Pb-1, Pb-4, Pb-6** and **Pb-10**

Compounds substituted with cyclohexyl and cyclopentyl ring exhibit similar IC_{50} values (7.74 μM and 7.14 μM). The orientation of both the molecules was quite similar. The additional hydrogen bonding with Gln72 in **Pb-2** changes in the PS inhibitory data with the IC_{50} of 7.74 μM. The ligand interaction diagram for the compound **Pb-2** and **Pb-3** was shown in Figure 5.34.

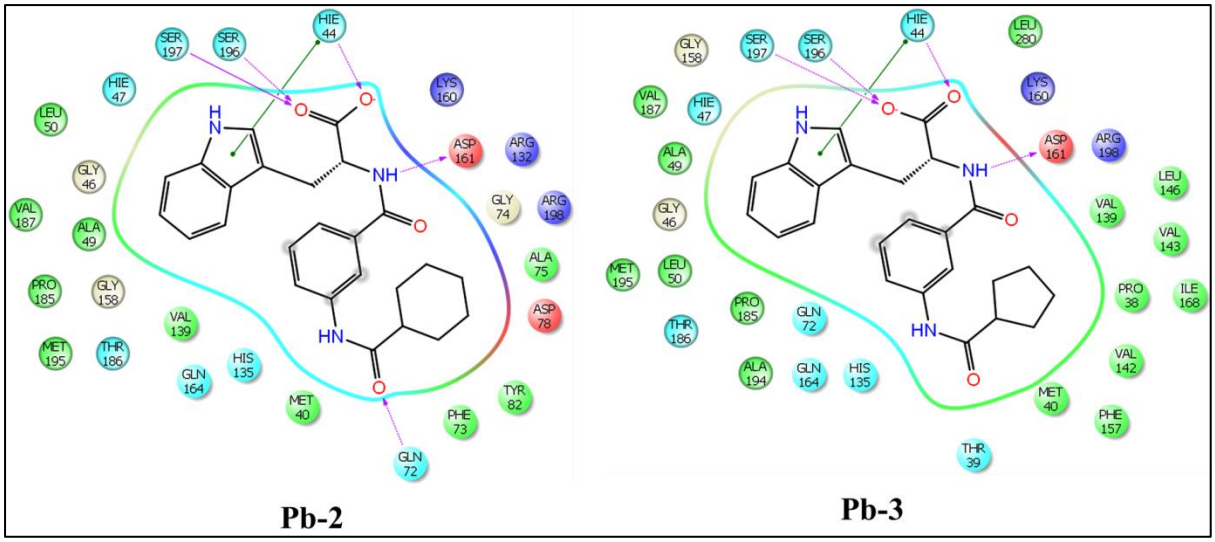

Figure 5.34: Ligand interaction diagram for the compound **Pb-2**and **Pb-3**

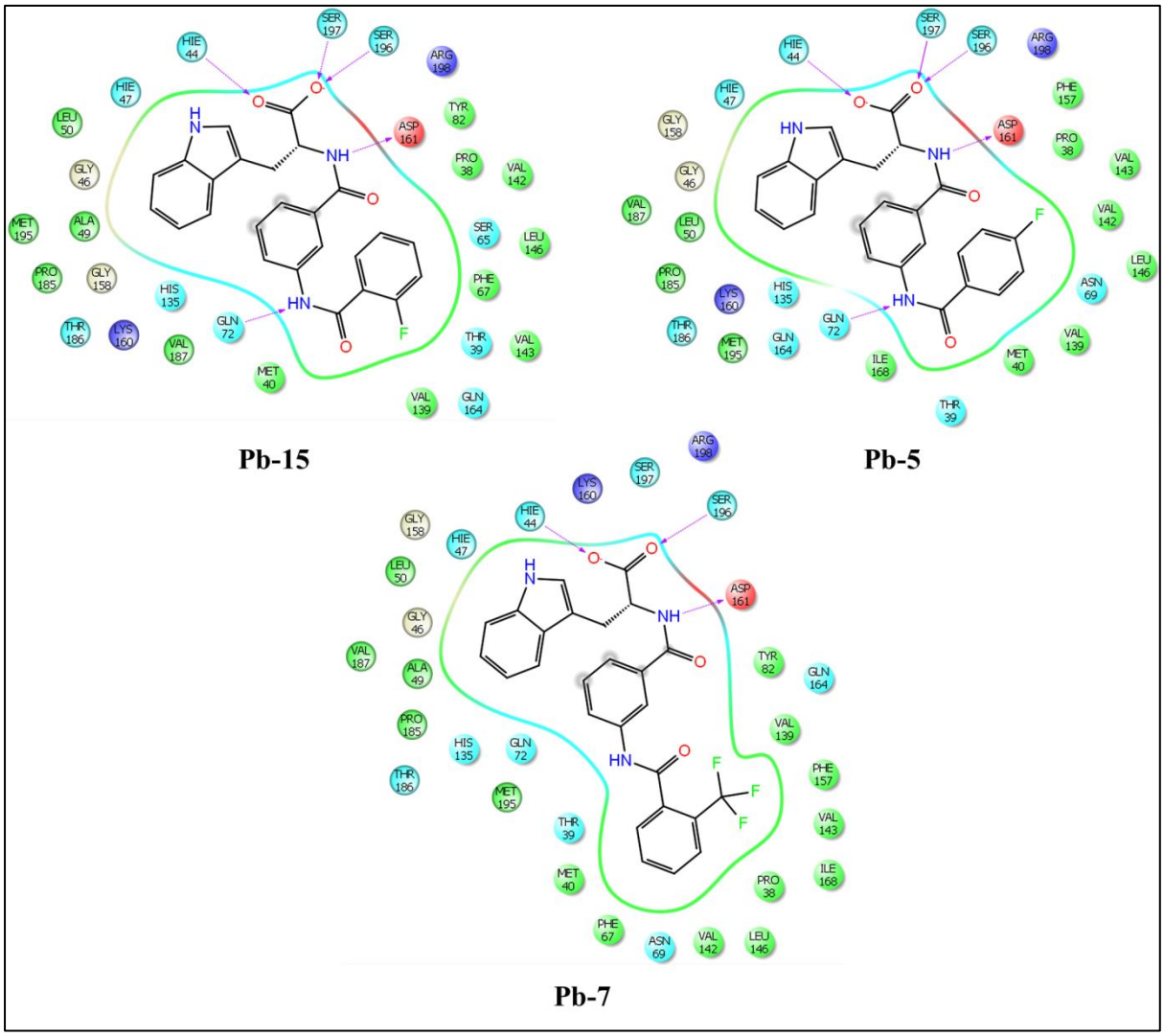

Figure 5.35: Ligand interaction diagram for the compound **Pb-15**, **Pb-5**, and **Pb-7**

With respect to the modification attempted to understand the effect of chain length at R-position with 2-fluoro, 4-fluorophenyl and 2-trifluoromethyl phenyl were substituted. It was found that an increase in chain length as in the case of compound **Pb-7**was seen to significantly hamper the activity, this as understood and due to loss of two hydrogen bonds that the compounds **Pb-15** and **Pb-5** maintained with Gln72 and Ser197 (Figure 5.35).

Among the various chlorophenyl substitutions attempted in synthesis (**Pb-11, Pb-9** and **Pb-8**), compound **Pb-8** emerged as the promising lead with PS inhibitory IC_{50} of 5.23 μM. The binding analysis of these compounds showed that the molecule oriented nicely into the active site cavity. Additionally, **Pb-8** was found to be involved in common hydrogen bonding with Ser197, Ser196 and Asp161 as shown in Figure 5.36.

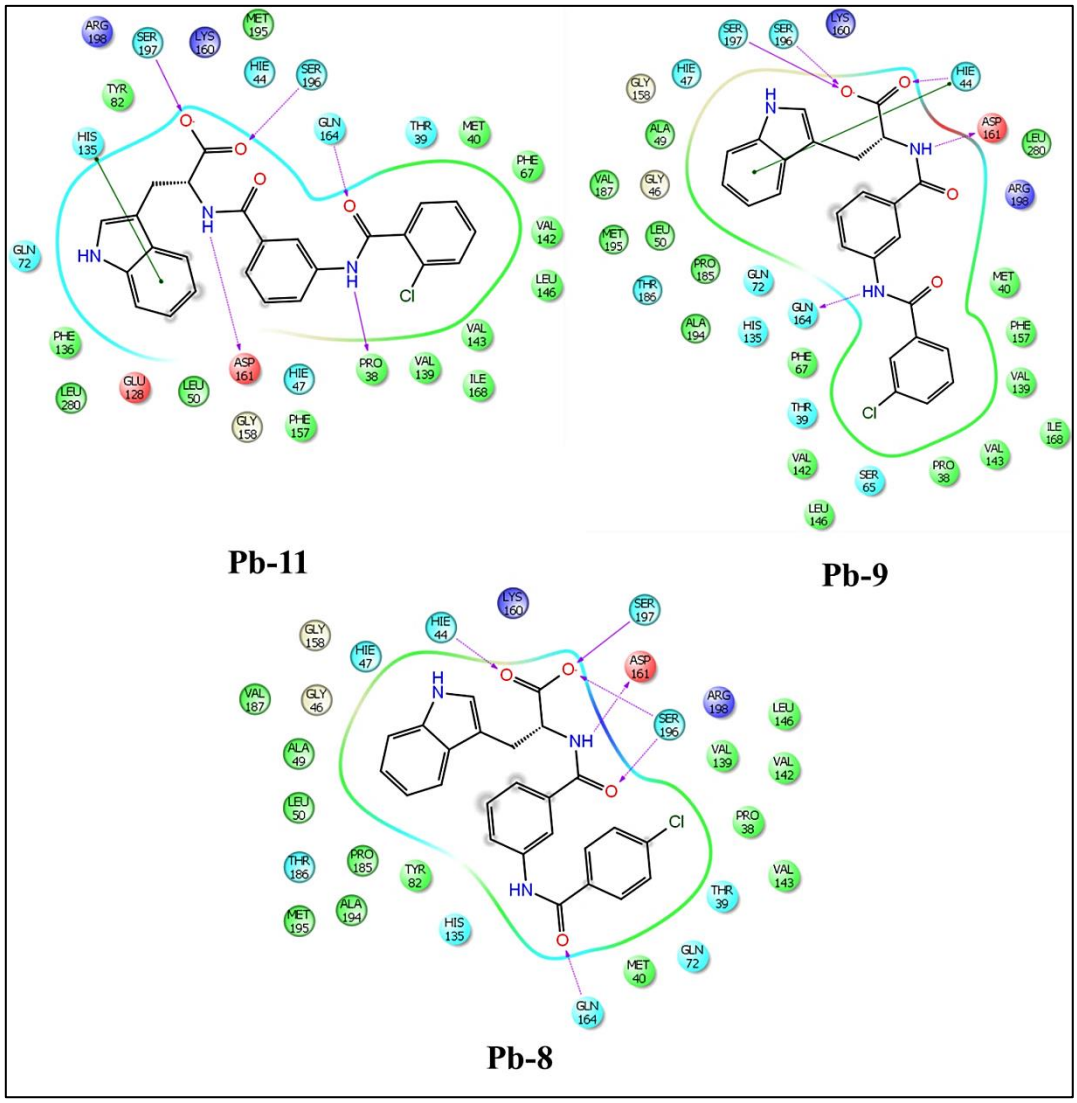

Figure 5.36: Ligand interaction diagram for the compound **Pb-11, Pb-9,** and **Pb-8**

The substitution with 3 and 4-nitrophenyl exhibited wide range of PS inhibition at enzymatic level. An in-silico investigation into the same revealed that the molecule is oriented in a completely opposite manner to the active analogue throwing the indole ring slightly away from the pocket. This implied less activity profile of compound **Pb-12** than **Pb-13** as shown in Figure 5.37.

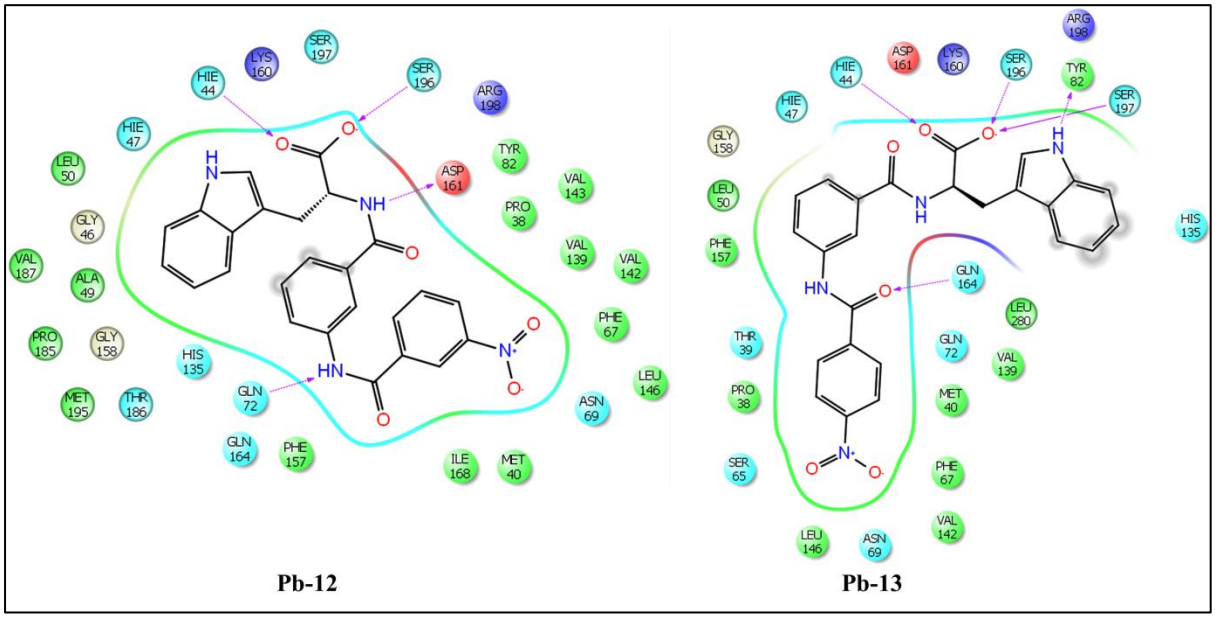

Figure 5.37: Ligand interaction diagram for the compound **Pb-12** and **Pb-13**

5.2.9. In-vitro anti-mycobacterial screening

Further the synthesized compounds were screened for their in-vitro anti-mycobacterial activities against log phase culture of Mtb H37Rv by MABA assay method for the determination of MIC in duplicates. MICs of the synthesized compounds along with the standard drugs (isoniazid (0.72 µM) and ethambutol (7.64 µM)) as positive controls are reported in Table 5.12. Out of 16 molecules tested, 6 compounds (**Pb-3**, **Pb-5**, **Pb-6**, **Pb-10**, **Pb-14** and **Pb-16)** showed MIC less than 30 µM; whereas remaining compounds (**Pb-1, Pb-2, (Pb-4**, **Pb-7**, **Pb-8**, **Pb-9**, **Pb-11**, **Pb-12**, **Pb-13** and **Pb-15)** showed MICs in the range of 51.39 µM - 102.77 µM. The most prominent molecules **Pb-5** and **Pb-12** possessed MIC value of 27.20 µM and 51.39 µM respectively which did not correlate with enzymatic assay. The compound **Pb-5** was two times more potent than parent lead **PII-10** but **Pb-12** almost possessed similar MIC values. This could probably be due to cell wall permeability or due to efflux pump transportation. In general, the compounds substituted with cyclopentyl, 4-fluorophenyl, methoxy benzyl, trifluoromethyl phenyl, 2-furoyl, phenyl and *tert*-butyl phenyl

showed good MICs. Also efflux studies need to be carried out in the presence of efflux inhibitors verapamil and piperine to check whether these compounds exhibited better activity.

5.2.10. In-vitro cytotoxicity evaluation for the synthesized compounds

Finally, the cytotoxicity of the compounds was also tested in-vitro toxicity against HEK293 cell lines at 50 μM concentration using MTT assay. Few compounds **Pb-6**, **Pb-11**, **Pb-15** and **Pb-16** showed cell toxicity about ≥50 %. All other compounds including the most promising compounds like **Pb-5** and **Pb-12** were found to be non-toxic. Percentage inhibition at 50 μM concentration is reported in Tables 5.12.

5.2.11. ADME predictions for the synthesized compounds

Finally, we predicted pharmaceutical properties for the synthesized compounds to check for drug-likeness. The predicted logP, HERG activity, blood brain barrier and rule of five violations of all the modified compounds were in the acceptable ranges except for few compounds. The compounds were modified with different bulky groups to make the molecules more lipophilic in-order to permeate into the cell wall of mycobacteria. In this series, the compounds substituted with 2-pyrazinyl (**Pb-1**) and nitrophenyl substitutions (**Pb-12** and **Pb-13**) showed less Caco-2 cell permeability property. The Caco-2 cell permeability property indicated oral absorption of a drug molecule in humans from its permeability across the Caco-2 monolayer. These compounds were found to be lipophilic and hence shared poor bioavailability. The most active compound **Pb-5**, substituted with 4-fluorophenyl was highly lipophilic. Also, this compound showed high oral absorption. The ADME predictions for the synthesized compounds are shown in Table 5.13. All the compounds passed the rule of five with no or one violation.

Table 5.13: ADME predictions for the synthesized compounds

Compound ID	QPlogPo/w[a]	QPlogHERG[b]	QPPCaco[c]	QPlogBB[d]	% Human oral absorption[e]	Rule of 5[f]
Lead PII-10	4.792	-4.165	90.669	-1.512	85.516	0
Pb-1	3.048	-5.705	16.49	-2.427	66.577	0
Pb-2	4.724	-5.194	47.309	-1.933	84.584	0
Pb-3	4.419	-5.093	50.064	-1.87	83.237	0
Pb-4	4.412	-5.662	42.182	-1.835	81.862	0
Pb-5	4.757	-5.868	44.229	-1.832	84.256	0
Pb-6	4.63	-5.877	44.211	-2.04	83.505	0
Pb-7	5.3	-5.59	61.28	-1.517	77.007	1
Pb-8	5.02	-5.881	45.789	-1.773	73.104	1
Pb-9	5.019	-5.881	45.791	-1.773	73.1	1
Pb-10	3.862	-5.688	39.903	-1.94	78.21	0
Pb-11	4.913	-5.844	47.448	-1.773	85.713	0
Pb-12	3.835	-5.886	5.276	-3.171	62.329	0
Pb-13	3.883	-5.967	5.683	-3.156	63.186	0
Pb-14	4.525	-6.001	44.208	-1.932	82.891	0
Pb-15	4.682	-5.865	45.96	-1.835	84.112	0
Pb-16	5.529	-5.983	47.505	-1.698	76.369	1

[a]Predicted octanol/water partition coefficient logP (acceptable range: −2.0 to 6.5);[b]Predicted IC50 value for blockage of HERG K+ channels.(below -5);[c]Predicted apparent Caco-2 cell permeability in nm/sec (<25 poor; >500 great); [d]Predicted brain/blood partition coefficient (-3.0 to 1.2); [e]Percent human oral absorption (<25% is poor and >80% is high); [f]Rule of 5 violation (mol_MW < 500, QPlogPo/w < 5, donorHB ≤ 5, accptHB ≤10)

5.2.12 Biophysical characterization of potent compound

The binding of the ligand **Pb-5** was evaluated by measuring the fluorescence of the native protein and protein-ligand in complex in the presence of a fluorescent dye whose fluorescence increased when exposed to non-polar residues of the protein and reached the maximum when the protein got denatured. Figure 5.38 represents the thermal shift assay of the molecule **Pb-5**. The protein showed melting temperature (T_m) of 42.30°C, whereas with molecule **Pb-5** the corresponding melting temperature was found to be 44.30°C. The difference in the melting temperature values showed how effectively the ligand stabilized the protein due to binding with the protein. Compound **Pb-5** displayed a T_m shift of 2°C which was correlated with its PS IC_{50} of 2.28 μM which is three times more potent than the parent lead compound **PII-10** with the IC_{50} of 6.63 μM.

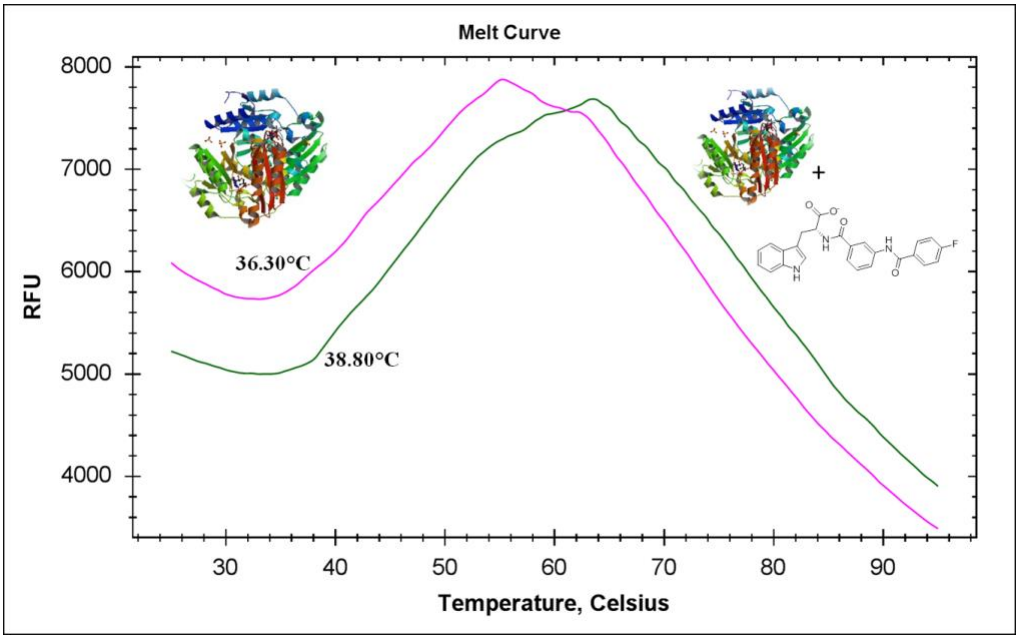

Figure 5.38: Thermal shift pattern for the protein (pink line) and in complex with the potent molecule **Pb-5** (green line)

5.3 Summary and Conclusion

We utilized the medicinal chemistry tools of structure based drug design with two design strategies. One with reaction intermediate approach was performed in-order to identify new scaffold molecules. This strategy revealed hitherto unknown binding pockets and inhibitor binding modes distinct from the earlier reported inhibitors and was exploited successfully in further drug development process. In another strategy, we utilized inhibitor based approach in-order to modify reported ligand with a promising molecule.

DESIGN I: MTB PS INHIBITORS BASED ON REACTION INTERMEDIATE BOUND TO PS PROTEIN

In this study, structure-based e-pharmacophore modelling was employed to identify structurally diverse, small molecule inhibitors of Mtb PS enzyme based on the crystal structure co-crystalized with reaction intermediate. Ten active compounds from varied structural classes were identified and out of which, four molecules showed Mtb PS activity with IC_{50} <10 µM, and the compound that resembled crystal ligand was selected as lead to further synthesize a library of 19 molecules.

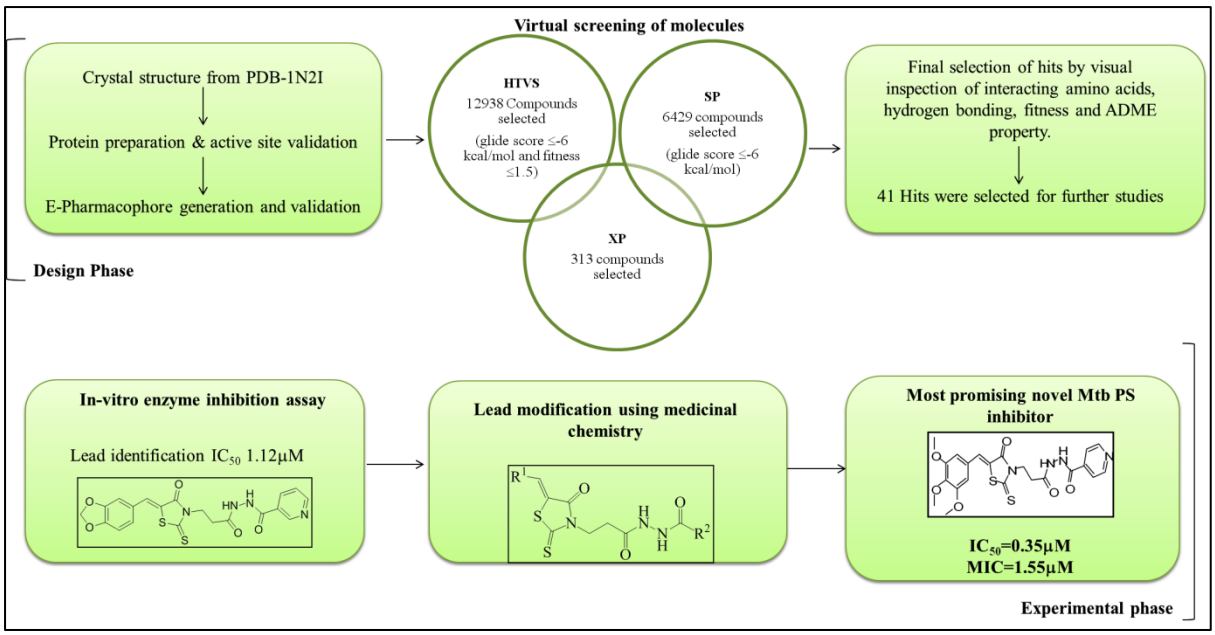

All these compounds were subjected to Mtb PS inhibition assay, further their binding and enhanced protein stability was biophysically confirmed by DSF. It was gratifying to report that the best inhibitory compounds **Pa-9** and **Pa-12** showed a greater positive shift in DSF, indicating an increase in thermal stability of the inhibitor–protein complex that correlated well with their enzyme inhibition. Furthermore, compounds **Pa-9** and **Pa-12** showed better activity against dormant Mtb. thereby making these compounds a potential chemical class to be developed as Mtb PS inhibitors.

DESIGN II: Mtb PS INHIBITORS BASED ON INHIBITOR BOUND TO PS PROTEIN

In design II strategy, we successfully demonstrated based on the first generation of hit identification step; an optimized **Lead PII-10** by medicinal chemistry approach and identified a potential compound **Pb-5** useful as inhibitor of Mtb PS. Further the compound was biophysically confirmed by DSF that improved stability of the protein. It was satisfying to see the that **Lead PII-10** was modified to compound **Pb-5** (after lead optimization) that showed a positive shift in T_m, indicating an increase in thermal stability of the complex inhibitor–protein that matched the best in-vitro enzyme inhibition as well.

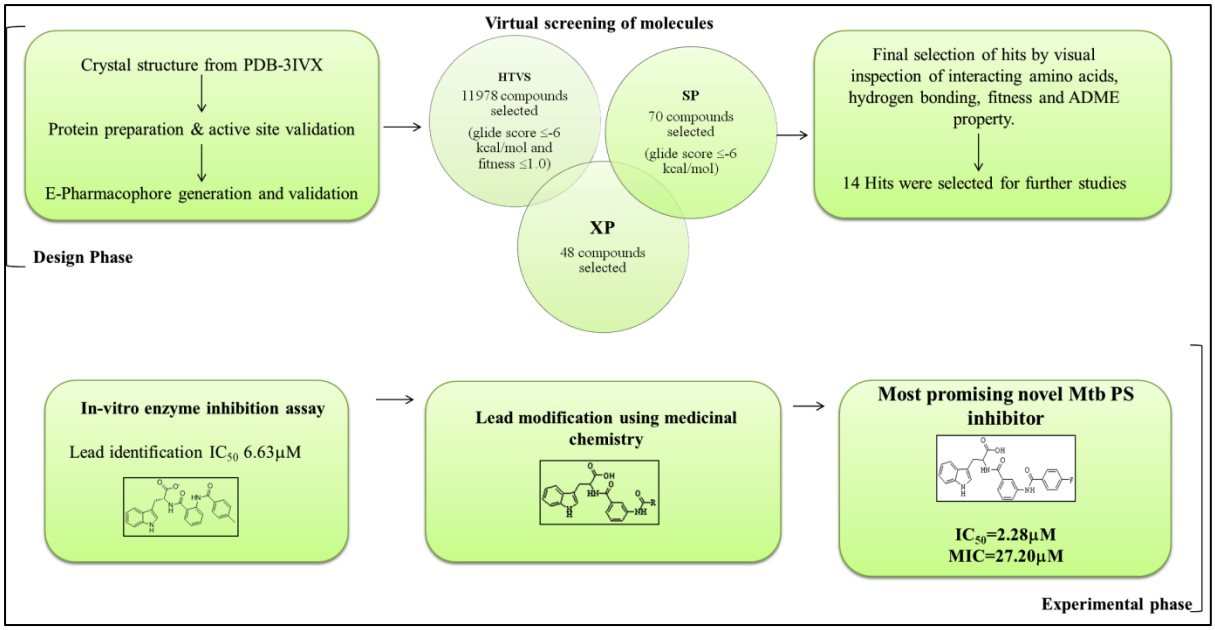

In conclusion, when comparing with both the design strategy, the Design I strategy worked well with the enzyme PS and two novel leads were identified than the Design II as we did not obtained promising leads as that of Design I strategy. These results also well correlated with the Mtb MIC without efflux inhibitors, Mtb MIC in presence of efflux inhibitors, by dormant Mtb studies and bio-physical characteristics was proved that the inhibitor is stabilizing the protein ligand which implied the strong inhibitor binding towards the protein molecule. Thus with the help of Design I strategy we could identify numerous novel molecules which can be target specific inhibitors for the Mtb infection.

Chapter 6

Result and Discussion for Development of Mycobacterial Lysine Aminotransferase Inhibitors

As seen from the extensive literature search it is clear that, in nutrient starved condition *lat* gene is upregulated in the multiples of 40 times in Mtb. Another study showed that Mtb adapted to external environment into stable and latent form in which *lat* gene was found upregulated [Voskuil M.I., *et al*., 2004]. Literatures revealed that *lat* gene expression was associated with dynamics of bacterial infection, which was potentially ideal as drug targets. However, so far none of the literature reported to have anti-TB effects of LAT inhibitors.

In the present study, we employed two attempts to develop new diverse inhibitors as exemplified below.

Design I: Structure-based lead identification as LAT inhibitors based on substrate lysine bound protein.

Design II: Structure-based lead identification as LAT inhibitors based on substrate α-ketoglutarate bound to LAT protein.

6.1. DESIGN I: MTB LAT INHIBITORS BASED ON SUBSTRATE LYSINE BOUND PROTEIN

The present study was directed towards the active site of LAT, using high throughput screening of compound library. It was reported earlier that LAT has been an important cellular target for TB, which we employed structure-based design to effectively develop and inhibitors. As there were no reported inhibitors available till date, we took substrate lysine bound along with Pyridoxal 5-phosphate (PLP) with the LAT protein. Our aim was to identify novel small molecule inhibitors that could bind to the active site of Mtb LAT protein utilizing e-pharmacophore approach. The crystal structure of LAT from MTB in external aldimine form in complex with its substrate lysine (PDB ID: 2CJD) with 2.00 Å resolution [Figure 6.1].

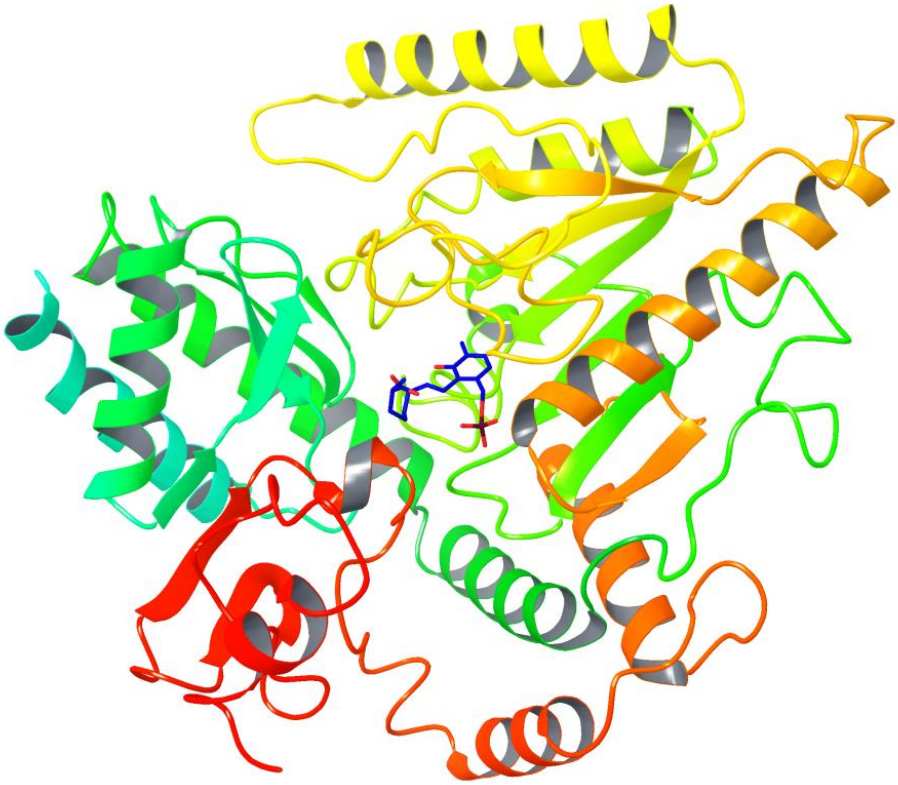

Figure 6.1: Crystal structure of LAT protein bound with lysine (2CJD)

6.1.1. Protein preparation and active site validation

The retrieved protein was prepared using protein preparation wizard by adding hydrogen atoms, removing water molecules and minimization of energy by converging the heavy atoms using OPLS_2005 as force field. The orientations of the ligand in the active site pocket and its interactions between with the protein residues were visualized. To validate the method in predicting binding energy and possible interaction between ligands and receptor, at first existing ligand in crystal structure was re-docked in 2CJD. The active site of the protein was located and grid files were generated using receptor grid generation panel. Grid size was found to be 18Å and was used for all docking analysis. The ligand showed docking score of -7.86 kcal mole^{-1} with the important amino acid interactions with Arg170, Gln274, Ala129, Gly128 and π-π stacking interaction with Phe167. The diagrammatic representation of re-docking results of crystal ligand towards the active site of protein and its ligand interaction diagram are shown in Figure 6.2.

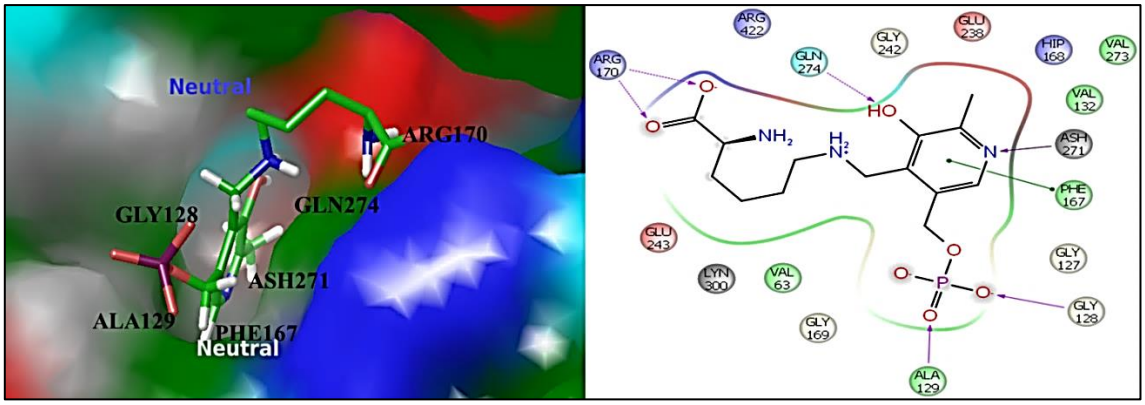

Figure 6.2: Binding analysis and ligand interaction of reference ligand towards the active site of the protein

The superimposition of reference ligand and the docked ligand was performed and the RMSD was found to be 0.20 Å and hence this technique could be for next predictions (Figure 6.3).

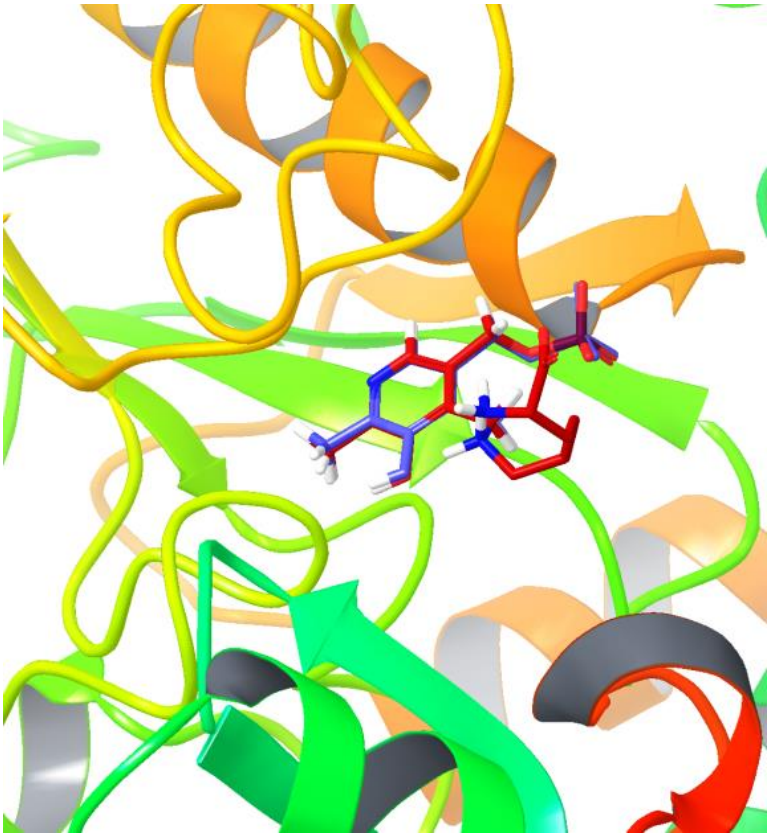

Figure 6.3: Superimposition of docking pose of ligand lysine and original pose towards the active site of the protein; where violet colour indicates docked pose and red colour indicates original pose of the ligand

6.1.2. E-pharmacophore generation

Pharmacophore hypotheses based on mapping of the energetic terms from the XP, Glide scoring function onto atom centres were obtained using Phase. We followed similar protocol employed for Mtb PS inhibitors as presented in materials and methods in section 4.1.3. A six-point e-pharmacophore model was generated with Mtb LAT protein bound to lysine with PLP. Initially for generating the model, we kept features for 10 and we got prominent features with energy scores and ranking. The pharmacophoric sites established included three hydrogen bond acceptors (A1, A3 and A4), one ring aromatic (R14) and two negative ionizable groups (N9 and N11) (Figure 6.4). Based on the energy score we have selected two different pharmacophore hypotheses. We selected five sites as A1, A3, R14 N9 and N11 as one hypothesis and A1, A3, R14, A4 and N9 as another hypothesis for further virtual screening of a commercial database Asinex. As there are no reported inhibitors till date, e-pharmacophore validation was not performed.

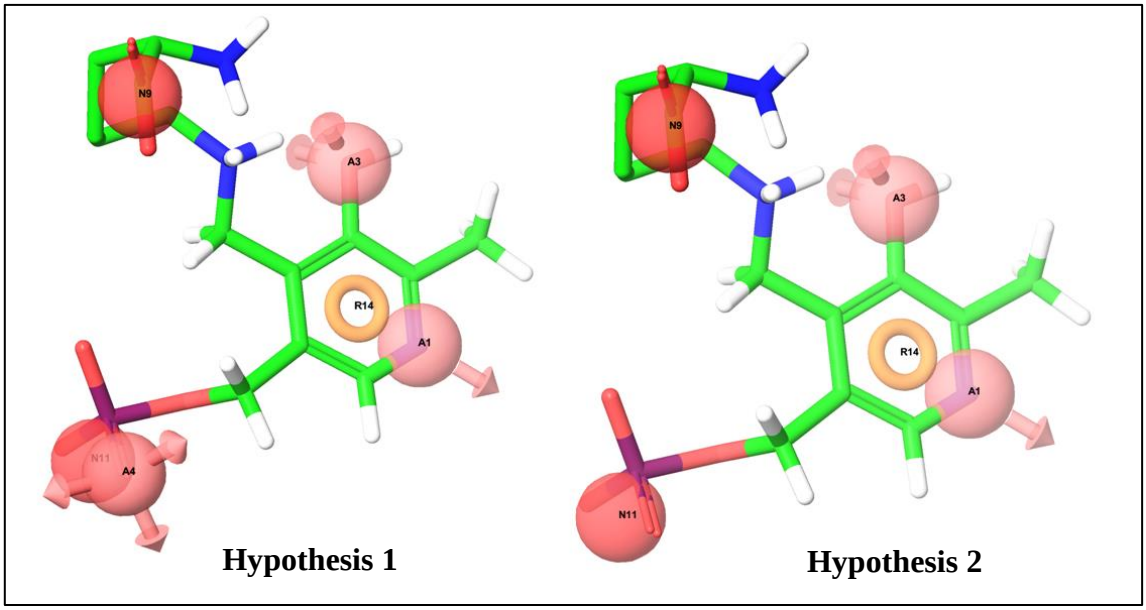

Figure 6.4: Energy based pharmacophore features for virtual screening

6.1.3. Virtual screening of molecules and docking

From PHASE find matches module output of two e-pharmacophore hypotheses AAARN and AARNN for 2CJD, we selected fitness above 1.0 as a limit for HTVS docking and selected 5648 hits with different clusters. These ligands were docked into Mtb LAT active site using the grid generated and finally 1247 compounds were shortlisted as hits with the criteria of docking score of ≤ -4.0 kcal mol^{-1} and with at least two or more hydrogen bonds. These hits were then subjected to another round of docking by Glide XP and 63 hits were selected.

Glide XP combined accurately with the parameters physics-based scoring terms and thorough sampling resulted in compounds with docking scores between -7.649 to -6.222 kcal mol^{-1}. The final shortlisting of the molecules was based on the protein ligand interaction in the active site cleft through hydrogen bonding with Arg170, Gln274, Ala129 and Gly128; π-π stacking interactions with Phe167 and predicted pharmacokinetic properties. The fitness, docking score, hydrogen bonding and ligand interaction towards the active site of the protein for the top five selected leads were represented in Table 6.1. The structures of the lead compounds are presented in Figure 6.5.

Table 6.1: Docking parameters for the top five leads

Compound ID	Docking score	Hydrogen bond	Fitness	Interaction
Crystal ligand	-7.86	5	1.47	Arg170, Gln274, Ala129, Gly128, Phe167
Lead LI-1	-6.72	5	1.33	Lys300.Asp271,Gly128
Lead LI-2	-6.61	4	1.43	Lys300,Gly128,Ala129,Asp271
Lead LI-3	-6.68	7	1.59	Asp271,Arg170,Thr180,Glu243,Gln274
Lead LI-4	-6.47	4	1.60	Asp271,Lys300,Arg170
Lead LI-5	-6.45	5	1.32	Gly128,Ala129,Arg170

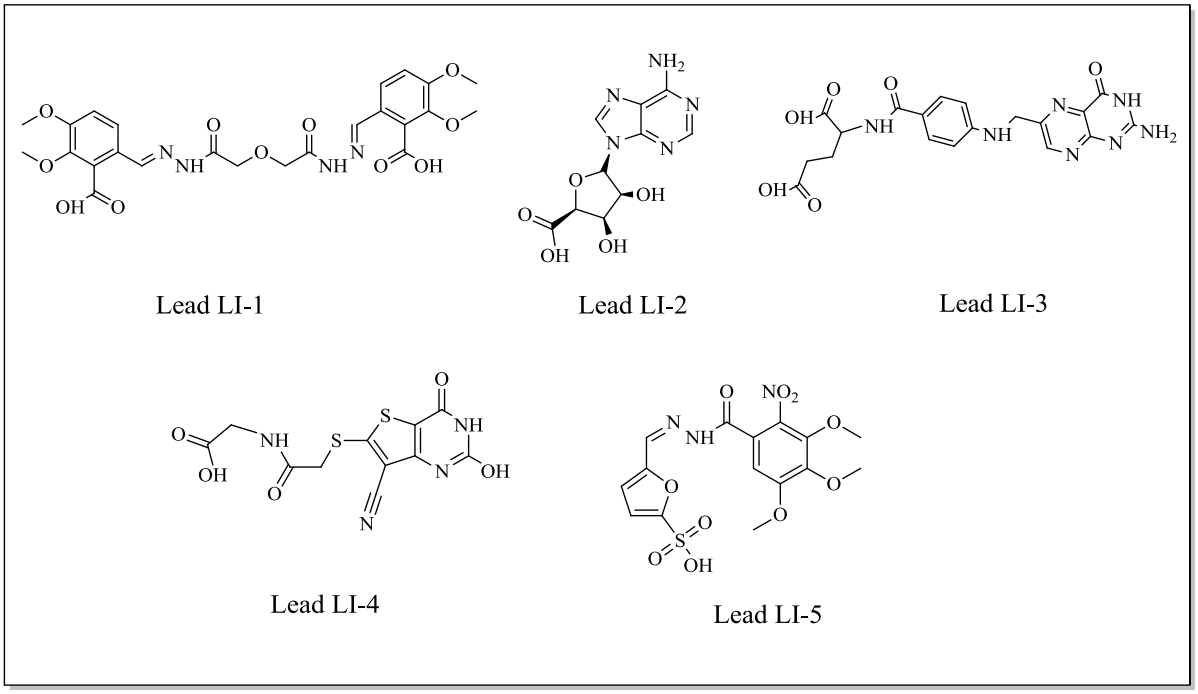

Figure 6.5: Structure of the selected compounds for in-vitro screening

6.1.4. ADME predictions for the designed compounds

ADME predictions would help in identifying selected compounds with pharmaceutical importance which could be further developed into a drug-like molecule. All the selected designed compouds were subjected to in-silico ADME properties using QikProp module in Schrodinger (Table 6.2). The compounds **Lead LI-1** and **Lead LI-3** shortlisted were not found to violate in the Lipinski's rule of five. Various other important properties like Predicted octanol/water partition coefficient logP, predicted IC_{50} value for blockage of HERG K+ channels, predicted apparent Caco-2 cell permeability in nm/sec, predicted brain/blood partition coefficient, percent human oral absorption were determined for the selected compounds and checked for any deviations. Predicted logP values for the top five hits were in the acceptable range except for **Lead LI-3** and **Lead LI-4**. Predicted Caco-2 cell permeability property was in the expected range and hence indicated of problems in intestinal absorption. Whereas predicted blood brain barrier and % human oral absorption were also found out of the range for the compounds except **Lead LI-2**. The polar surface area was considered as the significant descriptor for the drugs to transport in membranes and barrier penetrations. These hit molecules were highly electronegative in nature and hence the reason for these to have failed. Moreover, these predictions of ADME properties could be useful in further modifications of active molecules after preliminary enzymatic screening.

Table 6.2: ADME predictions for the designed compounds

Compoud ID	QPlogPo/w[a]	QPlogHERG[b]	QPPCaCo[c]	QPlogBB[d]	% Human oral absorption[e]	Rule of 5[f]
Lead LI-1	2.444	-3.182	0.701	-4.329	12.577	2
Lead LI-2	-1.176	-1.937	3.647	-2.176	30.115	0
Lead LI-3	-0.347	-2.612	0.051	-4.884	0	2
Lead LI-4	-0.061	-2.581	0.558	-3.262	22.048	0
Lead LI-5	1.371	-2.847	23.648	-2.01	46.605	1

[a]Predicted octanol/water partition coefficient logP (acceptable range: −2.0 to 6.5);[b]Predicted IC_{50} value for blockage of HERG K+ channels.(below -5);[c]Predicted apparent Caco-2 cell permeability in nm/sec (<25 poor; >500 great); [d]Predicted brain/blood partition coefficient (-3.0 to 1.2);[e]Percent human oral absorption (<25% is poor and >80% is high);[f]Rule of 5 violation (mol_MW < 500, QPlogPo/w < 5, donorHB ≤5, accptHB ≤10)

6.1.5. Biological assessments

The finally shortlisted 5 lead compounds were procured from the commercial source (Asinex). The enzyme inhibition studies were performed as discussed in materials and methods 4.3.2.3. Initially, the range finding experiments were performed to check the concentration of enzyme which was found to be 6.89 pM. Further, the two substrates lysine

and α-ketoglutarate were varied with α-ketoglutarate as constant and later lysine as constant and determined K_m and V_{max} using Michaels-Menton equation. The K_m was calculated using Graphpad Prism software and was found to be 1.65 mM for lysine and 1.02 mM for α-ketoglutarate. The kinetic parameters for both lysine and α-ketoglutarate were shown in the Figure 6.6.

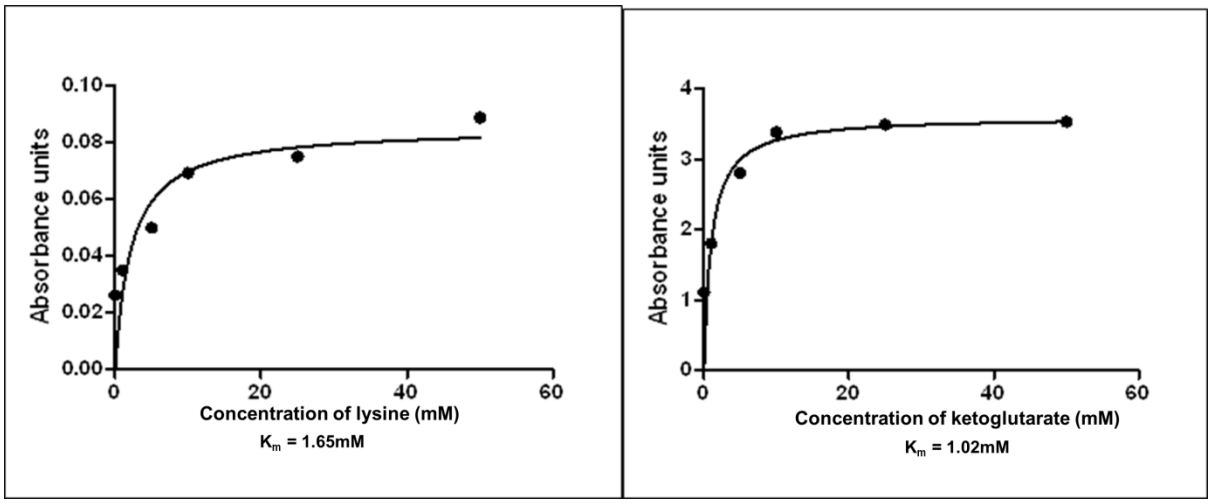

Figure 6.6: Kinetic parameters of lysine and α-ketoglutarate

The designed compounds were added to the plates with the concentrations varied from 50 μM to 1 μM. The reaction components except Mtb LAT were mixed in the well and the background reaction was measured; Mtb LAT was then added and the reaction kinetics was monitored. The reaction mixture was incubated at 37°C for 1 hr. The reaction was terminated by the addition of 10% trichloroacetic acid in ethanol. The product piperidene 6-carboxylate and glutamate was measured due to its colour intensity of its adduct with o-aminobenzaldehyde at 465 nm and 280 nm in a heat-controlled PerkinElmer Victor X3 spectrophotometer. As there were no reported inhibitors available for Mtb LAT till date, we couldn't use any positive control for comparision. In the initial screening at 50 μM, all the designed compounds showed good inhibition. The designed molecules and their calculated IC_{50} values are presented in Table 6.3. Among the five hits, four compounds showed IC_{50}'s in the range of 18-75 μM and two compounds **Lead LI-1** and **Lead LI-4** emerged as promising inhibitors of Mtb LAT with IC_{50}s of 23.83 μM and 18.06 μM respectively.

Table 6.3: Preliminary enzyme inhibition screening of designed compounds

S.No	Compound ID	IC_{50} values (μM)
1	**Lead LI-1**	23.83±0.15
2	**Lead LI-2**	75.26±0.06
3	**Lead LI-3**	>50
4	**Lead LI-4**	18.06±0.12
5	**Lead LI-5**	44.33±0.10

After preliminary enzyme inhibition studies, the designed compounds were again visually inspected for their interacting amino acids. The ligand interaction diagram for the active compounds is depicted in Figure 6.7.

The docking orientation of the **Lead LI-1**, when compared with the crystal ligand, revealed important hydrogen bonding interactions with Arg170, Gln274 and Ash271(Asparagine at ω position) was observed as shown in Figure 6.7. In addition to hydrogen bonding interactions the dimethoxyphenyl ring interacted *via* pi-pi interaction with Phe167 and there was a hydrogen bonding interaction with Gly128, which was analogues to the one observed with the crystal ligand (Figure 6.2). The orientation of lead compound was found to be closely similar to that of crystal ligand exhibiting a very good fitness in the active site pocket making this compound promising with IC_{50} of 23.83 μM.

Leads LI-2 and **LI-4** were found to show a new hydrogen bonding interaction with Lys300 which was not seen with the crystal ligand. Four ligands (**LI-1**, **LI-2**, **LI-3** and **LI-5**) showed interaction with Gly128 except **LI-4** while interaction with Gln274 was observed with all compounds except **LI-2**. The π-π stacking interaction with Phe167 was exhibited by all leads except **LI-5** while **LI-2** exhibited two π-π stacking interactions. The **LI-3** showed additional hydrogen bonding interactions with Thr180 and Glu238 which was not observed in **Leads LI-1**, **LI-2**, **LI-4** and **LI-5**. As compared with crystal ligand, the important hydrogen bond interaction Ala129 was missing all the Leads. Also, another interaction with Gly128 is missing in **Leads LI-2**, **LI-3**, **LI-4** and **LI-5**.

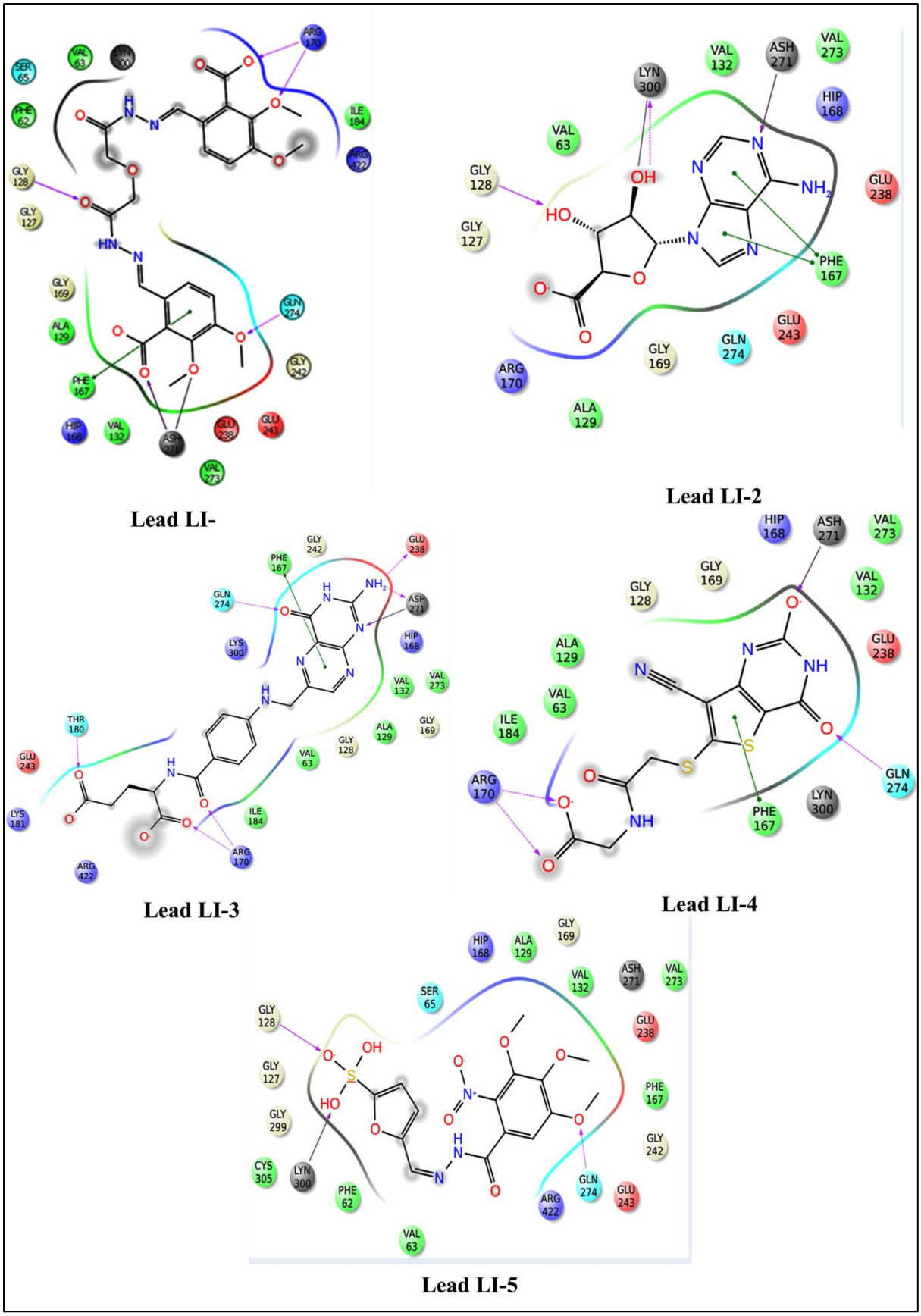

Figure 6.7: Ligand interaction diagram for the designed compounds

6.1.7. Lead optimization using medicinal chemistry

Based on the enzyme assay results, **Leads LI-1** and **LI-4** were screened for anti-mycobacterial potency using the MABA assay procedure. **Lead LI-1** exhibited better activity with the MIC of 18.06 μM when compared to **Lead LI-4** which showed MIC of 46.42 μM. Hence a library was designed with the goal of obtaining a series of compounds with tractable SAR and potencies better than **Lead LI-1**. A library of 48 compounds was synthesized with the collaboration of medicinal chemistry drug discovery group at Department of Pharmacy. The scheme utilized for developing the analogues is depicted in Figure 6.8

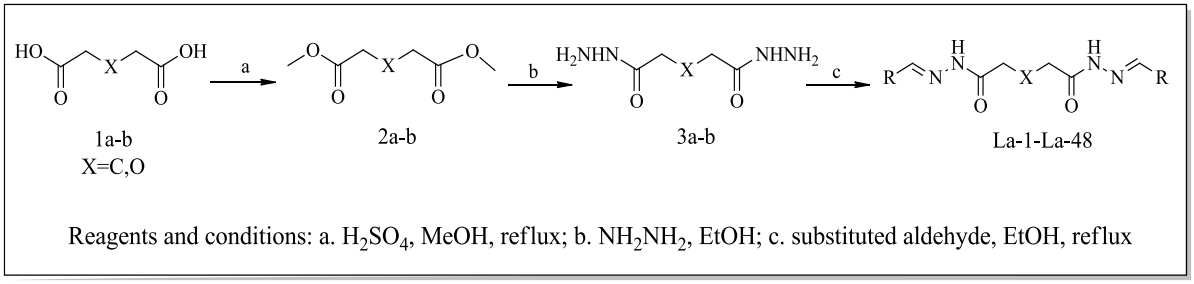

Figure 6.8: Scheme utilized for developing Mtb LAT leads-lysine based approach

The physical data and spectral data of the compounds are given in annexure III at the end of the thesis. The designed target molecules were synthesized *via* three steps in a classical way starting with commercially available and less expensive glutaric and diglycolic acid as shown in Scheme 2a. In the first step the corresponding acids (**1a-b**) were converted into esters (**2a-b**) by following the conventional sulphuric acid-methanol method well established in literature. The obtained esters after refluxing with hydrazine hydrate yielded corresponding hydrazide derivatives (**3a-b**) in good yields and purity. The transformation of the resultant hydrazides into imines by employing various substituted aldehydes afforded final compounds **La-1- La-48)**.

6.1.8. In-vitro LAT inhibition assay for the synthesized compounds

Synthesized compounds were assayed for in-vitro Mtb LAT inhibition as described earlier. The end product piperidene-6-carboxylate was measured due to its colour intensity of its adduct with o-aminobenzaldehyde at 465 nm and the glutamate product was measured at 280 nm in a heat-controlled PerkinElmer Victor X3 spectrophotometer. Of all the synthesized compounds, 16 compounds showed ≤ 10 μM IC_{50}s. Most of the compounds (about 30) were found to be better than the parent **Lead LI-1**. Among these compounds, **La-28** and **La-30**

emerged as the most active inhibitors of Mtb LAT with IC_{50}s ≤ 1 μM, whose dose response curves have been presented in Figure 6.9.

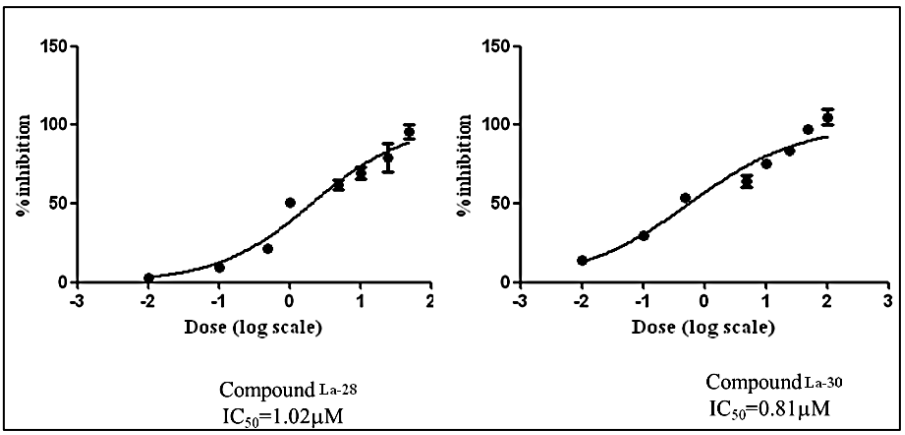

Figure 6.9: Dose response curve for the active molecules **La-28** and **La-30**

The biological evaluation for the synthesized compounds substituted with 'C' linker and 'O' linker are shown in Tables 6.4 and 6.5.

Table 6.4: Biological evaluation for the synthesized compounds with 'C' linker

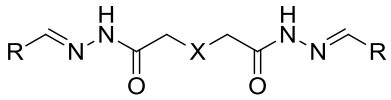

Compound ID	R	X	IC_{50}(μM) [a]	MIC(μM) [b]	% Cytotoxicity at 50μM [c]
Lead LI-1	2,3 dimethoxy benzoate	O	23.83±0.15	11.44	15.68±0.73
La-1	2-Methyl phenyl	C	4.09±0.09	34.3	25.82 ±0.06
La-2	3-Methyl phenyl	C	19.83±0.08	68.6	43.87±0.12
La-3	4-Methyl phenyl	C	15.49±0.02	34.3	33.98±0.09
La-4	2-Fluoro phenyl	C	10.17±0.08	67.14	37.81±0.03
La-5	3-Fluoro phenyl	C	14.44±0.02	67.14	27.73±0.14
La-6	4-Fluoro phenyl	C	21.59±0.06	67.14	18.25±0.03
La-7	2-Methoxy phenyl	C	26.26±0.02	31.53	46.39±0.04
La-8	4-Methoxy phenyl	C	20.04±0.01	63.06	26.51±0.04
La-9	2-Nitro phenyl	C	17.31±0.09	29.32	40.59±0.07
La-10	4-Nitro phenyl	C	20.02±0.01	14.66	11.33±0.16
La-11	2-Benzyloxy phenyl	C	55.46±0.01	45.57	46.26±0.57
La-12	3-Benzyloxy phenyl	C	19.6±0.02	22.78	0.54±0.25
La-13	3-Hydroxy phenyl	C	9.93±0.05	67.86	45.38±0.30
La-14	4-Hydroxy phenyl	C	13.75±0.05	47.82	37.96±0.02
La-15	3-Bromo phenyl	C	4.66±0.01	12.65	41.99±0.28
La-16	4-Bromo phenyl	C	18.93±0.01	25.29	37.80±0.10
La-17	4-N,N-dimethyl amino phenyl	C	4.34±0.01	59.17	46.10±0.09
La-18	Piperidine	C	16.41±0.02	17.83	44.29±0.11
La-19	Morpholine	C	20.65±0.03	70.54	36.21±0.01
La-20	2-Bromo phenyl	C	11.37±0.03	25.29	48.01±0.09
La-21	2-Naphthyl	C	7.28±0.05	3.44	31.03±0.07
La-22	3-Trifluoro methyl phenyl	C	8.02±0.04	26.46	25.62±0.03
La-23	2-Nitro thiophene	C	8.56±0.03	3.42	3.70±0.18
La-24	2-Hydroxy phenyl	C	10.35±0.09	33.93	45.91±0.05
Isoniazid	-	-	-	0.72	ND
Rifampicin	-	-	-	0.15	ND
Ethambutol	-	-	-	7.64	ND
Moxifloxacin	-	-	-	1.24	ND

[a]Mtb LAT enzyme inhibitory assay; [b]Minimum Inhibitory concentration against Mtb H37Rv; [c]**%** inhibition of HEK293 cells; ND: not determined

Table 6.5: Biological evaluation for the synthesized compounds with 'O' linker

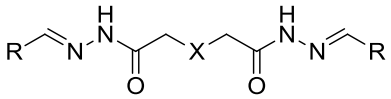

Compound ID	R	X	IC_{50}(μM) [a]	MIC(μM) [b]	% Cytotoxicity at 50μM [c]
Lead LI-1	2,3 dimethoxy benzoate	O	23.83±0.15	11.44	15.68±0.73
La-25	2-Methyl phenyl	O	11.5±0.02	68.23	43.85±0.08
La-26	3-Methyl phenyl	O	2.78±0.05	68.23	44.08±0.09
La-27	4-Methyl phenyl	O	39.33±0.02	68.23	43.49±0.01
La-28	2-Fluoro phenyl	O	1.02±0.08	16.71	36.34±0.02
La-29	3-Fluoro phenyl	O	44.55±0.03	33.41	46.43±0.06
La-30	4-Fluoro phenyl	O	0.81±0.08	16.71	25.57±0.02
La-31	2-Methoxy phenyl	O	54.01±0.02	62.75	57.30±0.06
La-32	4-Methoxy phenyl	O	95.3±0.09	31.38	35.87±0.01
La-33	2-Nitro phenyl	O	6.14±0.09	58.36	13.97±0.08
La-34	4-Nitro phenyl	O	65.4±0.06	116.71	19.47±0.04
La-35	2-Benzyloxy phenyl	O	5.46±0.02	90.81	9.20±0.09
La-36	3-Benzyloxy phenyl	O	1.96±0.07	45.41	26.24±0.11
La-37	3-Hydroxy phenyl	O	42.3±0.08	67.49	40.81±0.08
La-38	4-Hydroxy phenyl	O	41.68±0.03	67.49	54.27±0.09
La-39	3-Bromo phenyl	O	>50	25.19	45.77±0.02
La-40	4-Bromo phenyl	O	36.97±0.09	50.38	58.55±0.08
La-41	4-N,N-dimethyl amino phenyl	O	39.11±0.04	58.93	43.10±0.08
La-42	Piperidine	O	65.49±0.05	35.47	49.15±0.06
La-43	Morpholine	O	51.96±0.09	70.15	58.60±0.06
La-44	2-Bromo phenyl	O	>60	50.38	61.14±0.07
La-45	2-Naphthyl	O	27.03±0.03	57.01	20.80±0.06
La-46	3-Trifluoro methyl phenyl	O	91.59±0.05	105.4	2.77±0.05
La-47	2-Nitro thiophene	O	93.04±0.02	113.53	42.30±0.02
La-48	2-Hydroxy phenyl	O	8.47±0.03	67.49	44.64±0.07
Isoniazid	-	-	NA	0.72	ND
Rifampicin	-	-	NA	0.15	ND
Ethambutol	-	-	NA	7.64	ND
Moxifloxacin	-	-	NA	1.24	ND

[a]Mtb LAT enzyme inhibitory assay; [b]Minimum Inhibitory concentration against Mtb H37Rv; [c]**%** inhibition of HEK293 cells; ND: not determined

A closer analysis of the structural modification attempted with **Lead LI-1**, the terminal aryl functions (R) were varied and the linker atom (X) was studied with either carbon or oxygen. A total of 48 compounds each with C-linker and O-linker were synthesized. Overall it appeared that the C-linker compounds were more active than the O-linker, but surprisingly the top two most potent inhibitors emerged from the O-linker on enzyme inhibition; docking of these compounds was undertaken and the ligand interaction plots were generated to support SAR. Among these, the most active compound **La-30** with a 4-fluorophenyl group at R position and O atom at X position showed good in-vitro inhibitory activity with an IC_{50} of 0.81±0.018 µM which showed a 28 times more increment in activity when compared to the lead compound **Lead LI-1**. While the other fluoro phenyl substituted compound where carbon atom is substituted on X position **La-6** also showed lesser activity with IC_{50} of 21.59 µM. In compound **La-30**, 4-fluoro phenyl group at R position was found involved in the polar contacts with Gln274, Glu238, Glu243 and Thr180 as illustrated in Figure 6.10. In-silico analysis of this compound indicated that the molecules oriented in a similar manner to that crystal ligand maintaining hydrogen bonding interaction with Arg170 and also π-π interaction with Phe167 amino acid. The compounds were further stabilized by the various hydrophobic interactions with Ile184, Val63, Ala416, Pro415, Ala129, Val132 and Val273 amino acid residues. While, the predicted binding pose of the less active compound (**La-6**) suggested that the orientation of the molecule also changed which resulted in lesser activity of the compound than **La-30**.

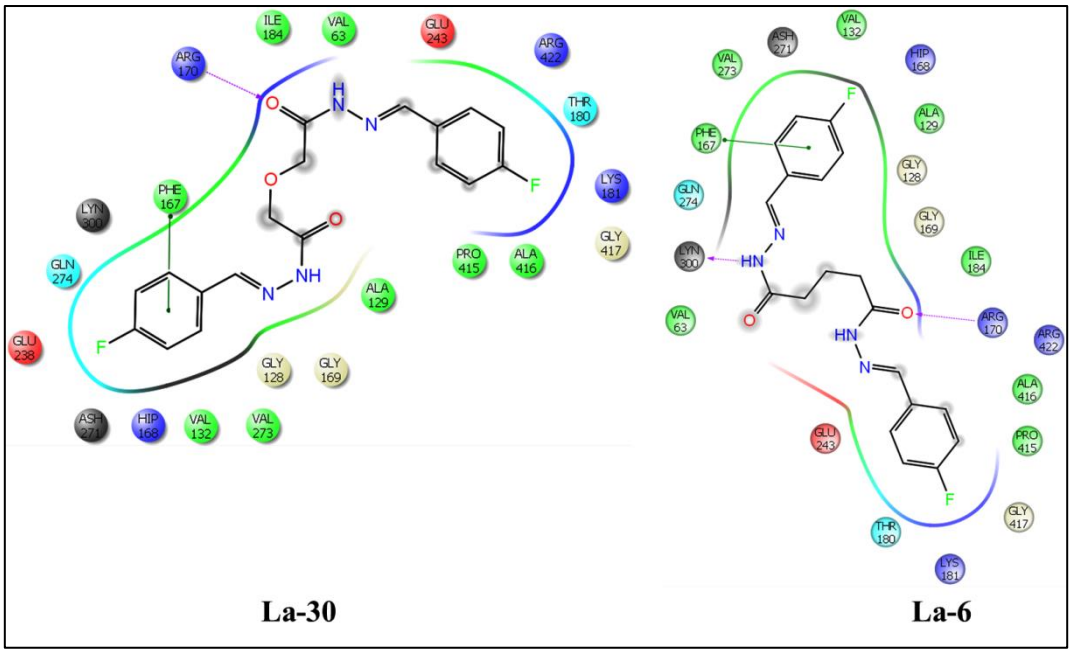

Figure 6.10: Ligand interaction diagram for the compounds **La-30** and **La-6**

The 2-fluoro phenyl substitution at R position on O-linker showed good Mtb PS inhibition at 1.02 µM whereas the substitution on C-linker showed PS inhibition at 10.17 µM. These two molecules (**La-28** and **La-4**) were found to have similar interaction pattern displaying prominent H-bonding and stacking bonding with Lys300 and Phe167. The change in the orientation of the compound **Lb-4** made less potent than **La-28**. Additional interaction with Ala129 made this compound potent as this interaction was crucial for enzyme inhibition. The ligand interaction diagram for the two compounds is shown in Figure 6.11.

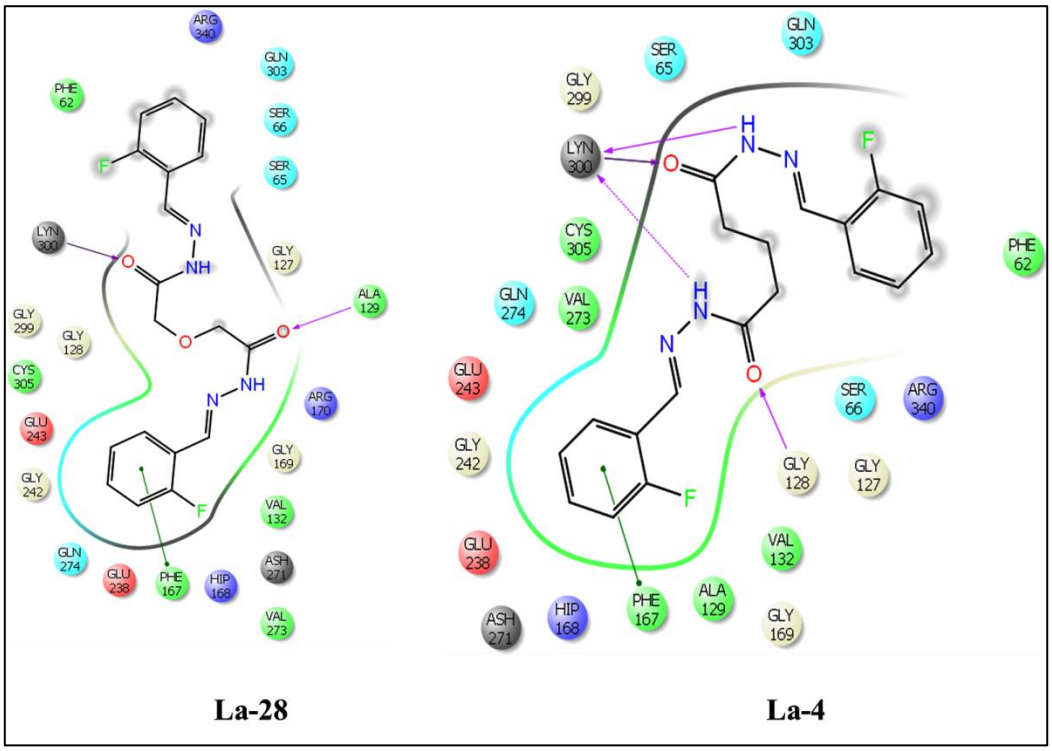

Figure 6.11: Ligand interaction diagram for the compounds **La-28** and **La-4**

Substitution with 2-methyl phenyl at R position on C-linker and O-linker showed Mtb PS inhibition of 4.09 µM and 11.50 µM. These two compounds were found to be oriented in the similar manner, but **La-1** retained hydrogen bonding with Ala129 which was earlier stated to be crucial for enzyme inhibition and thus may have resulted in reduced activity when compared to **La-1**. The ligand interaction diagram for the compounds **La-25** and **La-1** is shown in Figure 6.12.

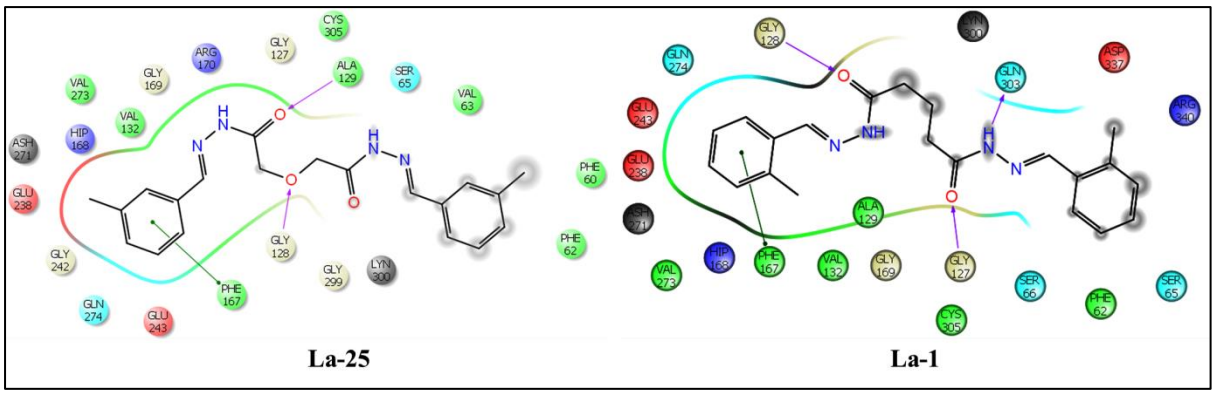

Figure 6.12: Ligand interaction for the compound **La-25** and **La-1**

Substitution with 3-hydroxy phenyl at R-position on C-linker and O-linker showed wide range of activity (9.93 μM and 42.3 μM respectively). The SAR study revealed that, hydrophobic phenyl group increased hydrophobicity of the compounds which was crucial for inhibition of enzyme; whereas the hydrophobicity was missing in the compound **La-37**. There was an additional positive charged amino acid interaction with Glu238 in **La-13** which was missing in **La-37**. The ligand interaction diagram for the compounds **La-13** and **La-37** are depicted in Figure 6.13.

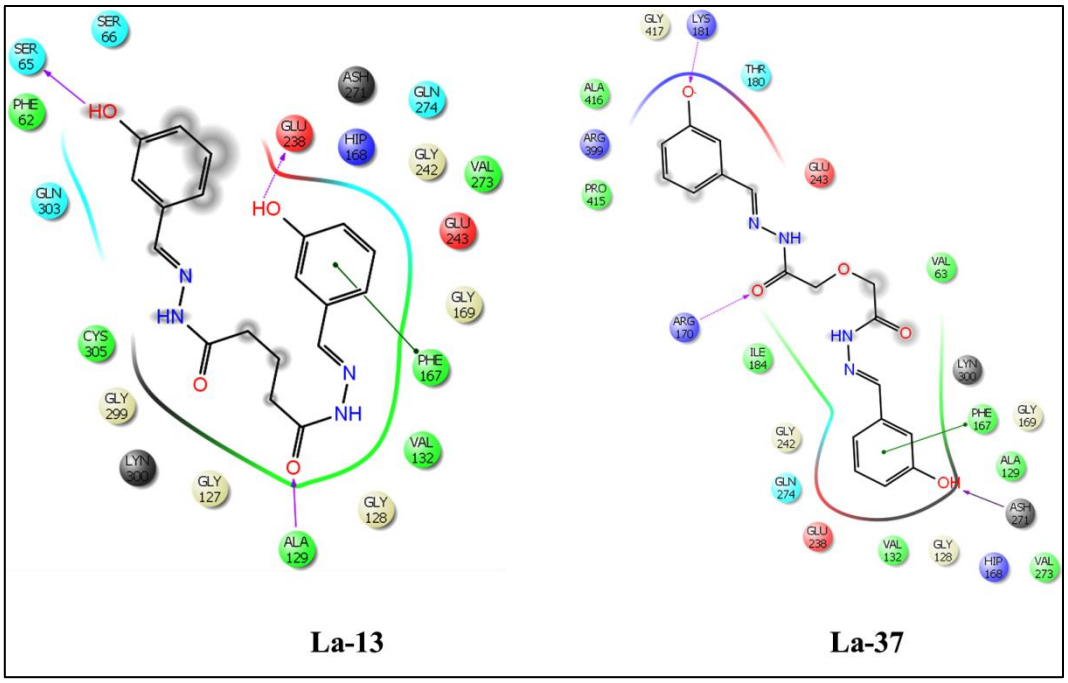

Figure 6.13: Ligand interaction diagram for the compounds **La-13** and **La-37**.

Substitution with 3-bromophenyl at R-position on C-linker and O-linker revealed that there was a wide range of Mtb PS inhibition differences. The presence of lipophilic bromophenyl substituents increased non-polar interactions in both **La-15** and **La-39**. In contrast, the

presence of bulky substituents at right hand bromophenyl core oriented the moiety slightly away from the active site, resulting in the loss of activity. The ligand interaction diagram for the compounds is depicted in Figure 6.14.

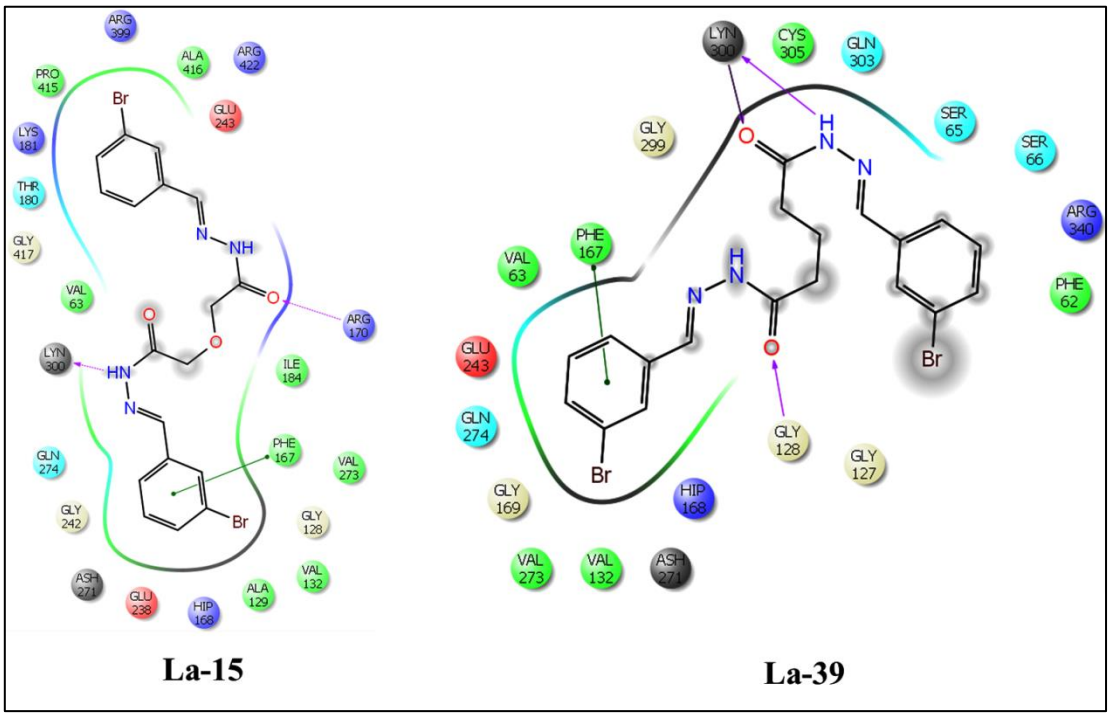

Figure 6.14: Ligand interaction diagram for the compounds **La-15** and **La-39**

The R-substituent with 4-N,N-dimethyl aminophenyl in C-linker and O-linker showed PS inhibition with IC_{50} of 4.34 μM and 39.11 μM respectively. The complete orientation change in these molecules made differences in their activity. Also, the compound **La-17** is stabilized with stacking interaction with Phe167 and hydrogen bonding with Ala129 which was turn to be crucial for enzyme activity. The ligand interaction diagram for the compounds is shown in Figure 6.15.

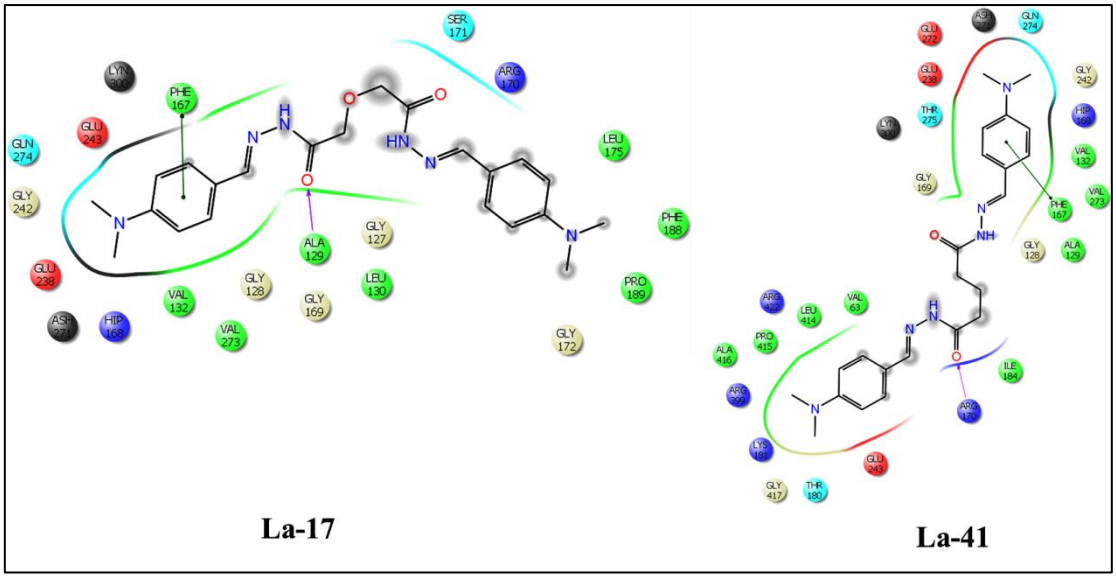

Figure 6.15: Ligand interaction diagram for the compound **La-17** and **La-41**

The naphthyl substituent at R-position showed PS inhibitory activity 7.28 μM on C-linker and 27.03 μM on O-linker. The good activity profile of compound **La-21** can be attributed to the polar contact with Arg422. Also, the right hand side naphthyl group is deep into the hydrophobic pocket, which was further stabilized by π-π stacking interaction with Phe167. The lesser activity of compound **La-45** emphasizes the importance of hydrophobic contacts on the right hand side. The ligand interaction diagram for the compounds is depicted in Figure 6.16.

Nitrothiophene substitution at R-position on C-linker and O-linker showed activity at 8.56 μM and 93.04 μM respectively. The ligand interaction pictures also gave us an insight into the differences in the binding pattern of the molecules. The compound **La-23** was making prominent interaction with Phe167, Gly128 and Gly127 which was considered to be crucial for the enzyme inhibition. Missing interactions in **La-47** made this compound less potent than **La-23**. The ligand interaction diagram for the compounds is depicted in Figure 6.17.

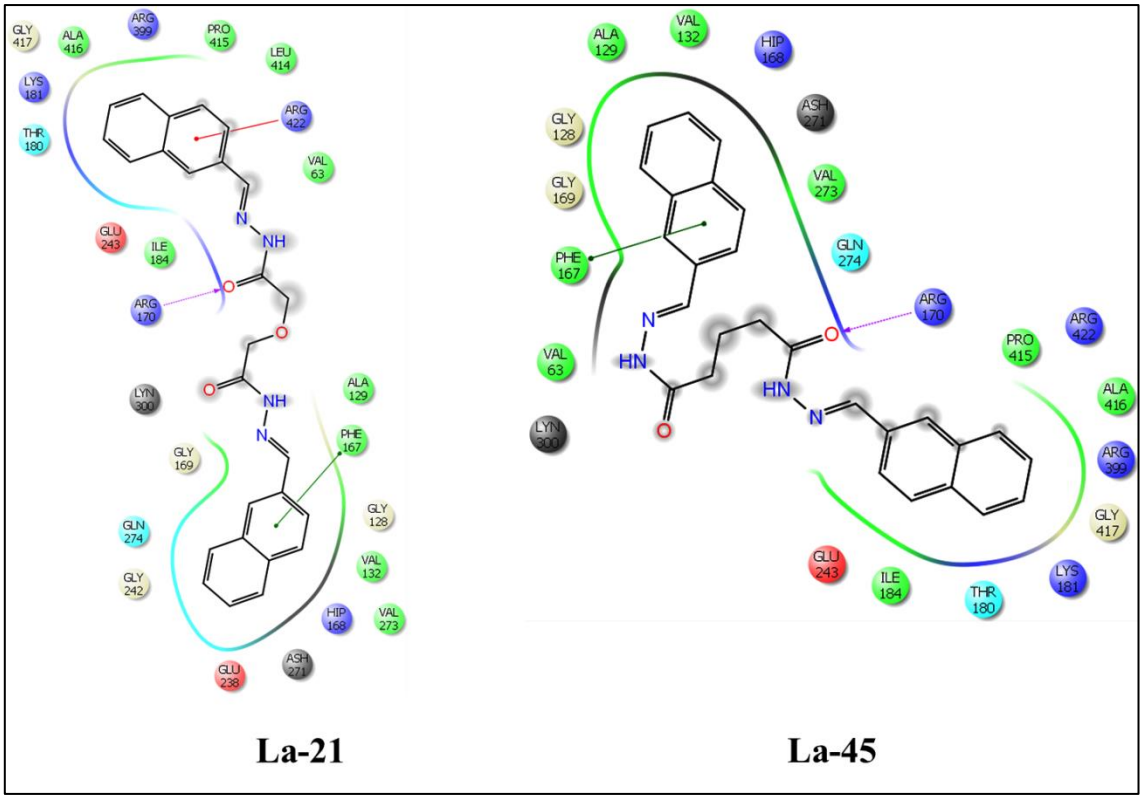

Figure 6.16: Ligand interaction diagram for the compound **La-21** and **La-45**

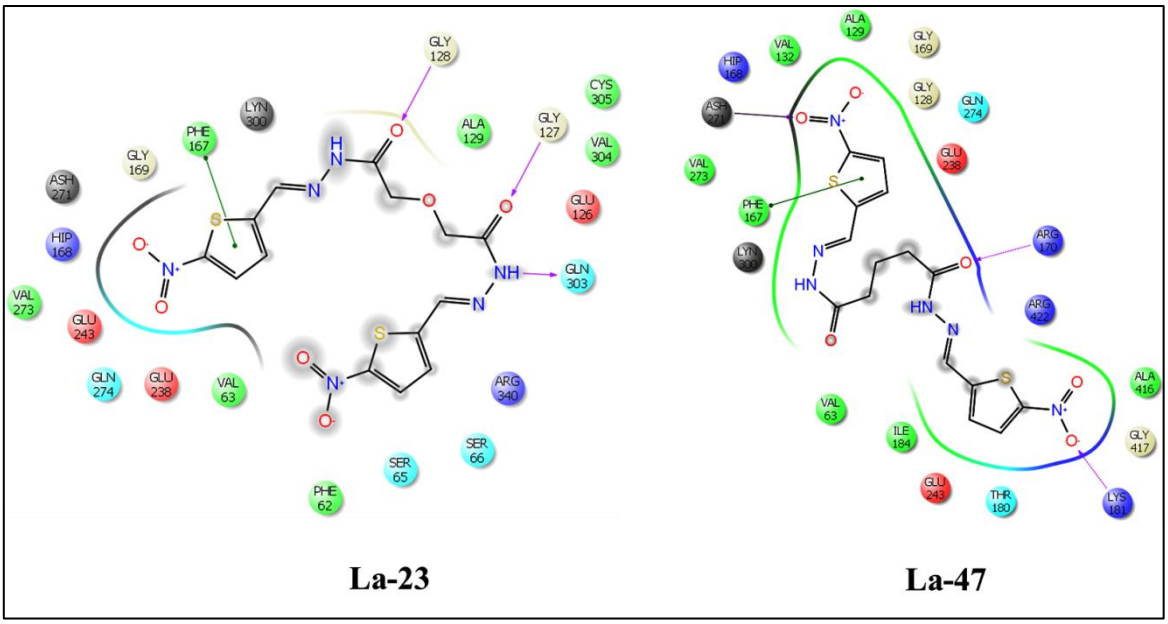

Figure 6.17: Ligand interaction diagram for the compounds **La-23** and **La-47**

6.1.9. In-vitro anti-mycobacterial screening

The synthesized compounds were evaluated for its anti-mycobacterial activity against Mtb H37Rv using MABA assay as described in materials and methods section 4.3.3.1. The MICs were determined for each compound and presented in Table 6.4. Isoniazid and Ethambutol were used as reference compounds for comparison. All the synthesized compounds showed activity against Mtb with MIC ranging from 3.42 to 116.71 µM. Seven compounds (**La-10**, **La-17**, **La-20**, **La-22**, **La-24**, **La-28** and **La-30**) inhibited Mtb with MIC <20 µM. All the compounds were less potent than isoniazid, rifampicin, ethambutol and moxiflaxicin;, while compound **La-21** and **La-23** were two times more potent than ethambutol and the parent **Lead LI-1**. The most potent enzyme inhibitors **La-28** and **La-30** exhibited MIC of 16.71 µM. Similar to the enzyme inhibition profile, the C-linked compounds (**La-1-La-24**) were more effective anti-mycobacterials compared to that of O-linked compounds (**La-25-La-48**). In the Mtb LAT enzyme inhibition assay, **La-28** and **La-30** from the O-linked derivatives emerged promising but in the anti-mycobacterial screening, **La-21** and **La-23** from the C-linked derivatives were found effective. Hence further fine tuning in molecular manipulations are needed to correlate well the enzyme-level and cell-level activities.

6.1.10. In-vitro cytotoxicity evaluation for the synthesized compounds

The synthesized compounds were also tested for in-vitro cytotoxicity against HEK 293 cells at 50 µM concentration in duplicates. Percentage inhibition was calculated and reported in Table 6.4. The most promising compound **La-30** showed only 25.57% of inhibition at 50 µM concentration. Five compounds (**La-31**, **La-38**, **La-43** and **La-44)** that were ineffective in enzyme, Mtb assays and cytotoxicity of all other compounds including parent compounds were non-cytotoxic.

6.1.11. Nutrient starved condition of dormant Mtb

The nutrient starvation conditions were established for Mtb to arrest growth, minimize aerobic metabolism and that were resistant to the existing anti-mycobacterial drugs. The LAT protein in this model was found to be overexpressed 41 times. Owing to its simplicity, reproducibility and handling, we utilized this model for testing potent LAT inhibitors for their effectiveness against dormant form of Mtb. The nutrient starved bacteria were grown according to the procedure discussed in the materials and methods section 4.3.3.5. The plates were incubated at 37°C for 4 weeks and the wells with visible bacterial growth were counted as positive and Most probable numbers (MPN) values were calculated using statistical

methods [Salina E., *et al*., 2014]. At 10 μg/ml concentration, standard first-line antitubercular drugs isoniazid and rifampicin reduced ~1.2 and 2.0 log bacterial reduction respectively, whereas Moxifloxacin showed high log reduction of ~2.5. Ten compounds (**La-15**, **La-17**, **La-18**, **La-21**, **La-23**, **La-30**, **La-33**, **La-35**, **La-36** and **La-38**) were chosen based on wide range of inhibition of the Mtb LAT enzyme. Three compounds (**La-17**, **La-30**, and **La-33**) showed similar log bacterial reduction when compared with isoniazid. Compound **La-23** was found equipotent to moxifloxacin and more potent than rifampicin and isoniazid; interestingly this compound also exhibited LAT enzyme inhibition with IC_{50} of 8.56 μM. Compound **La-48** was found ineffective in this study. The graphical representation of bacterial count and log of bacterial reduction are presented in Figure 6.18 and Table 6.6 respectively. Thus these results was first of its kind in proving Mtb LAT inhibitors to be effective in attenuating dormant Mtb which is the need of the one.

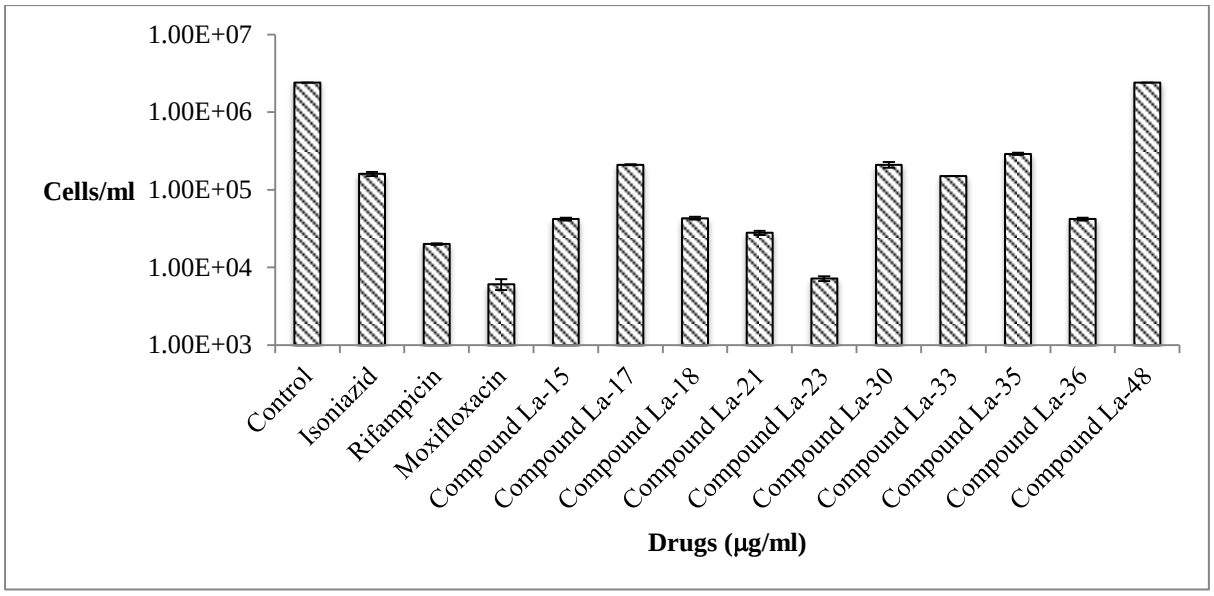

Figure 6.18: Graphical representation for bacterial count by nutrient starvation model for the top active compounds. (Error bars represent the standard deviation)

Table 6.6: Bacterial growth Log reduction values of active compounds with standard drugs

Drug (10µg/ml)	No. of Bacteria	SD*	Log reduction values
Control	2400000	0	NIL
La-15	42000	1802.77	1.5
La-17	210000	2886.75	1.1
La-18	43000	1887.45	1.5
La-21	28000	1750	1.8
La-23	7200	529.15	2.3
La-30	210000	18027.75	1.1
La-33	150000	0	1.2
La-35	290000	10000	0.8
La-36	42000	1802.77	1.5
La-48	2400000	0	NIL
Isoniazid	160000	10000	1.1
Rifampicin	20000	500	2
Moxifloxacin	6100	1000	2.4

*SD-Standard deviation

6.1.12. ADME predictions for the synthesized compounds

Among synthesized compounds the promising leads were were subjected to in-silico ADME predictions using QikProp module in Schrodinger. Various important properties like predicted octanol/water partition coefficient logP, predicted IC_{50} value for blockage of HERG K+ channels, predicted brain/blood partition coefficient, and percent human oral absorption were determined and presented in Table 6.7. LogP values predicted for the compounds were found to be acceptable being >1, due to bulky aryl functional groups present in all these compounds. Predicted Caco-2 cell permeability was very poor for the parent compound **Lead LI-1** which was found to be very much improved with the analogues while leads **La-10, La-23,** and **La-33** were still found in a lower range. Log HERG property was considered important to predict potential cardio toxicity associated with these compounds as the parent **Lead LI-1** was found to cardiotoxic having value more than -5. All the derivatized compounds were found to be safe as their predicted log HERG value were found to be < -5. Encouragingly the oral absorption for all the derivatized compounds was found to be improved many times compared to parent **Lead LI-1**.

Table 6.7: ADME predictions for the synthesized compounds

Compound ID	QPlogPo/w[a]	QPlogHERG[b]	QPPCaco[c]	QPlogBB[d]	% Human oral absorption[e]	Rule of 5[f]
Lead LI-1	2.444	-3.182	0.701	-4.329	12.577	2
La-1	4.769	-7.346	624.326	-1.551	100	0
La-3	4.792	-7.416	491.312	-1.739	100	0
La-5	4.643	-7.41	491.73	-1.459	100	0
La-7	4.515	-7.498	574.453	-1.77	100	0
La-8	4.368	-7.381	490.936	-1.85	100	0
La-10	2.777	-7.411	7.024	-4.282	45.401	1
La-13	2.619	-7.393	45.375	-3.131	71.934	0
La-14	2.627	-7.401	46.306	-3.125	72.141	0
La-15	5.311	-7.477	491.818	-1.356	93.264	1
La-16	5.313	-7.477	491.867	-1.356	93.274	1
La-17	5.03	-7.461	458.557	-1.979	91.071	1
La-18	3.573	-5.465	242.296	-1.896	90.541	0
La-19	1.648	-5.094	232.867	-1.801	78.962	0
La-20	5.194	-7.378	697.031	-1.19	95.287	1
La-21	6.067	-8.778	491.3	-1.789	100	1
La-22	6.135	-7.444	491.9	-1.2	100	1
La-23	2.524	-6.887	5.874	-4.195	42.53	1
La-26	3.869	-7.26	386.171	-1.828	95.895	0
La-28	3.652	-7.259	382.428	-1.572	94.554	0
La-30	3.733	-7.27	379.782	-1.561	94.972	0
La-33	1.959	-7.319	7.295	-4.122	40.904	1
La-35	7.051	-10.04	390.896	-2.461	88.707	2
La-36	7.11	-10.194	378.169	-2.547	88.794	2
La-48	1.887	-7.273	55.085	-2.925	69.155	0

[a]Predicted octanol/water partition coefficient logP (acceptable range: −2.0 to 6.5);[b]Predicted IC_{50} value for blockage of HERG K+ channels.(below -5); [c]Predicted apparent Caco-2 cell permeability in nm/sec (<25 poor; >500 great); [d]Predicted brain/blood partition coefficient (-3.0 to 1.2); [e]Percent human oral absorption (<25% is poor and >80% is high); [f]Rule of 5 violation (mol_MW < 500, QPlogPo/w < 5, donorHB ≤5, accptHB ≤10)

6.1.13. Biophysical characterization of promising compounds

The stabilization of native protein and in complex with ligands was evaluated by measuring the fluorescence of native protein and ligand-protein complexes when exposed to hydrophobic residues of the protein. A positive shift in T_m of protein-ligand complexes compared with native protein signified better stabilization of protein by the ligand binding. The most potent compounds **La-1** and **La-28** show good positive shifts complexed to native protein Mtb LAT. The native protein shows T_m of 50.60°C whereas protein with ligand

complexes shows T_m of 51.70°C, and 53.60°C respectively; which proved better stabilization of the ligand towards the native protein (Figure 6.19 and Figure 6.20) respectively.

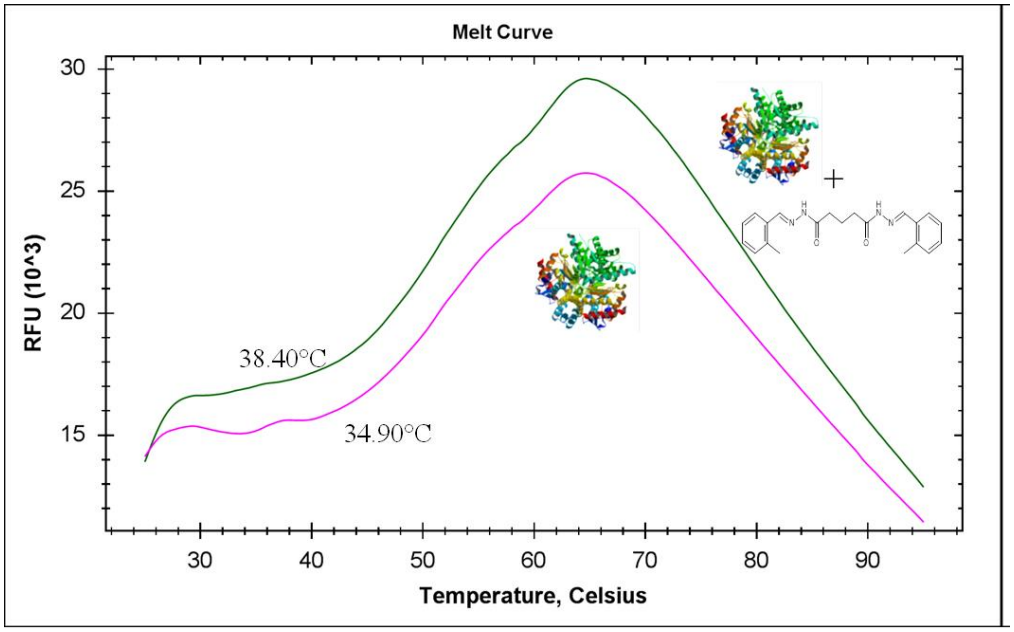

Figure 6.19: Thermal shift analysis for the active compound **La-1** using DSF

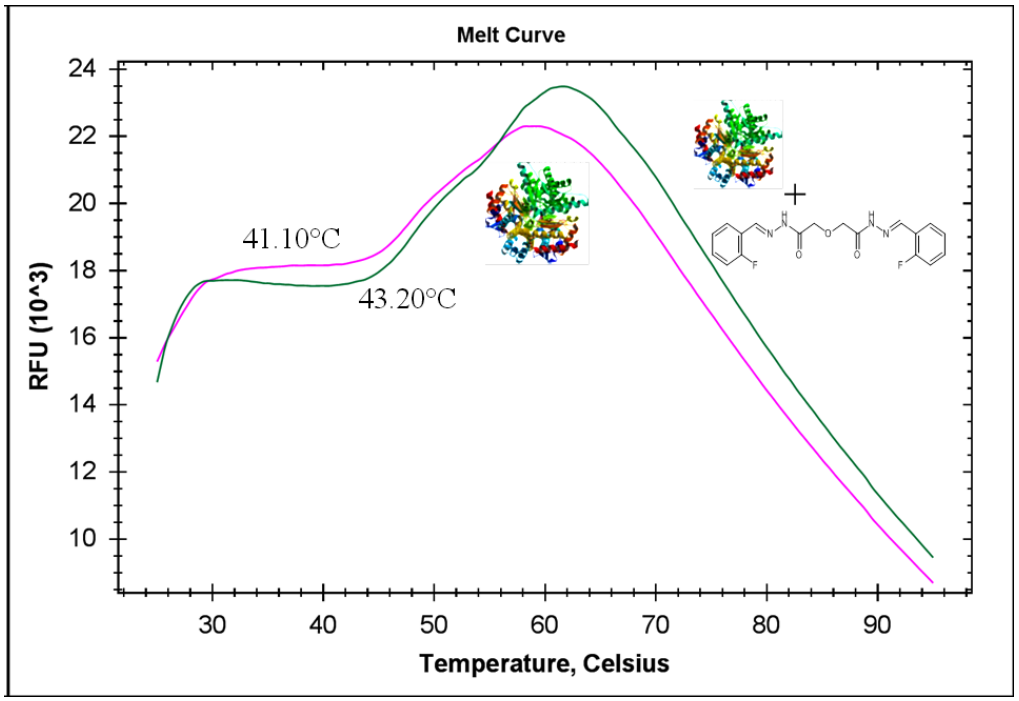

Figure 6.20: Thermal shift analysis for the active compound **La-28** using DSF

6.2: DESIGN II: DESIGN OF INHIBITORS BASED ON SUBSTRATE α-KETOGLUTARATE WITH PLP BOUND TO Mtb LAT

As earlier mentioned there were no reported inhibitor available for Mtb LAT, we utilized also the crystal structure of Mtb LAT bound to α-ketoglutarate with PLP. In the present study, we identified some novel small molecule inhibitors that could bind to the active site of Mtb LAT protein with the help of e-pharmacophore modelling using the crystal structure with PDB ID: 2CJH and 2.00 Å resolution. The crystal structure of the protein bound with α-ketoglutarate and PLP was shown in Figure 6.21.

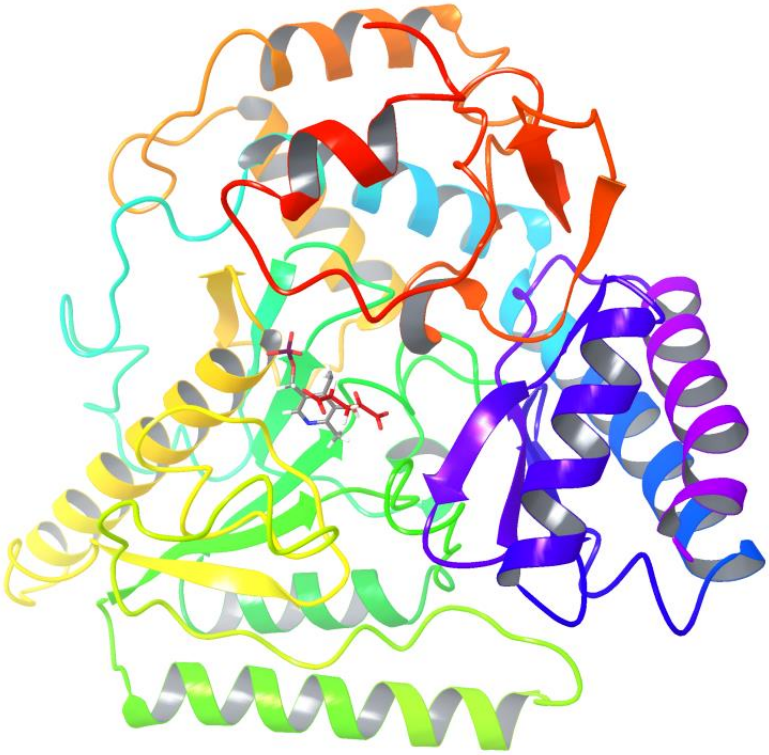

Figure 6.21: Crystal structure of LAT bound with α-ketoglutarate (2CJH)

6.2.1. Protein preparation and active site cavity validation

The retrieved protein was prepared using protein preparation wizard as mention earlier. The diagrammatic representation of crystal ligand bound in the active site of protein and its ligand interaction diagram are shown in Figure 6.22.

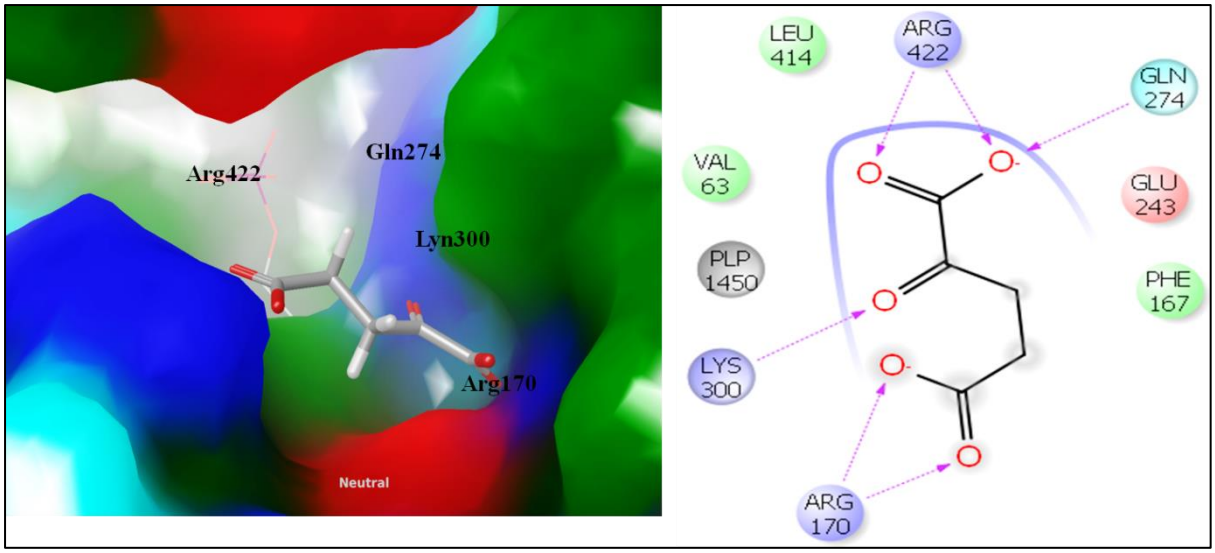

Figure 6.22: Binding analysis and ligand interaction diagram for reference ligand

To validate the method in prediction of binding energy and possible interaction between ligands and receptor, at first existing ligand in crystal structure was re-docked in 2CJH. The reference ligand was redocked and showed docking score of -5.58 kcal mole^{-1} with the important interactions retained with Gln274, Arg422, Lys300 and Arg170. After superimposition, RMSD of 0.34Å was gained and showed that this technique could be utilized for next predictions (Figure 6.23).

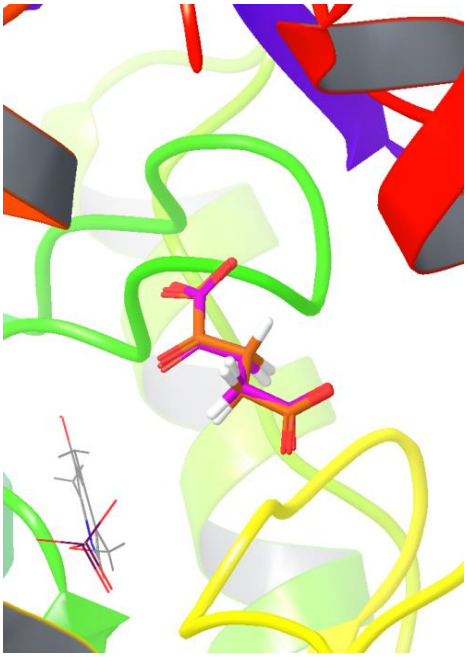

Figure 6.23: Superimposition of reference ligand α-ketoglutarate in crystal and docked pose where, orange colour represents docked and purple colour represents original ligand

The active site of the protein was located and grid files were generated using receptor grid generation panel. Grid size was calculated was found to be 15Å and further docking studies.

6.2.2. E-pharmacophore generation

Pharmacophore hypothesis based on mapping of the energetic terms from the extra precision (XP) Glide XP scoring function onto atom centres were obtained using PHASE. A three-point e-pharmacophore model was generated with Mtb LAT protein based with α-ketoglutarate (Figure 6.24). The pharmacophoric sites included one hydrogen bond acceptor (A1) and two negative ionizable groups (N2 and N3). This e-pharmacophore was further used for virtual screening of a commercial database Asinex.

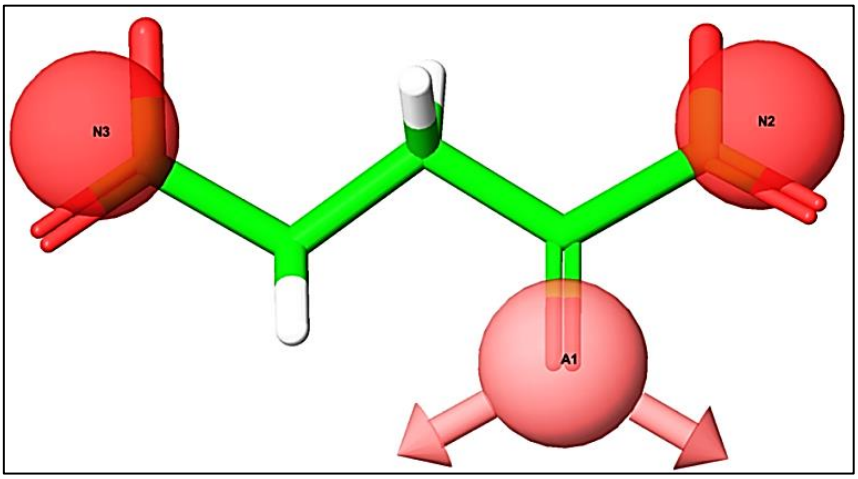

Figure 6.24: E-pharmacophore model based on α-ketoglutarate

6.2.3. Virtual screening of molecules and docking

We followed similar protocol as reported in the previous sections utilizing 2CJD, wherein first pharmacophore filter was performed on the commercial database (Asinex). The hits derived at each stage were validated based on fitness score which indicated how well they matched the pharmacophore features. The compounds with the high fitness scores were shortlisted for high-throughput virtual screening. The ligands were docked into the Mtb LAT active site using the grid generated and selected 256 hits from HTVS with a criterial of docking score above ≤ -3.0 kcal mol^{-1}. These hits were further subjected to another round of docking by Glide XP. Finally, 67 hits were identified from XP docking, with docking scores between -5.22 to -7.80 kcal mol^{-1}. Top eight compounds were selected based on visual inspection on interactions and their structures are illustrated in Figure 6.25. The compounds belonged to five different diverse scaffolds; the final shortlisting of the molecules was based on the protein ligand interaction in the active site cleft through hydrogen bonding with

Arg170, Arg422, Gln274 and Lys300. The docking scores, fitness, hydrogen bonding and ligand interaction for the top hits are represented in Table 6.8.

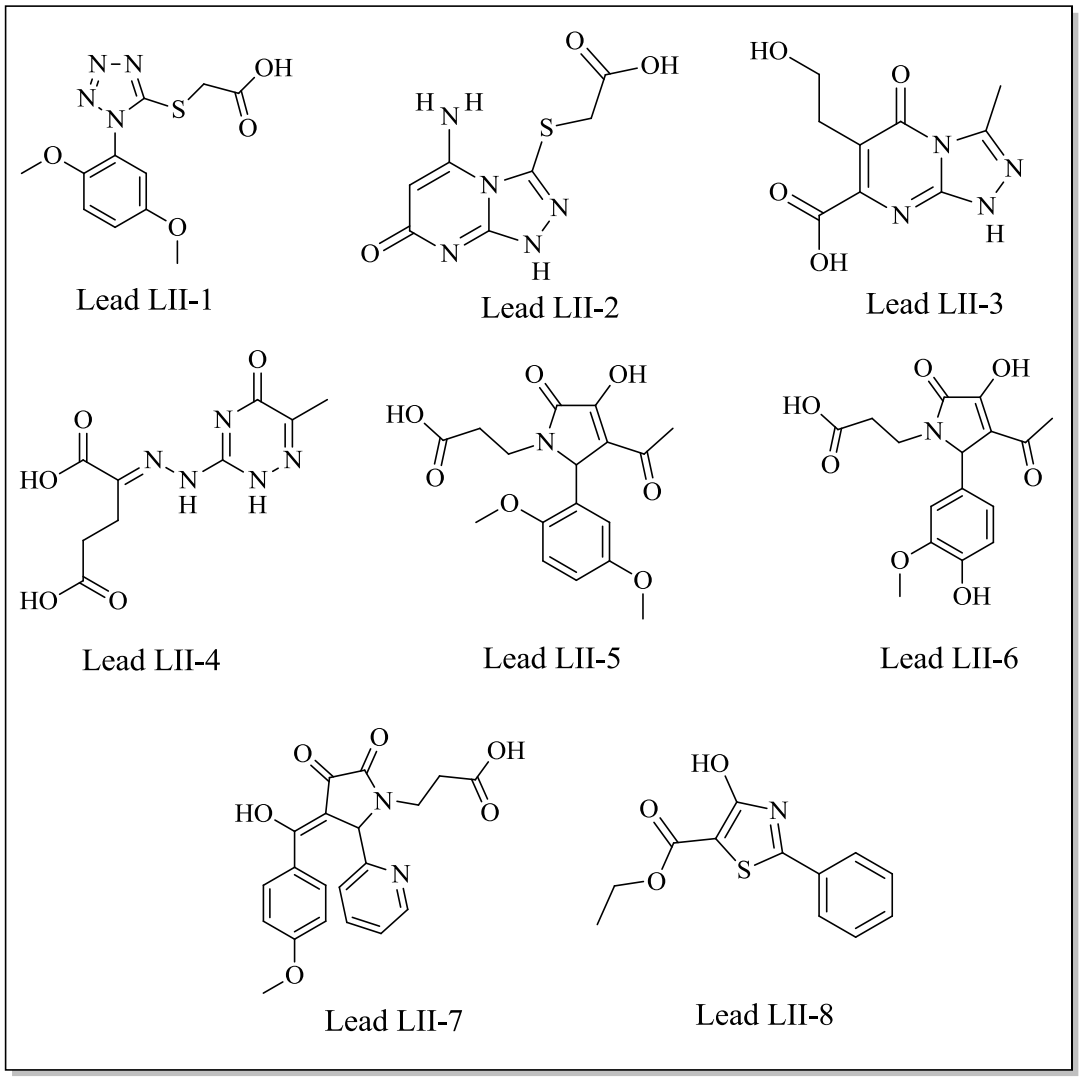

Figure 6.25: Chemical structures for the selected designed inhibitors by virtual screening

Table 6.8: Computational analysis for the designed compounds

Compound ID	Docking score	Hydrogen bond	Fitness	Interaction
Crystal ligand	-5.58	4	2.18	Gln274, Arg422, Lys300 , Arg170
Lead LII-1	-6.53	4	2.04	Arg422,Gln274,phe167,Arg170
Lead LII-2	-6.23	5	2.1	Gln274,Arg170,Lys300,Arg422
Lead LII-3	-7.14	5	2.13	Aerg422,Gln274,Arg170
Lead LII-4	-7.96	7	2.35	Arg170, Gln274,Arg422,Lys300
Lead LII-5	-7.55	5	2.23	Arg422,gln274,Lys300,Arg170
Lead LII-6	-8.8	6	2.17	Arg422,Lys300,Gln274,Arg170
Lead LII-7	-7.75	2	2.32	Arg422, Gln274
Lead LII-8	-7.65	3	2.24	Arg422, Lys300, Phe167

6.2.4. ADME prediction for the designed compounds

All the selected designed compouds were subjected to in-silico ADME properties using QikProp module in Schrodinger. The compounds shortlisted were found to be in accordance with Lipinski's rule of five which was the preliminary criteria for drug-like molecules. Various important properties like predicted octanol/water partition coefficient logP, predicted IC_{50} value for blockage of HERG K+ channels, predicted apparent Caco-2 cell permeability in nm/sec, predicted brain/blood partition coefficient, predicted human oral absorption were determined for the selected compounds and checked for any deviations. The predicted logP values were not in the acceptable range for the Leads **LII-2**, **LII-3** and **LII-4**. Most of the compounds (**Lead LII-1**-**Lead LII-7**) were predicted to be associated with HERG cardiotoxicity. The Caco-2 cell permeability property was not in the acceptable range for the compounds (**Lead LII-2- Lead LII-7**). As mentioned earlier, the permeation of drugs through the membrane could occur by hydrogen bond cleavage in aqueous environment. Potentially, molecules could make more hydrogen bonds leading to more energy to cleavage of hydrogen bond which was unfavourable property that would result in low permeability and absorption. Thus these molecules were predicted to make more hydrogen bonding which might have made these compounds to fail in Caco-2 cell permeability. Predicted % human oral absorption was very poor for the compound **Lead LII-4**. However these compounds were found to pass the Lipinski rule of five properties. The predicted properties for selected compounds are tabulated in the Table 6.9.

Table 6.9: ADME predictions for the designed compounds

Compound ID	QPlogPo/w[a]	QPlogHERG[b]	QPPCaCo[c]	QPlogBB[d]	% Human oral absorption[c]	Rule of 5[f]
Lead LII-1	1.522	-2.064	47.159	-1.222	65.811	0
Lead LII-2	-0.279	-2.024	4.154	-2.201	36.378	0
Lead LII-3	-0.187	-1.661	10.234	-1.855	43.93	0
Lead LII-4	-0.878	-0.628	0.333	-3.14	13.25	0
Lead LII-5	1.528	-2.632	13.767	-2.096	56.274	0
Lead LII-6	1.017	-2.575	8.809	-2.244	49.81	0
Lead LII-7	2.292	-4.021	19.656	-2.078	63.519	0
Lead LII-8	3.101	-5.215	758.826	-0.666	96.649	0

[a]Predicted octanol/water partition coefficient logP (acceptable range: −2.0 to 6.5);[b]Predicted IC_{50} value for blockage of HERG K+ channels.(below -5);[c]Predicted apparent Caco-2 cell permeability in nm/sec (<25 poor; >500 great); [d]Predicted brain/blood partition coefficient (-3.0 to 1.2);[e]Percent human oral absorption (<25% is poor and >80% is high);[f]Rule of 5 violation (mol_MW < 500, QPlogPo/w < 5, donorHB ≤5, accptHB ≤10)

6.2.5. Biological assessments

Enzyme inhibition studies were performed as discussed in the materials and methods section 4.3.2.3. The range finding experiments and enzyme kinetics studies were performed as described in the section 6.1.5 and the K_m for the substrates lysine and α-ketoglutarate were carried throughout the reactions. The designed eight compounds were tested in concentrations of inhibitor varied from 50 μM to 1 μM. The reaction components except Mtb LAT were mixed in the well and the background reaction was measured. Mtb LAT was then added and the reaction kinetics was monitored. The reaction mixture was incubated at 37°C for 1 hr. The reaction was terminated by the addition of 10% trichloroacetic acid in ethanol. The product piperidene 6-carboxylate was measured due to its colour intensity of its adduct with o-aminobenzaldehyde at 465 nm in a heat-controlled PerkinElmer Victor X3 spectrophotometer. In the initial screening, at 50 μM the designed compounds showed good range of inhibition and the IC_{50} values were calculated and tabulated in Table 6.10. Among the eight compounds, five compounds (**Lead LII-2-LII-5** and **Lead LII-8**) showed good IC_{50} values. The **Lead LII-8** showed the best IC_{50} of 5.32±0.32 μM.

Table 6.10: Preliminary enzyme inhibition screening for the designed compounds

Compound ID	IC_{50} values (μM)
Lead LII-1	>50
Lead LII-2	17.37±0.17
Lead LII-3	39.10±0.09
Lead LII-4	19.14±0.27
Lead LII-5	25.05±0.42
Lead LII-6	>50
Lead LII-7	>50
Lead LII-8	5.32±0.32

To evaluate the difference in potency of these compounds, the docking orientations were compared with the crystal ligand and the lead compounds revealed important hydrogen bonding interactions with Lys300 and Arg422 (Figure 6.26). With regard to **Lead LII-8**, in addition to hydrogen bonding interactions the thiazole ring was found to participate with π-π stacking interaction with Phe167 which was absent with other compounds making **Lead LII-8** more potent thatn other compounds.

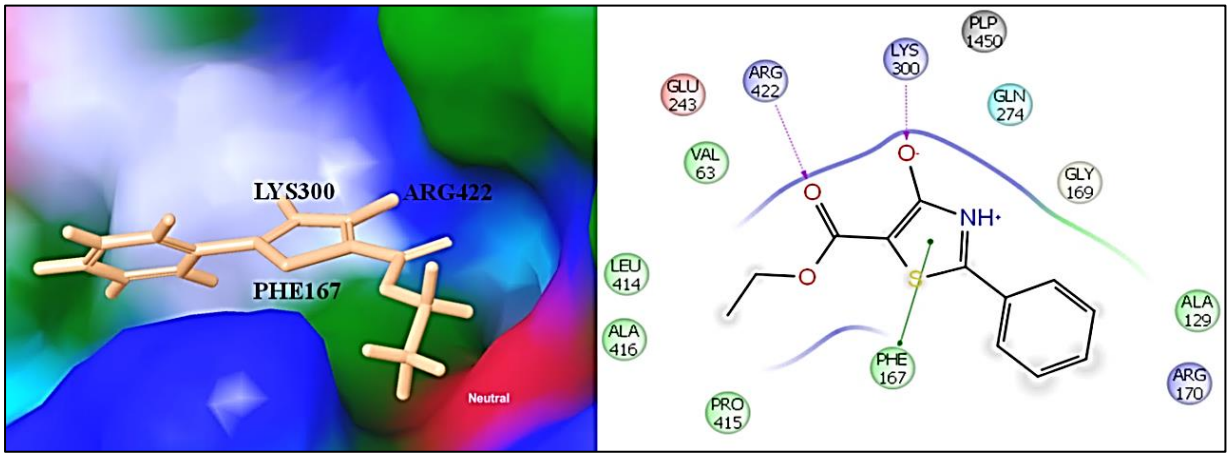

Figure 6.26: Binding analysis and ligand interaction diagram for **Lead LII-8**

The ligand interaction diagrams of other active compounds as depicted in the Figure 6.27, revealed that **Leads LII-2** and **LII-4** which were promising next to **LII-8** were found to interact with PLP1450 which was absent in other compounds including **LII-8**. Lead compounds **LII-3** and **LII-5** lacked hydrogen bonding with Arg170 which could be responsible for lower activity. Though this interaction was found missing with the most active **Lead LII-8**, hydrophobic interaction with Phe167 could have compensated for this.

The most potent **Lead LII-8** with IC_{50} of 5.32 µM was taken as a reference molecule for further derivatization in-order to optimise the activity at lower concentrations.

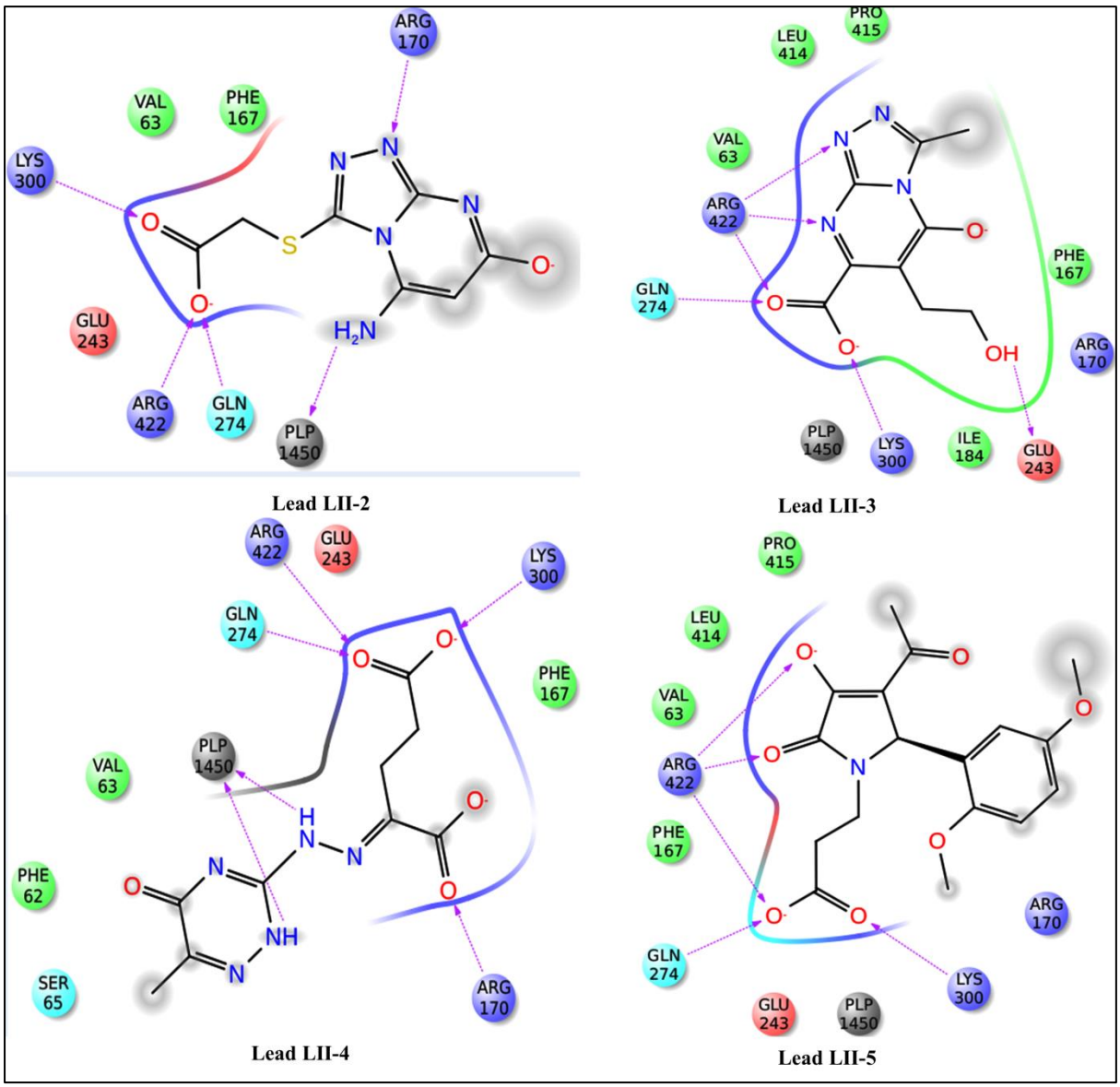

Figure 6.27: Ligand interaction diagram for the active compounds (**Lead LII-2**, **LII- 3**, **LII-4** and **LII-5**) based on preliminary screening

6.2.6. Lead optimization using medicinal chemistry

Further, **Lead LII-8** was optimized and a series of 36 compounds was synthesized by collaboration with medicinal chemistry drug discovery group in department of pharmacy. The detailed procedure to synthesis, its physical data and spectral data were given in annexure IV at the end of the thesis. The scheme utilized is depicted in as Figure 6.28.

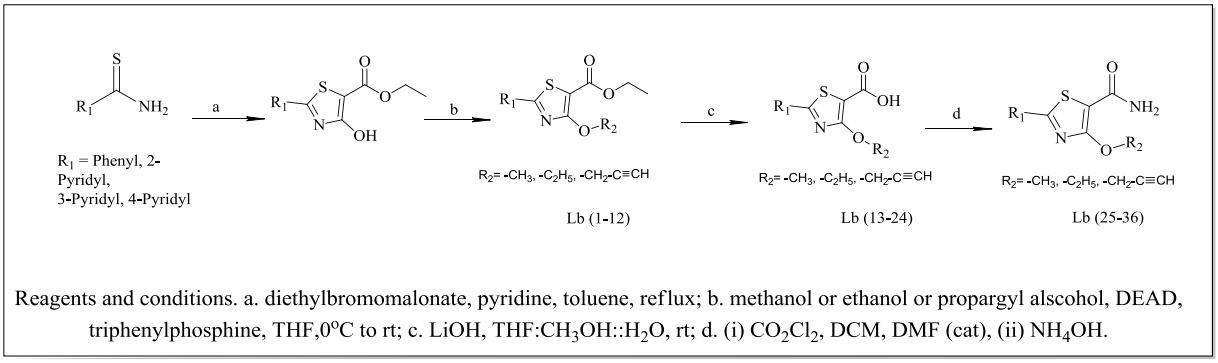

Reagents and conditions. a. diethylbromomalonate, pyridine, toluene, reflux; b. methanol or ethanol or propargyl alscohol, DEAD, triphenylphosphine, THF,0^0C to rt; c. LiOH, THF:CH_3OH::H_2O, rt; d. (i) CO_2Cl_2, DCM, DMF (cat), (ii) NH_4OH.

Figure 6.28: Scheme utilized for developing Mtb LAT leads-α-ketoglutarate based approach

Synthesis of the thiazole core began by condensing commercially available aryl (phenyl, 2-pyridyl, 3-pyridyl and 4-pyridyl) thioamides with diethyl bromo malonate in toluene under refluxing conditions giving the corresponding 4-hydroxy thiazole derivatives in desired yield [Kerdesky F.A.J., *et al.,* 1991 and Jeankumar V.U., *et al.,* 2013]. The alkyl tail at R_2 position was fused into the thiazole core by mistnobu reaction of hydroxyl group in the thiazole core with various alcohols (*viz*: methyl, ethyl and propargyl) to yield ether linked derivatives **Lb-1-Lb-12** in good yields. These analogues **Lb-1-Lb-12** were further hydrolysed into their corresponding acid derivatives **Lb-13-Lb-24** and later converted to their amide derivatives **Lb-25-Lb-36** as well, in an effort to understand the ideal site for introducing chemical diversity.

6.2.7. In-vitro LAT inhibition assay for the synthesized compounds

The synthesized compounds were assayed for in-vitro Mtb LAT inhibition study as described earlier. The end product piperidene 6-carboxylate was measured due to its colour intensity of its adduct with o-aminobenzaldehyde at 465 nm in a heat-controlled Perkinelmer Victor X3 spectrophotometer. Mostly all compounds exhibited good IC_{50} values in the range of 1.21-15 μM towards Mtb LAT. The activity data for all the synthesized compounds are presented in Table 6.11. About half of the compounds synthesized were found to more active (<5 μM) than the parent compounds **Lead LII-8**. Compounds **Lb-2**, **Lb-8**, **Lb-21, Lb-16**, and **Lb-29**, were found to be most potent compounds towards Mtb LAT with IC_{50}s less than 2 μM.

Table 6.11: Biological evaluation of synthesized molecules

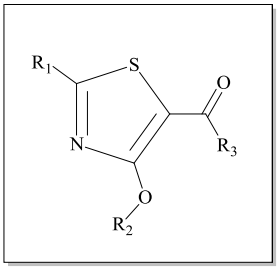

Compound ID	R_1	R_2	R_3	IC_{50} (μM)[a]	MIC (μM)[b]	% Cytotoxicity at 50 μM[c]
Lead LII-8	Phenyl	H	OC_2H_5	5.32±0.32	50.16	43.86±0.59
Lb-1	Phenyl	Methyl	OC_2H_5	7.96±0.13	189.89	28.60±0.01
Lb -2	2-Pyridyl	Methyl	OC_2H_5	1.87±0.28	23.65	41.83±0.03
Lb -3	3-Pyridyl	Methyl	OC_2H_5	4.91±0.12	47.29	36.64±0.01
Lb -4	4-Pyridyl	Methyl	OC_2H_5	6.48±0.31	94.59	25.79±0.10
Lb -5	Phenyl	Ethyl	OC_2H_5	4.68±0.12	90.15	36.64±0.01
Lb -6	2-Pyridyl	Ethyl	OC_2H_5	10.45±0.23	89.82	22.78±0.01
Lb -7	3-Pyridyl	Ethyl	OC_2H_5	8.75±0.22	22.46	38.76±0.01
Lb -8	4-Pyridyl	Ethyl	OC_2H_5	1.99±0.14	89.82	28.37±0.09
Lb -9	Phenyl	Propargyl	OC_2H_5	8.25±0.13	43.5	30.62±0.32
Lb -10	2-Pyridyl	Propargyl	OC_2H_5	6.60±0.41	173.42	42.06±0.08
Lb -11	3-Pyridyl	Propargyl	OC_2H_5	9.76±0.15	86.7	48.91±0.08
Lb -12	4-Pyridyl	Propargyl	OC_2H_5	4.01±0.31	21.68	54.44±0.07
Lb -13	Phenyl	Methyl	OH	13.66±0.16	212.54	38.60±0.01
Lb -14	2-Pyridyl	Methyl	OH	6.82±0.22	52.91	34.49±0.04
Lb -15	3-Pyridyl	Methyl	OH	6.54±0.32	26.46	30.44±0.05
Lb -16	4-Pyridyl	Methyl	OH	1.21±0.21	211.65	24.87±0.09
Lb -17	Phenyl	Ethyl	OH	9.08±0.12	100.29	26.69±0.01
Lb -18	2-Pyridyl	Ethyl	OH	5.70±0.61	24.97	28.16±0.08
Lb -19	3-Pyridyl	Ethyl	OH	2.95±0.31	24.97	29.14±0.01
Lb -20	4-Pyridyl	Ethyl	OH	5.47±0.72	49.95	42.08±0.03
Lb -21	Phenyl	Propargyl	OH	1.82±0.22	12.05	24.46±0.06
Lb -22	2-Pyridyl	Propargyl	OH	15.36±0.51	48.03	30.77±0.01
Lb -23	3-Pyridyl	Propargyl	OH	4.55±0.21	24.01	36.47±0.05
Lb -24	4-Pyridyl	Propargyl	OH	15.26±0.64	48.03	33.75±0.03
Lb -25	Phenyl	Methyl	NH_2	4.85±0.21	106.71	34.95±0.02
Lb -26	2-Pyridyl	Methyl	NH_2	4.98±0.51	53.13	32.40±0.05
Lb -27	3-Pyridyl	Methyl	NH_2	5.003±0.62	106.27	29.97±0.02
Lb -28	4-Pyridyl	Methyl	NH_2	2.81±0.71	53.13	22.36±0.01
Lb -29	Phenyl	Ethyl	NH_2	1.72±0.64	25.17	34.99±0.01

Contd

Compound ID	R_1	R_2	R_3	IC_{50} (μM)[a]	MIC (μM)[b]	% Cytotoxicity at 50 μM[c]
Lb -30	2-Pyridyl	Ethyl	NH_2	2.16±0.42	100.28	29.60±0.02
Lb -31	3-Pyridyl	Ethyl	NH_2	5.56±0.61	100.29	38.80±0.01
Lb -32	4-Pyridyl	Ethyl	NH_2	2.40±0.81	50.14	26.47±0.05
Lb -33	Phenyl	Propargyl	NH_2	8.74±0.71	193.58	27.65±0.02
Lb -34	2-Pyridyl	Propargyl	NH_2	3.33±0.93	48.21	30.78±0.03
Lb -35	3-Pyridyl	Propargyl	NH_2	4.82±0.11	48.21	52.18±0.07
Lb -36	4-Pyridyl	Propargyl	NH_2	8.51±0.91	96.42	43.50±0.08
Isoniazid	-	-	-	ND	0.72	NIL
Rifampicin	-	-	-	ND	0.15	NIL
Ethambutol	-	-	-	ND	7.64	NIL
Moxifloxacin	-	-	-	ND	1.24	NIL

[a]Mtb LAT enzyme inhibitory assay; [b]Minimum Inhibitory concentration against *M. tuberculosis* H37Rv; [c]**%** inhibition of HEK293 cells; ND indicates not determined

The dose response curve for the most active compounds was plotted using non-linear regression analysis GraphPad Prism software (Figure 6.29 and Figure 6.30).

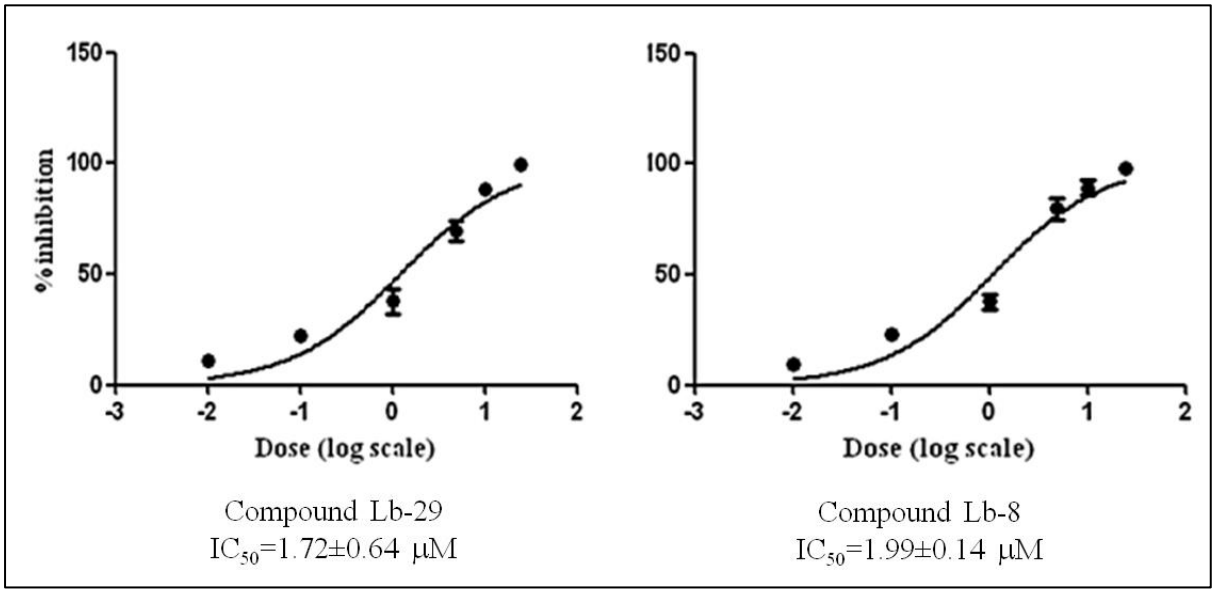

Figure 6.29: Dose response curve for the active compounds (**Lb-29** and **Lb-8**)

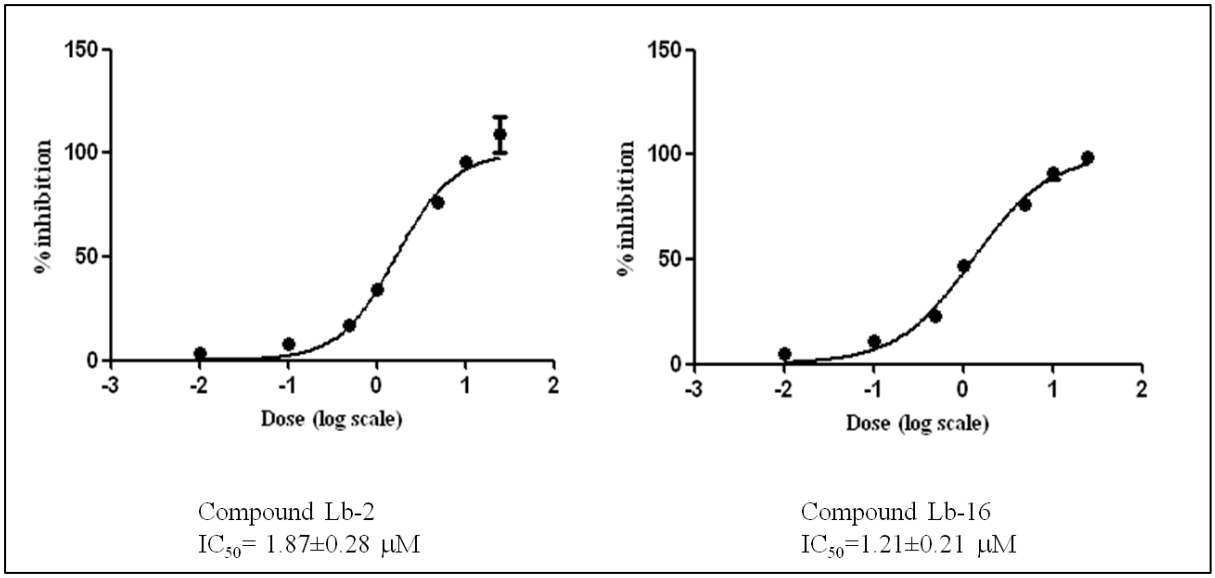

Figure 6.30: Dose response curve for the compound **Lb-2** and **Lb-16**

Overall the activities of the derivatives were based on R_3 substitutions. The amide derivatives were more active than the ethyl ester derivatives which were better thatn simple carboxylic acid compounds. Among the ester compounds (**Lb-1-Lb-12**) the order of activity based on R_1 substitution was found to be 4-pyridyl > 2-pyridyl > phenyl = 3-pyridyl. With regard to R_2 substitution, methyl and ethyl were well tolerated compared to propargyl group. In this series, compounds **Lb-2** and **Lb-8** emerged as promising hits compared to the parent **Lead LII-8**.

With regard to carboxylic acid compounds (**Lb-13-Lb-24**), the order of activity of R_1 substitution was found to be 3-pyridyl > 4-pyridyl > phenyl > 2-pyridyl. In this series, 3-pyridyl substitution was favourable compared to ester compounds. An ethyl substitution at R_2 was more favourable than methyl and propargyl group similar to parent **Lead LII-8**. Among these compounds, **Lb-16** emerged as the most potential LAT inhibitor which had 4-pyridyl substitution at R_1 and methyl group at R_3 position.

Lastly when the amide compounds (**Lb-25-Lb-36**) were analyzed, the 2-pyridyl group at R_1 was more favoured than phenyl and then 4-pyridyl and 3-pyridyl. Among the R_2 substituents ethyl was more preferred than methyl and propargyl groups. The most potent inhibitor in the amide series was found to be **Lb-29**.

A closer analyses of all the most active compounds (**Lb-2**, **Lb-8**, **Lb-16**, **Lb-21** and **Lb-29**) in the Mtb LAT protein revealed that all the compounds made favourable interactions with important amino acid residues such as Arg170/Arg440, and Lys300 hydrogen bond distances less than 2.5 Å which made stable protein-ligand complex. In-order to study the structure-

activity relationships of the **Lead LII-8** derivatives, 36 different analogues were prepared and could divided into three subsets. The R_1 position was substituted with different aromatic groups like phenyl, 2-pyridyl, 3-pyridyl and 4-pyridyl; whereas the R_2 was substituted with simple alkyl groups like methyl, ethyl and propargyl respectively. Also, the R_3 was substituted with ethoxy, hydroxyl or amino groups. Further to support the activity we performed docking for these compounds. All the compounds were docked in to the active site of Mtb LAT protein using Glide (Glide v5.7, Schrodinger, LLC, New York, NY). The hydrophobic pocket of Mtb LAT was defined by the side chains of Phe415, Leu414, Val63, and Phe167.

The compounds **Lb-2**, **Lb-8**, **Lb-16** and **Lb-29** showed similar inhibitory effect. The active site of the Mtb LAT protein was small, thus due to the inherent flexibility of their side chain, this is more likely simply a favourable electrostatic interaction. The hydrophobic pocket of Mtb LAT was defined by the side chains of Phe415, Leu414, Val63, and Phe167. Our most active ligand 4-methoxy-2-(pyridin-4-yl)thiazole-5-carboxylic acid (**Lb-16**) on docking gave a highest docking score of -8.31 kcal mol^{-1}. It showed three hydrogen bonding interactions with Arg422, Gln274 and Lys300 amino acid residues. The binding pattern within the active site pocket of the crystal ligand and reference ligand was quite similar and additionally some hydrophobic interaction with Leu414, Phe167 and Val63 constituted for a stable binding profile of the molecule as shown in the Figure 6.31**.** It has been found that Gln274 amino acid interaction was missing in the compounds **Lb-2**, **Lb-8** and **Lb-29**. Also, **Lb-2** was stabilized by π-π stacking interaction. The Arg170 amino acid interaction was found to be common in compounds **Lb-29** and **Lb-8**. The most prominent hydrogen bonding interaction with Lys300 in all these compounds (**Lb-2**, **Lb-8**, **Lb-21** and **Lb-29**) hydrogen was found to be crucial for LAT inhibition.

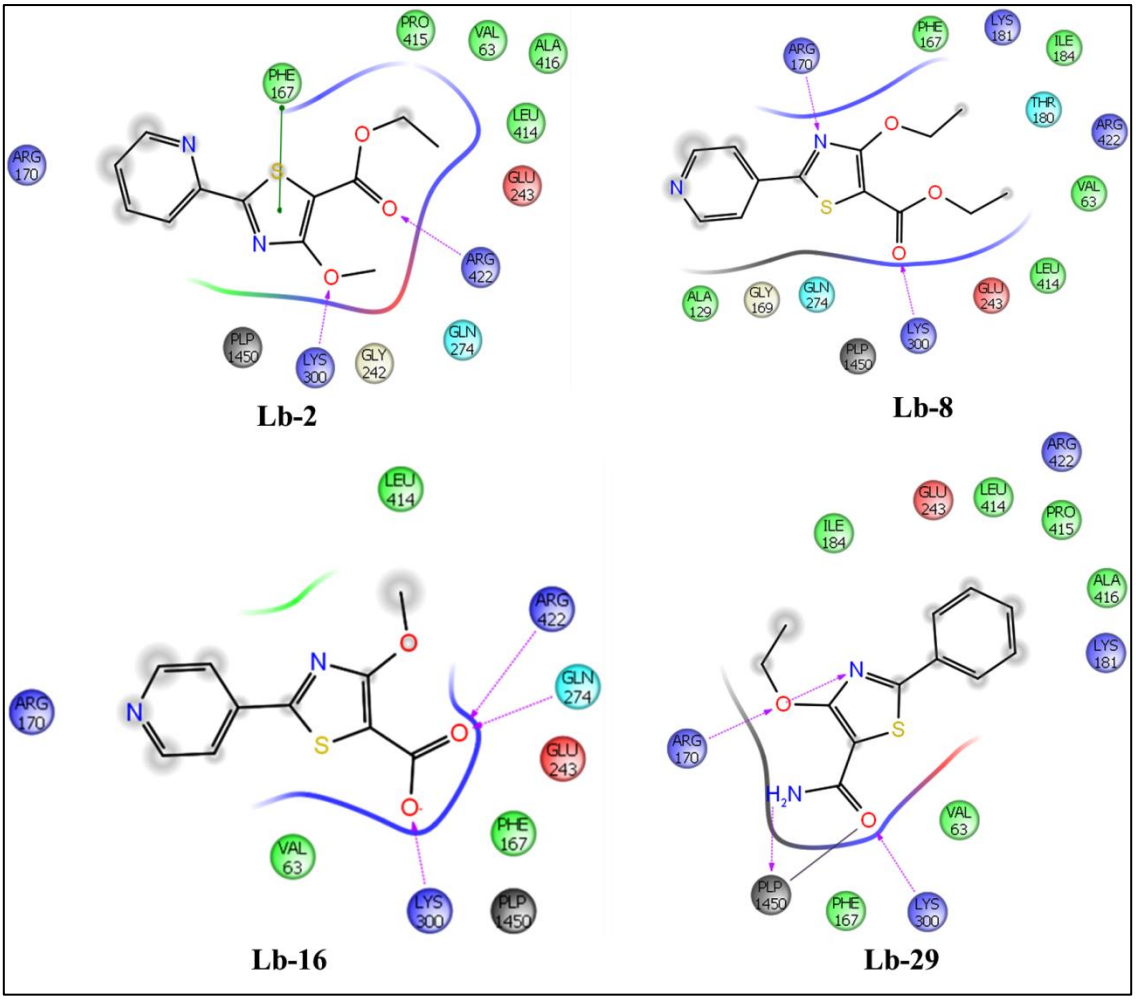

Figure 6.31: Ligand interaction diagram for the compounds **Lb-2, Lb-8, Lb-16** and **Lb-29**

6.2.8. In-vitro anti-mycobacterial screening in active Mtb model

The synthesized compounds were assayed for in-vitro anti-mycobacterial assay in active Mtb as described earlier. The MIC was determined for each compound which was measured as the minimum concentration of compound required to completely inhibit the mycobacterial growth. Of all the 36 synthesized compounds, only compound **Lb-21** showed low MIC value of 12.05 µM. Isoniazid and ethambutol were used as reference compounds for comparison. The MIC values of the synthesized compounds along with the standard drugs for comparison are presented in Table 6.10. All the synthesized compounds showed activity against Mtb with MIC ranging from 12.05 to 212.54 µM. All the compounds were found to be less potent than isoniazid and ethambutol. In general, compounds from carboxylic acid series were found to be more active compared to ester derivatives and least effective were from amide series. The promising in-vitro potency observed at the enzymatic level was not translated in anti-

mycobacterial potency. This could probably be due to poor cell permeability or due to efflux pump transportation.

6.2.9. In-vitro cytotoxicity evaluation of synthesized compounds

The synthesized compounds were also tested for in-vitro cytotoxicity HEK 293 cells at 50 μM concentration in duplicates. Percentage inhibition was calculated and reported in Table 6.10. Compounds inhibited in the range of 22.36 to 54.44 μM. The most promising compounds **Lb-2**, **Lb-16**, **Lb-21** and **Lb-29** were found to be non-cytotoxic at 50 μM concentration. Only compound **Lb-12** showed moderate cytotoxicity at 50 μM with 54% inhibition.

6.2.10. Nutrient starved condition for dormant Mtb screening

As mention earlier in the literature review, *lat* gene has been found to be over-expressed about 40 times in nutrient starved conditions. So with this importance of *lat* gene in dormant model we established nutrient starved condition for Mtb bacteria to study the potencies of prominent compounds (**Lb-2**, **Lb-8**, **Lb-12**, **Lb-16**, **Lb-18**, **Lb-21**, **Lb-23**, **Lb-25**, **Lb-28-Lb-31** and **Lb-34**). As a hypothesis we selected compounds from each subset *i.e.* in $–OC_2H_5$, –OH substation, and amino substitution inorder to check the activity dormant model of Mtb. The nutrient starved bacterium was grown according to the procedure discussed earlier. After incubation of Mtb bacteria with 10 μg/ml concentration of potencies compounds were evaluated and compared with standard drugs like isoniazid, rifampicin and moxiflaxicin. These standard drugs were found to reduce ~1.2, 2.0 and 2.3 of log bacterial counts. All the fourteen compounds were one fold more potent than first-line anti-tubercular drug isoniazid in the range of ~2.0 to 2.8 log bacterial population reduction. 11 compounds (**La-2, La-8**, **La-12**, **La-16**, **La-18**, **La-21**, **La-25**, **La-28**, **La-29**, **La-30**, and **La-31**) showed ~2.2-2.8 log bacterial population reduction better than standard drugs. The compound **La-12** and **Lb-29** were found to be more potent in nutrient starved bacteria with the bacterial log reduction of ~2.8; which was 0.4 times more than the promising standard drug moxiflaxicin. These compounds were also found to inhibit Mtb LAT with the IC_{50} of 4.01 μM and 1.72 μM respectively. The graphical representation of bacterial count and log of bacterial reduction data are shown in Figure 6.32 and Table 6.12 respectively.

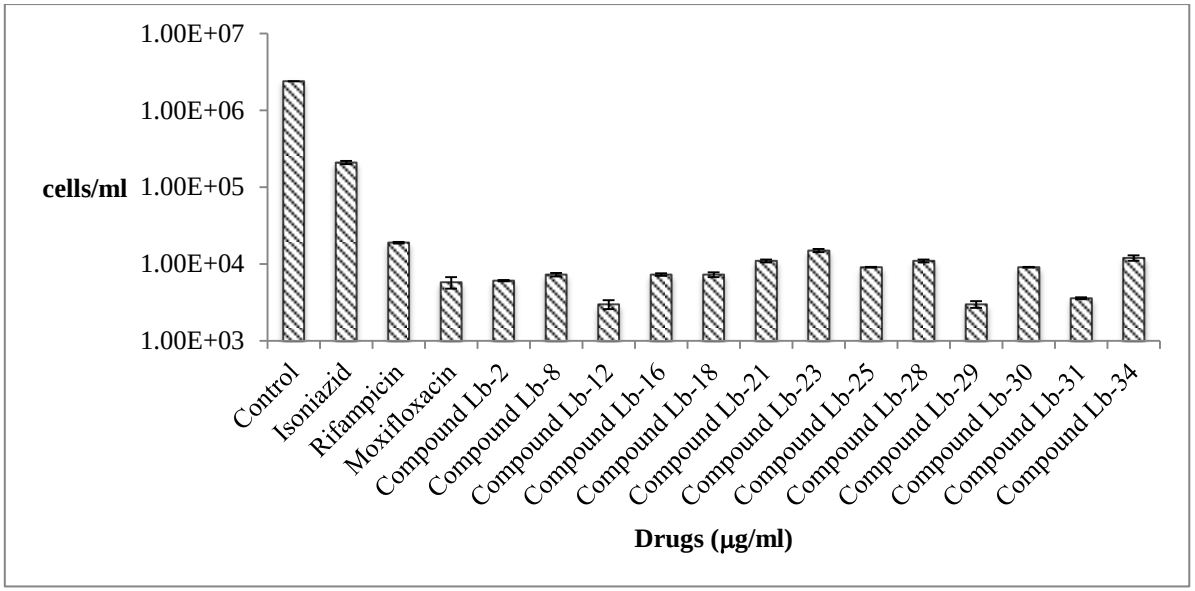

Figure 6.32: Graphical representation for bacterial count by nutrient starvation model for top active compounds. Error bars represents the standard deviation.

Table 6.12: Bacterial growth Log reduction values of active compounds with standard drugs

Drug (µg/ml)	No. of Bacteria	SD*	Log reduction values
Control	2400000	0	-
Lb-2	6100	100	2.4
Lb-8	7300	400	2.3
Lb-12	3000	400	2.8
Lb-16	7300	300	2.3
Lb-18	7300	500	2.3
Lb-21	11000	500	2.2
Lb-23	15000	700	2
Lb-25	9100	100	2.3
Lb-28	11000	500	2.2
Lb-29	3000	300	2.8
Lb-30	9100	100	2.2
Lb-31	3600	100	2.6
Lb-34	12000	1000	2
Isoniazid	210000	10000	1.1
Rifampicin	19000	500	2
Moxifloxacin	5800	1000	2.4

*SD-Standard deviation

6.2.11. ADME predictions for the synthesized compounds

The promising synthesized compounds were subjected to in-silico ADME predictions using QikProp module in Schrodinger. The compounds were found to be in accordance with Lipinski's rule of five which was important for drug-likeness. Predicted IC_{50} values for blockage of HERG k+ channels for the compounds **Lb-16**, **Lb-18**, **Lb-19**, **Lb-23**, **Lb-25-Lb-32** were not in the considerable range (below -5). The most potent compounds **Lb-16, Lb-2, Lb-21** and **Lb-29** showed considerable pharmacokinetic properties but the HERG K+ activity seem to be a deterrent factor for compounds **Lb-16**, **Lb-21** and **Lb-29**. As these are predictions, HERG K+ activity should be evaluated for these compounds experimentally to estimate their toxicity levels. LogP values were as expected for all compounds except **Lb-27** and **Lb-28**. All other properties were within acceptable range including Lipinski rule of five where no violations was reported. All the properties determined are listed out in Table 6.13**.**

Table 6.13: ADME predictions for the synthesized compounds

Compound ID	QPlogPo/w[a]	QPlogHERG[b]	QPPCaco[c]	QPlogBB[d]	% Human oral absorption[e]	Rule of Five[f]
Lead LII-8	3.101	-5.215	758.826	-0.666	96.649	0
Lb -2	2.682	-5.255	1942.267	-0.267	100	0
Lb -3	2.289	-5.141	1426.074	-0.407	96.803	0
Lb -5	3.824	-5.623	2844.845	-0.188	100	0
Lb -8	2.768	-5.412	1540.64	-0.467	100	0
Lb -12	3.058	-5.856	1482.477	-0.563	100	0
Lb -16	1.69	-2.595	118.285	-0.696	73.945	0
Lb -18	2.538	-3.098	161.304	-0.704	81.321	0
Lb -19	2.131	-2.932	128.077	-0.783	77.142	0
Lb -21	2.93	-3.619	227.23	-0.635	86.276	0
Lb -23	2.272	-3.407	123.404	-0.889	77.677	0
Lb -25	1.766	-4.666	777.08	-0.506	89.019	0
Lb -26	1.207	-4.619	530.801	-0.67	82.781	0
Lb -27	0.928	-4.444	421.616	-0.743	79.358	0
Lb -28	0.927	-4.443	420.783	-0.744	79.338	0
Lb -29	2.2	-4.945	858.584	-0.566	92.335	0
Lb -30	1.511	-4.41	641.435	-0.624	86.034	0
Lb -31	1.345	-4.726	465.839	-0.814	82.574	0
Lb -32	1.344	-4.725	464.946	-0.814	82.555	0
Lb -34	1.75	-5.326	608.4	-0.793	87.025	0
Lb -35	1.414	-5.211	446.224	-0.926	82.646	0

[a]Predicted octanol/water partition coefficient logP (acceptable range: −2.0 to 6.5);[b]Predicted IC_{50} value for blockage of HERG K+ channels.(below -5);[c]Predicted apparent Caco-2 cell permeability in nm/sec (<25 poor; >500 great); [d]Predicted brain/blood partition coefficient (-3.0 to 1.2);[e]Percent human oral absorption (<25% is poor and >80% is high);[f]Rule of 5 violation (mol_MW < 500, QPlogPo/w < 5, donorHB ≤ 5, accptHB ≤10)

6.2.12. Biophysical characterization of the promising compound

The stabilization of native protein and the complexes with ligands was evaluated by DSF experiment as reported earlier. A positive shift in melting temperature (T_m) of protein-ligand complexes compared with native protein signified better stabilization of protein. The most potent compound **Lb-29** which exhibited significant enzyme inhibition and was effective in dormant Mtb assay showed the temperature of 52.10 °C whereas the native protein showed Tm of 50.60 °C. This proved a better stabilization of the protein by **Lb-29**. The graph Mtb LAT protein and in complex with top active ligand is illustrated in Figure 6.33.

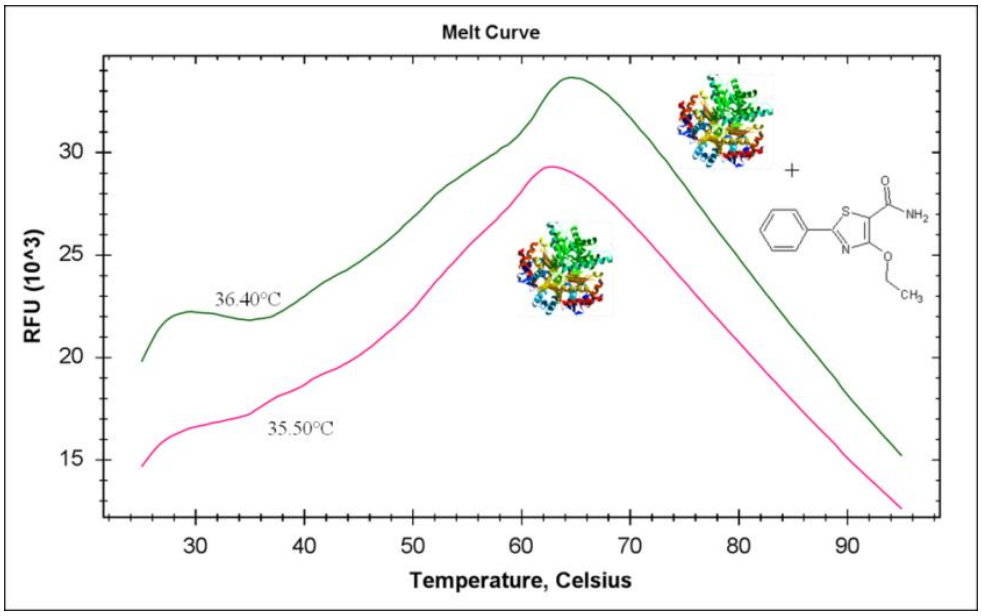

Figure 6.33: Melt curve for the protein complexes with compound **Lb-29** using DSF where pink colour represents the native protein and green colour represents the protein bound with ligand

6.2.13. Summary and conclusion

Design I: Mtb LAT INHIBITORS BASED ON SUBSTRATE LYSINE WITH PLP BOUND

To conclude, this chapter focussed on virtual screening of large database using the co-crystallized Mtb LAT with substrate lysine bound with PMP was attempted to identify novel inhibitors. Top five hits identified were screened experimentally and **Lead LII-1** with IC_{50}=23.83 μM was found to be the primary molecule for further development. 48 optimized derivatives were synthesized and evaluated for their ability to inhibit Mtb LAT, activity against Mtb and cytoxicity as steps towards the structure-activity relationships and lead

optimization. It could be concluded that substitutions like methyl phenyl, fluorophenyl, benzyloxy phenyl and hydroxy phenyl on the lead molecule were favourable in terms of activity against Mtb LAT. Presence of carbon atom as linker was advantageous oxygen as the linker as they were involved in the orientation of the compound at the active site for interactions.

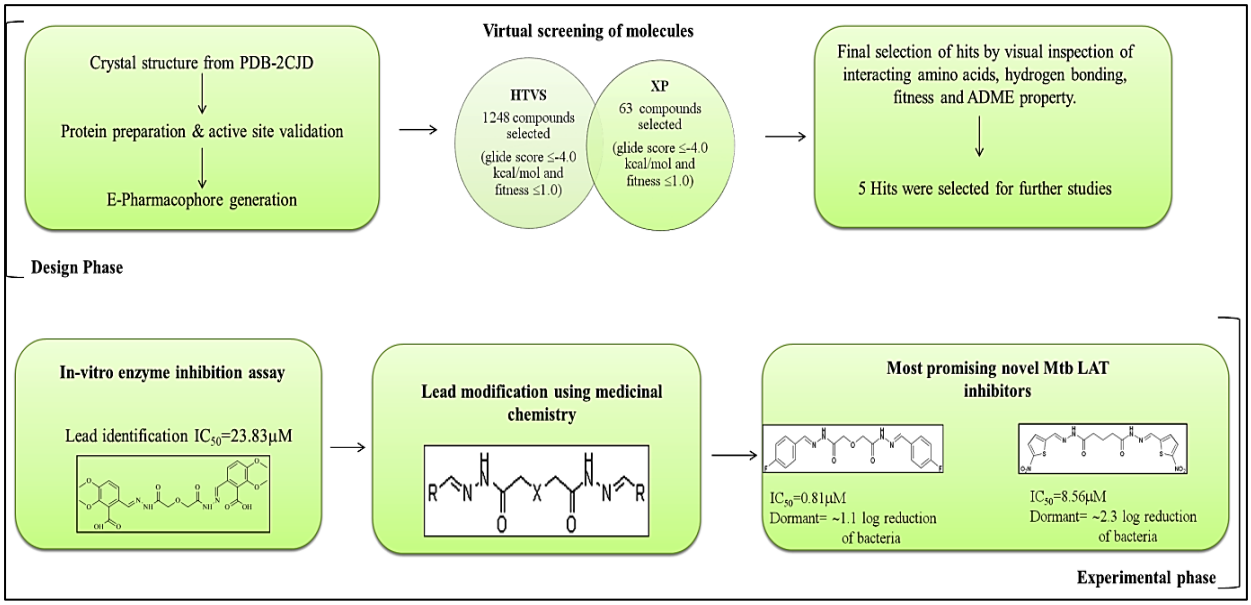

Compounds **La-1** and **La-17** with C-linker showed good inhibition of Mtb LAT with IC_{50}s 4.09±0.099 µM and 4.34±0.015 µM respectively; whereas, compounds **La-28** and **La-30** with O-linker showed IC_{50}s of 1.02±0.018 µM and 0.81±0.018 µM respectively. The active Mtb and dormant Mtb data for these compounds were found to be satisfactory. Compound **La-23** with IC_{50}=8.56 µM showed good activity against dormant Mtb bacteria with bacterial log reduction of ~2.3 which is found equipotent to moxiflaxicin (~2.4), and more potent than rifampicin (~2.0). The safety profile of these compounds revealed that these compounds were not cytotoxic till 50 µM in HEK cells. Thus, in need of anti-mycobacterial drugs, we believe that the present work could be useful for further optimization through in-vivo studies, mutagenesis, and pharmacokinetic approaches.

Design II: MTB LAT INHIBITORS BASED ON SUBSTRATE α-KETOGLUTARATE WITH PLP BOUND TO LAT PROTEIN

In this study, virtually the LAT inhibitors were designed to identify top eight hits from the co-crystallized substrate α-ketoglutarate bound with PLP. The **Lead LII-8** was identified as potential hit for further lead optimization and a series of 36 compounds were derivatized with R_1 position substituted with different aromatic groups like phenyl, 2-pyridyl, 3-pyridyl and 4-

pyridyl along with R_2 substituted with simple alkyl groups like methyl, ethyl and propargyl and the R_3 position was substituted with ethoxy, hydroxyl and amine groups. Almost all the compounds showed good activity data with IC_{50}s <20 μM towards Mtb LAT.

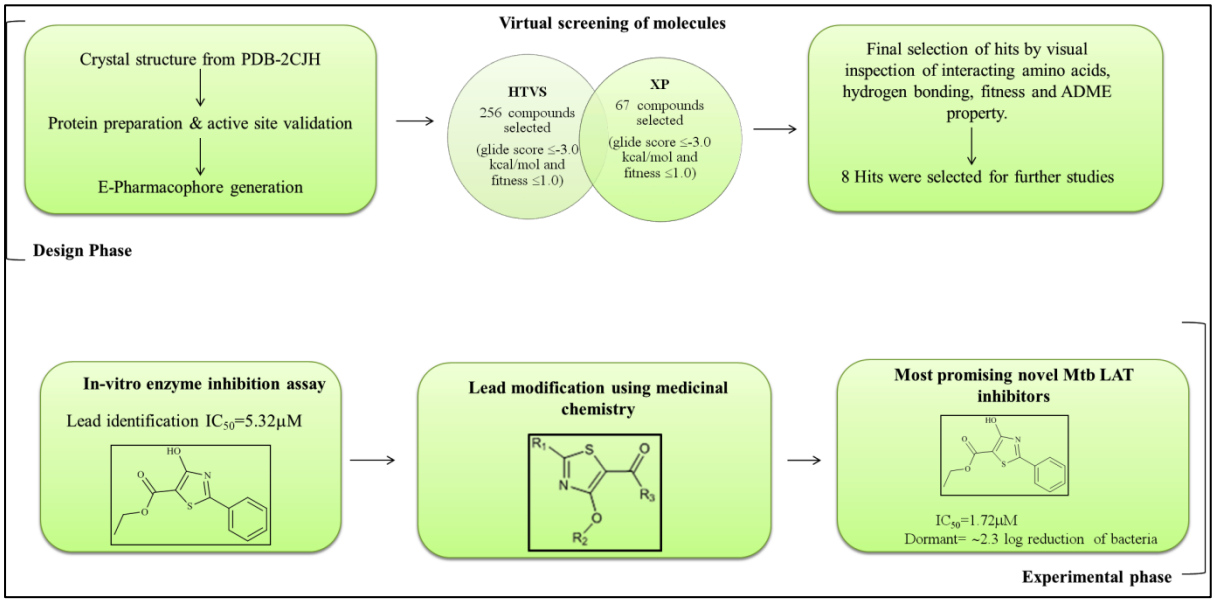

In this study, virtually the LAT inhibitors were designed to identify top eight hits from the co-crystallized substrate α-ketoglutarate bound with PLP. The **Lead LII-8** was identified as potential hit for further lead optimization and a series of 36 compounds were derivatized with R_1 position substituted with different aromatic groups like phenyl, 2-pyridyl, 3-pyridyl and 4-pyridyl along with R_2 substituted with simple alkyl groups like methyl, ethyl and propargyl and the R_3 position was substituted with ethoxy, hydroxyl and amine groups. Almost all the compounds showed good activity data with IC_{50}s <20 μM towards Mtb LAT. Compounds **Lb-12** and **Lb-29** with IC_{50} of 4.01 μM and 1.72 μM respectively exhibited (~2.3 bacterial growth reduction) promising results in nutrient starved condition when compared with standard first line drugs isoniazid (~1.2) and rifampicin (~2.0). Also, it was more active than moxiflaxicin. Further studies with these thiazole derivatives could be helpful for developing as novel Mtb LAT inhibitors, since there are no reported inhibitors till date in the market.

In conclusion, these two design strategies helped us to find and develop more potent leads as Mtb LAT inhibitors as there were no reported inhibitors available till date in the market for the dormant Mtb. Further, the identified lead could be used as the initial scaffolds to derivatize more promising leads for the Mtb infections in dormant conditions.

Chapter 7
Recapitulation and Future perspectives

As there is an urgent need of drugs for current global population, development of new drugs is of main importance. Based on the biological investigation and literature report, the Mtb PS and Mtb LAT found to be an important target for the treatment of Mtb infection in both active and dormant model. Thus, the present study focused on the design of novel inhibitors for Mtb infection.

7.1. Development of mycobacterial PS inhibitors

In summary, a high throughput virtual screening campaign against Mtb PS using a library comprising 500000 compounds, we successfully identified two novel scaffolds viz., Rhodanine and tryphtophan moieties as Mtb PS inhibitors. In total, 35 series of compounds have been derivatized using medicinal chemistry approach and evaluated for its biological activity. Further, the biophysical characterization was evaluated using differential scanning flourimetry experiments. Compound **Pa-09** and **Pa-12** emerged as the most potent Mtb PS inhibitor with the PS inhibitory IC_{50} of 0.35 μM and 0.37 μM; Mtb MIC of 1.55 μM and 1.71 μM and was not cytotoxic till 50 μM concentration. Further, efflux pump analysis was performed with the known inhibitors piperine and verapamil and found that the most promising lead was more effective than standard drugs Isoniazid (0.72 μM) and Ethambutol (7.62 μM) with the Mtb MIC of 0.38 μM and 0.85 μM respectively. Thus, these two strategies suggests that, if a crystal structure retrieved from either substrate or intermediate we can develop many novel scaffolds and make that molecule towards target specificity.

7.2. Development of mycobacterial LAT inhibitors

Similarly, using virtual screening of compounds with Mtb LAT, we successfully identified two novel scaffolds viz., glutarohydrazide and thiazole moieties Mtb LAT inhibitors. Totally, 84 series of compounds have been derivatized using synthetic approach and evaluated using biological approaches. Further, in order to confirm the binding of ligand to the protein, differential scanning flourimetry experiments were performed. Compound **La-30** (from glutarohydrazide series) and **Lb-16** (from thiazole series) emerged as the most potent novel Mtb LAT inhibitors with the inhibitory concentration of 0.81 μM and 1.21 μM; Mtb MIC

16.71 μM and 211.65 μM and was not cytotoxic till 50 μM concentration against human embryonic kidney cells. Dormant nutrient starved model of Mtb bacteria was established and the compounds were tested against nutrient starved bacteria. The most promising results show that compounds **Lb-12** and **Lb-29** showed good reduction in the bacterial growth (~2.8) at 10μg/ml when compared with the standard drug moxiflaxicin (~2.3), Rifampicin (~2.0) and Isoniazid (~1.1).

In conclusion, the class of compounds described here are the most promising lead compounds for further optimization and development to yield novel drugs for fast growing bacterial infections. The study also provides the basis for further chemical and biological optimization of these potent inhibitors as potential anti-tubercular agents.

7.3. Future perspectives

The PS and LAT biosynthetic pathways are absent in humans but essential for the survival of bacterial populations, suggesting that it acts as potential targets for the development of novel anti-mycobacterial compounds.

The present study could be extended to resolve the x-ray crystallography of LAT and PS bound to these novel inhibitors as there were no/not much reported inhibitors till date. The synthesized compounds were focussed to possess significant in-vitro activity; studies are still required to confirm in-vivo, pharmacokinetic and pharmacodynamics profiles of the active leads including safety profile. Also, further mutational studies and macrophage infection studies could be evaluated for the most promising leads specific to LAT and PS. The advancement of any of the compound presented in the thesis along with the development path would require significant investment.

References

Alexander F.W., Sandmeierm E., Mehta P. K., Christen P., Evolutionary relationships among pyridoxal-5'-phosphate-dependent enzymes. Region-specific alpha, beta and gamma families. *Eur. J. Biochem*, 1994. *219*, 953–960.

Alibert S., Pages J-M. Efflux pump inhibitors in bacteria. *Expert Opin. Ther. Pat*, 2007. *17*, 883-888

Alvin W., Hung H., Leonardo S., Shijun W., Alessio C.,Tom L., Blundell., Chris A. Application of Fragment Growing and Fragment Linking to the Discovery of Inhibitors of *Mycobacterium tuberculosis* Pantothenate Synthetase. *Drug discovery*, 2009. *48*, 8452-8456.

ASINEX Platinum Collection, ASINECorp, Winston-Salem, NC, USA, http://www.asinex.com.

Asselineau J., Lederer E., Structure of the mycolic acids of mycobacteria. Nature, 1950, *166*, 782–783.

Banerjee S.K., Bhatt K., Rana S., Misra P., Chakraborti P.K. Involvement of an efflux system in mediating high level of fluoroquinolone resistance in *Mycobacterium smegmatis*. *Biochem. Biophys. Res. Commun*, 1996. *226*, 362-368

Battu M.B., Chandra A.M., Sriram D., Yogeeswari P., Pharmacophore-Based 3DQSAR and Molecular Docking studies to Identify new Non-Peptidic inhibitors of Cathepsin S, *Curr Med Chem*, 2013. Sep 17.

Bernstein J, W.A. Lott, B.A. Steinberg, H.L. Yale, Chemotherapy of experimental tuberculosis. Isonicotinic acid hydrazide (Nydrazid) and related compounds, *American Review of Tuberculosis*. 1952, *65*, 357-364.

Betts J.C., Luckey P.T., Robb L.C., McAdam R.A., Duncan K., Evaluation of a nutrient starvation model of *Mycobacterium tuberculosis* persistence by gene and protein expression profiling. *Mol. Microbiol*, 2002, *43*, 717–731.

Binda G., Domenichini E., Gottardi A., Orlandi B., Ortelli E., Pacini B., Fowst G. Rifampicin, a general review. *Arzneimittelforschung*. 1971, *12*, 1907-1977.

Brennan P.J., Structure, function, and biogenesis of the cell wall of *Mycobacterium tuberculosis*. *Tuberculosis (Edinb),* 2003, *83*, 91-97.

Brian L., Jorge C., Mark S., Louis G., Luz C., Pilar., Robert H.,Gilman., David., Inter-and Intra-assay Reproducibility of Microplate Alamar Blue Assay Results for Isoniazid, Rifampicin, Ethambutol, Streptomycin, Ciprofloxacin and Capreomycin Drug susceptibility testing of *M.tuberculosis*, *Clinical Microbiology*, 2008. 3526-3528.

Cappelli G., Volpe E., Grassi M., Liseo B., Colizzi V., Mariani F., Profiling of *Mycobacterium tuberculosis* gene expression during human macrophage infection: upregulation of the alternative sigma factor G, a group of transcriptional regulators, and proteins with unknown function, *Res Microbiol*, 2006. *157*, 445–455.

Chan E.D., Strand M.J., Iseman M.D. Treatment outcomes in extensively resistant tuberculosis. *New Engl. J. Med.* 2008, *359*, 657-659

Chopra P., Meena L.S., Singh Y., New drugs for *Mycobacterium tuberculosis*, Indian J Med Res, 2003, 117, 1-9

Christopher W., Murray., David C., The rise of fragment-based drug discovery *Nature chemistry*, 2009. *1*, 187.

Ciulli A., Scott D.E., Ando M., Reyes F., Saldanha S.A., Tuck K.L., Chirgadze D.Y., Blundell T.L., Abell C., Inhibition of *Mycobacterium tuberculosis* pantothenate synthetase by analogues of the reaction intermediate, *ChemBioChem*, 2008. *9*, 2606

Coker R.J. Review: Multidrug-resistant tuberculosis: public health challenges. *Trop. Med. Int. Health*, 2004. *9*, 25-40.

Cole S.T, Eiglmeier K., Parkhill J., James K.D., Thomson N.R., Wheeler P.R., Honore N., Garnier T., Churcher C., Harris D., Massive gene decay in the leprosy bacillus, *Nature*, 2001. *409*, 1007–1011.

Cole S.T., Brosch R., Parkhill J., Garnier T., Churcher C., Harris D., Gordon S.V., Eiglmeier K., Gas S., Barry III C.E., Tekaia F., Badcock K., Basham D., Brown D., Chillingworth T., Connor R., Davies R., Devlin K., Feltwell T., Gentles S., Hamlin N., Holroyd S., Hornsby H., Jagels K., Krogh A., McLean J., Moule S., Murphy L., Oliver K., Osborne J., Quail M.A., Rajandream M.A., Rogers J., Rutter S., Seeger K., Skelton J., Squares R., Squares S., Sulston J.E., Taylor K., Whitehead S., Barrell B.G. Deciphering the biology of *Mycobacterium tuberculosis* from the complete genome sequence. *Nature*, 1998, *393*, 537-544.

Corbett E.L., Watt C.J., Walker N., Maher D., Williams B.G., Raviglione M.C., Dye C. The growing burden of tuberculosis: global trends and interactions with the HIV epidemic. *Arch. Intern. Med*, 2003. *163*, 1009-1021

Cox H.S., Ford N., Reeder J.C., Are we really that good at treating tuberculosis?. Lancet Infect, 2009, *9*, 138-139.

Crick D.C., Mahapatra S., Brennan P.J., Biosynthesis of the arabinogalactan-peptidoglycan complex of *Mycobacterium tuberculosis*, *Glycobiology,* 2001. *11*, 107R-118R.

Dixon S.L., Smondyrev M., Rao S.N., PHASE: A novel approach to Pharmacophore modeling and 3D database searching, *Chem Biol Drug Des*, 2006. *67*, 370-372.

Dorman S.E., Chaisson R.E. From magic bullets back to the Magic Mountain: the rise of extensively drug-resistant tuberculosis. *Nat. Med*, 2007. *13*, 295-298

Dube D., Tripathi S.M., Ramachandran R., Identification of in-vitro inhibitors of *Mycobacterium tuberculosis* Lysine aminotransferase by pharmacophore mapping and three-dimensional flexible searches, *Med Chem Res*, 2007. *17*, 182-188.

Dye C., Williams B.G., The population dynamics and control of tuberculosis. Science, 2010, *328*, 856-861.

Elzinga G., Raviglione M.C., Maher D., Scale up: meeting targets in global tuberculosis control. Lancet, 2004, *363*, 814-819.

Fattorini L, Piccaro G, Mustazzolu A, Giannoni F. Targeting dormant bacilli to fight tuberculosis, *Mediterr J Hematol Infect Dis.* 2013, *5*, e2013072.

Fernandes N.D., Wu Q.L., Kong D., Puyang X., Garg S., Husson R.N., A mycobacterial extra cytoplasmic sigma factor involved in survival following heat shock and oxidative stress, *J Bacteriol*, 1999. *181*, 4266–4274.

Gerlier D., Thomasset N. Use of MTT colorimetric assay to measure cell activation. *J. Immunol. Methods*, 1986. *94*, 57-63.

Gomez M., Doukhan L., Nair G., Smith I., sigA is an essential gene in *Mycobacterium smegmatis*, *Mol Microbiol*, 1998. *29*, 617–628.

Graham J.E., Clark-Curtiss J.E., Identification of *Mycobacterium tuberculosis* RNAs synthesized in response to phagocytosis by human macrophages by selective capture of transcribed sequences (SCOTS), *Proc Natl Acad Sci* USA, 1999. *96*, 11554–11559.

Grant S.S., Kaufmann B.B., Chand N.S., Haseley N., Hung D.T., Eradication of bacterial persisters with antibiotic-generated hydroxyl radicals. Proc Natl Acad Sci U S A, 2012,109, 12147-52.

Hahn M.Y., Raman S., Anaya M., Husson R.N., The *Mycobacterium tuberculosis* extra cytoplasmic function sigma factor SigL regulates polyketide synthases and secreted or membrane proteins and is required for virulence, *J Bacteriol*, 2005. *187*, 7062–7071.

Hajduk P. J., Greer J., A decade of fragment-based drug design: strategic advances and lessons learned *Nature reviews of drug discovery*, 2007, *6*, 211-219

Hayashi H., Pyridoxal enzymes: mechanistic diversity and uniformity, *J. Biochem*. 1995, *118*, 463–473.

Houben EN, Nguyen L, Pieters J., Interaction of pathogenic mycobacteria with the host immune system, *Current Opinion in Microbiology.* 2006, *9*, 76-85.

Hu Y., Coates A.R., Increased levels of sigJ mRNA in late stationary phase cultures of *Mycobacterium tuberculosis* detected by DNA array hybridisation, *FEMS Microbiol Lett*, 2001. *202*, 59–65.

Hu Y., Coates A.R., Transcription of two sigma 70 homologue genes, sigA and sigB, in stationary-phase *Mycobacterium tuberculosis*, *J Bacteriol*, 1999. *181*, 469–476.

Hung A.W., Silvestre H.L., Wen S., Ciulli A., Blundell T.L., Abell C., Application of fragment growing and fragment linking to the discovery of inhibitors of *Mycobacterium tuberculosis* pantothenate synthetase, *Angew. Chem. Int. Ed*. 2009. *48*, 8452–8456.

Jackowski S., Biosynthesis of pantothenic acid and coenzyme A. Escherichia coli and *Salmonella typhimurium*, *Cellular and molecular biology*, 1996. 2nd ed., vol. 1, pp. 687–694. *American Society for Microbiology*, Washington, DC.

Jeankumar, V. U.; Renuka, J.; Santosh, P.; Sridevi, J. P.; Suryadevara, P.; Yogeeeswari, P.; Sriram, D. *Eur. J. Med. Chem*, 2013. *70*, 140−153.

John R.A., Pyridoxal phosphate-dependent enzymes, *Biochem. Biophys. Acta*, 1995. *1248*, 81–96.

Jones D., Metzger H.J., Schatz A., Waksman S.A. Control of gram-negative bacteria in experimental animals by streptomycin, *Science*. 1944, *100*, 103-105.

Kerdesky F.A.J., Holms J.H., Moore J.L., Bell R.L., Dyer R.D., Carter, G.W., Brooks, D.W. *J. Med. Chem*, 1991. *34*, 2158-2165.

Kimerling M.E, Kluge H., Vezhnina N., Iacovazzi T., Demeulenaere T., Portaels F., Inadequacy of the current WHO re-treatment regimen in a central Siberian prison: treatment failure and MDR-TB. 1999, Int J Tuberc Lung Dis, 1999, *3* , 451-453.

Koul, E. Arnoult, N. Lounis, J. Guillemont, K. Andries, The challenge of new drug discovery for tuberculosis, *Nature*. 2011, *469*, 483-490.

Kumar A., Casey A., Odingo J., Kesicki E.A., Abrahams G., Vieth M., Masquelin T., Mizrahi V., Hipskind P.A., Sherman D.R., Parish T., A high-throuput screen against pantothenate synthetase (*PanC*) identifies 3-biphenyl-4-cyanopyrrole-2-carboxylic acids as a new class of inhibitor with activity against *Mycobacterium tuberculosis*, *Plos one*, 2013. *8*, 1-8.

Lange C, Mori T. Advances in the diagnosis of tuberculosis, *Respirology*. 2010, *15*, 220–40.

Lee J.H., Geiman D.E., Bishai W.R., Role of stress response sigma factor SigG in *Mycobacterium tuberculosis*, *J Bacteriol*, 2008. *190*, 1128–1133.

Lucile E., Kristen S., Larry R., Sara C., Rachel B., Melinda I.S. Anna M., Lynn R., Celia G., David E., Thomas M., A Novel Inhibitor of *Mycobacterium tuberculosis* Pantothenate Synthetase, *Journal of biomolecular screening*, 2006. 100-102.

Maas W.K., The biosynthesis of pantothenic acid. *Proc. Int. Congr. Biochem*, 1960. 11, 161–168.

Maestro, Version 9.3, Schrödinger, LLC, New York, NY, 2012

Manganelli R., Dubnau E., Tyagi S., Kramer F.R., Smith I., Differential expression of 10 sigma factor genes in *Mycobacterium tuberculosis*, *Mol Microbiol*, 1999. *31*, 715–724.

Manganelli R., Provvedi R., Rodrigue S., Beaucher J., Gaudreau L., Smith I., Sigma factors and global gene regulation in *Mycobacterium tuberculosis*, *J Bacteriol*, 2004. *186*, 895–902.

Manganelli R., Voskuil M.I., Schoolnik G.K., Dubnau E., Gomez M., Smith I., Role of the extracytoplasmic- function sigma factor sigma(H) in *Mycobacterium tuberculosis* global gene expression. *Mol Microbiol*, 2002. *45*, 365–374.

Mehta P.K., Hale T.I., Christen P., Aminotransferases: demonstration of homology and division into evolutionary subgroups, *Eur. J. Biochem*, 1993. *214*, 549–561.

Merkel W.K., Nichols B.P., Characterization and sequence of the Escherichia coli panBCD gene cluster, *FEMS Microbiol.Let*t, 1996. *143*, 247-252.

Michele T.M., Ko C., Bishai W.R., Exposure to antibiotics induces expression of the *Mycobacterium tuberculosis* sigF gene: implications for chemotherapy against mycobacterial persistors, *Antimicrob Agents Chemother*, 1999. *43*, 218–225.

Miyahara I., Hirotsu B. M., Snell E. E., *J. Biochem*, 1994. *116*, 1001–1012.

Miyatake K., Nakano Y., Kitaoka S., Pantothenate synthetase from *Escherichia coli*, *Methods Enzymol*, 1979. *62*, 215–219.

Murphy D.J., Brown J.R., Identification of gene targets against dormant phase *Mycobacterium tuberculosis* infections, *BMC infectious diseases.* 2007. *7*, 84

Murray C.W., Rees D.C, The rise of fragment-based drug discovery, *Nature Chemistry*, 2009, *1*, 187-192.

Nagamani S., Kesavan C., Muthusam K., E-Pharmacophore mapping and docking studies on Vitamin D receptor (VDR), *Bioinformation*, 2012. *15*, 705-710.

Niesan F.H., Berglund H., Vedadi M., The use of differential scanning fluorimetry to detect ligand interactions that promote protein stability, *Nature protocols*, 2007.321

Online text book of bacteriology, tuberculosis, Todar K.

Pendzich J., Maksymowicz-Mazur W., Mazurek U., Dworniczak S., Oklek K., Kozielski J., Wilczok T., Quantitative analysis of sigma genes expression in *Mycobacterium tuberculosis* cultures exposed to rifampicin and isoniazid, *Wiad Lek*, 2004. *57*, 233–240.

Pethe K., Bifani P., Jang J., Kang S., Park S., Ahn S., Jiricek J., Jung J., Jeon H.K., Cecjetto J., Christophe T., Lee H., Kempf M., Jackson M., Lenaerts A.J., Pham H., Jones V., Seo M.J., Kim Y.M., Seo M., Seo J.J., Park D., Ko Y., Choi I., Kim R., Kim. S.Y., Lim S., Yim S-A., Nam J., Kang H., Kwon H., Oh C-T., Cho Y., Jang Y., Kim J., Chua A., Tan B.H., Nanjundappa M.B., Rao S.P.S., Barnes W.S., Walker J.R., Alonso S., Lee S., Kim J., Oh S., Oh T., Nehrbass U., Han S-J., No Z., Lee J., Brodin P., Cho S.N., Nam K., Kim J. Discovery of Q203, a potent clinical candidate for the treatment of tuberculosis, *Nat. Med*, 2013. *19*, 1157-1160.

Pieters J., *Mycobacterium tuberculosis* and the macrophage: maintaining a balance, *Cell Host Microbe*, 2008. *3*, 399–407.

Provvedi R., Boldrin F., Falciani F., Palu G., Manganelli R., Global transcriptional response to vancomycin in *Mycobacterium tuberculosis*, *Microbiology*, 2009. *155*, 1093–1102.

Raman S., Hazra R., Dascher C.C., Husson R.N., Transcription regulation by the *Mycobacterium tuberculosis* alternative sigma factor SigD and its role in virulence, *J Bacteriol*, 2004. *186*, 6605–6616.

Raman S., Puyang X., Cheng T.Y., Young D.C., Moody D.B., Husson R.N., *Mycobacterium tuberculosis* SigM positively regulates *Esx* secreted protein and non-ribosomal peptide synthetase genes and down regulates virulence-associated surface lipid synthesis, *J Bacteriol* 2006. *188*, 8460–8468.

Rodrigue S., Provvedi R., Jacques P.E., Gaudreau L., Manganelli R., The sigma factors of *Mycobacterium tuberculosis*, *FEMS Microbiol Rev*, 2006. *30*, 926– 941.

Sachdeva P., Misra R., Tyagi A.K., Singh Y., The sigma factors of *Mycobacterium tuberculosis*: regulation of the regulators, *the FEBS journal*, 2009. doi:10.1111/j.1742-4658.2009.07479.x

Salam N.K., Nuti R., Sherman W., Novel Method for Generating Structure-Based Pharmacophores Using Energetic Analysis, *J. Chem. Inf. Model*, 2009. *49*, 2356-2368.

Samala G., Devi P.B., Nallangi R., Sridevi J.P., Saxena S., Yogeeswari P., Sriram D., Identification and development of 2-methylimidazo[1,2-a]pyridine-3-carboxamides as *Mycobacterium tuberculosis* pantothenate synthetase inhibitors, *Bioorg Med Chem*, 2014. *22*, 4223-4232

Samala G., Devi P.B., Nallangi R., Yogeeswari P., Sriram D., Development of 3-phenyl-4,5,6,7-tetrahydro-1*H*-pyrazolo[4,3-c] pyridine derivatives as novel *Mycobacterium tuberculosis* pantothenate synthetase inhibitors, *Eur J Med Chem*, 2013. *69*, 356-364

Samala G., Devi P.B, Nallangi R., Sridevi J.P., Saxena S., Yogeeswari P., Sriram D., Development of novel tetrahydrothieno[2,3-c]pyridine-3-carboxamide based *Mycobacterium tuberculosis* pantothenate synthetase inhibitors: Molecular hybridization from known antimycobacterial leads, *Bioorg Med Chem*, 2014. *22*, 1938-1947

Sambandamurthy V.K., Derrick S.C., Jalapathy K.V., Chen B., Russell R.G., Morris S.L., Jacobs W.R., Long-term protection against tuberculosis following vaccination with a severely attenuated double lysine and pantothenate auxotroph of *Mycobacterium tuberculosis*, *Infec Immun*. 2005, *73*, 1196-1203.

Sambandamurthy V.K., Wang X., Chen B., Russell R.G., Derrick.S., Collins F.M., Morris S.L and Jacobs W.R., A pantothenate auxotroph of *Mycobacterium tuberculosis* is highly attenuated and protects mice against tuberculosis, *Nat. Med*. 2002, *8*, 1171–1174.

Saxena S., Devi P.B., Soni V., Yogeeswari P., Sriram D., Identification of novel inhibitors against *Mycobacterium tuberculosis* L-alanine dehydrogenase (MTB-AlaDH) through structure-based virtual screening, *J Mol Graph Model*, 2014. *47*, 37–43.

Schatz A, Bugie E, Waksman SA. Streptomycin, a substance exhibiting antibiotic activity against Gram-positive and Gram negative bacteria, *Proc Soc Exp Biol Med.* 1944, *55*, 66–69.

Scudiero D.A., Shoemaker R.H., Paull K.D., Monks A., Tierney S., Nofziger T.H., Currens M.J., Seniff D., Boyd M.R., "Evaluation of a soluble tetrazolium/formazan assay for cell growth and drug sensitivity in culture using human and other tumor cell lines" *cancer research*, 1988. 4827-4828.

Shen B. W., Henning M., Hohenester E., Jansonius J. N., Schirmer T., Crystal structure of human recombinant ornithine aminotransferase, *J. Mol. Biol*, 1998. *277*, 81–102.

Silva P.E., Bigi F., Santangelo M.P., Romano M.I., Martin C., Cataldi A., Ainsa J.A. Characterization of P55, a multidrug efflux pump in *Mycobacterium bovis* and *Mycobacterium tuberculosis*. *Antimicrob. Agents Chemother,* 2001. *45*, 800-804.

Soda K., Misono H., Yamamoto T., L-lysine and α-ketoglutarate aminotransferase: I. Indentification of product, Δ1-piperidine-6-carboxylic acid, *Biochemistry*, 1968a. *7*, 4102–4109.

Soda K., Misono H., L-lysine α-ketoglutarate aminotransferase. II. Purification, crystallization, and properties, *Biochemistry*, 1968b. *7*, 4110–4119.

Storici P., Biase D.D., Bossa F., Bruno S., Mozzarelli A., Peneff C., Structures of γ-aminobutyric acid (GABA) aminotransferase, a pyridoxal 5′-phosphate, and [2Fe-2S] cluster containing enzymes, complexed with γ-ethynyl-GABA and with the anti-epilepsy drug vigabatrin, *J. Biol. Chem*, 2004. *279*, 363–373.

STRING - Known and Predicted Protein-Protein Interactions; http://string-db.org/

Takayama K., Wang C., Besra G.S., Pathway to synthesis and processing of mycolic acids in *Mycobacterium tuberculosis*. *Clinical Microbiology Reviews*, 2005. *18*, 81-101

Theras P.J., Manvar D., Kondepudi S., Battu M.B., Sriram D., Basu A., Yogeeswari P., Basu N.K., Multiple e-pharmacophore modelling, 3D-QSAR, and High-Throughput Virtual screening of Hepatitis C Virus NS5B Polymerase Inhibitors, *J.Chem.Inf.Model*, 2014. *54*, 539-552

Thomas J.P, Baughn, C.O., Wilkinson R.G., Shepherd R.G., A new synthetic compound with antituberculous activity in mice: ethambutol (dextro-2,2'-(ethylenediimino)-di-l-butanol), *Am. Rev. Respir. Dis*. 1961. *83*, 891-893.

Trauner A, Borrell S, Reither K, Gagneux S, Evolution of Drug Resistance in Tuberculosis: Recent Progress and Implications for Diagnosis and Therapy, *Drugs*, 2014. *74*, 1063–1072.

Tripathi S.M., Ramachandran R., Overexpression, purification and crystallization of lysine epsilon-aminotransferase (Rv3290c) from *Mycobacterium tuberculosis* H37Rv, *Acta Crystallogr., Sect. F: Struct. Biol. Cryst. Commun*, 2006. *62*, 572–575.

Velaparthi S., Brunsteiner M., Uddin R., Wan B., Franzblau S.G., Petukhov P.A., 5-*tert*-Butyl-N-pyrazol-4-yl-4,5,6,7-tetrahydrobenzo[*d*]isoxazole-3-carboxamide derivatives as novel potent inhibitors of *Mycobacterium tuberculosis* pantothenate synthetase: Initiating a quest for new antitubercular drugs, *J.Med.Chem*., 2008. *51*, 1999-2002.

Velick S.F., Vavra J., A kinetic and equilibrium analysis of the glutamic oxaloacetate transaminase mechanism, *J. Biol. Chem*, 1962. *237*, 2109–2122.

Vergne I., Fratti R. A., Hill P. J., Chua J., Belisle J., Deretic V., *Mycobacterium tuberculosis* phagosome maturation arrest: mycobacterial phosphatidylinositol analog phosphatidylinositol mannoside stimulates early endosomal fusion, *Mol. Biol. Cell. 15*, 751–760.

Villemagne B., Crauste C., Flipo M., Baulard A.R., Deprez B., Willand N., Tuberculosis: the drug development pipeline at a glance, *Eur J Med Chem*. 2012, *51*, 1-16

Volpe E., Cappelli G., Grassi M., Martino A., Serafino A., Colizzi V., Sanarico N., Mariani F., Gene expression profiling of human macrophages at late time of infection with *Mycobacterium tuberculosis*, *Immunology*, 2006. *118*, 449–460.

Von Delft F., Lewenodon A., Dhanaraj V., Blundell T.L., Abell C., Smith A.G., The crystal structure of *E.coli* pantothenate synthetase confirms it as a member of the cytidylyltransferase superfamily, *Structure*, 2001. *9*, 439-450.

Voskuil, M. I., *Mycobacterium tuberculosis* gene expression during environment conditions associated with latency, *Tuberculosis*, 2004a, *84*, 138–143

Voskuil M.I., Visconti K. C., Schoolnik G. K., *Mycobacterium tuberculosis* gene expression during adaptation to stationary phase and low oxygen dormancy, *Tuberculosis*, 2004b. *84*, 218–227.

Waagmeester A., Thompson J., Reyrat J.M., Identifying sigma factors in *Mycobacterium smegmatis* by comparative genomic analysis, *Trends Microbiol*, 2005. *13*, 505–509.

Wang S., Eisenberg D., Crystal structures of a pantothenate synthetase from *Mycobacterium tuberculosis* and its complexes with substrates and a reaction intermediates, *Protein Sci*. 2003, *45*, 1554-1561.

Wayne L.G., Sohaskey C.D., Non-replicating persistence of *Mycobacterium tuberculosis*. *Annu Rev Microbiol*, 2001. *55*, 139–63.

White E. L., Southworth K., Ross L., Cooley S., Gill R.B., Sosa M.I., Manouvakhova A., Rasmussen L., Goulding C., Eisenberg D., Fletcher T.M, A novel inhibitor of *Mycobacterium tuberculosis* pantothenate synthetase, *Journal of Biomolecular Screening*, 2007. *12*, 100–105.

Wieland T., Lowe W., Kreiling A., Pfleiderer G., On pantothenic acid synthetase from *E. coli:* Pantoyladenylate as the acylating component in the enzymatic synthesis of pantothenic acid. *Biochem*, 1963. *339*, 1–7.

Williams L., Zheng R., Blanchard J.S., Raushel F.M., Steady-state and pre-steady state kinetic analysis of *Mycobacterium tuberculosis* pantothenate synthetase, *Biochemistry*, 2003. 12904-12912

World Health Organization Global tuberculosis control: WHO report 2013. (WHO/HTM/TB/2013.7). Geneva, Switzerland: WHO, 2013.

Wu Q.L., Kong D., Lam K., Husson R.N., A mycobacterial extra cytoplasmic function sigma factor involved in survival following stress, *J Bacteriol*, 1997. *179*, 2922–2929.

Yang Y., Gao P., Liu Y., Ji X., Gan M., Guan Y., Hao X., Li Z., Xiao C., A discovery of novel *Mycobacterium tuberculosis* pantothenate synthetase inhibitors based on the molecular mechanism of actinomycin D inhibition, *Bioorganic & Medicinal chemistry letters*, 2011. *21*, 3943-3946.

Zahrt T.C, V. Deretic, Reactive nitrogen and oxygen intermediates and bacterial defenses: unusual adaptations in *Mycobacterium tuberculosis*, *Antioxid. Redox Signal*. 2002, 4, 141–159.

Zhang Y., The magic bullets and tuberculosis drug targets, *Annu. Rev. Pharmacol. Toxicol.*, 2005, *45*, 529-564.

Zheng R., Blanchard J.S., Steady-state and pre-steady state kinetic analysis of *Mycobacterium tuberculosis* pantothenate synthetase, *Biochemistry.* 2001, *40*, 12904-12912.

Zheng R., Dam T.K., Brewer F.C., Blanchard T.S., Active site residues in *Mycobacterium tuberculosis* pantothenate sythetase required in the formation and stabilization of the adenylate intermediate, *Biochemistry*, 2004, *43*, 7171-7178.

Zumla A.I., Gillespie S.H., Hoelscher M., Philips P.P., Cole S.T., Abubakar I., McHugh T.D., Schito M., Marurer M., Nunn A.J. New antituberculosis drugs, regimens, and adjunct therapies: needs, advances, and future prospects, *Lancet Infect. Dis.* 2014. *14*, 327-340.

Zumla, A.; Nahid, P.; Cole, S. T. Advances in the development of new tuberculosis drugs and treatment regimens, *Nature Rev. Drug Discovery.* 2013, *12*, 388−404.

Annexures

Annexure I: Synthesis of pantothenate synthetase inhibitors using substrate based approach-Rhodanine derivatives

The procedures and characterization data are given for all the synthesized compounds.

Preparation of 3-(4-oxo-2-thioxothiazolidin-3-yl)propanoic acid (II).

30% Aqueous KOH (26.3 ml, 141.2 mmol) was added drop wise to a stirred solution of compound **I** (7.0 g, 78.65 mmol) in H_2O (30 ml) at 0 °C, then CS_2 (6.57 g, 86.52 mmol) was added drop wise to the reaction mixture at same temperature and allowed to stir at room temperature for 3 hours, then bromoacetic acid (10.8 g, 78.65 mmol) was added as a solid in small portions over about 20 minutes. The reaction was allowed to mix at room temperature for an additional 3 hours, during which time a precipitate formed. The reaction mixture pH was adjusted to 3-4 using Con.H_2SO_4 and stirred for 1 hour. The product was filtered off and washed with water, dried in vacuum oven to get compound **II** as an off-white solid (9.7 g, 60%): ^{1}H NMR (300 MHz, $CDCl_3$): δ=2.50 (t, *J* = 7.6 Hz, 2H), 4.30 (s, 2H), 4.32 (t, *J* = 7.6 Hz, 2H), 12.45 (s, 1H); MS (ES, 70eV) m/z 206 $[M+H]^+$

General procedure for the preparation of compound III.

Aldehyde (1.0 equiv), compound **II** (1.0 equiv) and piperidine (catalytic) were taken in EtOH, and stirred under reflux conditions for 6 h. The reaction mixture was concentrated under reduced pressure and the obtained solid compound was filtered and washed with hexanes to get compound **III.**

Preparation of (Z)-3-(5-(benzo[d][1,3]dioxol-5-ylmethylene)-4-oxo-2-thioxothiazolidin-3-yl)propanoic acid.

Piperonal (2.19 ml, 14.63 mmol), and piperidine (catalytic) were added to a stirred solution of compound **II** (3.0 g, 14.63 mmol) in EtOH (25 ml) at room temperature, and allowed to reflux for 6 h. The reaction mixture was concentrated under reduced pressure and the obtained solid compound was filtered and washed with hexanes to get compound **III** as an off-white solid (4.5 g, 91%): ^{1}H NMR (300 MHz, $[D_6]$DMSO): δ=2.70 (t, *J* = 7.6 Hz, 2H), 4.39 (t, *J* = 7.6 Hz, 2H), 6.30 (s, 2H), 6.90 (d, *J* = 7.2 Hz, 1H), 7.23 (d, *J* = 7.6 Hz, 1H), 7.27 (s, 1H), 7.9 (s, 1H), 12.54 (s, 1H); MS (ES, 70eV) m/z 338 $[M+H]^+$.

General procedure for the preparation of compound IV.

To the stirred solution of compound **III** (1.0 equiv) in CH_2Cl_2, were added EDCI (1.3 equiv), HOBt (1.3 equiv) and Et_3N (2.2 equiv) at 0 °C, stirred for few minutes then added $R_2CONHNH_2$ (1.2 equiv) and allowed reaction mixture to stir at room temperature for 4 h. The solids formed in the reaction mixture were filtered and washed with H_2O, hexanes and diethyl ether. The obtained solid compound was dried in vacuum oven to get compound **IV**.

(*Z*)-*N'*-(3-(5-(Benzo[d][1,3]dioxol-5-ylmethylene)-4-oxo-2-thioxothiazolidin-3 yl)propanoyl)benzohydrazide (Pa-1).

To the stirred solution of (Z)-3-(5-(benzo[d][1,3]dioxol-5-ylmethylene)-4-oxo-2-thioxothiazolidin-3-yl)propanoic acid (0.3 g, 0.89 mmol) in CH_2Cl_2 (4 ml) were added EDCI (0.22 g, 1.15 mmol), HOBt (0.16 g, 1.15 mmol) and Et_3N (0.28 ml, 1.96 mmol) at 0 °C, stirred the reaction mixture for few minutes then added benzohydrazide (0.15 g, 1.06 mmol) and allowed reaction mixture to stir at room temperature for 4 h. The solids formed in the reaction mixture were filtered and washed with H_2O (3 × 20 ml), hexanes and diethyl ether. The solid compound was dried in vacuum oven to get title compound as an off-white solid (0.35 g, 87%): m.p. 231–232 °C; ^{1}H NMR (400 MHz, [D_6]DMSO) δ=2.79 (t, *J* = 7.2 Hz, 2H), 4.41 (t, *J* = 7.2 Hz, 2H), 6.42 (s, 2H), 7.27 (d, *J* = 6.8 Hz, 1H), 7.54 (s, 1H), 7.54–7.63 (m, 3H), 7.81–7.92 (m, 4H), 9.70 (bs, 2H); ^{13}C NMR (100 MHz, [D_6]DMSO) δ=37.6, 47.5, 102.0, 108.2, 115.0, 126.6(2C), 127.1, 128.3(2C), 129.2, 132.4, 142.2, 142.7, 147.7, 148.3, 149.9, 164.6, 165.6, 179.4, 189.2: MS (ES, 70eV) m/z 456 $[M+H]^+$; Anal. calcd for $C_{21}H_{17}N_3O_5S_2$: C, 55.37; H, 3.76; N, 9.22% Found C, 55.41; H, 3.79; N, 9.27%.

(*Z*)-*N'*-(3-(5-(Benzo[d][1,3]dioxol-5-ylmethylene)-4-oxo-2-thioxothiazolidin-3-yl)propanoyl)isonicotinohydrazide (Pa-2).

Yield: 91%, m.p. 260–261 °C; ^{1}H NMR (400 MHz, [D_6]DMSO) δ=2.62 (t, 2H), 4.71 (t, *J* = 7.2 Hz, 2H), 6.62 (s, 2H), 7.47 (d, *J* = 7.2 Hz, 1H), 7.62–7.72 (m, 3H), 7.72 (s, 1H), 7.90–8.10 (m, 3H), 9.72 (bs, 2H); ^{13}C NMR (100 MHz, [D_6]DMSO) δ 188.6, 172.6, 168.3, 164.6, 151.9, 148.4(2C), 147.2, 141.9, 141.2, 133.9, 128.7, 126.7(2C), 125.4, 119.0, 108.7, 101.7, 49.7, 38.3: MS (ES, 70eV) m/z 457 $[M+H]^+$; Anal. calcd for $C_{20}H_{16}N_4O_5S_2$: C, 52.62; H, 3.53; N, 12.27% Found C, 52.71; H, 3.61; N, 12.31%.

(*Z*)-*N'*-(3-(5-(Benzo[d][1,3]dioxol-5-ylmethylene)-4-oxo-2-thioxothiazolidin-3-yl)propanoyl)-1-naphthohydrazide (Pa-3).

Yield: 88%, m.p. 249–250 °C; ^{1}H NMR (400 MHz, [D_6]DMSO) δ=2.57 (t, *J* = 8.4 Hz, 2H), 4.77 (t, *J* = 8.8 Hz, 2H), 6.59 (s, 2H), 7.49 (s, 1H), 7.53–7.74 (m, 2H), 7.89 (d, *J* = 7.6 Hz, 2H), 8.21–8.91 (m, 6H), 10.21 (bs, 2H); ^{13}C NMR (100 MHz, [D_6]DMSO) δ=36.3, 45.9, 108.7, 121.6, 123.4, 124.6, 125.4, 126.9, 127.4, 128.7, 129.4, 132.1, 132.8, 133.0, 133.9, 142.0, 142.5, 147.3, 148.8, 149.1, 151.9, 165.0, 165.3, 177.6, 190.6: MS (ES, 70eV) m/z 506 $[M+H]^+$; Anal. calcd for $C_{25}H_{19}N_3O_5S_2$: C, 59.39; H, 3.79; N, 8.31% Found C, 59.41; H, 3.82; N, 8.37%.

(*Z*)-*N'*-(3-(5-(4-Chlorobenzylidene)-4-oxo-2-thioxothiazolidin-3 yl)propanoyl)benzohydrazide (Pa-4).

Yield: 79%, m.p. 246–247 °C; ^{1}H NMR (400 MHz, [D_6]DMSO) δ=2.44 (t, *J* = 7.6 Hz, 2H), 4.18 (t, *J* = 7.6 Hz, 2H), 7.31 (d, *J* = 6.8 Hz, 2H), 7.42 (s, 1H), 7.56–7.69 (m, 5H), 7.80 (d, *J* = 6.8 Hz, 2H), 9.60 (s, 1H), 9.70 (s, 1H); ^{13}C NMR (100 MHz, [D_6]DMSO) δ=37.1, 45.7, 125.7(2C), 126.1(2C), 127.1(2C), 128.2(2C), 130.2, 133.6, 135.8, 136.7, 142.3, 146.9, 169.6, 177.6, 178.4, 188.2: MS (ES, 70eV) m/z 446 $[M+H]^+$; Anal. calcd for $C_{20}H_{16}ClN_3O_3S_2$: C, 53.87; H, 3.62; N, 9.42% Found C, 54.01; H, 3.69; N, 9.47%.

(*Z*)-*N'*-(3-(5-(4-Chlorobenzylidene)-4-oxo-2-thioxothiazolidin-3 yl)propanoyl)isonicotinohydrazide (Pa-5).

Yield: 72%, m.p. 259–260 °C;. ^{1}H NMR (400 MHz, [D_6]DMSO) δ=2.25 (t, *J* = 7.2 Hz, 2H), 3.99 (t, *J* = 7.6 Hz, 2H), 7.40 (d, *J* = 6.8 Hz, 2H), 7.54–7.66 (m, 5H), 8.40 (d, *J* = 7.2 Hz, 2H), 9.40 (s, 1H), 9.60 (s, 1H); ^{13}C NMR (100 MHz, [D_6]DMSO) δ=38.3, 46.2, 124.7, 125.6(2C), 126.0(2C), 126.7(2C), 130.7, 132.6, 133.8, 136.7, 144.3, 149.9, 165.6, 175.0, 176.6, 181.6: MS (ES, 70eV) m/z 447 $[M+H]^+$; Anal. calcd for $C_{19}H_{15}ClN_4O_3S_2$: C, 51.06; H, 3.38; N, 12.54% Found C, 51.11; H, 3.39; N, 12.61%.

(*Z*)-*N'*-(3-(5-(4-Chlorobenzylidene)-4-oxo-2-thioxothiazolidin-3-yl)propanoyl)-1-naphthohydrazide (Pa-6).

Yield: 70%, m.p. 269–270 °C; ^{1}H NMR (400 MHz, $CDCl_3$) δ=2.32 (t, *J* = 7.6 Hz, 2H), 3.91 (t, *J* = 7.2 Hz, 2H), 7.39 (d, *J* = 8.8 Hz, 2H), 7.54–7.63 (m, 6H), 7.80–8.10 (m, 4H), 9.60 (bs, 2H); ^{13}C NMR (100 MHz, $CDCl_3$) δ=39.3, 44.9, 121.7, 124.0, 124.7, 125.1, 125.7, 126.6(2C), 129.5(2C), 132.6, 132.7, 133.8, 134.5, 136.4, 137.6, 138.7, 143.3, 145.9, 164.6,

169.0, 176.9, 178.6: MS (ES, 70eV) m/z 496 $[M+H]^+$; Anal. calcd for $C_{24}H_{18}ClN_3O_3S_2$: C, 58.12; H, 3.66; N, 8.47% Found C, 58.17; H, 3.71; N, 8.53%.

(*Z*)-*N'*-(3-(5-(4-Chlorobenzylidene)-4-oxo-2-thioxothiazolidin-3-yl)propanoyl)nicotinohydrazide (Pa-7).

Yield: 89%, m.p. 246–247 °C; ^{1}H NMR (400 MHz, [D_6]DMSO): δ=2.40 (t, *J* = 8.0 Hz, 2H), 4.12 (t, *J* = 8.4 Hz, 2H), 7.45 (d, *J* = 8.4 Hz, 2H), 7.60–7.81 (m, 4H), 8.10 (d, *J* = 7.2 Hz, 1H), 8.40 (d, *J* = 7.6 Hz, 1H), 8.80 (s, 1H), 9.40 (s, 1H), 9.60 (s, 1H); ^{13}C NMR (100 MHz, [D_6]DMSO) δ=37.8, 47.2, 123.7, 124.4, 125.6, 126.3(2C), 127.5(2C), 132.2, 133.5, 136.4, 137.7, 145.3, 147.6, 164.6, 172.5, 177.4, 180.7: MS (ES, 70eV) m/z 447 $[M+H]^+$; Anal. calcd for $C_{19}H_{15}ClN_4O_3S_2$: C, 51.06; H, 3.38; N, 12.54% Found C, 51.14; H, 3.42; N, 12.63%.

Preparation of (*Z*)-*N'*-(3-(4-oxo-2-thioxo-5-(3,4,5-trimethoxybenzylidene)thiazolidin-3-yl)propanoyl)benzohydrazide (Pa-8).

Yield 86%, m.p. 245–247 °C; ^{1}H NMR (400 MHz, [D_6]DMSO) δ=2.52 (t, *J* = 7.6 Hz, 2H), 3.90 (s, 9H), 4.23 (t, *J* = 8.0 Hz, 2H), 7.11 (s, 2H), 7.40 (s, 1H), 7.65–7.72 (m, 3H), 7.90 (d, *J* = 7.2 Hz, 2H), 9.72 (s, 1H), 9.81 (s, 1H); ^{13}C NMR (100 MHz, [D_6]DMSO) δ=38.3, 49.2, 56.4, 61.2(2C), 123.9, 124.4, 125.3(2C), 126.6, 127.2(2C), 127.8, 132.7, 133.9, 134.5, 138.6, 144.3, 145.6, 164.6, 168.5, 172.4, 176.7: MS (ES, 70eV) m/z 502 $[M+H]^+$; Anal. calcd for $C_{23}H_{23}N_3O_6S_2$: C, 55.08; H, 4.62; N, 8.38% Found C, 55.14; H, 4.72; N, 8.40%.

(*Z*)-*N'*-(3-(4-Oxo-2-thioxo-5-(3,4,5-trimethoxybenzylidene)thiazolidin-3-yl)propanoyl)isonicotinohydrazide (Pa-9).

Yield: 92%, m.p. 196–198 °C; ^{1}H NMR (400 MHz, [D_6]DMSO) δ=2.49 (t, *J* = 7.6 Hz, 2H), 3.93 (s, 9H), 4.32 (t, *J* = 8.0 Hz, 2H), 7.23 (s, 2H), 7.60 (s, 1H), 7.90 (d, *J* = 7.8 Hz, 2H), 8.40 (d, *J* = 8.0 Hz, 2H), 9.61 (s, 1H), 9.72 (s, 1H); ^{13}C NMR (100 MHz, [D_6]DMSO) δ=39.4, 48.6, 57.4, 59.8(2C), 123.4, 124.1, 124.9(2C), 125.1, 126.2, 126.6, 132.3, 133.1, 133.4, 137.4, 143.2, 144.5, 164.3, 169.4, 174.6, 178.7: MS (ES, 70eV) m/z 503 $[M+H]^+$; Anal. calcd for $C_{22}H_{22}N_4O_6S_2$: C, 52.58; H, 4.41; N, 11.15% Found C, 52.64; H, 4.52; N, 11.23%.

(*Z*)-*N'*-(3-(4-Oxo-2-thioxo-5-(3,4,5-trimethoxybenzylidene)thiazolidin-3-yl)propanoyl)-1-naphthohydrazide (Pa-10).

Yield: 75%, m.p. 238–240 °C; ^{1}H NMR (400 MHz, $CDCl_3$): δ=2.36 (t, *J* = 8.4 Hz, 2H), 3.79 (s, 9H), 4.27 (t, *J* = 8.0 Hz, 2H), 7.19 (s, 2H), 7.65–7.80 (m, 3H), 8.13–8.85 (m, 5H), 10.20 (bs, 2H); ^{13}C NMR (100 MHz, $CDCl_3$) δ=37.9, 49.6, 57.8(3C), 121.4, 123.1, 124.3(2C),

125.4, 126.0, 126.6, 127.2, 127.6, 128.3, 129.5, 132.1, 132.7, 133.0, 133.4, 138.2, 141.2, 143.6, 166.3, 171.7, 172.6, 180.7: MS (ES, 70eV) m/z 552 $[M+H]^+$; Anal. calcd for $C_{27}H_{25}N_3O_6S_2$: C, 58.79; H, 4.57; N, 7.62% Found C, 58.84; H, 4.62; N, 7.73%.

(*Z*)-*N'*-(3-(4-Oxo-2-thioxo-5-(3,4,5-trimethoxybenzylidene)thiazolidin-3-yl)propanoyl)nicotinohydrazide (Pa-11).

Yield: 84%, m.p. 234–236 °C; ^{1}H NMR (400 MHz, [D_6]DMSO) δ=2.34 (t, *J* = 8.4 Hz, 2H), 3.87 (s, 9H), 4.19 (t, *J* = 7.6 Hz, 2H), 7.21 (s, 2H), 7.54 (s, 1H), 7.60 (t, *J* = 8.8 Hz, 1H), 8.10 (s, 1H), 8.64 (s, 1H), 8.71 (s, 1H), 9.61 (d, *J* = 11.2 Hz, 2H); ^{13}C NMR (100 MHz, [D_6]DMSO) δ=40.0, 49.3, 56.7, 58.3(2C), 121.9, 123.6, 124.2(2C), 124.9, 125.6, 126.1, 132.5, 132.9, 133.9, 138.6, 142.5, 144.8, 163.9, 169.1, 174.2, 177.9: MS (ES, 70eV) m/z 503 $[M+H]^+$; Anal. calcd for $C_{22}H_{22}N_4O_6S_2$: C, 52.58; H, 4.41; N, 11.15% Found C, 52.62; H, 448; N, 11.21%.

(*Z*)-*N'*-(3-(5-(4-Nitrobenzylidene)-4-oxo-2-thioxothiazolidin-3 yl)propanoyl)benzohydrazide (Pa-12).

Yield: 69%, m.p. 248–249 °C; ^{1}H NMR (400 MHz, [D_6]DMSO) δ=2.54 (t, *J* = 8.8 Hz, 2H), 4.12 (t, *J* = 8.4 Hz, 2H), 7.63–7.83 (m, 7H), 7.92 (s, 1H), 8.31 (d, *J* = 9.6 Hz, 2H), 9.60 (d, *J* = 11.6 Hz, 2H); ^{13}C NMR (100 MHz, [D_6]DMSO) δ=38.1, 46.9, 120.1, 120.6, 121.9(2C), 125.4, 126.1, 126.6, 133.9, 134.6, 135.4, 139.6, 141.6, 143.0, 143.5, 163.4, 168.5, 173.2, 174.9: MS (ES, 70eV) m/z 457 $[M+H]^+$; Anal. calcd for $C_{20}H_{16}N_4O_5S_2$: C, 52.62; H, 3.53; N, 12.27% Found C, 52.72; H, 3.59; N, 12.31%

(*Z*)-*N'*-(3-(5-(4-Nitrobenzylidene)-4-oxo-2-thioxothiazolidin-3-yl)propanoyl)isonicotinohydrazide (Pa-13).

Yield: 72%, m.p. 229–231 °C; ^{1}H NMR (400 MHz, [D_6]DMSO) δ=2.61 (t, *J* = 8.4 Hz, 2H), 4.23 (t, *J* = 7.6 Hz, 2H), 7.63–7.72 (m, 4H), 7.81 (d, *J* = 7.4 Hz, 2H), 8.03 (s, 1H), 8.22 (d, *J* = 7.8 Hz, 2H), 10.11 (d, *J* = 11.6 Hz, 2H); ^{13}C NMR (100 MHz, [D_6]DMSO) δ=34.8, 45.9, 121.1, 121.7, 123.4, 125.6, 126.0, 126.8, 134.2, 134.7, 136.4, 139.9, 143.7, 144.0, 145.7, 162.8, 167.4, 174.6, 176.3: MS (ES, 70eV) m/z 458 $[M+H]^+$; Anal. calcd for $C_{19}H_{15}N_5O_5S_2$: C, 49.88; H, 3.30; N, 15.31% Found C, 49.92; H, 3.39; N, 15.36%.

(*Z*)-*N'*-(3-(5-(4-Nitrobenzylidene)-4-oxo-2-thioxothiazolidin-3-yl)propanoyl)-1-naphthohydrazide (Pa-14).

Yield: 81%, m.p. 263–264 °C; ^{1}H NMR (400 MHz, [D$_6$]DMSO) δ=2.50 (t, *J* = 8.0 Hz, 2H), 4.21 (t, *J* = 7.6 Hz, 2H), 7.92–7.72 (m, 10H), 8.10 (d, *J* = 10.0 Hz, 2H), 9.70 (d, *J* = 12.0 Hz, 2H); ^{13}C NMR (100 MHz, [D$_6$]DMSO) δ=36.9, 46.3, 121.2, 121.6, 123.4, 124.2, 124.8, 125.3, 125.9, 126.4, 126.8, 133.4, 134.6, 135.4, 136.7, 137.7, 138.8, 143.3, 144.3, 145.8, 164.6, 166.9, 172.8, 177.3: MS (ES, 70eV) m/z 507 [M+H]$^+$; Anal. calcd for $C_{24}H_{18}N_4O_5S_2$: C, 56.91; H, 3.58; N, 11.06% Found C, 56.97; H, 3.62; N, 11.16%.

(*Z*)-*N'*-(3-(5-(4-Nitrobenzylidene)-4-oxo-2-thioxothiazolidin-3 yl)propanoyl)nicotinohydrazide (Pa-15).

Yield: 72%, m.p. 264–265 °C; ^{1}H NMR (400 MHz, CDCl$_3$) δ=2.41 (t, *J* = 8.4 Hz, 2H), 4.30 (t, *J* = 8.4 Hz, 2H), 8.01–7.81 (m, 6H), 8.13 (d, *J* = 9.6 Hz, 2H), 8.70 (s, 1H), 10.21 (d, *J* = 11.6 Hz, 2H); ^{13}C NMR (100 MHz, CDCl$_3$) δ=36.5, 47.4, 120.1, 121.9, 124.5, 125.8, 126.4, 127.4, 134.7, 135.4, 136.6, 138.9, 143.3, 145.3, 145.9, 163.6, 165.3, 176.6, 178.7: MS (ES, 70eV) m/z 458 [M+H]$^+$; Anal. calcd for $C_{19}H_{15}N_5O_5S_2$: C, 49.88; H, 3.30; N, 15.31% Found C, 49.90; H, 3.36; N, 15.37%.

(*Z*)-*N'*-(3-(5-(4-(Benzyloxy)benzylidene)-4-oxo-2-thioxothiazolidin-3-yl)propanoyl)benzohydrazide (Pa-16).

Yield: 70%, m.p. 223–224 °C; ^{1}H NMR (400 MHz, [D$_6$]DMSO) δ=2.46 (t, *J* = 7.6 Hz, 2H), 4.21 (t, *J* = 8.0 Hz, 2H), 5.20 (s, 2H), 7.20–7.62 (m, 13H), 7.90 (d, *J* = 9.2 Hz, 2H), 9.72 (d, *J* = 12.4 Hz, 2H); ^{13}C NMR (100 MHz, [D$_6$]DMSO) δ=36.5, 47.4, 72.9, 121.2(2C), 124.2(2C), 125.8(2C), 126.2(2C), 127.6, 134.7(2C), 135.4, 136.0, 136.6, 137.0, 138.9, 141.4, 143.8, 144.3, 145.4, 166.9, 168.3, 179.6, 182.7: MS (ES, 70eV) m/z 518 [M+H]$^+$; Anal. calcd for $C_{27}H_{23}N_3O_4S_2$: C, 62.65; H, 4.48; N, 8.12% Found C, 62.70; H, 4.56; N, 8.16%.

(*Z*)-*N'*-(3-(5-(4-(Benzyloxy)benzylidene)-4-oxo-2-thioxothiazolidin-3-yl)propanoyl)isonicotinohydrazide (Pa-17).

Yield: 79%, m.p. m.p. 233–234 °C; ^{1}H NMR (400 MHz, CDCl$_3$) δ=2.38 (t, *J* = 7.6 Hz, 2H), 4.12 (t, *J* = 8.0 Hz, 2H), 5.11 (s, 2H), 7.18–7.35 (m, 7H), 7.63–7.72 (m, 3H), 7.92 (d, *J* = 7.6 Hz, 2H), 8.31 (d, *J* = 7.2 Hz, 2H), 9.93 (d, *J* = 12.4 Hz, 2H); ^{13}C NMR (100 MHz, [D$_6$]DMSO) δ 180.7, 178.4, 166.3, 162.9, 143.5, 142.3, 142.0, 141.6, 139.5, 138.3, 136.9, 136.4, 135.6, 134.4(2C), 127.2(2C), 125.9(2C), 125.2, 124.7(2C), 123.2, 72.9, 47.4, 36.5: MS

(ES, 70eV) m/z 519 $[M+H]^+$; Anal. calcd for $C_{26}H_{22}N_4O_4S_2$: C, 60.21; H, 4.28; N, 10.80% Found C, 60.26; H, 4.36; N, 10.92%.

(*Z*)-*N'*-(3-(5-(4-(Benzyloxy)benzylidene)-4-oxo-2-thioxothiazolidin-3-yl)propanoyl)-1-naphthohydrazide (Pa-18).

Yield: 90%, m.p. 240–242 °C; ^{1}H NMR (400 MHz, [D_6]DMSO) δ=2.43 (t, *J* = 8.4 Hz, 2H), 4.21 (t, *J* = 8.8 Hz, 2H), 5.12 (s, 2H), 7.36–7.20 (m, 5H), 7.92–7.62 (m, 8H), 8.44–8.31 (m, 4H), 10.17 (d, *J* = 12.8 Hz, 2H); ^{13}C NMR (100 MHz, [D_6]DMSO) δ=38.3, 49.4, 69.6, 123.2, 124.7(2C), 125.2, 125.9(2C), 126.4, 127.5, 128.2(2C), 129.4, 132.5(2C), 133.3(2C), 135.6, 136.2, 136.9, 139.3, 140.7, 141.3, 141.7, 142.1, 143.3, 162.5, 164.3, 177.4, 179.7: MS (ES, 70eV) m/z 568 $[M+H]^+$; Anal. calcd for $C_{31}H_{25}N_3O_4S_2$: C, 65.59; H, 4.44; N, 7.40% Found C, 65.66; H, 4.46; N, 7.42%.

(*Z*)-*N'*-(3-(5-(4-(Benzyloxy)benzylidene)-4-oxo-2-thioxothiazolidin-3-yl)propanoyl)nicotinohydrazide (Pa-19).

Yield: 79%, m.p. 249–250 °C; ^{1}H NMR (400 MHz, [D_6]DMSO): δ=2.34 (t, *J* = 7.6 Hz, 2H), 4.09 (t, *J* = 8.0 Hz, 2H), 5.17 (s, 2H), 7.11–7.23 (m, 5H), 7.91–8.12 (m, 7H), 8.62 (d, *J* = 6.0 Hz, 1H), 8.80 (s, 1H), 9.92 (d, *J* = 12.4 Hz, 2H); ^{13}C NMR (100 MHz, [D_6]DMSO) δ=37.6, 48.2, 73.5, 123.7, 124.1(2C), 124.6, 126.3(2C), 127.2, 134.2(2C), 135.3, 136.0, 136.4, 137.3, 138.4, 141.8, 142.4, 142.6, 144.3, 164.1, 167.5, 179.6, 180.4: MS (ES, 70eV) m/z 519 $[M+H]^+$; Anal. calcd for $C_{26}H_{22}N_4O_4S_2$: C, 60.21; H, 4.28; N, 10.80% Found C, 60.24; H, 4.32; N, 10.88%.

Annexure II: Synthesis of pantothenate synthetase inhibitors using inhibitor based approach- tryptophan derivatives

The procedures and characterization data for representative compounds (Pb-5, Pb-8, Pb-14, Pb-15 and Pb-16) are presented.

Preparation of methyl D-tryptophanate (2)

To a solution of thionyl chloride (4.25 ml, 58 mmol) in methanol (50 ml) was added D-tryptophan (5 g, 24.5 mmol) and the resulting solution was heated under reflux for 18 h. After evaporation of the solvent, a white residue of hydrochloride salt was obtained, which was neutralized by a sodium carbonate solution and the ester was extracted with ethyl acetate (200 ml). The organic layer was dried over sodium sulphate and evaporated under reduced pressure to obtain 5 g (yield 93%) of compound as off-white solid.

^{1}H NMR (δ, ppm, DMSO-d_6, 300 MHz): 3.39 (m, 2H), 3.63 (s, 3H), 4.20 (t, 1H, J = 5.5), 7.07 (dt, 2H, J = 21), 7.26 (d, 1H, J = 3), 7.39 (d, 1H, J = 7.8), 7.53 (d, 1H, J = 7.8). ^{13}C NMR (DMSO-d_6, 100 MHz); 26.01, 52.61, 106.26, 111.45, 117.84, 118.50, 121.05, 124.80, 126.79, 136.13, 169.57; m/z 218 $[M+H]^+$.

Preparation of methyl 2-(3-aminobenzamido)-3-(1H-indol-3-yl)propanoate (3)

To a stirred solution of **2** (5.00 g, 22.9 mmol) and 3-aminobenzoic acid (3.45 g, 25.22 mmol) in DMF (80 ml) was added DIPEA (7.38 g, 57.25 mmol) followed by O-(benzotriazol-1-yl)-N,N,N',N'-tetramethyluronium tetrafluoroborate (8.82 g, 27.48 mmol). Then the reaction mixture was allowed to stir at room temperature for 16 h. The reaction mixture was diluted with water (50 ml) and extracted with EtOAc (100 ml); organic layer washed with water dried over sodium sulphate and evaporated under reduced pressure to obtain crude compound. This was purified by column chromatography to afford 5.10 g (yield 65%) of compound **3** as off-white solid.

^{1}H NMR (300 MHz, $CDCl_3$) δ:8.136 (bs,1H), 7.563 (d, *J* = 7.5 Hz, 1H), 7.350 (d, *J* = 8.1 Hz, 1H), 7.180 – 7.010 (m, 5 H), 6.663 – 6.531 (m, 3H), 5.498 (bs, 2H), 5.090 – 5.069 (m, 1H), 3.713 (s, 3H), 3.426 (d, *J* = 4.8 Hz, 2H); MS (ESI) m/z 338 $[M+H]^+$.

General procedure for preparation of compounds 4

To a stirred solution of compound **3** (1.00 equiv) in CH_2Cl_2 (10 vol) was added DIPEA (3.00 equiv) and cooled to 0°C and slowly added corresponding acid chloride (1.30 equiv) and allowed to stir at room temperature for 12 h. Reaction mixture washed with water followed

by 3N NaOH and brine; organic layer dried over sodium sulphate and evaporated under reduced pressure to obtain crude compound. This was purified by trituration with diisopropylether to afford **4** respectively.

General procedure for the synthesis of compounds 5 (Pb 1-Pb-16)

To a stirred solution of compound **4** (1.00 equiv) in methanol (8 vol) was added 3N NaOH (3.00 equiv) and stirred at room temperature for 4 h. Evaporated the methanol and diluted with water, washed the aqueous layer with EtOAc. Adjusted the aqueous layer pH to 2 by using conc. HCl and extracted with CH_2Cl_2 and concentrated and dried to afford the compounds **5 (Pb-1-Pb-16)** respectively.

The spectral data of representative compounds are given below,

2-(3-(4-Fluorobenzamido)benzamido)-3-(1H-indol-3-yl)propanoic acid (Pb-5): Yield: 92%; MS(ESI) m/z 444 $[M-H]^+$. ^{1}H NMR (400 MHz, DMSO-d_6) δ:12.2 (s, 1H), 10.8 (s, 1H), 9.07(d, , *J* = 8, 1H), 8.59(d, *J* = 8, 1H), 7.90 – 7.83(m, 3H), 7.61 – 7.55 (m, 2H), 7.39(t, , *J* = 8, 2H), 7.29(d, *J* = 8, 1H), 7.20(t, *J* = 8, 2H), 7.04(t, *J* = 8, 1H), 6.96(t, *J* = 8, 1H), 4.69 – 4.78 (m, 1H), 3.43 – 3.21 (m, 2H); ^{13}C NMR (100 MHz, DMSO-d_6) δ: 172.9, 168.7, 163.3, 139.2, 136.0, 132.46, 130.9, 129.6, 129.5, 128.4, 127.0, 123.5, 122.8, 120.9, 120.1, 119.8, 118.3, 118.0, 116.0, 115.8, 111.4, 110.2, 53.74, 26.42(2C)

2-(3-(4-Chlorobenzamido)benzamido)-3-(1H-indol-3-yl)propanoic acid (Pb-8): Yield: 89%; MS(ESI) m/z 460 $[M-H]^+$. ^{1}H NMR (400 MHz, DMSO-d_6) δ: 12.9 (bs, 1H), 12.2 (s, 1H), 10.803 (s, 1H), 9.07 (d, *J* = 8.0, 1H), 8.58 (d, *J* = 7.6, 1H), 7.85 – 7.81 (m, 3H), 7.646 – 7.550 (m, 4H), 7.29 (d, *J* = 15.6, 1H), 7.230 – 7.189 (m, 2H), 7.03 (t, *J* = 6.0, 1H), 6.96 (t, *J* = 7.2, 1H), 4.68 – 4.78 (m, 1H), 3.33 – 3.25 (m, 2H); ^{13}C NMR (100 MHz, DMSO-d_6) δ: 172.96, 168.71, 163.31, 139, 137.7, 136.8, 136.0, 133.1, 132.4, 131.1, 129.0, 128.7, 128.4, 127.0, 123.5, 122.9, 120.9, 119.9, 118.3, 118.0, 111.4, 110.2, 53.73, 26.80, 26.42

2-(2-Benzamidobenzamido)-3-(1H-indol-3-yl)propanoic acid (Pb-14):

Yield: 70% ^{1}H NMR (400 MHz, DMSO-d_6) δ:12.251 (s, 1H), 10.831 (s, 1H), 9.090 (d, *J* = 6.8 Hz, 1H), 8.667 (d, *J* = 8, 1H), 7.871 (d, *J* = 6.4, 2H), 7.644 – 7.569 (m, 6H), 7.337 – 7.193 (m, 3H), 7.086 – 6.998 (m, 2H), 4.764 (s, 1H), 3.406 – 3.295 (m, 2H); ^{13}C NMR (100 MHz, DMSO-d_6) δ: 173.02, 168.80, 164.38, 139.33, 136.11, 132.46, 128.93, 128.52, 128.45, 1 27.09, 126.86, 123.59, 122.70, 120.95, 120.13, 119.79, 118.37, 118.08, 111.44, 110.26, 53.77, 27.33; MS (ESI) m/z 426 $[M-H]^+$.

2-(2-(2-Fluorobenzamido)benzamido)-3-(1H-indol-3-yl)propanoic acid (Pb-15):

Yield: 65% ^{1}H NMR (400 MHz, DMSO-d_6) δ:11.830 (s, 1H), 10.809 (s, 1H), 8.978 (d, *J* = 7.6 Hz ,1H), 8.578 (d, *J* = 8.4 Hz, 1H), 7.864– 7.763 (m, 2H), 7.656– 7.545 (m, 3H), 7.399 – 7.342 (m, 3H), 7.319 – 7.299 (m, 2H), 7.047 (t, *J* = 7.2 Hz, 1H), 6.965 (t, *J* = 7.2 Hz, 1H), 4.697 – 4.643 (m, 1H), 3.363 – 3.209 (m, 2H); ^{13}C NMR (100 MHz, DMSO-d_6) δ: 173.02, 168.23, 161.41, 160.53, 158.05, 138.49, 136.09, 133.83, 133.74, 132.16, 130.59, 128.38, 127.10, 125.01, 124.98, 123.51, 122.87, 122.74, 120.91, 120.85, 120.79, 118.32, 118.06, 116.69, 116.49, 111.39, 110.25, 53.68, 26.41; MS (ESI) m/z 444 $[M-H]^+$.

2-(2-(4-tert-Butylbenzamido)benzamido)-3-(1H-indol-3-yl)propanoic acid (Pb-16): Yield: 75% ^{1}H NMR (400 MHz, $CDCl_3$) δ:11.945 (s, 1H), 8.729 (d, *J* = 8.4 Hz, 1H), 8.181 (bs, 1H), 7.989 – 7.925 (m, 1H), 7.561 – 7.409 (m, 4H), 7.253 – 7.187 (m, 2H), 7.127 (t, *J* = 7.2 Hz, 1H), 7.026 (t, *J* = 7.6 Hz, 1H), 6.912 – 6.804 (m, 4H), 5.131 – 5.099 (m, 1H), 3.478 – 3.387 (m, 2H), 1.255 (s, 9H) ;^{13}C NMR (100MHz,$CDCl_3$) δ: 175.35, 168.95, 165.93, 155.56, 139.95, 136.11, 133.01, 131.79, 130.14, 127.56, 126.97, 125.54, 123.10, 122.37, 121.65, 119.86, 118.48, 111.43, 109.44, 53.39, 35.00, 31.15; MS (ESI) m/z 482 $[M-H]^+$.

Annexure III: Synthesis of lysine aminotransferase inhibitors using substrate lysine based approach- glutarohydrazide derivatives

The procedures and characterization data are given for all the synthesized compounds.

General procedure for the synthesis of dimethyl ester (2a-b)

To a stirred solution of dicarboxylic acid (1a-b) (1 mmol) in methanol (15 ml) at room temperature was added concentrated sulphuric acid. The solution was refluxed for about 6 hrs (monitored by TLC & LCMS for completion), and solvent evaporated under reduced pressure. The residue was further diluted with water (30 ml) and ethyl acetate (50 ml) and the layers were separated. The organic layer was dried over anhydrous sodium sulphate and evaporated under reduced pressure. The residue was purified by silica gel column chromatography using hexane: ethylacetate as eluent to give the corresponding dimethyl glutarate (2a-b) in good yield.

Dimethyl glutarate (**2a)**:

The compound was synthesized according to the general procedure glutaric acid (**1a**) (1.5 g, 10.26 mmol) and concentrated sulphuric acid to afford **2a** (1.84 g, 82.4 %) as white solid. M.p: 222-224°C. ^{1}H NMR (DMSO-d_6): δ_H3.65 (s, 6H), 2.32-2.25(m, 6H). ^{13}C NMR (DMSO-d_6): δ_C 173.1(2C), 51.9(2C), 33(2C), 20. ESI-MS *m/z*161 $(M+H)^+$. Anal.Calcd.for$C_7H_{12}O_4$: C, 52.49; H, 7.55; Found: C, 52.47; H, 7.53%.

Dimethyl 2,2'-oxydiacetate (2b):

The compound was synthesized according to the general procedure diglycolic acid (1b) (1.5 g, 10.26 mmol) and concentrated sulphuric acid to afford 2b (1.84 g, 82.4 %) as white solid.M.p: 243-245°C. ^{1}H NMR (DMSO-d_6): δ_H 3.68 (s, 6H), 4.33(s, 4H). ^{13}C NMR (DMSO-d_6) :δ_C 169.2(2C), 70.1(2C), 51.9(2C). ESI-MS *m/z*163 $(M+H)^+$. Anal.Calcd.for$C_6H_{10}O_5$: C, 44.45; H, 6.22; Found: C, 44.43; H, 6.19%.

General procedure for the synthesis of hydrazide

To a stirred solution of ester (1 mmol) in ethanol (30 ml) was added hydrazine hydrate (2.5 mmol). The solution was refluxed for about 12 hours (monitored by TLC & LCMS for completion), and solvent evaporated under reduced pressure. The residue was further diluted with water (30 ml) and ethyl acetate (50 ml) and the layers were separated. The organic layer was dried over anhydrous sodium sulphate and evaporated under reduced pressure. The

residue was purified by silica gel column chromatography using hexane: ethylacetate as eluent to give the corresponding hydrazide in good yield.

Glutarohydrazide

The compound was synthesized according to the general procedure dimethyl glutarate (2a) (1.5 g, 10.26 mmol) andhydrazine hydrate to afford 3a (1.84 g, 82.4 %) as white solid. M.p: 216-218°C. ^{1}H NMR (DMSO-d_6): δ_H8 (s, 2H), 2.34-2(m, 10H). ^{13}C NMR (DMSO-d_6) :δ_C 176.6(2C), 38.1(2C), 22.8. ESI-MS *m/z*161 $(M+H)^+$. Anal.Calcd.for$C_5H_{12}N_4O_2$: C, 37.49; H, 7.55; N, 34.98. Found: C, 37.45; H, 7.57; N, 34.96%.

2,2'-Oxydi(acetohydrazide)

The compound was synthesized according to the general procedure dimethyl 2,2'-oxydiacetate (2b) (1.5 g, 10.26 mmol) andhydrazine hydrate to afford 3b(1.84 g, 82.4 %) as white solid. M.p: 195-197°C. ^{1}H NMR (DMSO-d_6): δ_H 8 (s, 2H), 4.26 (s, 4H), 2 (s,4H). ^{13}C NMR (DMSO-d_6) :δ_C 166.3 (2C), 69.1 (2C),. ESI-MS *m/z*163 $(M+H)^+$. Anal.Calcd.for $C_4H_{10}N_4O_3$: C, 29.63; H, 6.22; N, 34.55 Found: C, 29.65; H, 6.24; N, 34.58%.

General procedure for the synthesis of substituted (N'1E,N'5E)-N'1,N'5-diethylideneglutarohydrazide (La-1- La-24)

To a stirred solution of glutarohydrazide (**3a**) (1 mmol) in ethanol (15 ml) at room temperature was added aldehyde(1 mmol). The solution was refluxed for about 12 hours (monitored by TLC & LCMS for completion), and solvent evaporated under reduced pressure. The residue was further diluted with water (30 ml) and ethyl acetate (50 ml) and the layers were separated. The organic layer was dried over anhydrous sodium sulphate and evaporated under reduced pressure. The residue was purified by silica gel column chromatography using hexane: ethylacetate as eluent to give the corresponding $N^{1'}$,$N^{5'}$-diethylideneglutarohydrazide(**La-1-La-24**) in good yield.

(N'1E,N'5E)-N'1,N'5-Bis(2-methylbenzylidene)glutarohydrazide (La-1) :

The compound was synthesized according to the general procedure using glutarohydrazide (3a) (0.1 g, 0.62mmol) and o-tolualdehyde (0.149 g, 1.24mmol) to afford 4 (0.157 g, 69%) as white solid.M.p: 221-223 °C. ^{1}H NMR (DMSO-d_6): δ_H 11.06– 10.92 (m, 2H), 8.52– 7.21 (m, 10H), 2.45– 2.03 (m, 12H). ^{13}C NMR (DMSO-d_6): δ_C 167.2(2C), 143.2(2C), 135.4(2C), 131.3(2C), 130.7(2C), 129.2(2C), 126.1(2C), 125.8(2C), 38.5(2C), 22.8, 18.8(2C). ESI-MS

m/z 365 $(M+H)^+$. Anal.Calcd.for $C_{21}H_{24}N_4O_2$: C, 69.21; H, 6.64; N, 15.37; Found: C, 69.19; H, 6.66; N, 15.34

(N'1E,N'5E)-N'1,N'5-Bis(3-methylbenzylidene)glutarohydrazide (La-2):

The compound was synthesized according to the general procedure using glutarohydrazide (3a) (0.1 g, 0.62 mmol) and m-tolualdehyde (0.149 g, 1.24mmol) to afford 5 (0.169 g, 74.2 %) as white solid. M.p: 242-244 °C. ^{1}H NMR (DMSO-d_6): δ_H 11.07– 10.93 (m, 2H), 8.55 – 7.27 (m, 10H), 2.34– 2.02 (m, 12H). ^{13}C NMR (DMSO-d_6): δ_C 167.2(2C), 146.6(2C), 138.4(2C), 133.3(2C), 131.7(2C), 129.2(2C), 128.2(2C), 126.8(2C), 38.5(2C), 22.7, 21.1(2C). ESI-MS *m/z* 365 $(M+H)^+$. Anal.Calcd.for $C_{21}H_{24}N_4O_2$: C, 69.21; H, 6.64; N, 15.37; Found: C, 69.23; H, 6.65; N, 15.33.

(N'1E,N'5E)-N'1,N'5-Bis(4-methylbenzylidene)glutarohydrazide (La-3) :

The compound was synthesized according to the general procedure using glutarohydrazide (3a) (0.1 g, 0.62mmol) and p-tolualdehyde (0.149 g, 1.24mmol) to afford 6 (0.114 g, 50.1 %) white solid.M.p: 217-219 °C. ^{1}H NMR (DMSO-d_6): δ_H 11.06– 10.93 (m, 2H), 8.54 – 7.27 (m, 10H), 2.35–2.04 (m, 12H). ^{13}C NMR (DMSO-d_6): δ_C167.3(2C), 144.3(2C), 140.5(2C), 130.3(2C), 129.7(4C), 126.2(4C), 38.2(2C), 22.6, 21.4(2C). ESI-MS *m/z* 365 $(M+H)^+$. Anal.Calcd.for $C_{21}H_{24}N_4O_2$: C, 69.21; H, 6.64; N, 15.37; Found: C, 69.25; H, 6.61; N, 15.33.

(N'1E,N'5E)-N'1,N'5-Bis(2-fluorobenzylidene)glutarohydrazide (La-4) :

The compound was synthesized according to the general procedure using glutarohydrazide (3a) (0.1 g, 0.62mmol) and 2-fluoro benzaldehyde (0.154 g, 1.24mmol) to afford 7 (0.172 g, 73.9 %) as white solid.M.p: 187-189 °C. ^{1}H NMR (DMSO-d_6): δ_H 11.07– 10.95 (m, 2H), 8.55 – 7.28 (m, 10H), 2.35– 2.01 (m, 6H),. ^{13}C NMR (DMSO-d_6):δ_C 167.5(2C), 159.4(2C), 143.2(2C), 132.6(2C), 130.6(2C), 124.6(2C), 118.3(2C), 115.5(2C), 38.1(2C), 22.6. ESI-MS *m/z* 373$(M+H)^+$. Anal.Calcd.for $C_{19}H_{18}F_2N_4O_2$: C, 61.28; H, 4.87; N, 15.05; Found: C, 61.31; H, 4.85; N, 15.08.

(N'1E,N'5E)-N'1,N'5-Bis(3-fluorobenzylidene)glutarohydrazide (La-5) :

The compound was synthesized according to the general procedure using glutarohydrazide (3a) (0.1 g, 0.62mmol) and 3-fluoro benzaldehyde(0.154 g, 1.24mmol) to afford **8** (0.156 g, 67.1 %) as whitesolid.M.p: 199-201 °C. ^{1}H NMR (DMSO-d_6): δ_H 11.04– 10.97 (m, 2H), 8.54 – 7.36 (m, 10H), 2.34– 2.03(m, 6H). ^{13}C NMR (DMSO-d_6):δ_C 167.6(2C), 163.2(2C), 146.2(2C), 135.4(2C), 130.7(2C), 124.2(2C), 117.5(2C), 114.1(2C), 38.6(2C), 22.7.ESI-MS

m/z 373 $(M+H)^+$. Anal.Calcd.for $C_{19}H_{18}F_2N_4O_2$: C, 61.28; H, 4.87; N, 15.05; Found: C, 61.33; H, 4.86; N, 15.07.

(N'1E,N'5E)-N'1,N'5-Bis(4-fluorobenzylidene)glutarohydrazide (La-6) :

The compound was synthesized according to the general procedure using glutarohydrazide (3a) (0.1 g, 0.62mmol) and 4-fluoro benzaldehyde (0.154g, 1.24mmol) to afford 9 (0.132 g, 56.7 %) as white solid.M.p: 252-254 °C. ^{1}H NMR (DMSO-d_6): δ_H 11.02– 10.88 (m, 2H), 8.54 – 7.32 (m, 10H), 2.34– 2.01(m, 6H). ^{13}C NMR (DMSO-d_6):δ_C167.1(2C), 165.3(2C), 144.3(2C), 130.4(4C), 129.7(2C), 115.2(4C), 38.5(2C), 22.6.ESI-MS *m/z* 373 $(M+H)^+$. Anal.Calcd.for $C_{19}H_{18}F_2N_4O_2$: C, 61.28; H, 4.87; N, 15.05; Found: C, 61.31; H, 4.87; N, 15.04.

(N'1E,N'5E)-N'1,N'5-Bis(2-methoxybenzylidene)glutarohydrazide (La-7) :

The compound was synthesized according to the general procedure using glutarohydrazide (3a) (0.1 g, 0.62mmol) and 2-methoxy benzaldehyde (0.170g, 1.24mmol) to afford **10** (0.129 g, 52.1%) as whitesolid.M.p: 263-265 °C. ^{1}H NMR (DMSO-d_6): δ_H 11.04– 10.87 (m, 2H), 8.74 – 7.05 (m, 10H), 3.83(s,6H), 2.34– 2.01(m, 6H). ^{13}C NMR (DMSO-d_6):δ_C167.3(2C), 157.4(2C), 146.5(2C), 132.4(2C), 131.6(2C), 121.3(2C), 116.8(2C), 111.3(2C), 55.8(2C), 38.6(2C), 22.6.ESI-MS *m/z* 397 $(M+H)^+$. Anal.Calcd.for $C_{21}H_{24}N_4O_4$: C, 63.62; H, 6.10; N, 14.13; Found: C, 63.66; H, 6.14; N, 14.10.

(N'1E,N'5E)-N'1,N'5-Bis(4-methoxybenzylidene)glutarohydrazide (La-8):

The compound was synthesized according to the general procedure using glutarohydrazide (3a) (0.1 g, 0.62mmol) and 4-methoxy benzaldehyde (0.170 g, 1.24mmol) to afford 11 (0.149 g, 60.1 %) as white solid.M.p: 234-236 °C. ^{1}H NMR (DMSO-d_6):δ_H 11.04– 10.87 (m, 2H), 8.74 – 7.05 (m, 10H), 3.83(s,6H), 2.34– 2.01(m, 6H). ^{13}C NMR (DMSO-d_6):δ_C 167.3(2C), 162.7(2C), 144.6(2C), 130.1(4C), 126(2C), 114.5(4C), 55.6(2C), 38.3(2C), 22.7.ESI-MS *m/z* 397 $(M+H)^+$. Anal.Calcd.for $C_{21}H_{24}N_4O_4$: C, 63.62; H, 6.10; N, 14.13; Found: C, 63.63; H, 6.13; N, 14.11.

(N'1E,N'5E)-N'1,N'5-Bis(2-nitrobenzylidene)glutarohydrazide (La-9):

The compound was synthesized according to the general procedure using glutarohydrazide (3a) (0.1 g, 0.62mmol) and o-nitro benzaldehyde (0.188 g, 1.24mmol) to afford 12 (0.157 g, 58.9 %) as white solid.M.p: 266-268 °C. . ^{1}H NMR (DMSO-d_6): δ_H 11.04– 10.91 (m, 2H), 8.58 – 7.55 (m, 10H), 2.34– 2.01(m, 6H). ^{13}C NMR (DMSO-d_6): δ_C 167.4(2C), 147.7(2C),

143.5(2C), 134.6(2C), 131.1(2C), 130.3(2C), 128.2(2C), 124.3(2C), 38.8(2C), 22.7. ESI-MS *m/z* 427 $(M+H)^+$. Anal.Calcd.for $C_{19}H_{18}N_6O_6$: C, 53.52; H, 4.26; N, 19.71; Found: C, 53.55; H, 4.21; N, 19.69.

(N'1E,N'5E)-N'1,N'5-Bis(4-nitrobenzylidene)glutarohydrazide (La-10) :

The compound was synthesized according to the general procedure using glutarohydrazide (3a) (0.1 g, 0.62mmol) and p-nitro benzaldehyde (0.188 g, 1.24mmol) to afford 13 (0.176 g, 66.1 %) as white solid.M.p: 179-181 °C. ^{1}H NMR (DMSO-d_6): δ_H 11.04– 10.91 (m, 2H), 8.55 – 7.51 (m, 10H), 2.33– 2.01(m, 6H). ^{13}C NMR (DMSO-d_6): δ_C 167.1(2C), 150.3(2C), 144.4(2C), 139.4(2C), 124.3(4C), 124.1(4C), 38.5(2C), 22.4.ESI-MS *m/z* 427 $(M+H)^+$. Anal.Calcd.for $C_{19}H_{18}N_6O_6$: C, 53.52; H, 4.26; N, 19.71; Found: C, 53.49; H, 4.22; N, 19.68.

(N'1E,N'5E)-N'1,N'5-Bis(2-(benzyloxy)benzylidene)glutarohydrazide (La-11):

The compound was synthesized according to the general procedure using glutarohydrazide (3a) (0.1 g, 0.62mmol) and 2-benzyloxy benzaldehyde (0.264 g, 1.24mmol) to afford 14 (0.191 g, 55.7 %) as white solid.M.p: 234-236 °C. ^{1}H NMR (DMSO-d_6): δ_H 11.04– 10.87 (m, 2H), 8.75 – 6.57 (m, 20H), 5.14(s,4H), 2.33– 2.02(m, 6H). ^{13}C NMR (DMSO-d_6):δ_C 167.1(2C), 160.1(2C), 146.2(2C), 136.4(2C), 132.3(2C), 131.5(2C), 128.7(4C), 127.5(2C), 127.1(4C), 121.3(2C), 116.8(2C), 114.3(2C), 70.9(2C), 38.5(2C), 22.4.ESI-MS *m/z* 549 $(M+H)^+$. Anal.Calcd.for $C_{33}H_{32}N_4O_4$: C, 72.24; H, 5.88; N, 10.21; Found: C, 72.20; H, 5.86; N, 10.18.

(N'1E,N'5E)-N'1,N'5-Bis(3-(benzyloxy)benzylidene)glutarohydrazide (La-12):

The compound was synthesized according to the general procedure using glutarohydrazide (3a) (0.1 g, 0.62mmol) and 3-benzyloxy benzaldehyde (0.264 g, 1.24mmol) to afford 15 (0.181 g, 52.8 %) as white solid.M.p: 154-156 °C. ^{1}H NMR (DMSO-d_6): 8.55 – 7.04(m, 20H), 5.15(s,4H), 2.85 (s,2H), 2.35– 2.01(m, 6H). ^{13}C NMR (DMSO-d_6):δ_C167.2(2C), 160.9(2C), 146.7(2C), 138.4(2C), 136.3(2C), 129.5(2C), 128.7(4C), 127.5(2C), 127.1(4C), 121.3(2C), 116.6(2C), 111.1(2C), 38.5(2C), 22.5.ESI-MS *m/z* 549 $(M+H)^+$. Anal.Calcd.for $C_{33}H_{32}N_4O_4$: C, 72.24; H, 5.88; N, 10.21; Found: C, 72.28; H, 5.83; N, 10.23.

(N'1E,N'5E)-N'1,N'5-Bis(3-hydroxybenzylidene)glutarohydrazide (La-13) :

The compound was synthesized according to the general procedure using glutarohydrazide (3a) (0.1 g, 0.62mmol) and m-hydroxy benzaldehyde (0.152g, 1.24mmol) to afford 16 (0.123 g, 53.4 %) as white solid.M.p: 205-207 °C. . ^{1}H NMR (DMSO-d_6): δ_H 11.06– 10.86 (m, 2H),

8.53 – 7.02(m, 10H), 5.33(s,2H), 2.32– 2.01(m, 6H). ^{13}C NMR (DMSO-d_6):δ_C 167.1(2C), 158.5(2C), 146.2(2C), 138.7(2C), 130.3(2C), 121.5(2C), 118.7(2C), 114.5(2C), 38.5(2C), 22.4.ESI-MS *m/z* 367 $(M-H)^+$. Anal.Calcd.for $C_{19}H_{20}N_4O_4$: C, 61.95; H, 5.47; N, 15.21; Found: C, 61.93; H, 5.44; N, 15.23.

(N'1E,N'5E)-N'1,N'5-bis(4-hydroxybenzylidene)glutarohydrazide (La-14) :

The compound was synthesized according to the general procedure using glutarohydrazide (3a) (0.1 g, 0.62mmol) and p-hydroxy benzaldehyde (0.152 g, 1.24mmol) to afford 17 (0.125 g, 54.3 %) as white solid.M.p: 221-223 °C.^{1}H NMR (DMSO-d_6): δ_H 11.05– 10.89 (m, 2H), 8.56 – 6.87(m, 10H), 5.36(s,2H), 2.35– 2.02(m, 6H). ^{13}C NMR (DMSO-d_6):δ_C 167.3(2C), 160.4(2C), 144.2(2C), 130.7(4C), 126.3(2C),116.5(2C), 38.5(2C), 22.6.ESI-MS *m/z* 367 $(M-H)^+$. Anal.Calcd.for $C_{19}H_{20}N_4O_4$: C, 61.95; H, 5.47; N, 15.21; Found: C, 61.91; H, 5.42; N, 15.26.

(N'1E,N'5E)-N'1,N'5-Bis(3-bromobenzylidene)glutarohydrazide (La-15) :

The compound was synthesized according to the general procedure using glutarohydrazide (3a) (0.1 g, 0.62mmol) and 3-bromo benzaldehyde (0.231 g, 1.24mmol) to afford 18 (0.136 g, 44 %) as white solid. M.p: 233-235 °C. . ^{1}H NMR (DMSO-d_6): δ_H 11.06– 10.91 (m, 2H), 8.55 – 6.88(m, 10H), 2.35– 2.01(m, 6H). ^{13}C NMR (DMSO-d_6): δ_C 167.4(2C), 146.4(2C), 135.2(2C), 133.7(2C), 132.3(2C),129.5(2C), 128.5(2C), 123.3(2C), 38.5(2C), 22.6.ESI-MS *m/z* 496 $(M+2H)^+$. Anal.Calcd.for $C_{19}H_{18}Br_2N_4O_2$: C, 46.18; H, 3.67; N, 11.34; Found: C, 46.15; H, 3.66; N, 11.36.

(N'1E,N'5E)-N'1,N'5-Bis(4-bromobenzylidene)glutarohydrazide (La-16) :

The compound was synthesized according to the general procedure using glutarohydrazide (3a) (0.1 g, 0.62mmol) and 4-bromo benzaldehyde (0.231 g, 1.24mmol) to afford 19 (0.116 g, 37.5 %) as white solid.M.p: 245-247 °C. ^{1}H NMR (DMSO-d_6): δ_H 11.02– 10.96 (m, 2H), 8.52 – 6.87(m, 10H), 2.36– 2.01(m, 6H). ^{13}C NMR (DMSO-d_6):δ_C 167.2(2C), 144.4(2C), 132.2(2C), 131.7(4C), 128.3(4C),125.5(2C), 38.5(2C), 22.4.ESI-MS *m/z* 496 $(M+2H)^+$. Anal.Calcd.for $C_{19}H_{18}Br_2N_4O_2$: C, 46.18; H, 3.67; N, 11.34; Found: C, 46.21; H, 3.70; N, 11.38.

(N'1E,N'5E)-N'1,N'5-Bis(4-(dimethylamino)benzylidene)glutarohydrazide (La-17) :

The compound was synthesized according to the general procedure using glutarohydrazide (3a) (0.1 g, 0.62mmol) and p-Dimethylaminobenzaldehyde (0.186 g, 1.24mmol) to afford 20

(0.184 g, 69.7 %) as white solid.M.p: 227-229 °C. ^{1}H NMR (DMSO-d_6): δ_H 11.05– 10.94 (m, 2H), 8.53 – 6.84(m, 10H), 3.04(s, 12H), 2.35– 2.02(m, 6H). ^{13}C NMR (DMSO-d_6):δ_C 167.3(2C), 153.6(2C), 144.2(2C), 128.7(4C), 123.3(2C),111.5(4C), 41.4(4C), 38.5(2C), 22.6.ESI-MS *m/z* 423 $(M+H)^+$. Anal.Calcd.for $C_{23}H_{30}N_6O_2$: C, 65.38; H, 7.16; N, 19.89; Found: C, 65.36; H, 7.14; N, 19.91.

(N'1E,N'5E)-N'1,N'5-Bis(piperidin-1-ylmethylene)glutarohydrazide (La-18) :

The compound was synthesized according to the general procedure using glutarohydrazide (3a) (0.1 g, 0.62mmol) and N-Formylpiperidine (0.141 g, 1.24mmol) to afford 21(0.15 g, 54.3 %) aswhitesolid.M.p: 166-168 °C.^{1}H NMR (DMSO-d_6): δ_H 11.02– 10.92 (m, 2H), 7.51(s, 2H), 3.55– 1.52(m, 26H). ^{13}C NMR (DMSO-d_6):δ_C 167.2(2C), 146.(2C), 48.4(4C), 38.5(2C), 25.6(4C), 24.3(2C), 22.6.ESI-MS *m/z* 351 $(M+H)^+$. Anal.Calcd.for $C_{17}H_{30}N_6O_2$: C, 58.26; H, 8.63; N, 23.98; Found: C, 58.24; H, 8.65; N, 23.97.

(N'1E,N'5E)-N'1,N'5-Bis(morpholinomethylene)glutarohydrazide (La-19) :

The compound was synthesized according to the general procedure using glutarohydrazide (3a) (0.1 g, 0.62mmol) and 4-Formylmorpholine(0.143 g, 1.24mmol) to afford **22** (0.126 g, 56.9%) as whitesolid.M.p: 217-219 °C. ^{1}H NMR (DMSO-d_6): δ_H 11.04– 10.91 (m, 2H), 7.51(s, 2H), 3.62– 2.04(m, 22H). ^{13}C NMR (DMSO-d_6):δ_C 167.3(2C), 146.(2C), 66.4(4C), 48.6(4c), 38.5(2C), 22.6(1C). ESI-MS *m/z* 355 $(M+H)^+$. Anal.Calcd.for $C_{15}H_{26}N_6O_4$: C, 50.83; H, 7.39; N, 23.71; Found: C, 50.79; H, 7.43; N, 23.75.

(N'1E,N'5E)-N'1,N'5-Bis(2-bromobenzylidene)glutarohydrazide (La-20) :

The compound was synthesized according to the general procedure using glutarohydrazide (3a) (0.1 g, 0.62mmol) and 2-Bromobenzaldehyde (0.231 g, 1.24mmol) to afford 23 (0.146 g, 47.3%) aswhitesolid.M.p: 254-256 °C.^{1}H NMR (DMSO-d_6): δ_H 11.04– 10.93 (m, 2H), 8.54 – 7.41(m, 10H), 2.34– 2.01(m, 6H). ^{13}C NMR (DMSO-d_6):δ_C 167.2(2C), 143.4(2C), 135.2(2C), 132.7(2C), 130.3(2C),127.5(2C), 127.2(2C), 121.7(2C), 38.5(2C), 22.5.ESI-MS *m/z* 496 $(M+2H)^+$. Anal.Calcd.for $C_{19}H_{18}Br_2N_4O_2$: C, 46.18; H, 3.67; N, 11.34; Found: C, 46.12; H, 3.71; N, 11.35.

(N'1E,N'5E)-N'1,N'5-Bis(naphthalen-2-ylmethylene)glutarohydrazide (La-21) :

The compound was synthesized according to the general procedure using glutarohydrazide (3a) (0.1 g, 0.62mmol) and 2-Naphthaldehyde (0.194 g, 1.24mmol) to afford 24 (0.129 g, 47.3 %) as white solid.M.p: 266-268 °C. ^{1}H NMR (DMSO-d_6): δ_H 11.06– 10.91 (m, 2H), 8.52

– 7.57(m, 16H), 2.34– 2.01(m, 6H). ^{13}C NMR (DMSO-d_6):δ_C 167.2(2C), 146.4(2C), 136.2(2C), 133.7(2C), 128.3(2C),128.5(2C), 128.2(4C), 127.7(2C), 126.7(2C), 126.4(4C), 38.5(2C), 22.5.ESI-MS *m/z* 437 $(M+H)^+$. Anal.Calcd.for $C_{27}H_{24}N_4O_2$: C, 74.29; H, 5.54; N, 12.84; Found: C, 74.27; H, 5.56; N, 12.81.

(N'1E,N'5E)-N'1,N'5-Bis(3-(trifluoromethyl)benzylidene)glutarohydrazide (La-22) :

The compound was synthesized according to the general procedure using glutarohydrazide (3a) (0.1 g, 0.62mmol) and 3-(Trifluoromethyl)benzaldehyde (0.217 g, 1.24mmol) to afford 25 (0.147 g, 49.8%) as whitesolid.M.p: 237-239 °C.^{1}H NMR (DMSO-d_6): δ_H 11.05– 10.93 (m, 2H), 8.53 – 7.46(m, 10H), 2.34– 2.01(m, 6H). ^{13}C NMR (DMSO-d_6):δ_C 167.4(2C), 146.6(2C), 134.2(2C), 132.7(2C), 131.3(2C),129.5(2C), 127.2(4C), 125.7(2C), 124.7(2C), 38.6.ESI-MS *m/z* 473 $(M+H)^+$. Anal.Calcd.for $C_{21}H_{18}F_6N_4O_2$: C, 53.39; H, 3.84; N, 11.86; Found: C, 53.37; H, 3.81; N, 11.84.

(N'1E,N'5E)-N'1,N'5-Bis((5-nitrothiophen-2-yl)methylene)glutarohydrazide (La-23) :

The compound was synthesized according to the general procedure using glutarohydrazide (3a) (0.1 g, 0.62mmol) and 5-Nitro 2-thiophene carboxaldehyde (0.196 g, 1.24mmol) to afford 26 (0.163 g, 59.5 %) as white solid.M.p: 211-213 °C. ^{1}H NMR (DMSO-d_6): δ_H 11.05– 10.91 (m, 2H), 8.75 – 7.44(m, 6H), 2.34– 2.02(m, 6H). ^{13}C NMR (DMSO-d_6):δ_C 167.4(2C), 154.4(2C), 153.2(2C), 128.7(2C), 128.3(2C),125.5(2C), 38.4(2C), 22.7. ESI-MS *m/z* 439 $(M+H)^+$. Anal.Calcd.for $C_{15}H_{14}N_6O_6S_2$: C, 41.09; H, 3.22; N, 19.17; Found: C, 41.07; H, 3.19; N, 19.22.

(N'1E,N'5E)-N'1,N'5-Bis(2-hydroxybenzylidene)glutarohydrazide (La-24) :

The compound was synthesized according to the general procedure using glutarohydrazide (3a) (0.1 g, 0.62mmol) and Salicylaldehyde(0.152 g, 1.24mmol) to afford **27** (0.187 g, 81.3%) aswhite solid.M.p: 261-263 °C.^{1}H NMR (DMSO-d_6): δ_H 11.02– 10.96 (m, 2H), 8.73 – 7.05(m, 10H), 5.34(s, 2H), 2.34– 2.02(m, 6H). ^{13}C NMR (DMSO-d_6): δ_C 167.2(2C), 157.5(2C), 146.2(2C), 132.1(2C), 127.3(2C),121.5(2C), 118.4(2C), 117.6(2C), 38.4(2C), 22.3.ESI-MS *m/z* 367 $(M-H)^+$. Anal.Calcd.for $C_{19}H_{20}N_4O_4$: C, 61.95; H, 5.47; N, 15.21; Found: C, 61.98; H, 5.51; N, 15.17.

General procedure for the synthesis of substituted (N'E,N'''E)-2,2'-oxybis(N'-ethylideneacetohydrazide) (La-25-La-48)

To a stirred solution of 2,2'-oxydi(acetohydrazide) (3b) (1 mmol) in ethanol (15 ml) at room temperature was added aldehyde(1 mmol). The solution was refluxed for about 12 hours (monitored by TLC & LCMS for completion), and solvent evaporated under reduced pressure. The residue was further diluted with water (30 ml) and ethyl acetate (50 ml) and the layers were separated. The organic layer was dried over anhydrous sodium sulphate and evaporated under reduced pressure. The residue was purified by silica gel column chromatography using hexane: ethylacetate as eluent to give the corresponding (N'E,N'''E)-2,2'-oxybis(N'-ethylideneacetohydrazide) (**La-25-La-48**) in good yield.

(N'E,N'''E)-2,2'-Oxybis(N'-(2-methylbenzylidene)acetohydrazide) (La-25) : The compound was synthesized according to the general procedure using glutarohydrazide (**3b**) (0.1 g, 0.61mmol) and o-tolualdehyde(0.148 g, 1.23mmol) to afford **28** (0.123 g, 54.4%) aswhitesolid.M.p: 188-190 °C.^{1}H NMR (DMSO-d_6): δ_H 11.04– 10.90 (m, 2H), 8.51– 7.25 (m, 10H), 4.26(s,4H), 2.46(s, 6H). ^{13}C NMR (DMSO-d_6): δ_C 171.2(2C), 143.5(2C), 135.2(2C), 131.4(2C), 130.6(2C), 129.3(2C), 126.4(2C), 125.1(2C), 71.6(2C), 18.5(2C),. ESI-MS *m/z* 367 $(M+H)^+$. Anal.Calcd.for $C_{20}H_{22}N_4O_3$: C, 65.56; H, 6.05; N, 15.29; Found: C, 65.57; H, 6.01; N, 15.27.

(N'E,N'''E)-2,2'-Oxybis(N'-(3-methylbenzylidene)acetohydrazide) (La-26) :

The compound was synthesized according to the general procedure using glutarohydrazide (**3b**) (0.1 g, 0.61mmol) and m-tolualdehyde(0.148 g, 1.23mmol) to afford **29** (0.156 g, 69.1%) as whitesolid.M.p: 269-271 °C.^{1}H NMR (DMSO-d_6): δ_H 11.02– 10.88 (m, 2H), 8.52– 7.26 (m, 10H), 4.26(s,4H), 2.44(s, 6H). ^{13}C NMR (DMSO-d_6): δ_C 171.4(2C), 146.4(2C), 138.2(2C), 133.4(2C), 131.6(2C), 129.4(2C), 128.4(2C), 126.3(2C), 71.7(2C), 21.5(2C),. ESI-MS *m/z* 367 $(M+H)^+$. Anal.Calcd.for $C_{20}H_{22}N_4O_3$: C, 65.56; H, 6.05; N, 15.29; Found: C, 65.59; H, 6.04; N, 15.26.

(N'E,N'''E)-2,2'-Oxybis(N'-(4-methylbenzylidene)acetohydrazide) (La-27) :

The compound was synthesized according to the general procedure using glutarohydrazide (**3b**) (0.1 g, 0.61mmol) and p-tolualdehyde(0.148 g, 1.23mmol) to afford **30** (0.169 g, 74.8%) aswhitesolid.M.p: 266-268 °C.^{1}H NMR (DMSO-d_6): δ_H 11.03– 10.89 (m, 2H), 8.34– 7.26 (m, 10H), 4.24(s,4H), 2.35(s, 6H). ^{13}C NMR (DMSO-d_6): δ_C 171.1(2C), 144.2(2C),

140.4(2C), 130.1(2C), 129.6(4C), 126.4(4C), 71.6(2C), 21.4(2C),.ESI-MS *m/z* 367 $(M+H)^+$. Anal.Calcd.for $C_{20}H_{22}N_4O_3$: C, 65.56; H, 6.05; N, 15.29; Found: C, 65.57; H, 6.03; N, 15.25.

(N'E,N'''E)-2,2'-Oxybis(N'-(2-fluorobenzylidene)acetohydrazide) (La-28) :

The compound was synthesized according to the general procedure using glutarohydrazide (**3b**) (0.1 g, 0.61mmol) and 2-fluoro benzaldehyde(0.153 g, 1.23mmol) to afford **31** (0.149 g, 64.6 %) aswhitesolid.M.p: 153-155 °C.^{1}H NMR (DMSO-d_6): δ_H 11.01– 10.88 (m, 2H), 8.52–7.32 (m, 10H), 4.22(s,4H),. ^{13}C NMR (DMSO-d_6): δ_C 171.2(2C), 163.3(2C), 146.4(2C), 135.2(2C), 130.5(2C), 124.6(2C), 117.7(2C), 114.2(2C), 71.5(2C),.ESI-MS *m/z* 375 $(M+H)^+$. Anal.Calcd.for $C_{18}H_{16}F_2N_4O_3$: C, 57.75; H, 4.31; N, 14.97; Found: C, 57.77; H, 4.29; N, 14.99.

(N'E,N'''E)-2,2'-Oxybis(N'-(3-fluorobenzylidene)acetohydrazide) (La-29) :

The compound was synthesized according to the general procedure using glutarohydrazide (3b) (0.1 g, 0.61mmol) and 3-fluoro benzaldehyde (0.153 g, 1.23mmol) to afford 32 (0.116 g, 50.2 %) as white solid.M.p: 245-247 °C. ^{1}H NMR (DMSO-d_6): δ_H 11.03– 10.90 (m, 2H), 8.53– 7.34 (m, 10H), 4.24(s,4H),. ^{13}C NMR (DMSO-d_6):δ_C 171.1(2C), 163.2(2C), 146.7(2C), 135.1(2C), 130.5(2C), 124.7(2C), 117.5(2C), 114.1(2C), 71.6(2C),. ESI-MS *m/z* 375 $(M+H)^+$. Anal.Calcd.for $C_{18}H_{16}F_2N_4O_3$: C, 57.75; H, 4.31; N, 14.97; Found: C, 57.77; H, 4.28; N, 14.98.

(N'E,N'''E)-2,2'-Oxybis(N'-(4-fluorobenzylidene)acetohydrazide) (La-30) :

The compound was synthesized according to the general procedure using glutarohydrazide (3b) (0.1 g, 0.61mmol) and 4-fluoro benzaldehyde (0.153 g, 1.23mmol) to afford 33 (0.129 g, 55.9 %) as white solid.M.p: 252-254 °C. ^{1}H NMR (DMSO-d_6): δ_H 11.04– 10.89 (m, 2H), 8.36– 7.32 (m, 10H), 4.22(s,4H),. ^{13}C NMR (DMSO-d_6):δ_C 171.1(2C), 165.2(2C), 144.7(2C), 130.1(4C), 129.5(2C), 115.5(4C), 71.6(2C),. ESI-MS *m/z* 375 $(M+H)^+$. Anal.Calcd.for $C_{18}H_{16}F_2N_4O_3$: C, 57.75; H, 4.31; N, 14.97; Found: C, 57.74; H, 4.27; N, 14.95.

(N'E,N'''E)-2,2'-Oxybis(N'-(2-methoxybenzylidene)acetohydrazide) (La-31) :

The compound was synthesized according to the general procedure using glutarohydrazide (3b) (0.1 g, 0.61mmol) and 2-methoxy benzaldehyde (0.167 g, 1.23mmol) to afford 34 (0.132 g, 53.7 %) as white solid.M.p: 174-2176 °C. ^{1}H NMR (DMSO-d_6): δ_H 11.01– 10.92 (m, 2H), 8.76– 7.04 (m, 10H), 4.24(s,4H), 3.82(s, 4H),. ^{13}C NMR (DMSO-d_6): δ_C 171.1(2C), 157.3(2C), 146.2(2C), 132.1(2C), 131.4(2C), 121.1(2C), 116.8(2C), 111.1(2C), 71.8(2C),

55.6(2C). ESI-MS *m/z* 399 $(M+H)^+$. Anal.Calcd.for $C_{20}H_{22}N_4O_5$: C, 60.29; H, 5.57; N, 14.06; Found: C, 60.24; H, 5.61; N, 14.01.

(N'E,N'''E)-2,2'-Oxybis(N'-(4-methoxybenzylidene)acetohydrazide) (La-32):

The compound was synthesized according to the general procedure using glutarohydrazide (3b) (0.1 g, 0.61mmol) and 4-methoxy benzaldehyde (0.167 g, 1.23mmol) to afford 35 (0.176 g, 71.7 %) as white solid.M.p: 241-243 °C. ^{1}H NMR (DMSO-d_6): δ_H 11.03– 10.91 (m, 2H), 8.55– 7.01 (m, 10H), 4.23(s,4H), 3.81(s, 6H),. ^{13}C NMR (DMSO-d_6):δ_C 171.3(2C), 162.3(2C), 144.2(2C), 130.1(4C), 126.4(2C), 114.1(4C), 71.8(2C), 55.2(2C). ESI-MS *m/z* 399 $(M+H)^+$. Anal.Calcd.for $C_{20}H_{22}N_4O_5$: C, 60.29; H, 5.57; N, 14.06; Found: C, 60.27; H, 5.60; N, 14.02.

(N'E,N'''E)-2,2'-Oxybis(N'-(2-nitrobenzylidene)acetohydrazide) (La-33):

The compound was synthesized according to the general procedure using glutarohydrazide (3b) (0.1 g, 0.61mmol) and o-nitro benzaldehyde (0.186 g, 1.23mmol) to afford 36 (0.163 g, 61.5 %) as white solid.M.p: 168-170 °C. ^{1}H NMR (DMSO-d_6): δ_H 11.02– 10.93 (m, 2H), 8.52– 7.55 (m, 10H), 4.24(s,4H),. ^{13}C NMR (DMSO-d_6): δ_C 171.2(2C), 147.4(2C), 143.1(2C), 134.7(2C), 131.6(2C), 130.2(2C), 128.5(2C), 124.4(2C), 71.6(2C),. ESI-MS *m/z*429 $(M+H)^+$. Anal.Calcd.for $C_{18}H_{16}N_6O_7$: C, 50.47; H, 3.76; N, 19.62; Found: C, 50.44; H, 3.77; N, 19.61.

(N'E,N'''E)-2,2'-Oxybis(N'-(4-nitrobenzylidene)acetohydrazide) (La-34) :

The compound was synthesized according to the general procedure using glutarohydrazide (3b) (0.1 g, 0.61mmol) and p-nitro benzaldehyde (0.186 g, 1.23mmol) to afford 37 (0.119 g, 45 %) as white solid.M.p: 157-159 °C. ^{1}H NMR (DMSO-d_6): δ_H 11.04– 10.91 (m, 2H), 8.52– 8.05 (m, 10H), 4.22(s,4H),. ^{13}C NMR (DMSO-d_6): δ_C 171.1(2C), 150.1(2C), 144.3(2C), 139.7(2C), 124.6(4C), 124.2(4C), 71.6(2C),. ESI-MS *m/z* 429 $(M+H)^+$. Anal.Calcd.for $C_{18}H_{16}N_6O_7$: C, 50.47; H, 3.76; N, 19.62; Found: C, 50.48; H, 3.78; N, 19.65.

(N'E,N'''E)-2,2'-Oxybis(N'-(2-(benzyloxymethyl)benzylidene)acetohydrazide) (La-35) :

The compound was synthesized according to the general procedure using glutarohydrazide (3b) (0.1 g, 0.61mmol) and 2-benzyloxy benzaldehyde (0.261 g, 1.23mmol) to afford 38 (0.129 g, 38 %) as white solid.M.p: 221-223 °C. ^{1}H NMR (DMSO-d_6): δ_H 8.60-7.25 (m, 22H), 4.65-4.25 (s, 12H). ^{13}C NMR (DMSO-d_6): δ_C 171.4(2C), 143.7(2C), 137.7(2C), 134.6(2C), 131.2(4C), 128.9(4C), 127.1(8C), 124.2(4C), 72.8(4C), 71.7(2C),. ESI-

MS *m/z* 580 $(M+H)^+$. Anal.Calcd.for $C_{34}H_{34}N_4O_5$: C, 70.57; H, 5.92; N, 9.68; Found: C, 70.49; H, 6.01; N, 9.62.

(N'E,N'''E)-2,2'-Oxybis(N'-(3-(benzyloxymethyl)benzylidene)acetohydrazide) (La-36) :

The compound was synthesized according to the general procedure using glutarohydrazide (3b) (0.1 g, 0.61mmol) and 3-benzyloxy benzaldehyde (0.261 g, 1.23mmol) to afford 39 (0.187 g, 55.1 %) as white solid.M.p: 253-255 °C. ^{1}H NMR (DMSO-d_6): δ_H 8.42-7.35 (m, 22H), 4.65-4.24 (s, 12H). ^{13}C NMR (DMSO-d_6): δ_C 171.2(2C), 146.4(2C), 137.7(4C), 134.6(2C), 129.2(2C), 128.9(8C), 127.6(8C), 72.5(4C), 71.6(2C). ESI-MS *m/z* 580 $(M+H)^+$. Anal.Calcd.for $C_{34}H_{34}N_4O_5$: C, 70.57; H, 5.92; N, 9.68; Found: C, 70.53; H,6.00; N, 9.61.

(N'E,N'''E)-2,2'-Oxybis(N'-(3-hydroxybenzylidene)acetohydrazide) (La-37) :

The compound was synthesized according to the general procedure using glutarohydrazide (3b) (0.1 g, 0.61mmol) and m-hydroxy benzaldehyde (0.150 g, 1.23mmol) to afford 40 (0.125 g, 54.7 %) as white solid.M.p: 212-214 °C. ^{1}H NMR (DMSO-d_6): δ_H 11.05– 10.96 (m, 2H), 8.56– 7.04 (m, 10H), 5.34(s,2H), 4.25(s, 4H). ^{13}C NMR (DMSO-d_6): δ_C 171.6(2C), 158.3(2C), 146.2(2C), 138.5(2C), 130.6(2C), 121.4(2C), 118.4(2C), 114.3(2C), 71.6(2C),. ESI-MS *m/z* 369 $(M-H)^+$. Anal.Calcd.for $C_{18}H_{18}N_4O_5$: C, 58.37; H, 4.90; N, 15.13; Found: C, 58.33; H, 4.95; N, 15.11.

(N'E,N'''E)-2,2'-Oxybis(N'-(4-hydroxybenzylidene)acetohydrazide) (La-38) :

The compound was synthesized according to the general procedure using glutarohydrazide (3b) (0.1 g, 0.61mmol) and p-hydroxy benzaldehyde (0.150 g, 1.23mmol) to afford 41 (0.136 g, 59.6 %) as white solid.M.p: 259-261 °C. ^{1}H NMR (DMSO-d_6): δ_H 11.01– 10.95 (m, 2H), 8.56– 6.84(m, 10H), 5.33(s,2H), 4.24(s, 4H). ^{13}C NMR (DMSO-d_6): δ_C 171.5(2C), 160.2(2C), 144.1(2C), 130.5(4C), 126.6(4C), 116.4(2C), 71.4(2C),. ESI-MS *m/z* 369 $(M-H)^+$. Anal.Calcd.for $C_{18}H_{18}N_4O_5$: C, 58.37; H, 4.90; N, 15.13; Found: C, 58.35; H, 4.91; N, 15.14.

(N'E,N'''E)-2,2'-Oxybis(N'-(3-bromobenzylidene)acetohydrazide) (La-39) :

The compound was synthesized according to the general procedure using glutarohydrazide (3b) (0.1 g, 0.61mmol) and 3-bromo benzaldehyde (0.228 g, 1.23mmol) to afford 42 (0.149 g, 48.7 %) as white solid.M.p: 192-194 °C.^{1}H NMR (DMSO-d_6): δ_H 11.04– 10.91 (m, 2H), 8.54– 7.41(m, 10H), 4.26(s, 4H). ^{13}C NMR (DMSO-d_6): δ_C 171.2(2C), 146.2(2C), 135.7(2C), 133.1(2C), 132.4(2C), 129.8(2C), 128.4(2C), 123.5(2C), 71.4(2C),. ESI-MS *m/z* 498

$(M+2H)^+$. Anal.Calcd.for $C_{18}H_{16}Br_2N_4O_3$: C, 43.57; H, 3.25; N, 11.29; Found: C, 43.59; H, 3.21; N, 11.25.

(N'E,N'''E)-2,2'-Oxybis(N'-(4-bromobenzylidene)acetohydrazide) (La-40):

The compound was synthesized according to the general procedure using glutarohydrazide (3b) (0.1 g, 0.61mmol) and 4-bromo benzaldehyde (0.228g, 1.23mmol) to afford 43 (0.123 g, 40.2 %) as white solid.M.p: 205-207 °C. ^{1}H NMR (DMSO-d_6): δ_H 11.03– 10.90 (m, 2H), 8.53– 7.54(m, 10H), 4.24(s, 4H). ^{13}C NMR (DMSO-d_6): δ_C 171.1(2C), 144.7(2C), 132.5(2C), 131.2(4C), 128.4(4C), 125.8(2C),71.4(2C),. ESI-MS *m/z* 498 $(M+2H)^+$. Anal.Calcd.for $C_{18}H_{16}Br_2N_4O_3$: C, 43.57; H, 3.25; N, 11.29; Found: C, 43.55; H, 3.27; N, 11.31.

(N'E,N'''E)-2,2'-Oxybis(N'-(4-(dimethylamino)benzylidene)acetohydrazide) (La-41) :

The compound was synthesized according to the general procedure using glutarohydrazide (3b) (0.1 g, 0.61mmol) and p-Dimethylaminobenzaldehyde (0.184 g, 1.23mmol) to afford 44 (0.157 g, 60 %) as white solid.M.p: 237-239 °C. ^{1}H NMR (DMSO-d_6): δ_H 11.06– 10.88 (m, 2H), 8.51– 6.82(m, 10H), 4.22(s, 4H), 3.05(s, 6H),. ^{13}C NMR (DMSO-d_6): δ_C 171.1(2C), 153.7(2C), 144.5(2C), 128.2(4C), 123.4(2C), 111.8(4C),71.4(2C), 41.2(4C). ESI-MS *m/z* 425 $(M+H)^+$. Anal.Calcd.for $C_{22}H_{28}N_6O_3$: C, 62.25; H, 6.65; N, 19.80; Found: C, 62.22; H, 6.64; N, 19.83.

(N'E,N'''E)-2,2'-Oxybis(N'-(piperidin-1-ylmethylene)acetohydrazide) (La-42) :

The compound was synthesized according to the general procedure using glutarohydrazide (3b) (0.1 g, 0.61mmol) and N-Formylpiperidine (0.139g, 1.23mmol) to afford 45 (0.147 g, 67.7 %) as white solid.M.p: 234-236 °C. ^{1}H NMR (DMSO-d_6): δ_H 11.04– 10.90 (m, 2H), 7.51(s, 4H).4.24(s, 4H), 3.51–1.52(m, 20H). ^{13}C NMR (DMSO-d_6): δ_C 171.1(2C), 146.9(2C), 71.6(2C), 48.8(4C), 25.6(4C), 24.3(2C). ESI-MS *m/z*353 $(M+H)^+$. Anal.Calcd.for $C_{16}H_{28}N_6O_3$: C, 54.53; H, 8.01; N, 23.85; Found: C, 54.50; H, 8.05; N, 23.86.

(N'E,N'''E)-2,2'-Oxybis(N'-(morpholinomethylene)acetohydrazide) (La-43) :

The compound was synthesized according to the general procedure using glutarohydrazide (3b) (0.1 g, 0.61mmol) and 4-Formylmorpholine (0.142 g, 1.23mmol) to afford 46 (0.126 g, 57.3 %) as white solid.M.p: 217-219 °C. ^{1}H NMR (DMSO-d_6): δ_H 11.02– 10.90 (m, 2H), 7.52(s, 2H), 4.25(s, 4H), 3.66–3.14(m, 16H). ^{13}C NMR (DMSO-d_6): δ_C 171.3(2C), 146.2(2C), 71.4(2C), 66.8(4C), 48.6(4C),. ESI-MS *m/z*357 $(M+H)^+$. Anal.Calcd.for $C_{14}H_{24}N_6O_5$: C, 47.18; H, 6.79; N, 23.58; Found: C, 47.21; H, 6.77; N, 23.59.

(N'E,N'''E)-2,2'-Oxybis(N'-(2-bromobenzylidene)acetohydrazide) (La-44) :

The compound was synthesized according to the general procedure using glutarohydrazide (3b) (0.1 g, 0.61mmol) and 2-Bromobenzaldehyde (0.228 g, 1.23mmol) to afford 47 (0.191 g, 62.4 %) as white solid.M.p: 246-248 °C. ^{1}H NMR (DMSO-d_6): δ_H 11.06–10.96(m, 2H), 8.52–7.42(m, 10H), 4.25(s, 4H),. ^{13}C NMR (DMSO-d_6):δ_C 171.3(2C), 143.4(2C), 135.2(2C), 132.7(2C), 130.2(2C), 127.6(2C), 127.4(2C), 121.5(2C), 71.7(2C). ESI-MS *m/z* 498 $(M+2H)^+$. Anal.Calcd.for $C_{18}H_{16}Br_2N_4O_3$: C, 43.57; H, 3.25; N, 11.29; Found: C, 43.61; H, 3.21; N, 11.24.

(N'E,N'''E)-2,2'-Oxybis(N'-(naphthalen-2-ylmethylene)acetohydrazide) (La-45) :

The compound was synthesized according to the general procedure using glutarohydrazide (3b) (0.1 g, 0.61mmol) and 2-Naphthaldehyde (0.192 g, 1.23mmol) to afford 48 (0.157 g, 58.1 %) as white solid.M.p: 182-184 °C. ^{1}H NMR (DMSO-d_6): δ_H 11.04–10.92(m, 2H), 8.53–7.53(m, 16H), 4.24(s, 4H),. ^{13}C NMR (DMSO-d_6):δ_C 171.1(2C), 146.7(2C), 136.7(2C), 133.5(2C), 128.5(2C), 128.3(2C), 128.1(4C), 127.7(2C), 126.6(2C), 126.4(4C), 71.7(2C). ESI-MS *m/z* 439 $(M+H)^+$. Anal.Calcd.for $C_{26}H_{22}N_4O_3$: C, 71.22; H, 5.06; N, 12.78; Found: C, 71.25; H, 5.01; N, 12.77.

(N'E,N'''E)-2,2'-Oxybis(N'-(3-(trifluoromethyl)benzylidene)acetohydrazide) (La-46) :

The compound was synthesized according to the general procedure using glutarohydrazide (3b) (0.1 g, 0.61mmol) and 3-(Trifluoromethyl)benzaldehyde (0.214 g, 1.23mmol) to afford 49 (0.181 g, 61.9 %) as white solid.M.p: 251-253 °C. ^{1}H NMR (DMSO-d_6): δ_H 11.02–10.94(m, 2H), 8.52–7.42(m, 10H), 4.24(s, 4H),. ^{13}C NMR (DMSO-d_6): δ_C 171.4(2C), 146.4(2C), 136.2(2C), 133.8(2C), 128.5(2C), 128.3(2C), 128.31(2C), 127.5(2C), 126.6(2C), 71.6(2C). ESI-MS *m/z* 475 $(M+H)^+$. Anal.Calcd.for $C_{20}H_{16}F_6N_4O_3$: C, 50.64; H, 3.40; N, 11.81; Found: C, 50.62; H, 3.44; N, 11.79.

(N'E,N'''E)-2,2'-Oxybis(N'-((5-nitrothiophen-2-yl)methylene)acetohydrazide) (La-47) :

The compound was synthesized according to the general procedure using glutarohydrazide (3b) (0.1 g, 0.61mmol) and 5-Nitro 2-thiophene carboxaldehyde (0.193 g, 1.23mmol) to afford 50 (0.184 g, 67.8%) aswhitesolid.M.p: 182-184 °C.^{1}H NMR (DMSO-d_6): δ_H 11.05–10.93(m, 2H), 8.72–7.41(m, 6H), 4.22(s, 4H),. ^{13}C NMR (DMSO-d_6):δ_C 171.1(2C), 154.4(2C), 153.2(2C), 128.8(2C), 128.5(2C), 125.3(2C), 71.1(2C). ESI-MS *m/z* 441 $(M+H)^+$. Anal.Calcd.for $C_{14}H_{12}N_6O_7S_2$: C, 38.18; H, 2.75; N, 19.08; Found: C, 38.21; H, 2.73; N, 17.11.

(N'E,N'''E)-2,2'-Oxybis(N'-(2-hydroxybenzylidene)acetohydrazide) (La-48) :

The compound was synthesized according to the general procedure using glutarohydrazide (3b) (0.1 g, 0.61mmol) and Salicylaldehyde (0.15 g, 1.23mmol) to afford 51 (0.129 g, 56.5 %) as white solid.M.p: 243-245 °C. ^{1}H NMR (DMSO-d_6): δ_H 11.03–10.91(m, 2H), 8.73–7.01(m, 10H), 5.32(s, 2H), 4.26(s, 4H). ^{13}C NMR (DMSO-d_6): δ_C 171.3(2C), 157.2(2C), 146.7(2C), 132.8(2C), 127.5(2C), 121.3(2C), 118.4(2C), 117.6(2C), 71.6(2C). ESI-MS *m/z* 369 $(M-H)^+$. Anal.Calcd.for $C_{18}H_{18}N_4O_5$: C, 58.37; H, 4.90; N, 15.13; Found: C, 58.36; H, 4.89; N, 15.11.

Annexure IV: Synthesis of lysine aminotransferase inhibitors α-ketoglutarate based approach-thiazole derivatives

The procedures and characterization data are given for synthesized compounds (Lb-1-Lb-4, Lb-21-Lb-24, Lb-33-Lb-36).

General procedure for synthesis of ethyl 4-hydroxy-2-(phenyl/pyridyl)-thiazole-5-carboxylate (5-8)

Diethyl-2-bromomalonate (1 equiv) was added drop wise to a well stirred solution of the corresponding phenyl/pyridyl thioamide (1 equiv, 1 - 4) and pyridine (3 equiv) in toluene (60 ml) at room temperature (rt). The reaction mixture was then heated to reflux for 2-4 hours (monitored by TLC & LCMS for completion) and allowed to cool. The precipitate formed was filtered and re-crystallized form ethanol to afford the desired product (5 – 8) in good yield as described below.

Ethyl 4-hydroxy-2-phenylthiazole-5-carboxylate (05)

The compound was synthesized according to the above general procedure using thiobenzamide (01, 0.5 g, 3.64 mmol), diethylbromomalonate (0.87 g, 3.64 mmol), and pyridine (0.86 g, 10.9 mmol) to afford 05 (0.79 g, 86.81%) as pale yellow solid. ^{1}H NMR (DMSO-d_6): $\delta_{H.}$ 1.26 (t, J = 7.2 Hz, 3H), 4.23 (d, J = 7.2 Hz, 2H), 7.49- 7.95 (m, 5H). ^{13}C NMR (DMSO-d_6): δc. 167.3, 165.7, 161.3, 132.1, 131.6, 129.4, 126, 97.8, 60.3, 14.3. ESI-MS m/z 250.1 $(M+H)^+$. Anal Calcd for $C_{12}H_{11}NO_3S$; C, 57.82; H, 4.45; N, 5.62; Found: C, 57.79; H, 4.43; N, 5.61.

Ethyl 4-hydroxy-2-(pyridin-2-yl)thiazole-5-carboxylate (06)

The compound was synthesized according to the above general procedure using 2-pyridylthioamide (02, 0.5 g, 3.61 mmol), diethylbromomalonate (0.86 g, 3.61 mmol), and pyridine (0.86 g, 10.9 mmol) to afford 06 (0.73 g, 80.21%) as pale green solid. ^{1}H NMR (DMSO-d_6): $\delta_{H.}$ 1.28 (t, J = 7.1 Hz, 3H), 4.24 (q, J = 7.1 Hz, 2H), 7.41- 8.53 (m, 4H). ^{13}C NMR (DMSO-d_6): δc.166.6, 161.8 155.9, 149, 148.1, 142.3, 137.6, 125.3, 123.2, 60.4, 14.2. ESI-MS m/z 251.1 $(M+H)^+$. Anal Calcd for $C_{11}H_{10}N_2O_3S$ C, 52.79; H, 4.03; N, 11.19; Found: C, 52.8; H, 4.02; N, 11.21.

Ethyl 4-hydroxy-2-(pyridin-3-yl)thiazole-5-carboxylate (07)

The compound was synthesized according to the above general procedure using 3-pyridylthioamide (03, 0.5 g, 3.61 mmol), diethylbromomalonate (0.86 g, 3.61 mmol), and

pyridine (0.86 g, 10.9 mmol) to afford 07 (0.71 g, 78.02%) as pale green solid; ^{1}H NMR (DMSO-d_6): $\delta_{H.}$ 1.27 (t, J = 7.2 Hz, 3H), 4.22 (q, J = 7.2 Hz, 2H), 7.63- 8.93 (m, 4H). ^{13}C NMR (DMSO-d_6): δc.166.5, 153.1, 148.7, 147.9, 147.6, 141.9, 133.8, 133.1, 123.7, 60.4, 14.3. ESI-MS *m*/*z* 251 $(M+H)^+$. Anal Calcd for $C_{11}H_{10}N_2O_3S$ C, 52.79; H, 4.03; N, 11.19; Found: C, 52.78; H, 4.0; N, 11.19.

Ethyl 4-hydroxy-2-(pyridin-4-yl)thiazole-5-carboxylate (08)

The compound was synthesized according to the above general procedure using 4-pyridylthioamide (04, 0.5 g, 3.61 mmol), diethylbromomalonate (0.86 g, 3.61 mmol), and pyridine (0.86 g, 10.9 mmol) to afford 08 (0.76 g, 83.52%) as pale green solid. ^{1}H NMR (DMSO-d_6): $\delta_{H.}\delta_{H.}$ 1.26 (t, J = 7 Hz, 3H), 4.24 (q, J = 7 Hz, 2H), 7.98- 8.69 (m, 4H). ^{13}C NMR (DMSO-d_6): δc.166.7, 154, 150.1, 148, 143.6, 142.8, 121.4, 60.3, 14.3 ESI-MS *m*/*z* 251.1 $(M+H)^+$. Anal Calcd for $C_{11}H_{10}N_2O_3S$ C, 52.79; H, 4.03; N, 11.19; Found: C, 52.81; H, 4.01; N, 11.23.

General procedure for synthesis ethyl 4-(akyloxy)-2-(phenyl/pyridyl)thiazole-5-carboxylate (Lb-1-Lb-12)

To an ice cooled (0^{o}C) solution of Ethyl 4-hydroxy-2-(phenyl/pyridyl)-thiazole-5-carboxylate (04-08, 1 equiv) in dry THF (50ml) were added the propargyl alcohol (3 equiv) andtriphenylphosphine (3 equiv) one after another and maintained the same temperature for 15 min. To the above mixture, diethyl azodicarboxylate (3 equiv) was added drop wise and the reaction mixture was stirred at room temperature for 12 hours (monitored by TLC & LCMS for completion). The reaction mixture was evaporated under reduced pressure. The crude product was purified by column chromatography using hexane: ethyl acetate as eluent to give the desired product in good yield as described below.

Ethyl 4-(prop-2-yn-1-yloxy)-2-phenylthiazole-5-carboxylate (Lb-1)

The compound was synthesized according to the above general procedure using Ethyl 4-hydroxy-2-phenylthiazole-5-carboxylate (05, 0.5 g, 2 mmol), propargyl alcohol (0.34 g, 6 mmol) andtriphenylphosphine (1.57 g, 6 mmol) and diethyl azodicarboxylate (1.05 g, 6 mmol) to afford 09 (0.43 g, 74.65%) as white solid. ^{1}H NMR (DMSO-d_6): $\delta_{H.}$ 1.27 (t, J = 6.9 Hz, 3H), 3.6 (s, 1H), 4.24 (q, J = 6.9 Hz, 2H), 5.21 (s, 2H), 7.54- 8.01 (m, 5H). ^{13}C NMR (DMSO-d_6): δc.167, 163.5, 160, 131.9, 131.8, 129.4, 126.4, 101.2, 78.9, 78.2, 60.6, 58, 14.2. ESI-MS *m*/*z* 288.1 $(M+H)^+$. Anal Calcd for $C_{15}H_{13}NO_3S$; C, 62.70; H, 4.56; N, 4.87; Found: C, 62.68; H, 4.55; N, 4.85.

Ethyl 4-(prop-2-yn-1-yloxy)-2-(pyridin-2-yl)thiazole-5-carboxylate (Lb-2)

The compound was synthesized according to the above general procedure using ethyl 4-hydroxy-2-(pyridin-2-yl)thiazole-5-carboxylate (**06**, 0.5 g, 2 mmol), propargyl alcohol (0.34 g, 6 mmol) andtriphenylphosphine (1.57 g, 6 mmol) and diethyl azodicarboxylate (1.05 g, 6 mmol) to afford **10** (0.41 g, 71.2%) as off white solid. ^{1}H NMR (DMSO-d_6): $\delta_{H.}$1.27 (t, J = 6.7 Hz, 3H), 3.62 (s, 1H), 4.23 (q, J = 6.7 Hz, 2H), 5.23 (s, 2H), 7.43- 8.54 (m, 4H). ^{13}C NMR (DMSO-d_6): δc. 166.8, 162.1, 157.2, 149.4, 147.8, 146.2, 137.3, 124.4, 123.8, 78.8, 77.9, 60.6, 58.3, 14.3. ESI-MS *m*/*z* 289.2 $(M+H)^+$. Anal Calcd for $C_{14}H_{12}N_2O_3S$; C, 58.32; H, 4.20; N, 9.72; Found: C, 58.29; H, 4.18; N, 9.73.

Ethyl 4-(prop-2-yn-1-yloxy)-2-(pyridin-3-yl)thiazole-5-carboxylate (Lb-3)

The compound was synthesized according to the above general procedure using ethyl 4-hydroxy-2-(pyridin-3-yl)thiazole-5-carboxylate (07, 0.5 g, 2 mmol), propargyl alcohol (0.34 g, 6 mmol) andtriphenylphosphine (1.57 g, 6 mmol) and diethyl azodicarboxylate (1.05 g, 6 mmol) to afford 11 (0.36 g, 62.5%) as off white solid. ^{1}H NMR (DMSO-d_6): $\delta_{H.}$ 1.26 (t, J = 7 Hz, 3H), 3.61 (s, 1H), 4.24 (q, J = 7 Hz, 2H), 5.22 (s, 2H), 7.67- 8.98 (m, 4H). ^{13}C NMR (DMSO-d_6): δc.166.4, 153.3, 149, 148.2, 147.8, 147.5, 133.9, 133.2, 123.8, 78.7, 77.8, 60.5, 57.8, 14.2. ESI-MS *m*/*z* 289 $(M+H)^+$. Anal Calcd for $C_{14}H_{12}N_2O_3S$; C, 58.32; H, 4.20; N, 9.72; Found: C, 58.33; H, 4.19; N, 9.75.

Ethyl 4-(prop-2-yn-1-yloxy)-2-(pyridin-4-yl)thiazole-5-carboxylate (Lb-4)

The compound was synthesized according to the above general procedure using ethyl 4-hydroxy-2-(pyridin-4-yl)thiazole-5-carboxylate (08, 0.5 g, 2 mmol), propargyl alcohol (0.34 g, 6 mmol) andtriphenylphosphine (1.57 g, 6 mmol) and diethyl azodicarboxylate (1.05 g, 6 mmol) to afford 12 (0.39 g, 67.7%) as off white solid. ^{1}H NMR (DMSO-d_6): $\delta_{H.}$ 1.29 (t, J = 6.8 Hz, 3H), 3.6 (s, 1H), 4.23 (q, J = 6.8 Hz, 2H), 5.23 (s, 2H), 7.96- 8.71 (m, 4H). ^{13}C NMR (DMSO-d_6): δc. 166.7, 153.8, 149.8, 147.6, 143.6, 143.1, 121.2, 78.9, 78.1, 60.5, 57.9, 14.2. ESI-MS *m*/*z* 289.0 $(M+H)^+$. Anal Calcd for $C_{14}H_{12}N_2O_3S$; C, 58.32; H, 4.20; N, 9.72; Found: C, 58.34; H, 4.21 N, 9.7.

General procedure for synthesis of 4-(alkyloxy)-2-(phenyl/pyridyl) thiazole-5-carboxylic acid (Lb-13-Lb-24)

To a solution of the corresponding Ethyl 4-(akyloxy)-2-(phenyl/pyridyl)-thiazole-5-carboxylate (9-20, 1 equiv) in THF:Methanol:Water (1:1:1) system, was added lot wise lithium hydroxide (2 equiv). The reaction mixture was then heated at 60^{o}C for 4-5 hours

(monitored by TLC & LCMS for completion) and allowed to cool. Solvent was evaporated under vacuum, and the reaction mixture was diluted with water and acidified to pH 2 with 1N HCl. The precipitate formed was filtered and re-crystallized form ethanol to afford the desired product in good yield as described below.

4-(Prop-2-yn-1-yloxy)-2-phenylthiazole-5-carboxylic acid (Lb-21)

The compound was synthesized according to the above general procedure using ethyl 4-(prop-2-yn-1-yloxy)-2-phenylthiazole-5-carboxylate(17, 0.3 g, 1 mmol), and lithium hydroxide monohydrate (0.088 g, 2 mmol), to afford 29 (0.24 g, 88.6%) as white solid. ^{1}H NMR (DMSO-d_6):). $\delta_{H.}$ 3.61 (s, 1H), 5.18 (s, 2H), 7.54 – 8.00 (m, 5H). ^{13}C NMR (DMSO-d_6): δc.166.4, 162.9, 161.6, 132, 131.7, 129.4, 126.1, 102.7, 79.1, 78.2, 57.9. ESI-MS *m*/*z* 258.1 $(M-H)^+$. Anal Calcd for $C_{13}H_9NO_3S$; C, 60.22; H, 3.50; N, 5.40; Found: C, 60.21; H, 3.49; N, 5.38.

4-(Prop-2-yn-1-yloxy)-2-(pyridin-2-yl)thiazole-5-carboxylic acid (Lb-22)

The compound was synthesized according to the above general procedure using ethyl 4-(prop-2-yn-1-yloxy)-2-(pyridin-2-yl)thiazole-5-carboxylate(18, 0.3 g, 1 mmol), and lithium hydroxide monohydrate (0.088 g, 2 mmol), to afford 30 (0.22 g, 81.8%) as white solid. ^{1}H NMR (DMSO-d_6): $\delta_{H.}$3.62 (s, 1H), 5.22 (s, 2H), 7.39 – 8.57 (m, 4H). ^{13}C NMR (DMSO-d_6): δc.166.3, 161, 156.3, 149.2, 148.4, 143, 137.4, 124.8, 123.3, 79.1, 78, 60. ESI-MS *m*/*z* 259 $(M-H)^+$. Anal Calcd for $C_{12}H_8N_2O_3S$; C, 55.38; H, 3.10; N, 10.76; Found: C, 55.35; H, 3.12; N, 10.74.

4-(Prop-2-yn-1-yloxy)-2-(pyridin-3-yl)thiazole-5-carboxylic acid (Lb-23)

The compound was synthesized according to the above general procedure using ethyl 4-(prop-2-yn-1-yloxy)-2-(pyridin-2-yl)thiazole-5-carboxylate(19, 0.3 g, 1 mmol), and lithium hydroxide monohydrate (0.088 g, 2 mmol), to afford 31 (0.21 g, 77.49%) as white solid. ^{1}H NMR (DMSO-d_6): $\delta_{H.}$3.6 (s, 1H), 5.2 (s, 2H), 7.63 – 8.96 (m, 4H). ^{13}C NMR (DMSO-d_6): δc.166.1, 153.1, 149.1, 147.7, 147.5, 142.5, 134.1, 133.6, 123.9, 78.9, 77.8, 57.7. ESI-MS *m*/*z* 259.1 $(M-H)^+$. Anal Calcd for $C_{12}H_8N_2O_3S$; C, 55.38; H, 3.10; N, 10.76; Found: C, 55.37; H, 3.11; N, 10.76.

4-(Prop-2-yn-1-yloxy)-2-(pyridin-4-yl)thiazole-5-carboxylic acid (Lb-24)

The compound was synthesized according to the above general procedure using ethyl 4-(prop-2-yn-1-yloxy)-2-(pyridin-2-yl)thiazole-5-carboxylate(20, 0.3 g, 1 mmol), and lithium

hydroxide monohydrate (0.088 g, 2 mmol), to afford 32 (0.21 g, 77.49%) as white solid. ^{1}H NMR (DMSO-d_6): $\delta_{H.}$3.63 (s, 1H), 5.21 (s, 2H), 7.99 – 8.69 (m, 4H). ^{13}C NMR (DMSO-d_6): δc.166.3, 153.6, 149.9, 147.7, 143.4, 142.8, 121.3, 79.1, 77.9, 57.8. ESI-MS *m*/*z* 259.2 (M-H)$^{+}$. Anal Calcd for $C_{12}H_8N_2O_3S$; C, 55.38; H, 3.10; N, 10.76; Found: C, 55.40; H, 3.09; N, 10.78.

General procedure for synthesis of 4-(alkyloxy)-2-(phenyl/pyridyl) thiazole-5-carboxamide (Lb-25-Lb-36)

To a solution of the corresponding 4-(alkyloxy)-2-(phenyl/pyridyl) thiazole-5-carboxylic acid (21-32, 1 equiv) in DCM at 0^{o}C was added the oxalyl chloride (1.5 equiv) and catalytic amount of DMF. The reaction mixture was the stirred at rt (for the formation of the corresponding acid chloride) for about 2-3 hours and quenched into excess of ammonium hydroxide solution at 0^{o}C. The reaction mixture was then repeatedly extracted with ethyl acetate (2 * 20 ml), washed with brine (5 ml) dried over sodium sulphate. The combined organic phases were concentrated under reduced and re-crystallized form diethyl ether to afford the desired product in good yield as described below.

4-(Prop-2-yn-1-yloxy)-2-phenylthiazole-5-carboxamide (Lb-33)

The compound was synthesized according to the above general procedure using 4-(prop-2-yn-1-yloxy)-2-phenylthiazole-5-carboxylic acid (29, 0.25 g, 0.096 mmol) via 4-(prop-2-yn-1-yloxy)-2-phenylthiazole-5-carbonyl chloride to afford 41 (0.19 g, 76.3 %) as off white solid. ^{1}H NMR (DMSO-d_6): $\delta_{H.}$ 3.65 (s, 1H), 5.2 (s, 1H), 6.98 – 7.97(m, H). ^{13}C NMR (DMSO-d_6): δc.165.6, 161.2, 158.8, 132.2, 131.4, 129.3, 125.9, 109.5, 78.9, 78.5, 58.3. ESI-MS*m*/*z* 259.1 (M+H)$^{+}$. Anal Calcd for $C_{13}H_{10}N_2O_2S$; C, 60.45; H, 3.90; N, 10.85; Found: C, 60.43; H, 3.89; N, 10.83.

4-(Prop-2-yn-1-yloxy)-2-(pyridin-2-yl)thiazole-5-carboxamide (Lb-34)

The compound was synthesized according to the above general procedure using 4-(prop-2-yn-1-yloxy)-2-(pyridin-2-yl)thiazole-5-carboxylic acid (30, 0.25 g, 0.096 mmol) via 4-(prop-2-yn-1-yloxy)-2-(pyridin-2-yl)thiazole-5-carbonyl chloride to afford 42 (0.17 g, 68.3 %) as off white solid. ^{1}H NMR (DMSO-d_6): $\delta_{H.}$ 3.67 (s, 1H), 5.22 (s, 2H), 7.36 – 8.58 (m, 4H). ^{13}C NMR (DMSO-d_6): δc.165.4, 160.8, 156.2, 149.2, 147.8, 142.9, 137.4, 124.6, 123.5, 78.9, 78.3, 58.1. ESI-MS *m*/*z* 260.2 (M+H)$^{+}$. Anal Calcd for $C_{12}H_9N_3O_2S$; C, 55.59; H, 3.50; N, 16.21; Found: C, 55.61; H, 3.51; N, 16.19.

4-(Prop-2-yn-1-yloxy)-2-(pyridin-3-yl)thiazole-5-carboxamide (Lb-35)

The compound was synthesized according to the above general procedure using 4-(prop-2-yn-1-yloxy)-2-(pyridin-3-yl)thiazole-5-carboxylic acid (31, 0.25 g, 0.096 mmol) via 4-(prop-2-yn-1-yloxy)-2-(pyridin-2-yl)thiazole-5-carbonyl chloride to afford 43 (0.21 g, 84.3 %) as off white solid. ^{1}H NMR (DMSO-d_6): $\delta_{H.}$3.64 (s, 1H), 5.21 (s, 2H), 7.65 – 8.99 (m, 4H). ^{13}C NMR (DMSO-d_6): δc.165.3, 152.9, 149, 147.7, 147.4, 142.5, 134.2, 133.4, 123.9, 78.7, 78.1, 58. ESI-MS *m*/*z* 259.1 $(M+H)^+$. Anal Calcd for $C_{12}H_9N_3O_2S$; C, 55.59; H, 3.50; N, 16.21; Found: C, 55.58; H, 3.51; N, 16.2.

4-(Prop-2-yn-1-yloxy)-2-(pyridin-4-yl)thiazole-5-carboxamide (Lb-36)

The compound was synthesized according to the above general procedure using 4-(prop-2-yn-1-yloxy)-2-(pyridin-3-yl)thiazole-5-carboxylic acid (32, 0.25 g, 0.096 mmol) via 4-(prop-2-yn-1-yloxy)-2-(pyridin-2-yl)thiazole-5-carbonyl chloride to afford 44 (0.19 g, 76.3 %) as off white solid. NMR (DMSO-d_6): $\delta_{H.}$ 3.66 (s, 1H), 5.21 (s, 2H), 8.01 – 8.70 (m, 4H). ^{13}C NMR (DMSO-d_6): δc.165.5, 153.4, 149.7, 147.8, 143.4, 143, 121.1, 79, 78.4, 58.2. ESI-MS *m*/*z* 259.1 $(M+H)^+$. Anal Calcd for $C_{12}H_9N_3O_2S$; C, 55.59; H, 3.50; N, 16.21; Found: C, 55.61; H, 3.52; N, 16.23.

Appendix
List of publications

From thesis work

1. **Parthiban Brindha Devi**, Ganesh Samala, Jonnalagadda Padma Sridevi, Shalini Saxena, Mallika Alvala, Elena G Salina, Dharmarajan Sriram, Perumal Yogeeswari, Structure-guided design of novel thiazolidine derivatives as *Mycobacterium tuberculosis* pantothenate synthetase inhibitors, **ChemMedChem,** 9, 2538-2547.
2. **Parhiban Brindha Devi,** Shalini Saxena, Sridhar Jogula, Asireddy Parameshwar Reddy, Jonnalagadda Padma Sridevi, Dharmarajan Sriram, Perumal Yogeeswari, Structure-based drug design of novel *Mycobacterium tuberculosis* pantothenate synthetase inhibitors, **Molecular Informatics**, 2014, In Press
3. **Parthiban Brindha Devi**, Jonnalagadda Padma Sridevi, Shruti Singh Kakan, Shalini Saxena, Variam Ullas Jeankumar, Vijay Soni, Hasitha Shilpa Anantaraju, Perumal Yogeeswari, Dharmarajan Sriram, Discovery of novel lysine ε-aminotransferase inhibitors: An intriguing potential target for latent tuberculosis, **Molecular Biosystems** [Communicated]
4. **Parthiban Brindha Devi**, Jonnalagadda Padma Sridevi, Manoj Chandran, Shalini Saxena, Vijay Soni, Perumal Yogeeswari, Dharmarajan Sriram, Discovery of lysine aminotransferase inhibitors for latent tuberculosis, [To be Communicate].

Other Publications

1. Ganesh S Pedgaonkar, Jonnalagadda Padma Sridevi, Variam Ullas Jean Kumar, Shalini Saxena, **Parthiban Brindha Devi**, Janupally Renuka, Perumal Yogeeswari, Dharmarajan Sriram, Development of 2-(4-oxoquinazolin-3(4H)-yl)acetamide derivatives as novel enoyl-acyl carrier protein reductase (InhA) inhibitors for the treatment of tuberculosis, Eur. J. Med. Chem, DOI: 10.1016/j.ejmech.2014.09.028.

2. Renuka Janupally, Variam Ullas Jean Kumar, Bobesh K Andrews, Vijay Soni, **Parthiban Brindha Devi**, Pushkar Kulkarni, Priyanka Suryadevara, Perumal Yogeeswari, Dharmarajan Sriram, Structure-guided design and development of novel benzimidazole class of compounds targeting DNA Gyrase B enzyme of *Staphylococcus aureus*, Bioorg. Med. Chem.**,** DOI: 10.1016/j.bmc.2014.09.008.

3. Ganesh S Pedgaonkar, Jonnalagadda Padma Sridevi, Variam Ullas Jean Kumar, Shalini Saxena, **Parthiban Brindha Devi**, Janupally Renuka, Perumal Yogeeswari, Dharmarajan Sriram, Development of benzy[*d*]oxazol-2(3*H*)-ones derivatives as novel inhibitors of *Mycobacterium tuberculosis* InhA, Bioorg. Med. Chem., DOI: 10.1016/j.bmc.2014.08.031.

4. Ganesh Samala, Radhika Nallangi, **Parthiban Brindha Devi**, Shalini Saxena, Renu Yadav, Jonnalagadda Padma Sridevi, Perumal Yogeeswari, Dharmarajan Sriram, Identification and development of 2-methylimidazo[1,2-a] pyridine-3-carboxamides as *Mycobacterium tuberculosis* pantothenate synthetase Inhibitors, Bioorg. Med. Chem., DOI**:** 10.1016/j.bmc.2014.05.038

5. Ganesh Samala, Shruti Singh Kakan, Radhika Nallangi, **Parthiban Brindha Devi**, Jonnalagadda Padma Sridevi, Shalini Saxena, Perumal Yogeeswari, Dharmarajan Sriram, Investigating structure-activity relationship and mechanism of action of antitubercular 1-(4-chlorophenyl)-4-(4-hydroxy-3-methoxy-5-nitrobenzylidene) pyrazolidine-3,5-dione [CD59], International Journal of Mycobacteriology, **2014** 3(2):117-126

6. Ganesh Samala, **Parthiban Brindha Devi,** Radhika Nallangi, Jonnalagadda Padma Sridevi, Shalini Saxena, Perumal Yogeeswari, Dharmarajan Sriram, Development of Novel tetrahydrothieno[2,3-c] pyridine-3-carboxamide based *Mycobacterium tuberculosis* pantothenate synthetase inhibitors: Molecular hybridization from known antimycobacterial leads, Bioorg. Med. Chem., **2014**, 22(6); 1938-1947

7. Shalini Saxena, **Parthiban Brindha Devi**, Vijay Soni, Perumal Yogeeswari, Dharmarajan Sriram, Identification of novel inhibitors against *Mycobacterium tuberculosis* L-Alanine dehydrogenase (Mtb-AlaDH) through structure-based virtual screening, J Mol Graph Model, **2013**, 47:37-43.

8. Ganesh Samala, **Parthiban Brindha Devi,** Radhika Nallangi, Perumal Yogeeswari, Dharmarajan Sriram, Development of 3-phenyl-4,5,6,7-tetrahydro-1H-pyrazolo[4,3-c] pyridine derivatives as novel *Mycobacterium tuberculosis* pantothenate synthetase inhibitors, Eur. J. Med. Chem, **2013**, 69:356-364.

List of conferences papers

1. **Devi, P.B**., Saxena, S., Sriram, D., Yogeeswari, P., Screening and Identification of Potent Inhibitors against pantothenate synthetase- An important target *Mycobacterium tuberculosis* infection. 3rd ScienceOne Conference on Drug Discovery and Development (SCDDD), 21-23 January 2014, Dubai
2. **Devi, P.B**., Mallika A., P. Yogeeswari, D. Sriram, Development of Pantothenate Synthetase Inhibitors for Mycobacterium Tuberculosis Infection: Design and Enzyme Inhibition, 3rd World Congress on Biotechnology,13-15 Septemeber 2012, Hyderabad, India.
3. Ganesh, S.; Radhika, N.; **Devi, P.B**.; Yogeeswari, P.; Sriram, D. Design, synthesis and biological evaluation of 6-methylimidazo[2,1-b]thiazole-5-carboxylic acid derivatives as novel *Mycobacterium tuberculosis* pantothenate synthase inhibitors. 15th Tetrahedron Symposium- Asian Edition: Challenges in Bioorganic and Organic Medicinal Chemistry, 28-31 October 2014, Singapore

BIOGRAPHY OF BRINDHA DEVI P

Ms. P Brindha Devi completed her Bachelor of Technology and Master of Technology from Anna University, Chennai, Tamil Nadu. She has been appointed as JRF in OSDD-CSIR funded project at Birla Institute of Technology and Science, Pilani, Hyderabad campus from 2012-2014 under the supervision of Prof. P.Yogeeswari. She has published 10 scientific publications in well-renowned international journals and presented papers in various national and international conferences.

BIOGRAPHY OF PROF. P.YOGEESWARI

Dr. P. Yogeeswari is presently working in the capacity of Professor and Associate Dean (Sponsored Research and Consultancy Division), Department of Pharmacy, Birla Institute of Technology and Science, Pilani, Hyderabad Campus. She received her Ph.D. degree in the year 2001 from Banaras Hindu University; Varanasi. She has been involved in research for the last 14 years and in teaching for 13 years. APTI honoured her with YOUNG PHARMACY TEACHER AWARD for the year 2007. In 2010, ICMR honored her by awarding "Shakuntala Amir Chand Award" for her excellent biomedical research. She has been awarded for IASP 2014 "Excellence in Pain Research and Management in Developing Countries" under the basic science research category at Argentina in October 2014. She has collaborations with various national and international organizations that include National Institute of Health, Bethesda, USA, National Institute of Mental Health and Neurosciences, Bangalore, Karolinska Institute, Stockholm, Sweden, National Institute of Immunology, New Delhi, India, Pasteur Institute, University of Lille, France, Bogomoletz Institute of Physiology National Academy of Science, Ukraine, and Faculty of Medicine of Porto, Porto, Portugal,. She has to her credit more than 190 research publications and one Indian Patent, Application No: 1138/CHE/2009. She is an expert reviewer of many international journals like Journal of Medicinal Chemistry (ACS), Journal of Chemical Information & Modeling (ACS, USA), Bioorganic Medicinal Chemistry (Elsevier), Recent Patents on CNS Drug Discovery (Bentham), etc. She has also co-authored a textbook on organic medicinal chemistry with Dr. D Sriram titled "Medicinal Chemistry" published by Pearson Education and one book chapter in in Jan 2013 by IGI Global. She is a lifetime member of Association of Pharmacy Teachers of India and Indian Pharmacological Society. She has successfully completed many sponsored projects and currently handling projects sponsored by DST, DBT INDO-BRAZIL, ICMR-INSERM, and CSIR. She has guided nine Ph.D students and currently twelve students are pursuing their Ph.D. work.